SOME ASPECTS OF THE GEOCHEMISTRY OF HIGH-TEMPERATURE PERIDOTITES AND MEGACRYSTS FROM THE JAGERSFONTEIN KIMBERLITE PIPE, SOUTH AFRICA

by

Jennifer Jane Hops

Thesis submitted in fulfilment of the requirements
for the degree of Doctor of Philosophy

Department of Geochemistry
University of Cape Town

September, 1989

DECLARATION

I hereby declare that the work presented in this thesis is my own, except where otherwise stated in the text.

J.J.Hops

September, 1989

ABSTRACT

The Jagersfontein kimberlite contains an abundance of both deformed high-temperature peridotites and Cr-poor megacrysts. The Cr-poor megacryst suite is represented by olivine, orthopyroxene, clinopyroxene and garnet. The megacrysts show features which are unique to Jagersfontein, a particularly notable feature being the absence of ilmenite and ilmenite-silicate intergrowths. Major element and REE compositions of the Cr-poor megacryst suite are consistent with a magmatic fractionation sequence. $^{87}Sr/^{86}Sr$ and $^{143}Nd/^{144}Nd$ ratios of the Cr-poor clinopyroxene megacrysts indicate a source similar to that of non-DUPAL ocean island basalts.

Deformed peridotites at Jagersfontein have high calculated temperatures of equilibration (1132-1361^{o}C), which are slightly lower but which overlap with those of the Cr-poor megacryst suite. Both the high-temperature peridotites and the Cr-poor megacrysts yield similar pressures of equilibration (51$\pm$2 kbar), indicating their association with a thermal perturbation and supporting a close spatial association between them.

Olivine and pyroxenes in the high-temperature peridotites appear homogeneous, but compositional gradients were observed in several garnet porphyroclasts. These garnets show rim enrichments in TiO_2 and Na_2O. This zonation in the garnets is evidence for enrichment of the deformed peridotites shortly before kimberlite eruption. This

enrichment is likely to be due to interaction with the megacryst magma. In addition, the high-temperature peridotites show a general enrichment in Fe, Ti, Na and Al with decreasing Ca/(Ca+Mg). Such features support a magmatic aureole model, in that temperature and degree of enrichment might be expected to increase with proximity to the megacryst magma body.

$^{87}Sr/^{86}Sr$ and $^{143}Nd/^{144}Nd$ ratios of clinopyroxene separates from the high-temperature peridotites are similar to those from oceanic peridotites. Modal abundances and olivine forsterite contents of the high-temperature peridotites are consistent with an origin as residues of partial melting events involving basalt formation. It is suggested that partial melting events, in the upper mantle beneath Jagersfontein, resulted in the formation of a depleted protolith which underplated the base of the Archaean lithosphere. This depleted protolith was subsequently enriched by interaction with the Cr-poor megacryst magma just prior to kimberlite eruption. The high-temperature peridotites therefore represent samples from the base of the lithosphere rather than from the convecting asthenosphere.

Table of Contents

5 TRACE ELEMENTS AND RADIOGENIC ISOTOPE DATA

6 SYNTHESIS

Tables

Plates

Figures

PAGE

Appendices

CHAPTER 1

INTRODUCTION

1.1 MANTLE XENOLITHS

The discovery, at Jagersfontein in August 1870 (Williams, 1932), that kimberlite was a host rock for diamonds, prompted great interest in this volumetrically rare rock type. Apart from the possible occurrence of diamond, kimberlites have also proved invaluable in the study of the composition of the upper mantle. This is because xenoliths, representing fragments of the many heterogeneous reservoirs within the subcontinental upper mantle, are entrained by the kimberlite magma and transported to the surface. The study of the composition of these mantle-derived xenoliths, in combination with geophysical studies, yields clues to processes occurring in the lithosphere which then enable constraints to be placed on the petrology and structure of the upper mantle.

Extremely non-radiogenic Nd isotope ratios, indicative of old trace element enrichment, have been found in subcalcic peridotitic garnet inclusions in diamond (Richardson et al., 1984). Richardson et al. (op cit.) have interpreted this as an indication that the subcontinental lithosphere beneath the Kaapvaal craton has been stabilized for >3 b.y. Infiltration and crystallization of silicate melts and H_2O-rich fluids in the lithosphere beneath southern Africa over the last 3 b.y. will have overprinted original compositions to varying degrees by modal metasomatism and trace element

enrichment. The compositions of mantle-derived xenoliths might therefore reflect the effects of a number of processes.

Harte (1983) divided the mantle-derived xenoliths into four broad categories: a) peridotites and pyroxenites
b) eclogites and grospydites
c) megacrysts
d) glimmerites and MARID-suite rocks.

The peridotite group is commonly the most abundant at any particular locality, not surprisingly as peridotite is considered to be the basic constituent of the upper mantle. This peridotite group is represented by a broad spectrum of modal abundances of the minerals olivine, orthopyroxene, clinopyroxene and garnet. Peridotites are usually further subdivided according to petrography and mineral chemistry (Fig. 1.1). The division into coarse or deformed is based on textural-microstructural features, while the division into cold (<1100^{o}C) or hot (>1100^{o}C) is based on geothermometric estimates from mineral compositions (eg. Harte, 1983).

Xenoliths which yield high calculated temperatures of equilibration are of particular interest to this study. Various petrogenetic models have been proposed to account for the textures and the distinctive compositions of the high-temperature peridotites. These are discussed further in Chapter 6 in combination with petrogenetic models for the Cr-poor megacryst suite which has similar mineral

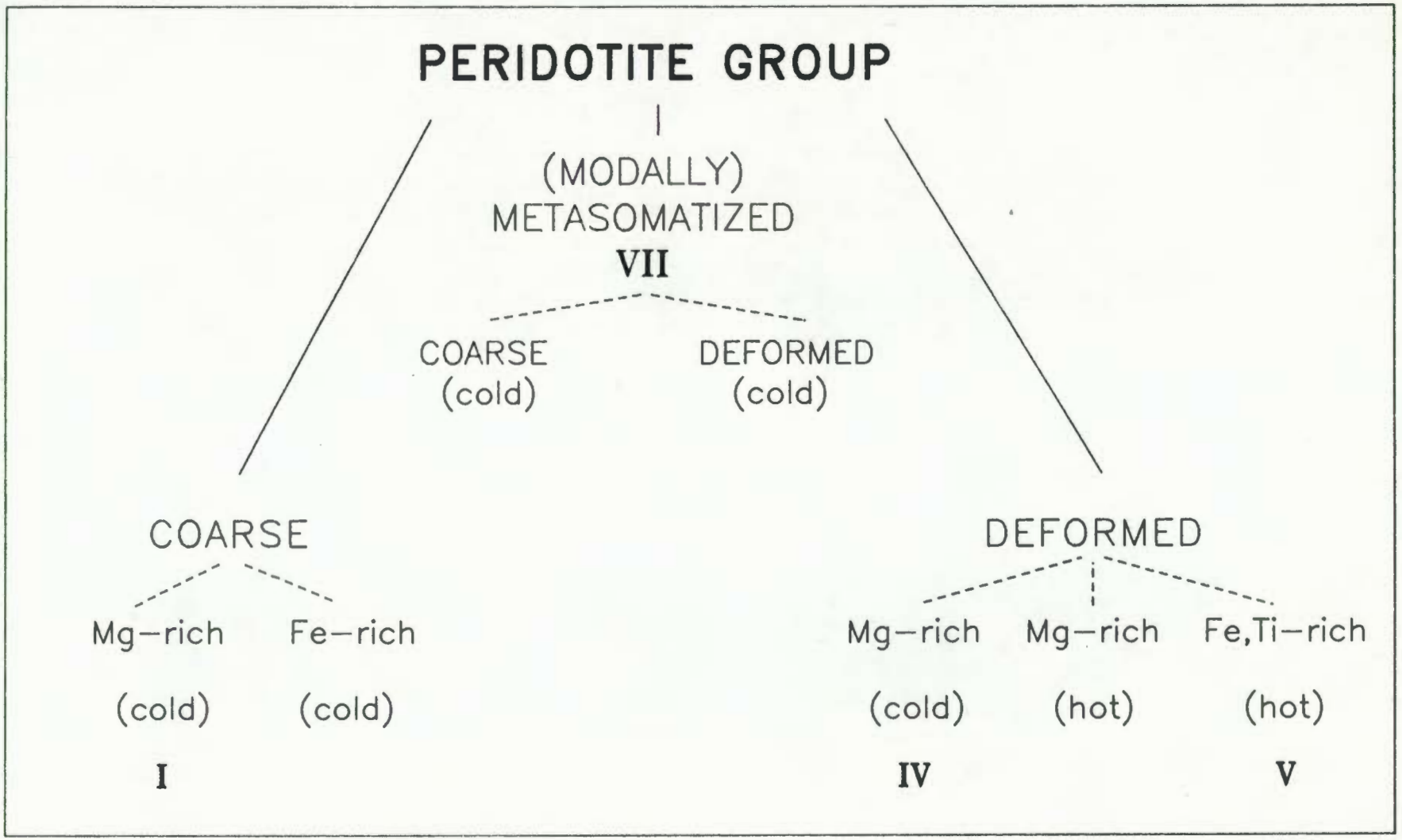

FIGURE 1.1: Major types of peridotites in kimberlites (after Harte, 1983). The Roman numerals indicate the correspondence with types in the Gurney and Harte (1980) classification.

compositions and temperatures of equilibration to the high-temperature peridotite xenoliths.

The major objective of this thesis is a detailed study of the high-temperature peridotite xenoliths and minerals of the Cr-poor megacryst suite. This represents an evaluation of the possible association between them as proposed by Harte and Gurney (1981), and by Ehrenberg (1979, 1982a) for xenoliths from The Thumb, a minette intrusion on the Colorado Plateau.

Comparisons of xenolith suites from kimberlites within the same cluster have revealed differences in both xenolith abundances and mineral compositions, suggesting localized mantle heterogeneities. In order to minimize these effects, samples for this study were chosen from a single locality. Although the Monastery kimberlite is widely regarded as the type locality for Cr-poor megacrysts (Jakob, 1977; Gurney et al., 1979; Moore, 1987), it does not contain many high-temperature deformed peridotites. The Jagersfontein kimberlite contains an abundance of both the high-temperature deformed peridotites and xenoliths from the Cr-poor megacryst suite and was selected as a superior sample locality for investigating their inter-relationships.

1.2 SAMPLE LOCALITY

The Jagersfontein kimberlite pipe ($29^{o}46'S$, $25^{o}28'E$) is situated southeast of Kimberley in the Orange Free State,

South Africa, close to the edge of the Kaapvaal craton (Fig. 1.2). The pipe intrudes Beaufort Group rocks (Permian to Triassic) of the Karoo Sequence. Jagersfontein is a Group 1 kimberlite (Smith, 1983) and has a U-Pb whole rock age of 89 $\pm$ 4 m.y. (Kramers and Smith, 1983) and a Rb-Sr phlogopite and whole-rock age of 85.6 $\pm$ 1.0 m.y. (Smith et al., 1985a); these have been interpreted as the age of pipe emplacement.

Previous studies of the peridotite xenolith suite at Jagersfontein include those by Johnston (1973), Harte and Gurney (1982), Haggerty (1983), Winterburn (1987) and Field et al. (1989). These sources will be used for complementary information on the coarse low-temperature and modally metasomatized peridotites at Jagersfontein.

1.3 SAMPLE COLLECTION

The peridotite xenoliths and megacrysts discussed in this thesis were chosen from samples collected by J.J. Gurney and B. Harte in 1979. This collection was supplemented both in July 1984 and October 1985. As mining of the Jagersfontein kimberlite pipe ceased in 1972, all the samples were collected from dumps in the floor areas on which the mined ground was spread.

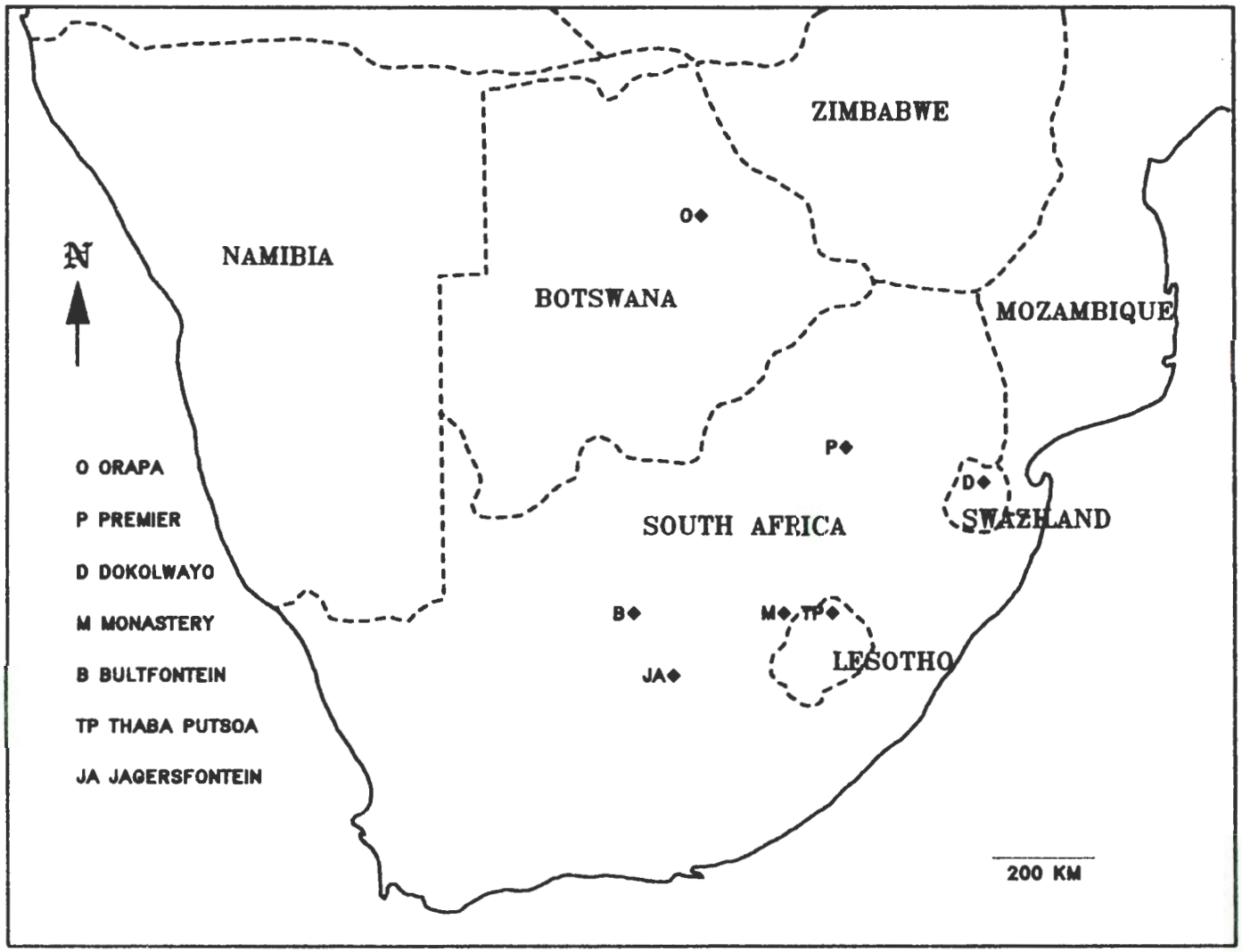

FIGURE 1.2:– Locality map of selected southern African kimberlites.

1.4 AIMS OF THIS STUDY

The results obtained from a study of the petrography, major and trace element mineral compositions of the peridotites and megacrysts and the Rb-Sr, Sm-Nd isotopic systematics of selected samples, will be combined to discuss:

- the possible relationship between the high-temperature deformed peridotites and the Cr-poor megacrysts;
- the possible association between the Cr-poor megacrysts and their host kimberlite;
- the possible association between hotspots and the Cr-poor megacryst source;
- a revised model for megacryst formation;
- the differences between the Cr-poor megacrysts and the Granny Smith megacrysts;
- the possible association between the Granny Smith megacrysts and their host kimberlite;
- the mineralogical characteristics of the lithosphere-asthenosphere boundary beneath the Kaapvaal craton.

CHAPTER 2

PETROGRAPHY AND MINERAL COMPOSITIONS OF THE PERIDOTITE XENOLITHS

2.1 XENOLITH NOMENCLATURE

The peridotite xenoliths analyzed in this study have been named according to the presence of primary minerals, as has become conventional in the study of mantle-derived xenoliths, even though this nomenclature does not strictly follow the classification of Streckeisen (1976). A garnet lherzolite is accordingly a xenolith containing the assemblage (olivine + orthopyroxene + garnet + clinopyroxene) even if the clinopyroxene content is < 5 volume percent, while a garnet harzburgite contains the assemblage (olivine + orthopyroxene + garnet). Modal abundances of the primary minerals in the peridotites analyzed were estimated by point-counting 700 points on one thin-section per xenolith. Estimated modal abundances of the peridotites are presented in Table 1.

2.2 TEXTURES

2.2.1 Textural classification

The textural classification followed in this study is that proposed by Harte (1977), which classifies peridotite xenoliths according to the extent of their olivine recrystallization (Table 2).

TABLE 1

TEXTURAL CLASSIFICATION AND MODES OF THE PERIDOTITES

Sample	Texture	Olv	Opx	Cpx	Gnt
JJH 1	Porphyroclastic	87.7	6.2	1.4	4.0
JJH 2	Fluidal Mosaic	72.7	16.7	1.4	9.1
JJH 3	Mosaic	65.4	24.0	1.5	9.0
JJH 4	Fluidal Mosaic	80.1	16.4	0.5	2.8
JJH 6	Porphyroclastic	75.4	22.8	0.0	1.7
JJH 7	Mosaic	80.5	16.7	1.2	1.4
JJH 8	Mosaic	81.2	14.2	1.0	3.4
JJH 9	Porphyroclastic	69.8	28.0	0.0	2.1
JJH 10	Mosaic	73.0	18.5	1.2	7.1
JJH 11	Mosaic	80.5	11.2	1.0	7.1
JJH 12	Mosaic	76.4	9.8	7.1	6.5
JJH 13	Mosaic	78.2	13.7	3.4	4.5
JJH 14	Porphyroclastic	75.7	19.0	1.4	3.8
JJH 15	Mosaic	66.8	22.1	2.1	8.8
JJH 17	Porphyroclastic	69.0	19.7	3.2	8.0
JJH 18	Fluidal Mosaic	76.8	18.4	0.0	4.7
JJH 19	Mosaic	76.7	21.2	0.0	1.4
JJH 20	Fluidal Mosaic	70.7	24.5	0.4	4.2
JJH 26	Mosaic	55.5	21.7	6.0	16.7
JJH 28	Porphyroclastic	75.0	17.1	2.1	5.7
JJH 29	Mosaic	84.0	13.5	0.0	2.1
JJH 30	Mosaic	89.0	9.2	1.7	0.0
JJH 31	Mosaic	78.4	17.4	2.4	1.7
JJH 32	Mosaic	76.7	16.8	1.0	5.4
JJH 33	Porphyroclastic	67.2	24.2	2.7	5.7
JJH 34	Laminar Mosaic	72.7	13.6	7.1	6.5
JJH 35	Porphyroclastic				
JJH 36	Mosaic	88.1	10.1	0.8	0.8
JJH 37	Mosaic	60.4	25.0	6.4	8.1
JJH 38	Mosaic	61.5	25.7	4.5	8.1
JJG 1710	Fluidal Mosaic	68.5	18.5	5.4	7.7
JJG 1713	Mosaic	68.2	13.0	6.8	11.8
JJG 1729	Porphyroclastic	58.5	19.2	7.2	12.0
JJG 1753	Mosaic	63.2	10.0	10.2	16.4
JJG 1798	Mosaic	81.0	12.1	2.0	4.8
J 117	Coarse	55.0	7.3	16.0	21.6

TABLE 2

GLOSSARY OF TEXTURAL TERMS (after Harte, 1977)

COARSE - Average grain size greater than 2.0 mm.

PORPHYROCLASTIC - More than 10 volume % of the olivine occurs as porphyroclasts

MOSAIC PORPHYROCLASTIC - More than 90 volume % of the olivine has recrystallized and pyroxenes are the dominant porphyroclast grain.

LAMINAR - Thin lenticles are associated with modal variations, essentially in olivine and orthopyroxene.

FLUIDAL - Narrow stripes of a mineral, present as tiny grains, are connected with porphyroclasts of the same mineral and extend across regions in which another mineral shows a dominantly mosaic texture.

The deformed peridotite xenoliths at Jagersfontein can be classified as porphyroclastic or mosaic-porphyroclastic. Thirty-five peridotites were chosen for analysis, of these, 9 have been classified as porphyroclastic, 20 as mosaic-porphyroclastic, 5 as fluidal mosaic-porphyroclastic and 1 as laminar mosaic-porphyroclastic. The differences in these textures are illustrated in Plates 1 to 4. The textural classification of each of the xenoliths is presented in Table 1.

The principal evidence for extensive deformation of the peridotites analyzed in this study is the bimodal grain size of the xenoliths. The large grain size of the porphyroclasts suggests that the porphyroclastic and mosaic-porphyroclastic peridotites were derived by deformation and recrystallization of coarse peridotites. At Jagersfontein however, both Johnston (1973) and Harte and Gurney (1982) noted a bias towards harzburgite for coarse peridotites and towards garnet lherzolite for deformed peridotites. As a result, Harte and Gurney (op cit.) proposed that the difference in modal abundances implied that the coarse peridotites found at the surface did not represent the coarse protoliths for the deformed peridotites. This is inconsistent with the model proposed by Gurney and Harte (1980), in which the high-temperature peridotites are derived by enrichment of the typical coarse low-temperature peridotites, and will be addressed further in Section 6.1.4.

The density of average low-temperature peridotite is estimated to be 3.32g/cm^3, in contrast to 3.38g/cm^3 for

Plate 1: A garnet harzburgite (JJH 6) showing a porphyroclastic texture. Magnification x17

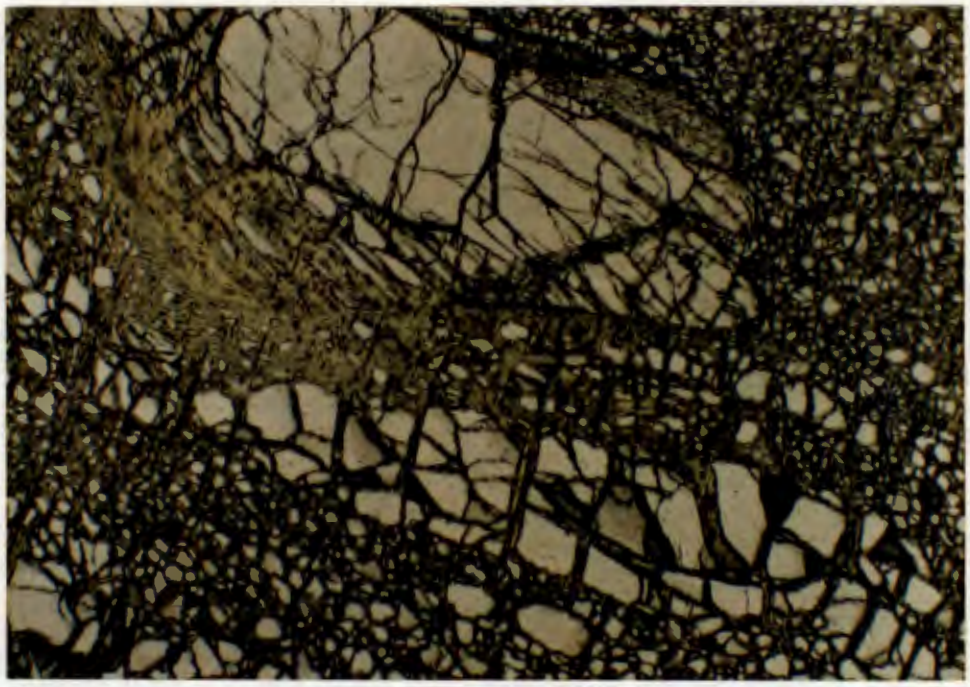

Plate 2: A garnet lherzolite (JJG 1713) showing a mosaic-porphyroclastic texture. Magnification x17

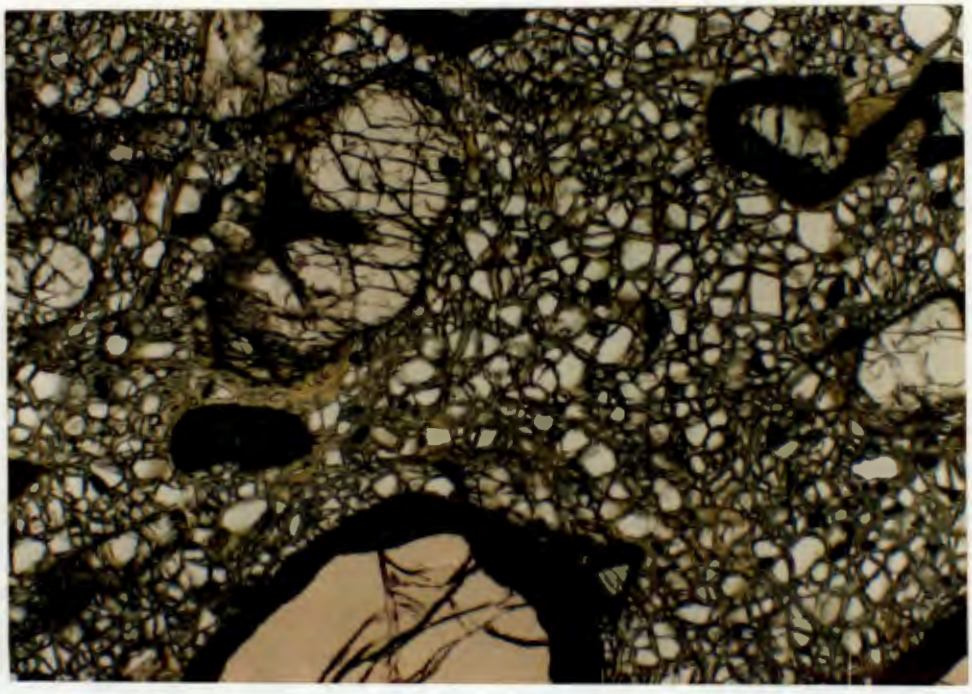

Plate 3: A garnet lherzolite (JJH 20) showing a fluidal mosaic-porphyroclastic texture. Magnification x17

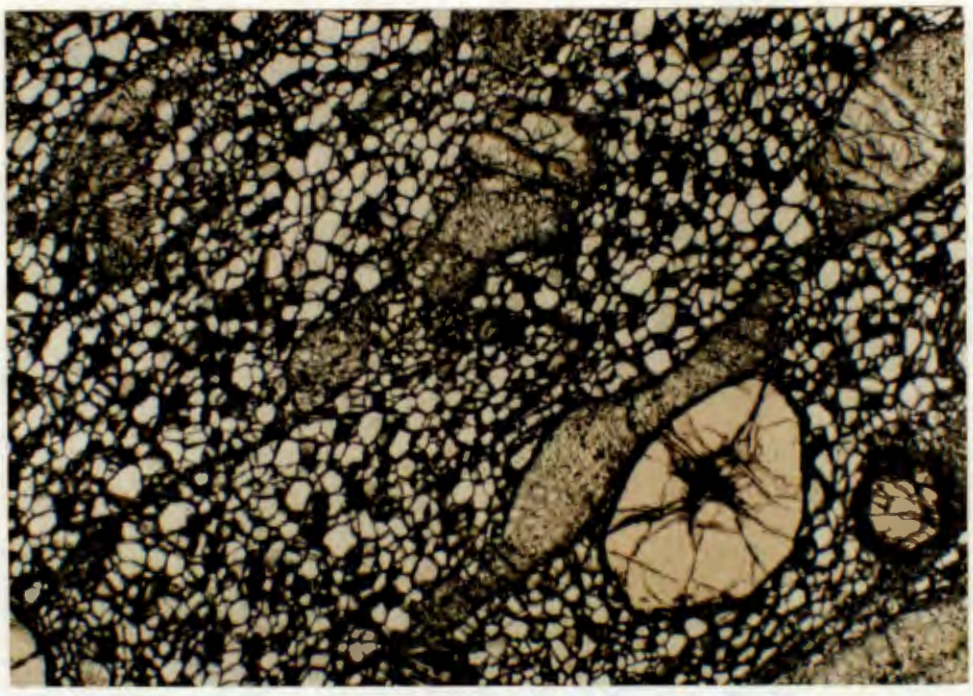

Plate 4: A garnet lherzolite (JJH 34) showing a laminar mosaic-porphyroclastic texture. Magnification x17

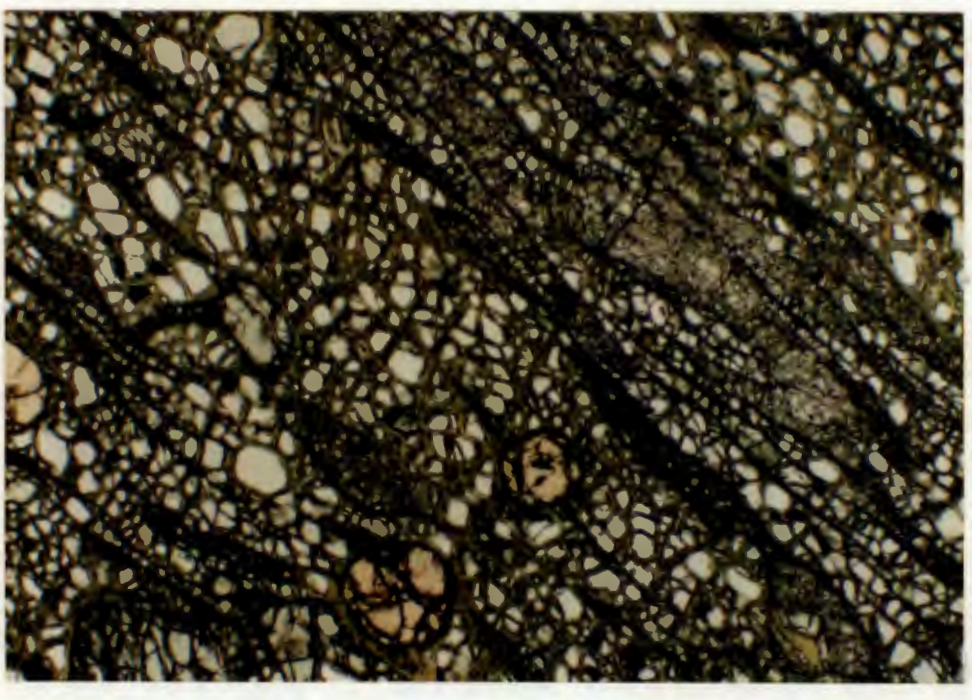

average high-temperature peridotite and 3.39g/cm^3 for the fertile garnet lherzolite PHN1611 (Boyd and McCallister, 1976). Jordan (1979) calculated that Fe-rich `fertile' garnet lherzolite would be denser than `depleted' lherzolite and suggested that chemical layering of the mantle would be an inherent feature. By virtue of their Fe-rich compositions relative to the low-temperature peridotites, the high-temperature peridotites would therefore be expected to represent a deeper portion of the upper mantle.

Anderson and Bass (1984) suggested, on the basis of seismic velocity, that above 140 km the shield lithosphere was olivine-rich and that the rapid drop in seismic velocity between 140 and 170 km was due to an increase in garnet and clinopyroxene relative to olivine and orthopyroxene. Modal abundance studies have, however, shown that the high-temperature peridotites are olivine-rich in comparison to the low-temperature peridotites (Boyd and Mertzman, 1987). The most significant modal difference between the low- and high-temperature peridotites is not so much in clinopyroxene + garnet as a difference in the proportions of orthopyroxene and olivine (Table 3). The average modal abundance calculated for the high-temperature peridotites from Jagersfontein is similar to that obtained for the combined average of high-temperature xenoliths from a number of localities on the Kaapvaal craton (Table 3). Boyd and Mertzman (1987) noted a similarity between modal abundances of oceanic peridotites and the high-temperature peridotites. They suggested that the high-temperature peridotites originated as a result of oceanic lithosphere being

TABLE 3

AVERAGE PERIDOTITE MODAL PROPORTIONS

	1	2	3	4	5
OLIVINE	62	79	73	75	66
ORTHOPYROXENE	31	13	17	16	20
CLINOPYROXENE	5	5	7	6	9
GARNET	2	4	3	3	5

1] Kaapvaal low-temperature peridotites (Boyd and Mertzman, 1987)

2] Abyssal peridotites (Boyd and Mertzman, 1987)

3] Average Jagersfontein high-temperature peridotites

4] Kaapvaal high-temperature peridotites (Boyd and Mertzman, 1987)

5] Premier high-temperature peridotites (Boyd and Mertzman, 1987)

1,2,4,5 Chemical modes
3 Optical mode

subducted beneath the southern margin of the Kaapvaal craton, possibly during the formation of the Namaqua-Natal mobile belt, approximately 1 b.y. ago. The feasibility of a subducted origin for the high-temperature peridotites at Jagersfontein will be addressed further in Section 6.1.4.

2.2.2 Review of textural studies

Textures observed in xenoliths are a function of a large number of variables. These include: temperature, pressure, strain rate, hydrolytic weakening, the number of metamorphic events the rock has been subjected to and modal composition. A study of the physical processes involved in producing the textures characteristic of the high-temperature deformed peridotites is beyond the scope of this thesis, but because any petrogenetic model for these peridotites must take the deformation into account, a short review of some salient features has been included.

The bimodal grain size which is characteristic of the deformed peridotites is the result of recrystallization. Recrystallization produces a generation of strain-free crystals (neoblasts and tablets) which progressively replace the original strained material through grain boundary migration. Recrystallization can take place during deformation (dynamic recrystallization) or during annealing (static recrystallization) (Mercier, 1979). Neoblasts are the result of dynamic (syntectonic) recrystallization, a process which yields a steady-state grain size with lognormal distribution. Tablets are the result of static

(annealing) recrystallization and are strain and dislocation free, this is in contrast to the neoblasts which have relatively high dislocation densities. The strain-free tablets grow at the expense of the strained porphyroclasts during post-deformation annealing. Drury and van Roermund (1988b) have noted that although it is possible that annealing occurred in the period between the end of deformation and entrainment in the kimberlite magma, recrystallization kinetics imply that this period is short. They suggested that growth of the tablets might also occur during ascent of the peridotite in the kimberlite magma, although translithospheric transport rates are also very rapid (cf. Section 6.1.3). Tablets form at the neoblast-porphyroclast recrystallization front, and the absence of tablets growing within the neoblast mosaic has been ascribed to the lower strain energy of the neoblasts (Mercier, 1979). Drury and van Roermund (1988b) noted that tablet grain boundaries were sub-parallel to crystal growth habits in olivine and orthopyroxene, and that this microstructure was characteristic of recrystallization by fluid-assisted grain boundary migration. In this process a semi-continuous fluid film is present along the grain boundary, and migration occurs by dissolution of the deformed grain, diffusion through the fluid and precipitation of the new grain. Although the nature of this fluid in the high-temperature deformed peridotites is still speculative, the occurrence of tablet grains in low-temperature deformed peridotites as well, suggests that the fluid might be a C-H-O-rich fluid derived from the kimberlite (Drury and van Roermund, 1988b). Once a xenolith is entrained in the kimberlite magma

however, fractures might be generated due to changes in pressure and temperature during uplift. Kimberlitic fluids could therefore infiltrate and destroy any evidence of a pre-existing grain boundary fluid.

The rheology of the upper mantle is to a first approximation controlled by the behaviour of olivine. As a result there have been extensive experimental studies on the flow properties of olivine. Comparison of the observed deformational microstructures in peridotite xenoliths with these experimental results allows constraints to be placed on the flow mechanisms operating in the mantle. The analysis of structures and mineral preferred orientations indicates that the flow mechanism in the deformed peridotites is dislocation creep controlled by recovery (Nicolas et al., 1973; Gueguen and Nicolas, 1980). The exception to this is the fluidal mosaic texture which Boullier and Nicolas (1975) ascribed to superplastic flow. In these flow conditions there is a ductility inversion between olivine and orthopyroxene and the deformation is controlled by the orthopyroxene.

Microstructural parameters are related to internal stresses. By assuming that internal and external stresses are almost equal, it is theoretically possible to determine palaeostresses from microstructural investigations. Nicolas (1978) noted that three piezometers were applicable to natural peridotites: dislocation densities, tilt wall spacings and syntectonically recrystallized grain sizes. Piezometry indicates that the deformed peridotites have

experienced minimum stresses of 500 bars, this is substantially more than the 10-100 bars ascribed to asthenospheric flow. Consequently strain rates were probably high and deformation was probably restricted to a narrow zone (Gueguen and Nicolas, 1980). Similarly, Ave Lallemant et al. (1980) noted that the microstructures must be associated with transport processes, since the strain rates were much too high to be representative of the steady-state rheological properties of the mantle.

In addition, the preservation of deformation features, to the degree observed in the Jagersfontein high-temperature deformed xenoliths, indicates that the peridotite was undergoing dynamic recrystallization during rapid flow at the time it was picked up by the magma. Mercier (1979) and Green and Gueguen (1983) have suggested that the peridotite reached the surface after not more than a few days (probably much less) in the magma.

2.3 HAND SPECIMEN DESCRIPTIONS

In their study of peridotite xenoliths from Jagersfontein, Harte and Gurney (1982) reported that the deformed peridotites comprised approximately 15% of the xenolith population >8 cm in diameter and approximately 35% of the xenolith population <8 cm in diameter. The xenoliths used in this study were mostly <8 cm in diameter and showed the characteristic rounding of edges caused by attrition during kimberlite ascent.

Both Johnston (1973) and Harte and Gurney (1982) noted that the deformed peridotites at Jagersfontein had high calculated temperatures of equilibration and that the coarse peridotites had low calculated temperatures of equilibration. As a result only deformed xenoliths were initially selected for analysis. A coarse garnet lherzolite (J117) was subsequently found by Harte (pers. comm.) to have an anomalously high temperature and this xenolith was included in this study. High-temperature coarse peridotites are not, however, a common occurrence at Jagersfontein and are not reported by Johnston (1973) or Harte and Gurney (1982).

Deformed peridotites are easily recognized in hand specimen, although the distinction between porphyroclastic and mosaic-porphyroclastic textures is not always readily apparent. The elongate light coloured orthopyroxene porphyroclasts are the most prominent feature on the weathered surfaces of the deformed peridotites. Large rounded garnets are also prominent in hand specimen. The garnets are commonly purple although some xenoliths contain garnets with an orange hue, similar in appearance to the Cr-poor garnet megacrysts. Clinopyroxene is bright green in hand specimen, but has a slightly darker green hue in those samples containing the orange garnets.

Olivine and orthopyroxene are always the dominant modal minerals in the high-temperature peridotites, with minor amounts of garnet and clinopyroxene. Garnet is present in all the peridotites analyzed. However, four of the

peridotites (JJH 6,9,19 and 29) lack clinopyroxene and are classified as garnet harzburgites.

2.4 PETROGRAPHY

Primary minerals in the deformed peridotites at Jagersfontein include olivine, orthopyroxene, clinopyroxene and garnet. In contrast to the coarse low-temperature peridotites, amphibole, spinel and phlogopite were not found as primary minerals in the deformed peridotites. All the peridotite xenoliths analyzed show evidence of late-stage alteration in the form of serpentine, and most have some phlogopite associated with the kelyphite rims around the garnet porphyroclasts.

Brief descriptions of each of the peridotites analyzed are given in Appendix 1. The following represent general observations which can be made for the primary minerals in the Jagersfontein deformed peridotites.

2.4.1 Olivine

Olivine forms the major component of all the deformed peridotites studied, modal abundances ranging from 55 to 89%. The percentage of olivine in the deformed peridotites which has been recrystallized ranges from approximately 80 to 100 %. Serpentinization is ubiquitous along all grain boundaries and along fractures in the porphyroclasts.

Olivine in the deformed peridotites can be found in one or more of three different morphologies: a) deformed porphyroclasts, b) dynamically recrystallized neoblasts and c) statically recrystallized tablets (Plate 5). The olivine porphyroclasts are commonly severely strained, showing pronounced undulose extinction. In contrast, the neoblasts and tablets are optically strain-free.

Olivine porphyroclasts range in size from 1 to 5 mm. Porphyroclastic peridotites are characterized by less olivine recrystallization and commonly have a wide range in neoblast size. In general the olivine neoblasts range in size from 0.05 to 0.3 mm, but very fine-grained neoblasts are commonly found in the porphyroclastic peridotites. The statically recrystallized tablets represent a minor proportion of the olivine population and were only observed in a few porphyroclastic peridotites.

Plate 5: A deformed garnet lherzolite (JJH 1) displaying three different olivine morphologies: a) deformed porphyroclast, b) neoblasts and c) tablets. Magnification x17

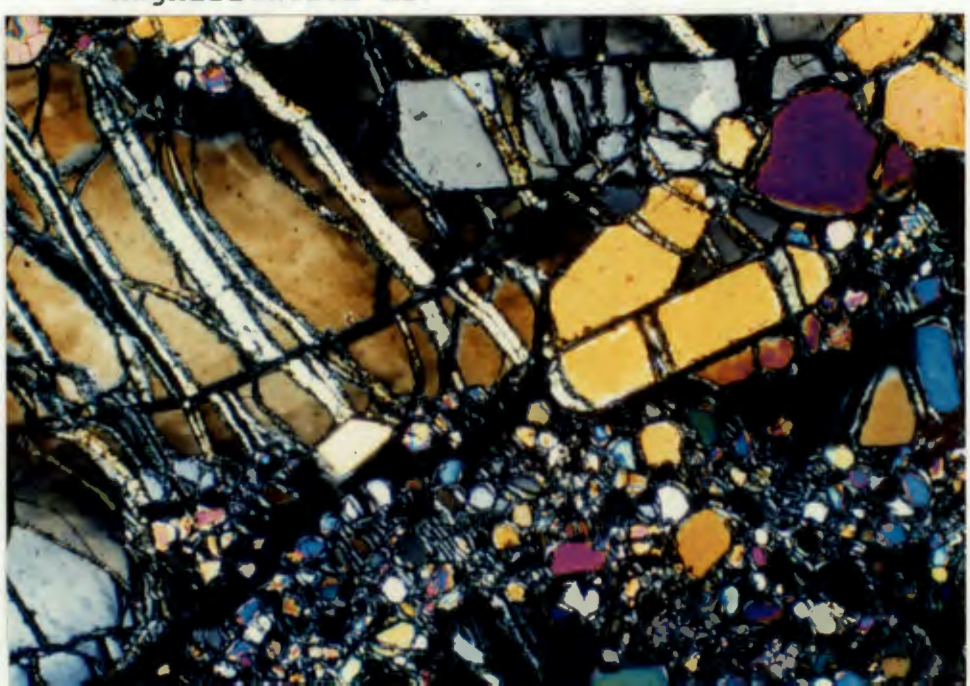

2.4.2 Orthopyroxene

Orthopyroxene is the second most abundant phase in the deformed peridotites, modal abundances ranging from 6 to 28%.

Orthopyroxenes are stronger than olivine and so are generally less extensively deformed. When they deform in nature they do so almost exclusively by slip along the system (100)[001], commonly accompanied by kinking (Carter, 1975).

The orthopyroxene porphyroclasts are anhedral and range in size from 0.5 to 4 mm. They are commonly severely strained and show pronounced undulose extinction. Orthopyroxene porphyroclasts show differing degrees of deformation depending on the texture of the xenolith ie. depending on the amount of olivine recrystallization. In porphyroclastic xenoliths, the orthopyroxene commonly recrystallizes within the original porphyroclast grain boundaries (Plate 6), whereas in the mosaic-porphyroclastic xenoliths the recrystallized orthopyroxene neoblasts are commonly strung-out, resulting in a fluidal texture.

Orthopyroxene neoblasts are smaller than olivine neoblasts and range in size from 0.01 to 0.1 mm. As a result there is a sharp contrast between orthopyroxene porphyroclast and neoblast grain size.

Rounded inclusions of olivine are occasionally found in the orthopyroxene porphyroclasts. These inclusions are in equilibrium contact with the orthopyroxene and do not appear to be related to fractures.

Plate 6: A deformed garnet lherzolite (JJH 26) showing recrystallization of an orthopyroxene porphyroclast within the original grain boundary.
Magnification x38

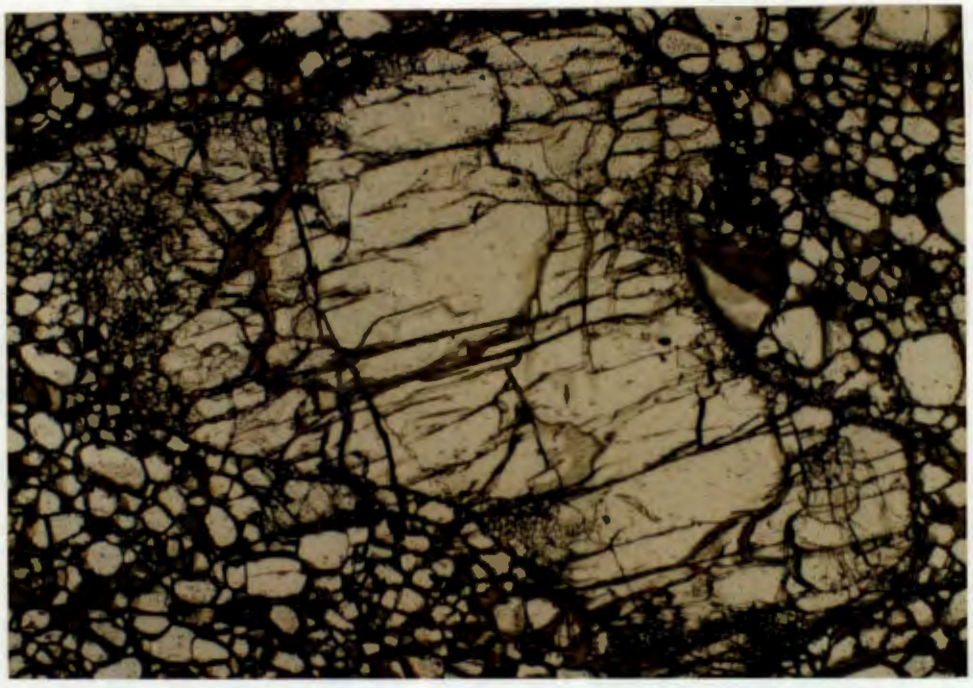

2.4.3 Garnet

Modal abundances of garnet porphyroclasts range from 0 to 22%. The garnets do not show any recrystallization features, but are commonly fractured. Garnet porphyroclasts range in shape from rounded to almost oval. They become elongate parallel to the foliation defined by the orthopyroxene porphyroclasts and neoblasts, the decreasing sphericity probably indicating increasing strain.

The garnet porphyroclasts are almost always surrounded by a kelyphitic rim, which in turn is often rimmed by phlogopite laths. The kelyphite rim, a secondary alteration product, varies in thickness and at extreme alteration can replace the entire garnet. Fractures are commonly filled with a kelyphitic alteration product as well. Kelyphite rims are optically irresolvable adjacent to the garnet, but occasionally coarsen into an optically resolvable assemblage of Al-rich spinel, aluminous clinopyroxene and aluminous orthopyroxene. The kelyphite may originate at depth in the mantle (Schandl and Clarke, 1982) or might be associated with ascent of the peridotite in the kimberlite.

Apart from the olivine porphyroclasts in some of the porphyroclastic xenoliths, the garnet is usually the mineral with the largest grain size. The garnet porphyroclasts range in size from 0.5 to 6 mm, many of the deformed peridotites having garnet porphyroclasts which are larger than those in the coarse xenolith J117. No correlation between garnet size and the degree of deformation was noted.

Rounded inclusions of olivine and occasionally clinopyroxene were found in some of the garnet porphyroclasts. As with the olivine inclusions in the orthopyroxene porphyroclasts, these inclusions were in equilibrium contact with the garnet and did not appear to be related to fracture.

A notable feature of the garnet in some of the xenoliths is the presence of polymineralic inclusions (Plate 7). The minerals in these inclusions include phlogopite, amphibole, aluminous clinopyroxene, aluminous orthopyroxene and aluminous spinel. Hunter and Taylor (1982) noted similar minerals as well as glass in garnets in peridotites from a kimberlite in Fayette County, Pennsylvania and interpreted them as products of incongruent melting of garnet. Similar inclusions have also been found in garnet and clinopyroxene megacrysts by Schulze (1985) and were interpreted as representing the high-pressure liquids from which the megacrysts crystallized. All the polymineralic inclusions observed in the Jagersfontein peridotites are, however, connected by fractures to the edge of the garnet porphyroclasts and have been affected by alteration. It is therefore difficult to determine whether these might have been primary inclusions or whether they are entirely the result of secondary processes.

Plate 7: A deformed garnet lherzolite (JJH 17) showing polymineralic inclusions in a garnet porphyroclast. Magnification x38

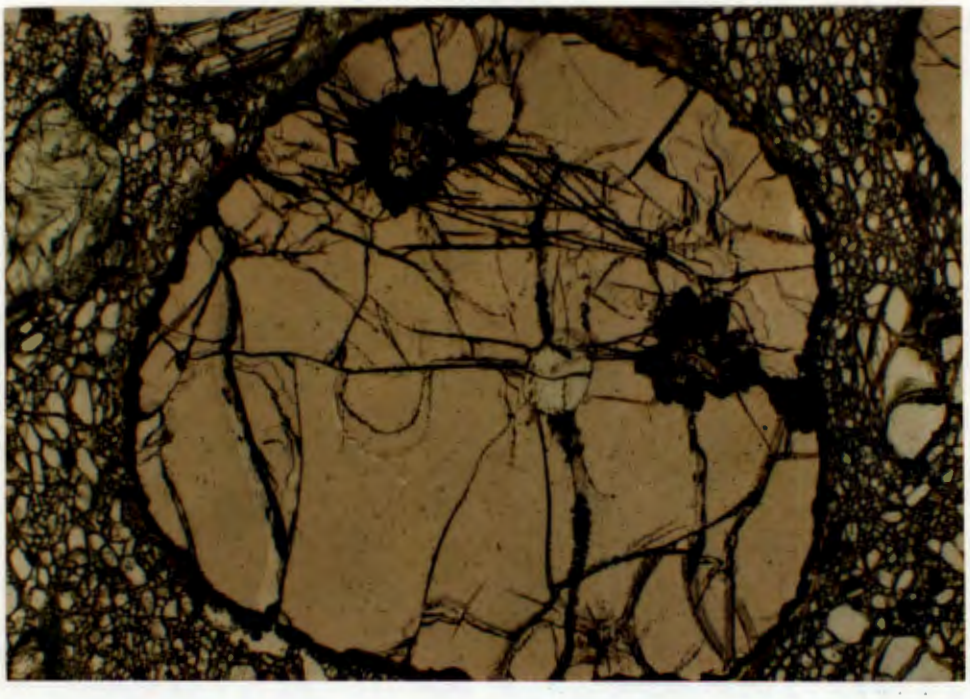

2.4.4 Clinopyroxene

Modal abundances of the clinopyroxene porphyroclasts range from 0 to 16%. Clinopyroxene porphyroclasts are almost always smaller than orthopyroxene porphyroclasts and range in size from 1 to 3 mm.

The clinopyroxene porphyroclasts commonly show little or no internal strain or recrystallization, but commonly have `spongy' borders (Plate 8). Carswell (1975) and Ehrenberg (1979) have attributed these `spongy' borders to a decompression reaction during kimberlite eruption.

Plate 8: A deformed garnet lherzolite (JJG 1713) showing `spongy' borders to the clinopyroxene porphyroclasts. Magnification x17

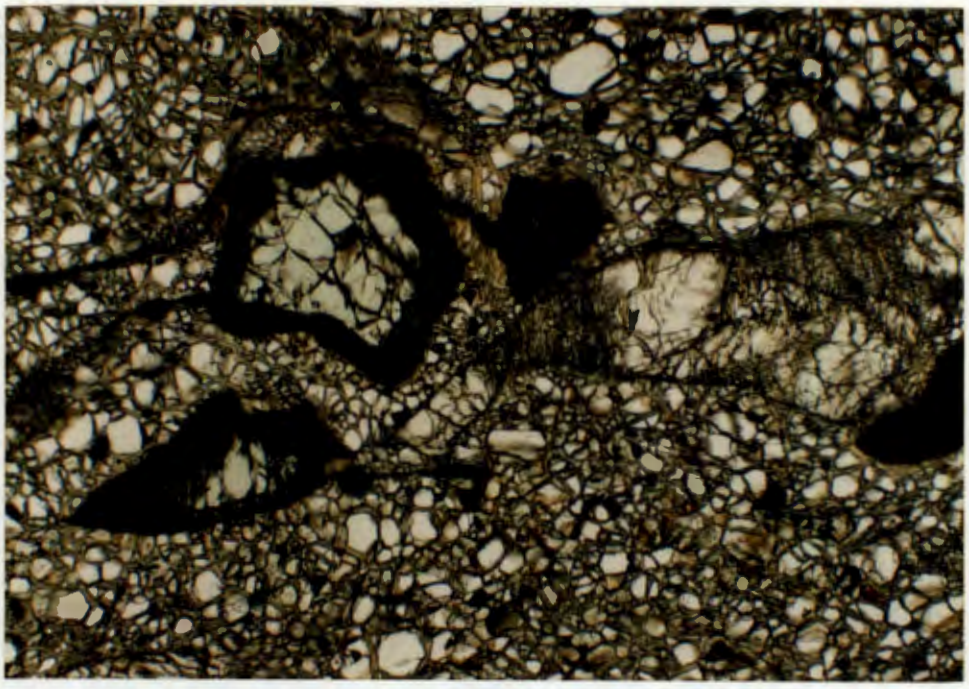

2.5 MINERAL COMPOSITIONS

The major element mineral compositions of the primary minerals in 35 deformed peridotites and 1 coarse peridotite have been determined. A polished section was made for each of the peridotites and analyses were performed using a Cameca/Camebax electron microprobe. Analytical conditions are listed in Appendix 2 and average mineral compositions for each peridotite are presented in Appendix 3.

The high-temperature deformed peridotites are generally considered `fertile' in comparison to the `depleted' low-temperature peridotites, where the terms `fertile' and `depleted' indicate the abundance of basaltic components, in particular CaO, Al_2O_3, FeO, TiO_2 and Na_2O.

Minerals in the deformed peridotite xenoliths are usually homogeneous, but compositional zoning has been noted in the garnet porphyroclasts of several of the xenoliths. Similarly, although most deformed peridotites have been shown to have similar neoblast and porphyroclast compositions, some of the xenoliths had orthopyroxene which differed in composition between porphyroclasts and neoblasts. These compositional differences may provide important constraints for modelling the nature and timing of events preceeding and associated with kimberlite eruption and will be discussed further in sections 2.6 and 6.1.4.

On the basis of mineral compositions, the high-temperature coarse xenolith (J117) is indistinguishable from the

deformed xenoliths so that, unless specifically referred to, deformed peridotite mineral compositions include those of J117.

2.5.1 Olivine

Olivine porphyroclasts in the deformed peridotites have 100(Mg/(Mg+Fe)) ratios (Mg#'s) which range from 89 to 92.5. Olivine porphyroclasts in the high-temperature coarse peridotite (J117) have a Mg# of 89, in comparison to Mg#'s of 91 to 93 observed in low-temperature coarse peridotites from Jagersfontein (Harte, 1983).

Harte (1983) suggested division of peridotite xenoliths into Fe-rich (Mg# < 91) and Mg-rich (Mg# > 91) varieties on the basis of whole-rock Mg#'s. Harte (op cit.) noted that olivine Mg#'s corresponded closely with whole-rock Mg#'s. On the basis of this classification the deformed peridotites from Jagersfontein would include both Fe- and Mg-rich xenoliths. No correlation between Mg# and the modal abundance of olivine was noted (Fig. 2.1).

The CaO concentration in the olivine porphyroclasts varies from 0.05 to 0.10 wt% and there appears to be a slight trend of increasing CaO with decreasing Mg# (Fig. 2.2). The Cr_2O_3 concentration varies from below detection limit (0.03 wt%) to 0.07 wt% (Fig. 2.3), while TiO_2 and Al_2O_3 are generally below detection limit (0.03 wt%). In a more detailed study (at ppm levels), Hervig et al. (1986) noted that high-temperature olivines had approximately 3-6 times the

abundances of Ti, Al, Ca and Na than low-temperature olivines.

The NiO concentration in the olivines varies from 0.28 to 0.41 wt% (Fig. 2.4), within the range for upper mantle olivine.

Olivine porphyroclasts in the deformed garnet harzburgites and garnet lherzolites are compositionally indistinguishable. No zoning was noted in the olivine porphyroclasts or neoblasts, and no differences between neoblast, tablet or porphyroclast compositions were noted.

FIGURE 2.1 Variation in modal % olivine with olivine Mg# in garnet lherzolites and garnet harzburgites from Jagersfontein

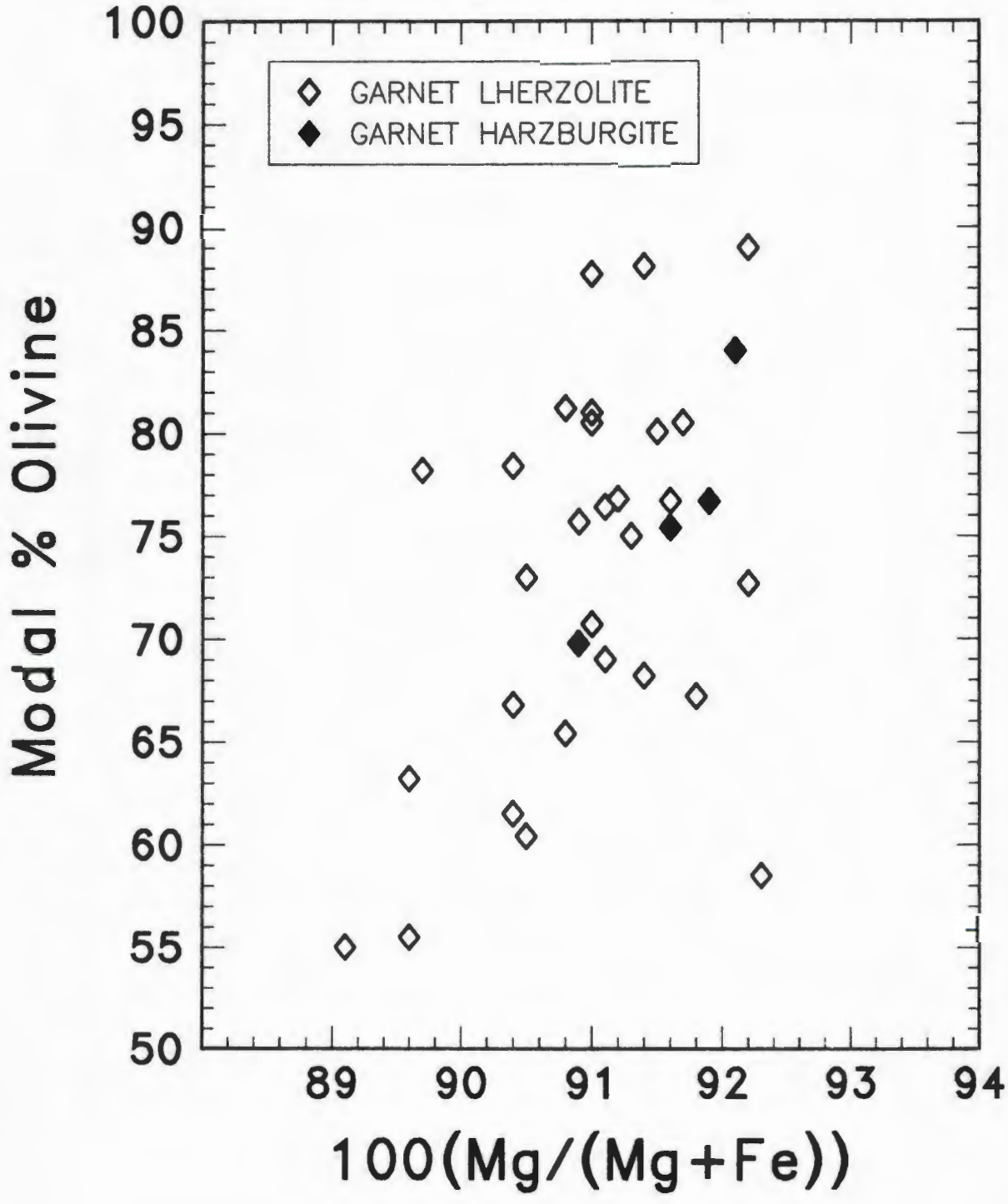

FIGURE 2.2 CaO wt% versus Mg# in olivine porphyroclasts from garnet lherzolites and garnet harzburgites

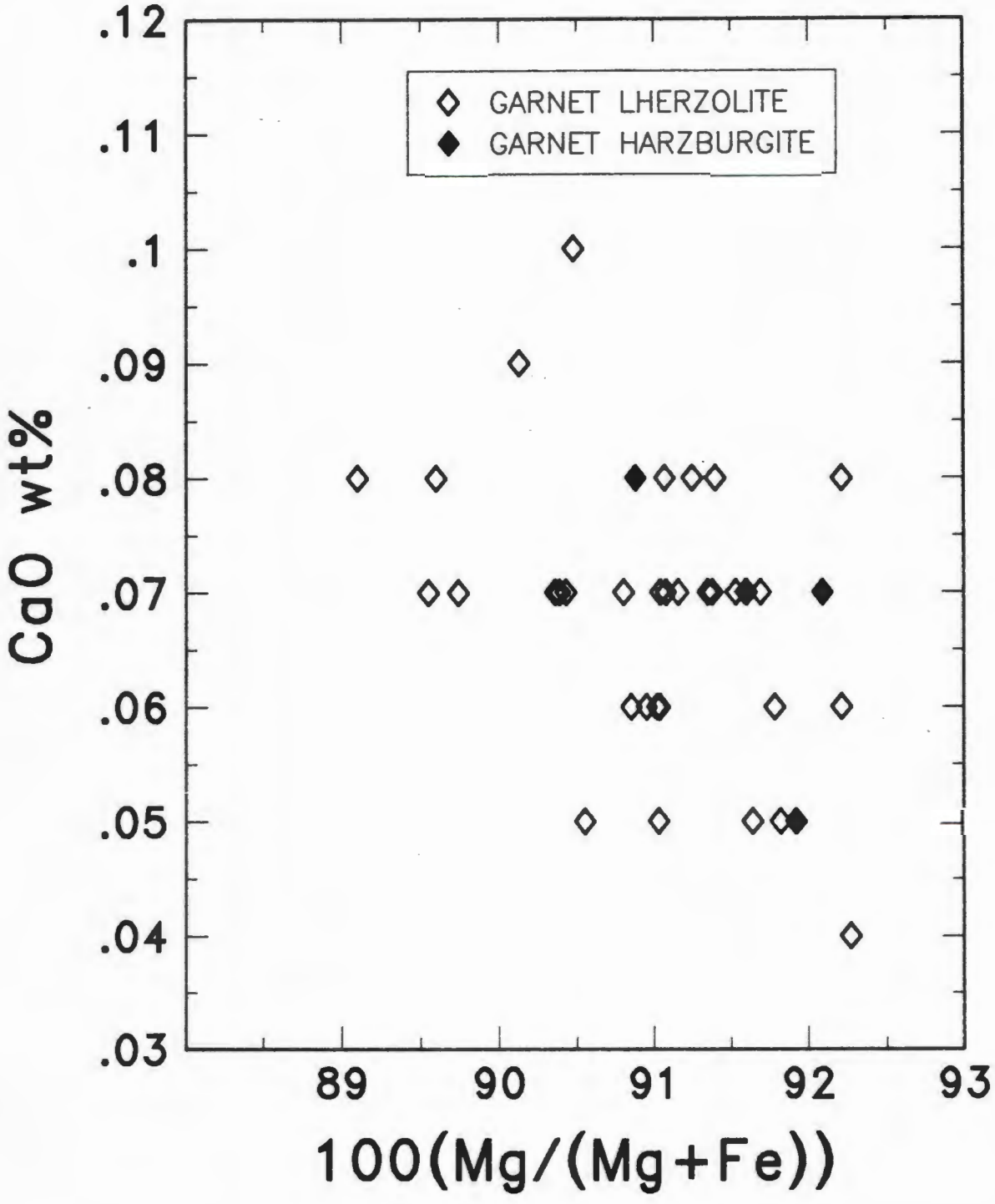

FIGURE 2.3 Cr_2O_3 wt% versus Mg# in olivine porphyroclasts from garnet lherzolites and garnet harzburgites

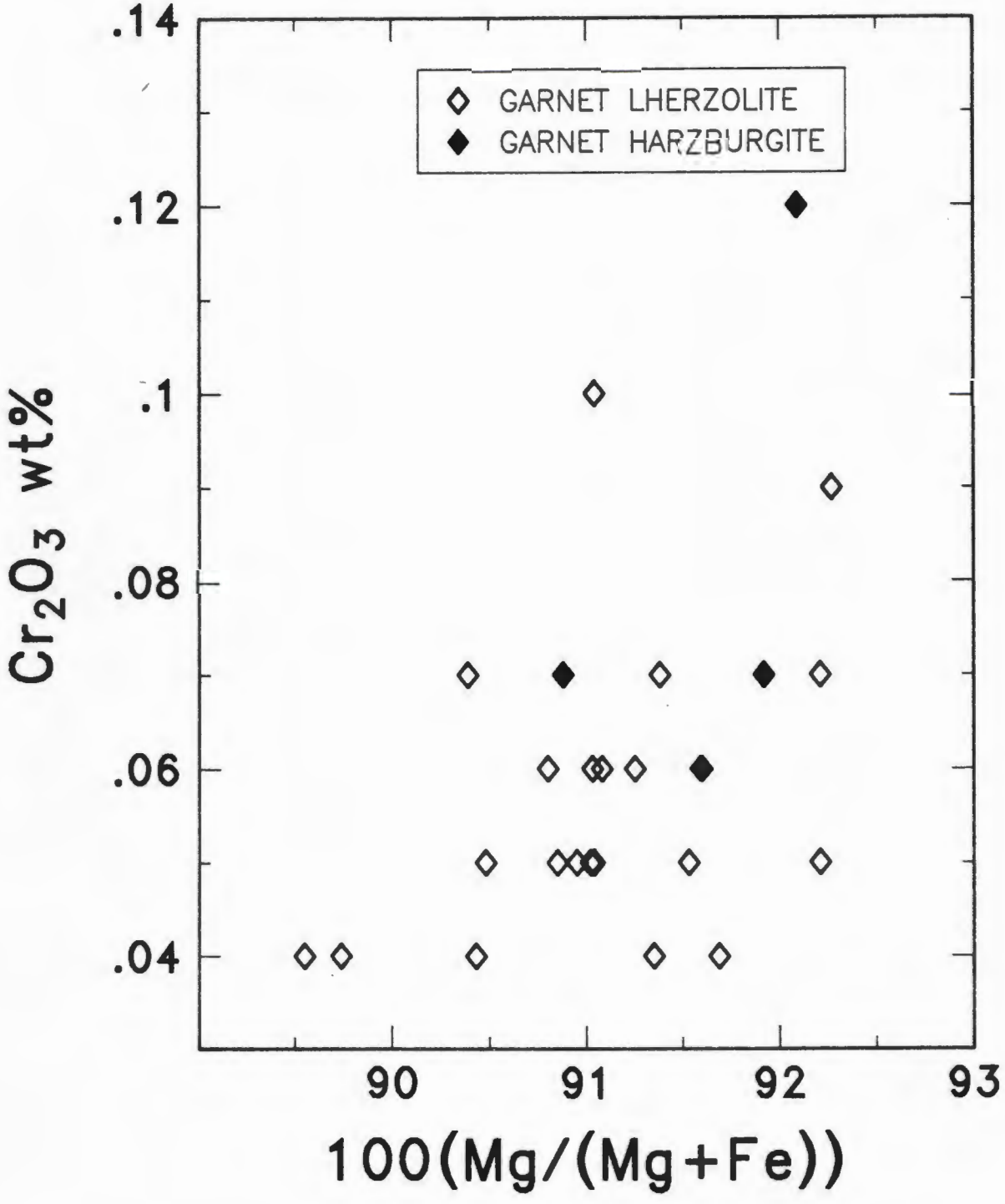

FIGURE 2.4 NiO wt% versus Mg# in olivine porphyroclasts from garnet lherzolites and garnet harzburgites

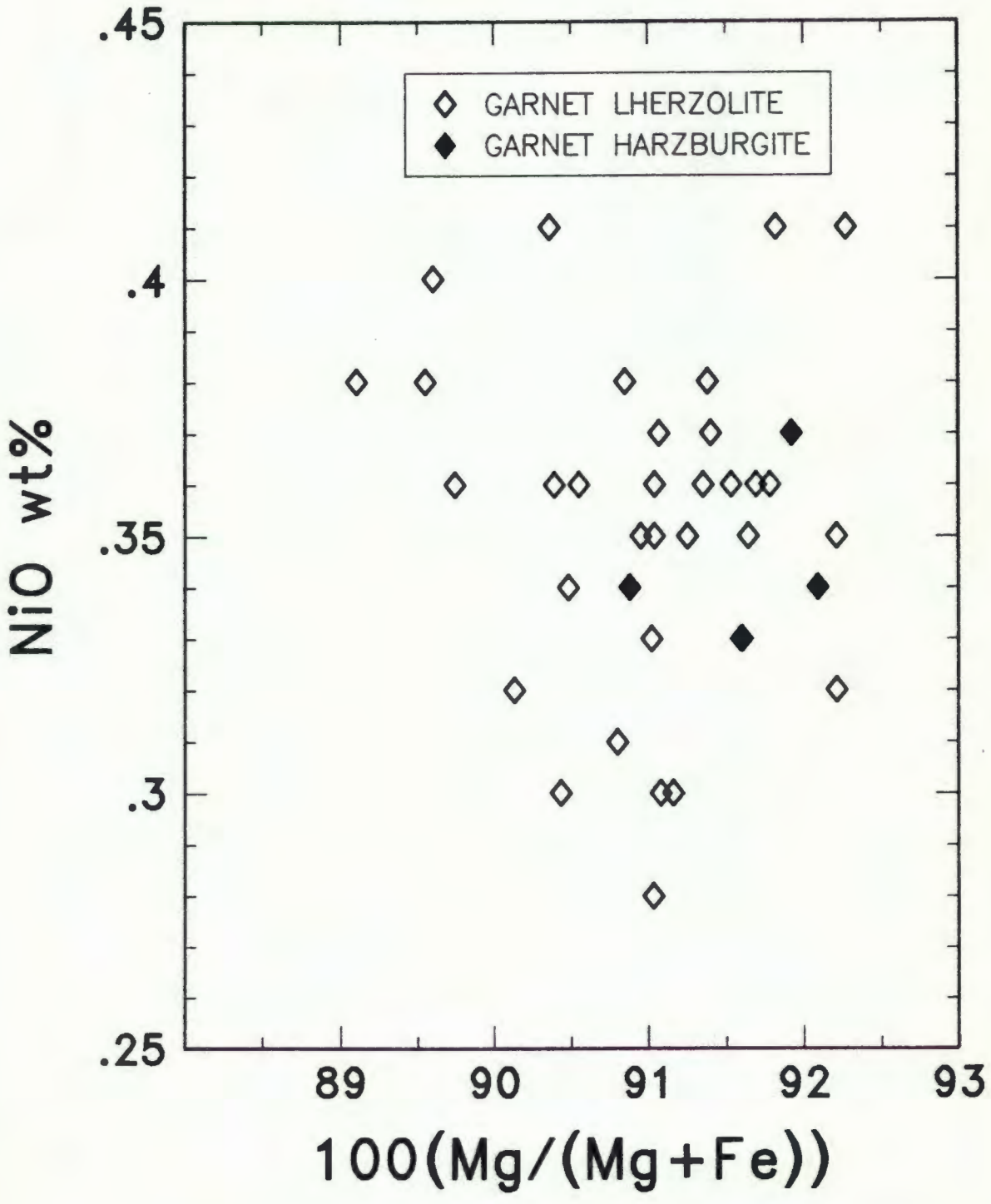

2.5.2 Orthopyroxene

Orthopyroxene porphyroclasts in the deformed peridotites have Mg#'s ranging from 90.5 to 93.5, and 100(Ca/(Ca+Mg)) ratios (Ca#'s) ranging from 1.5 to 2.4 (Fig. 2.5).

The orthopyroxene porphyroclasts show a trend of increasing Al_2O_3 (0.7 to 1.2 wt%) with increasing Ca#'s (Fig. 2.6). The orthopyroxenes from two of the deformed garnet harzburgites, however, have lower Al_2O_3 concentrations (0.54 and 0.59 wt%). The Na_2O concentrations (0.07 to 0.42 wt%) increase with increasing TiO_2 (n.d. to 0.24 wt%) and with increasing Al_2O_3 (0.5 to 1.1 wt%) (Fig. 2.7 and 2.8).

No zoning was noted in the orthopyroxene porphyroclasts and in most instances the porphyroclast and neoblast compositions are indistinguishable. Some of the neoblasts had higher Al_2O_3, CaO and Cr_2O_3 concentrations than the porphyroclasts. This is possibly due to their crystallization at lower pressures during kimberlite ascent.

FIGURE 2.5 Mg# versus Ca# in orthopyroxene porphyroclasts from garnet lherzolites and garnet harzburgites

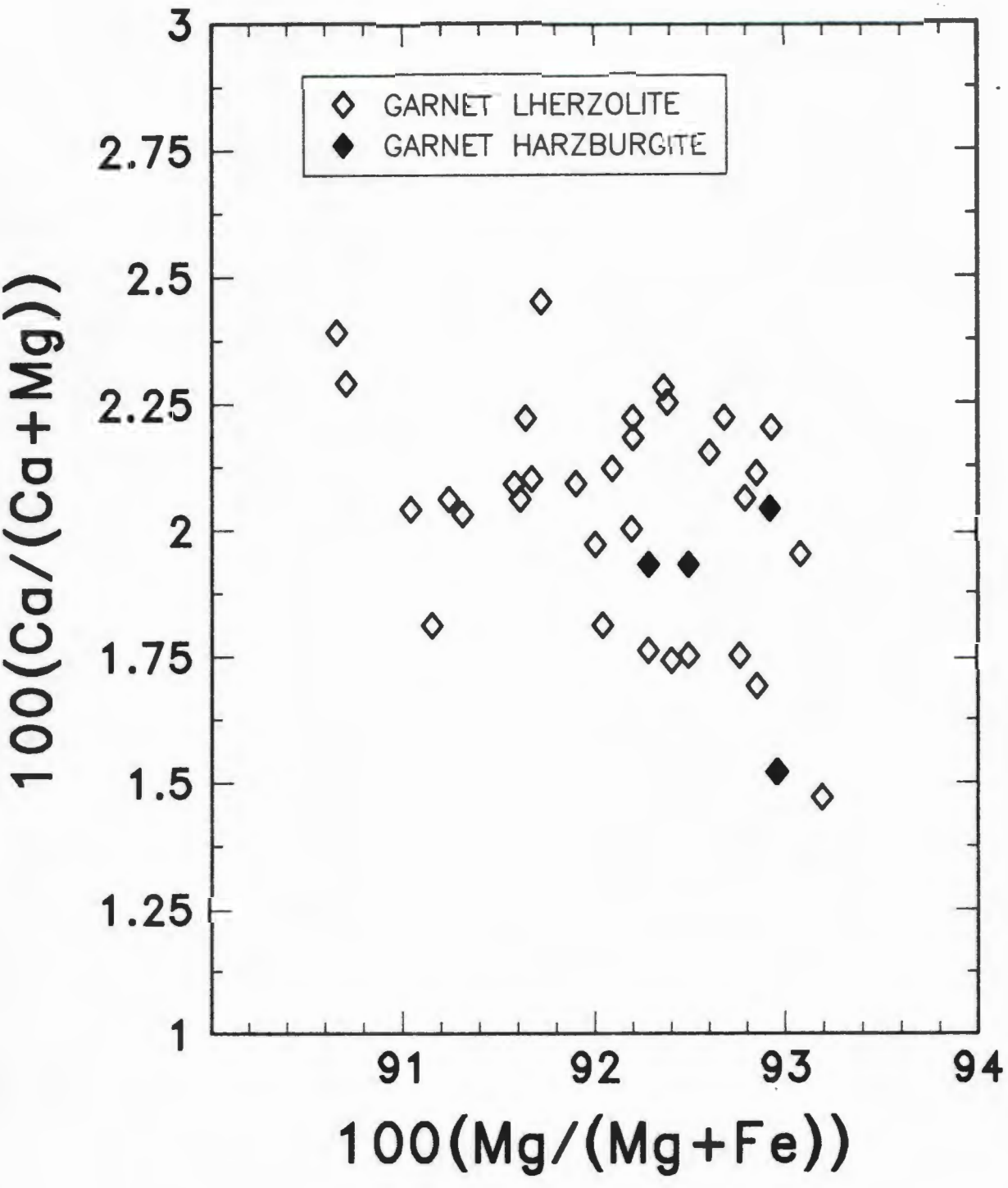

FIGURE 2.6 Ca# versus Al_2O_3 wt% in orthopyroxene porphyroclasts from garnet lherzolites and garnet harzburgites

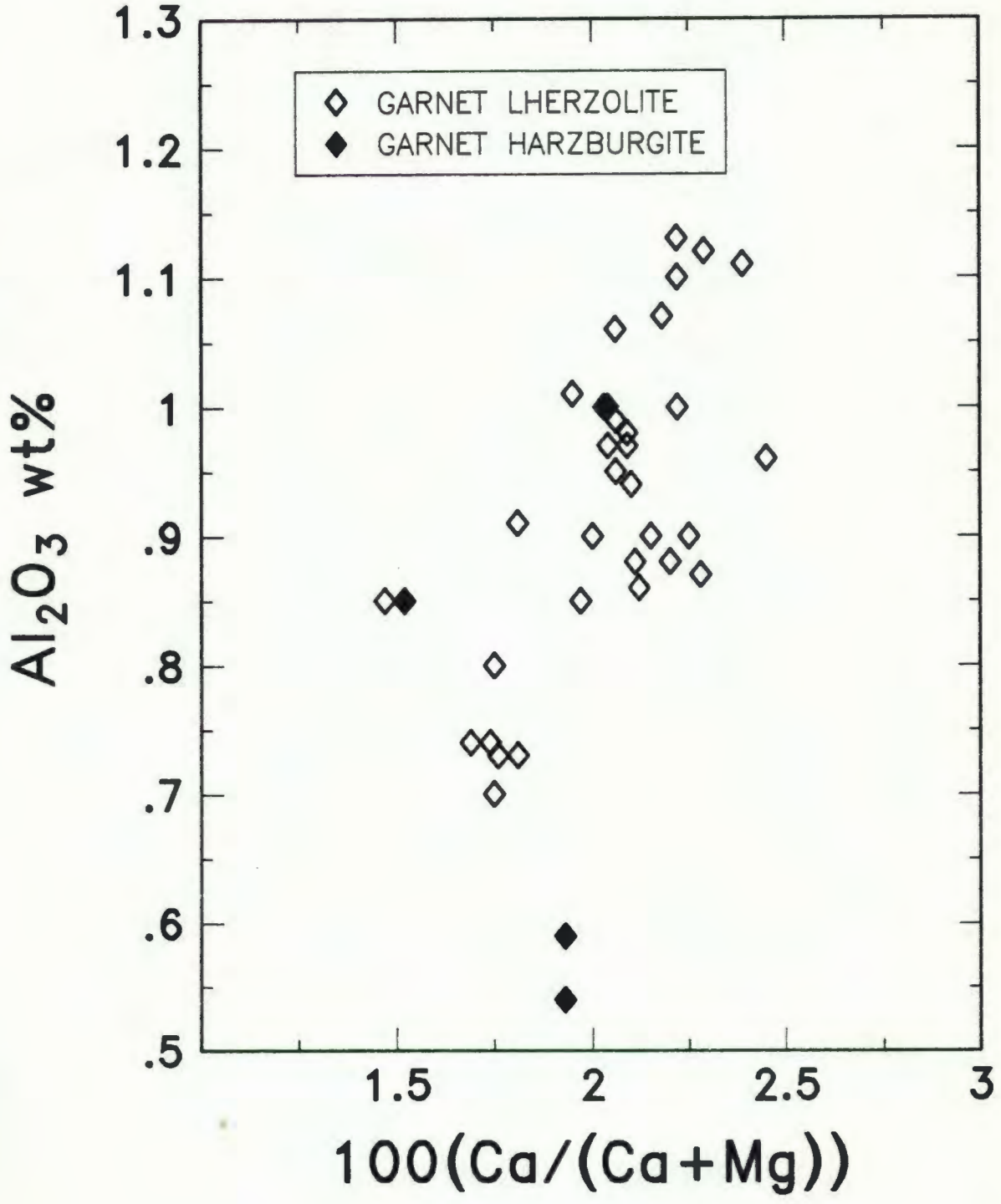

FIGURE 2.7 Na_2O wt% versus TiO_2 wt% in orthopyroxene porphyroclasts from garnet lherzolites and garnet harzburgites

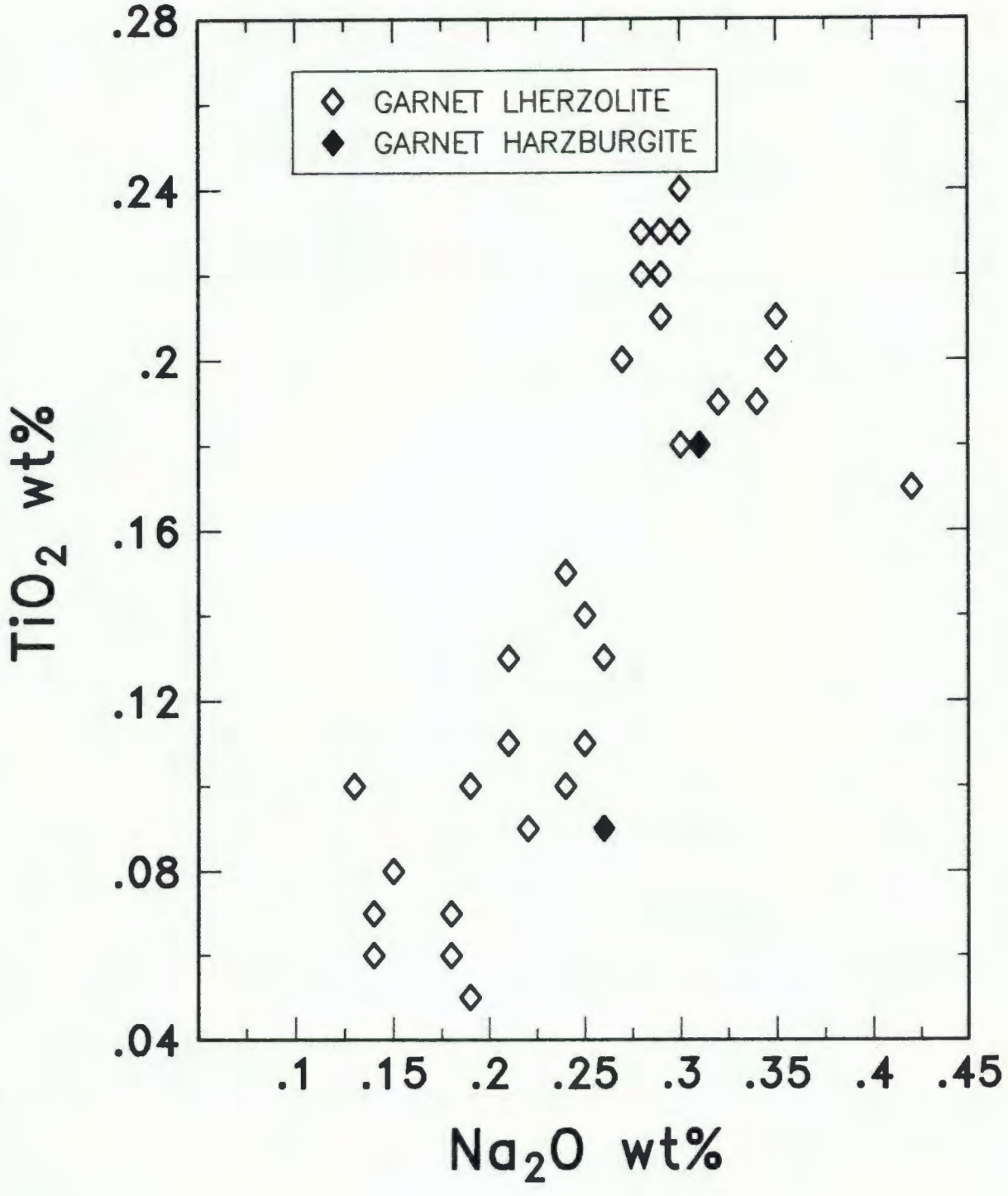

FIGURE 2.8 Na_2O wt% versus Al_2O_3 wt% in orthopyroxene porphyroclasts from garnet lherzolites and garnet harzburgites

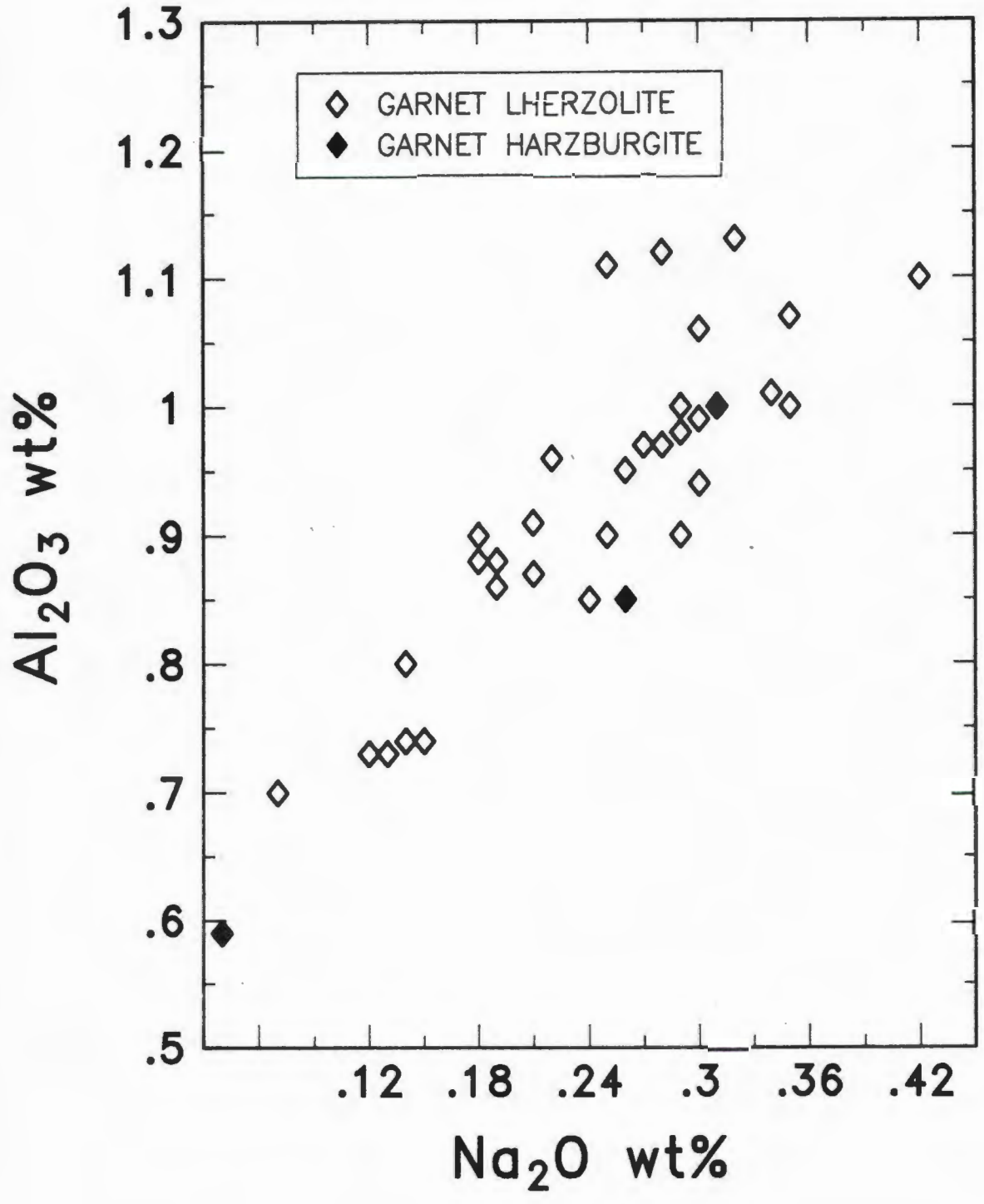

2.5.3 Garnet

The garnet porphyroclasts are pyrope-rich with Mg#'s of 81 to 86.

The CaO concentrations (4.2 to 8.4 wt%) increase with increasing Cr_2O_3 (1.6 to 11 wt%) (Fig. 2.9). This positive correlation between CaO and Cr_2O_3 contents is characteristic of the lherzolitic assemblage (Sobolev et al., 1973). The garnet porphyroclasts from two garnet harzbugites (JJH 6, JJH 9) are Cr- and Ca-rich compared to the lherzolite garnets, but still fall on the lherzolitic trend suggesting that they might have equilibrated in the presence of clinopyroxene. Only one of the garnet harzburgites (JJH 29) has a composition to the left of this trend.

The TiO_2 concentrations (n.d. to 1.1 wt%) increase with increasing Na_2O (n.d. to 0.13 wt%) (Fig. 2.10). These high Na_2O concentrations in the garnets are indicative of high pressures and temperatures.

Compositional zoning was noted in some of the garnet porphyroclasts. In these porphyroclasts the rims were enriched in TiO_2 and Na_2O relative to the cores (Fig. 2.11). Increases of up to .7 wt% TiO_2 and .05 wt% Na_2O were noted in some porphyroclasts. This zonation is most likely due to interaction between the garnet and a percolating melt. Takahashi (1986) noted a distribution coefficient (garnet/melt) of .65 at 50 kbar, this would require a melt containing 1.7 wt% TiO_2 to be in equilibrium with garnet

containing 1.1 wt% TiO_2. Possible sources of this melt will be discussed further in Section 6.1.4.

Rim enrichments in FeO and depletions in Cr_2O_3 were also noted, but these were not as systematic. The CaO and MgO concentrations occasionally showed differences in excess of analytical precision, but were not associated with the zonation. This zonation does not appear to be related to kelyphitic alteration as no zonation has been found associated with the kelyphite filling fractures crosscutting the porphyroclasts.

FIGURE 2.9 CaO wt% versus Cr_2O_3 wt% in garnet porphyroclasts from garnet lherzolites and garnet harzburgites

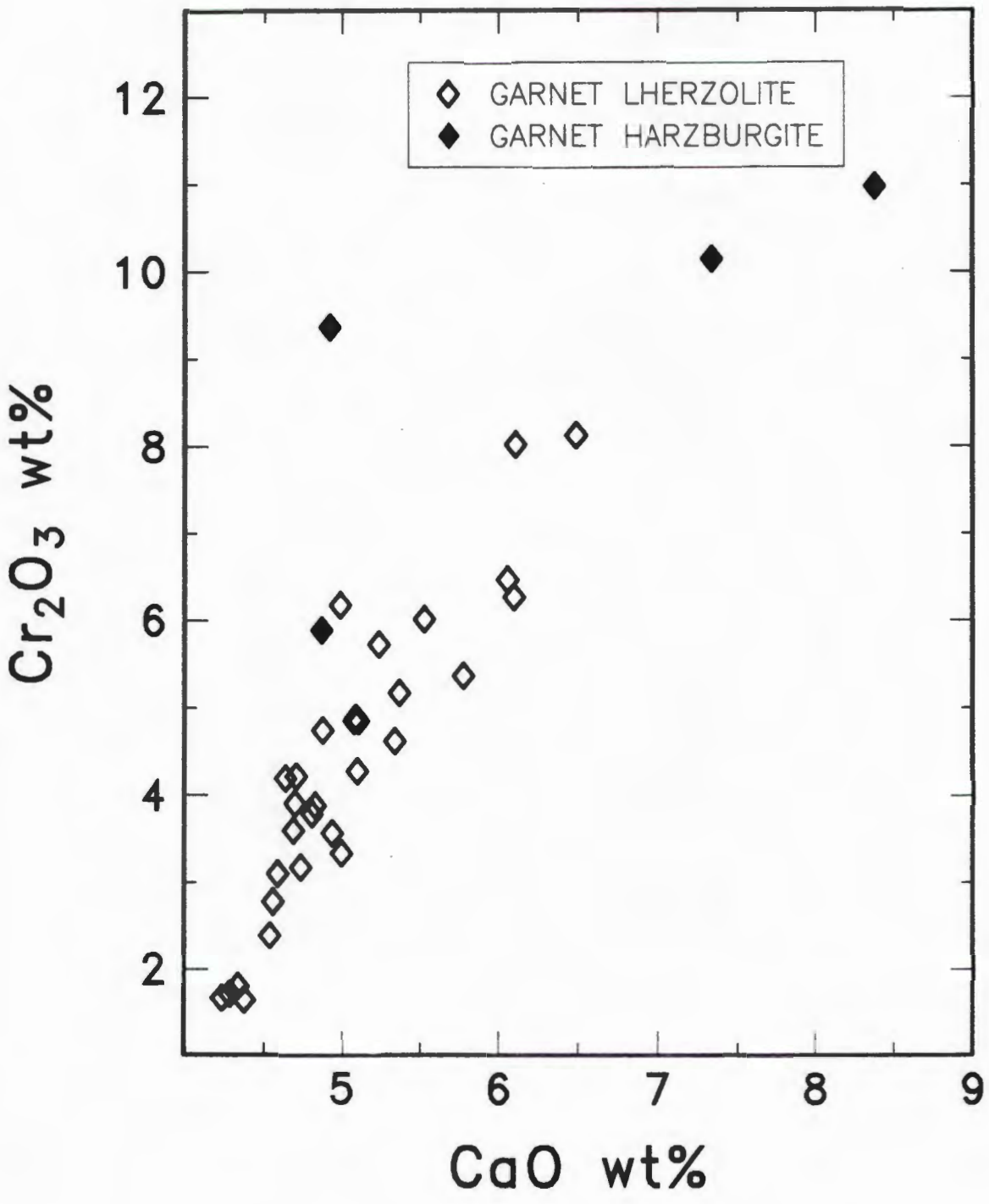

FIGURE 2.10 TiO_2 wt% versus Na_2O wt% in garnet porphyroclasts from garnet lherzolites and garnet harzburgites

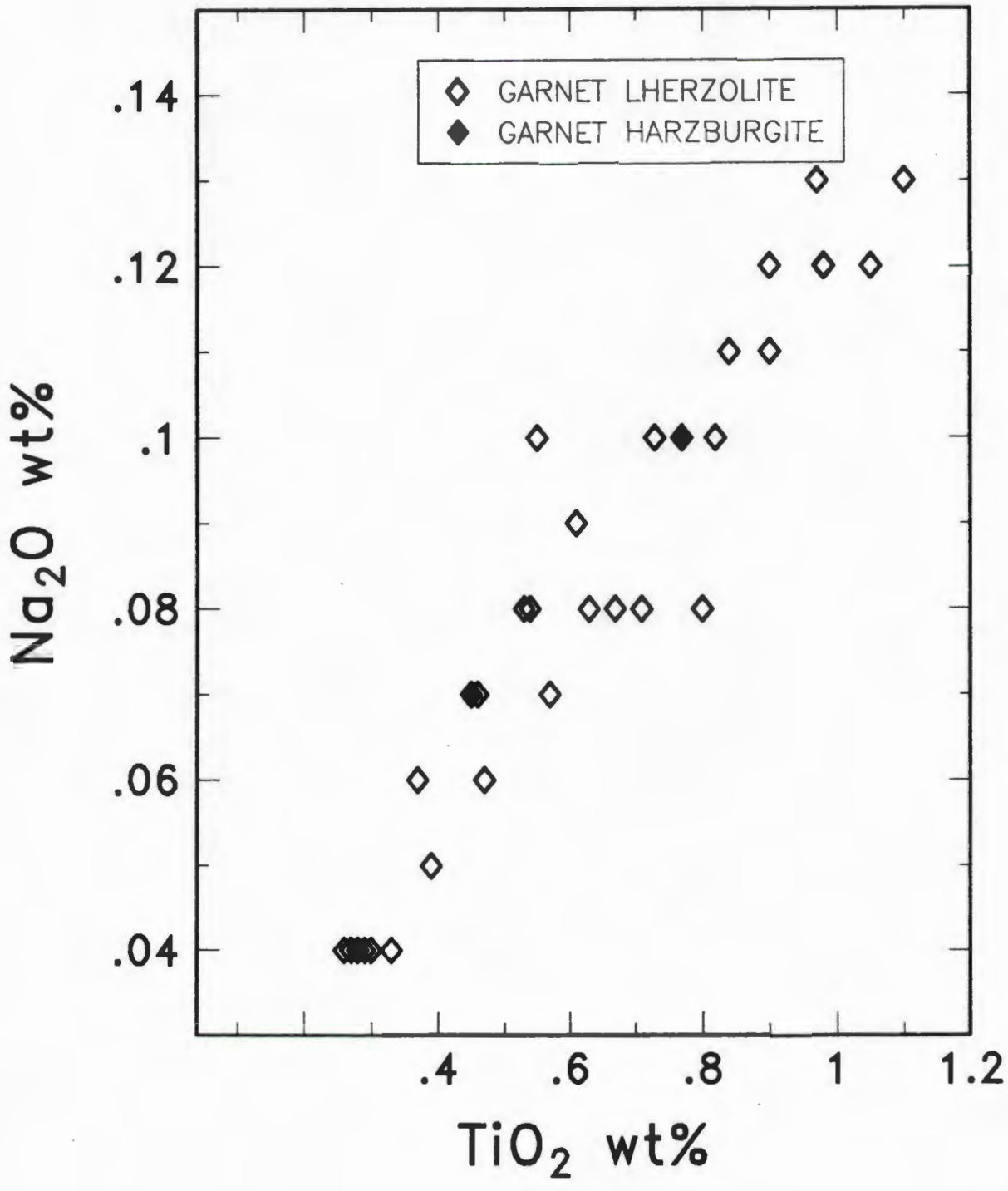

FIGURE 2.11 Zonation in TiO_2 and Na_2O in garnet porphyroclasts from Jagersfontein

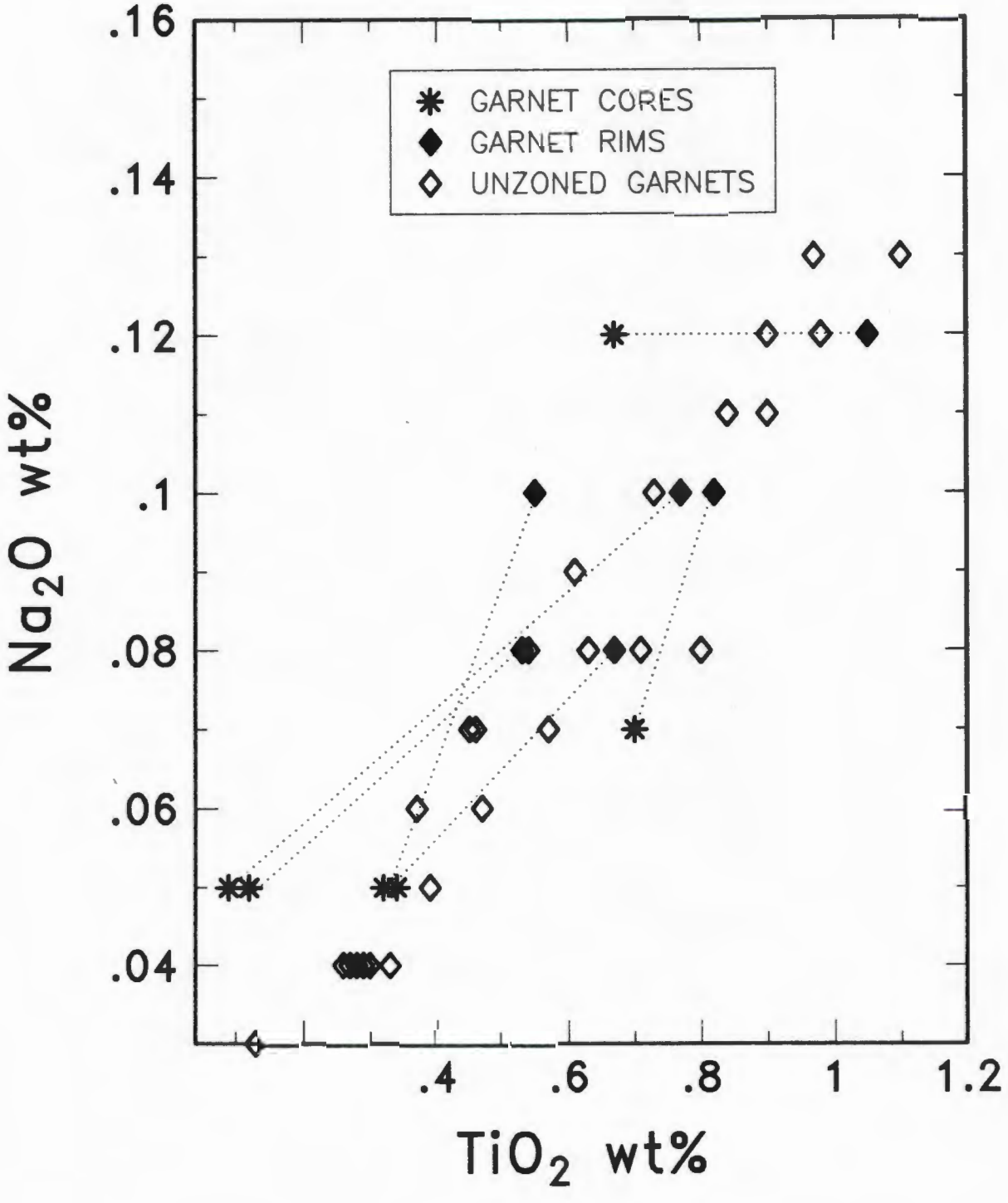

2.5.4 Clinopyroxene

The clinopyroxene porphyroclasts have Ca#'s ranging from 36 to 43. These are considerably lower than those for the coarse low-temperature peridotites from Jagersfontein (49 to 51) (Harte, 1983), reflecting their higher temperatures of equilibration. Clinopyroxene porphyroclasts in deformed peridotites from Thaba Putsoa have lower Ca#'s (29 to 36) reflecting even higher temperatures of equilibration (Boyd and Nixon, 1975). No correlation between Ca# and Mg# (88.5 to 92.5) was noted (Fig. 2.12).

The TiO_2 (n.d. to 0.52 wt%), Na_2O (0.68 to 2.7 wt%) and Al_2O_3 (1.0 to 3.1 wt%) concentrations of the clinopyroxene porphyroclasts all increase with decreasing Ca#'s (increasing temperature) (Fig. 2.13 to 2.15). The Na_2O concentrations increase regularly with increasing Al_2O_3, reflecting an increase in jadeite content. The TiO_2 concentrations increase with increasing Na_2O (Fig. 2.16) as was observed in the garnet porphyroclasts.

No zoning was observed in the clinopyroxene porphyroclasts except in those clinopyroxenes which had 'spongy' borders. The 'spongy' borders to some of the clinopyroxene porphyroclasts are inhomogeneous and have lower Al_2O_3 and Na_2O and higher CaO contents than the cores. As noted in section 2.4.4 these are thought to be related to decompression and Ehrenberg (1982a) suggested that the kelyphite rims might provide the sink for the Al_2O_3 and Na_2O.

One of the deformed peridotites (JJH 34) was found to have a clinopyroxene inclusion in a garnet porphyroclast. This inclusion clinopyroxene had lower Na_2O, TiO_2 and FeO and higher CaO concentrations than the clinopyroxene porphyroclasts in the same xenolith. Lower diffusion rates in the garnet (Smith and Wilson, 1985) have shielded the inclusion from the effects of enrichment. This clinopyroxene inclusion provides important evidence of the original pre-enrichment composition of this xenolith, indicating a relatively depleted composition and a lower temperature of equilibration.

FIGURE 2.12 Ca# versus Mg# in clinopyroxene porphyroclasts from garnet lherzolites

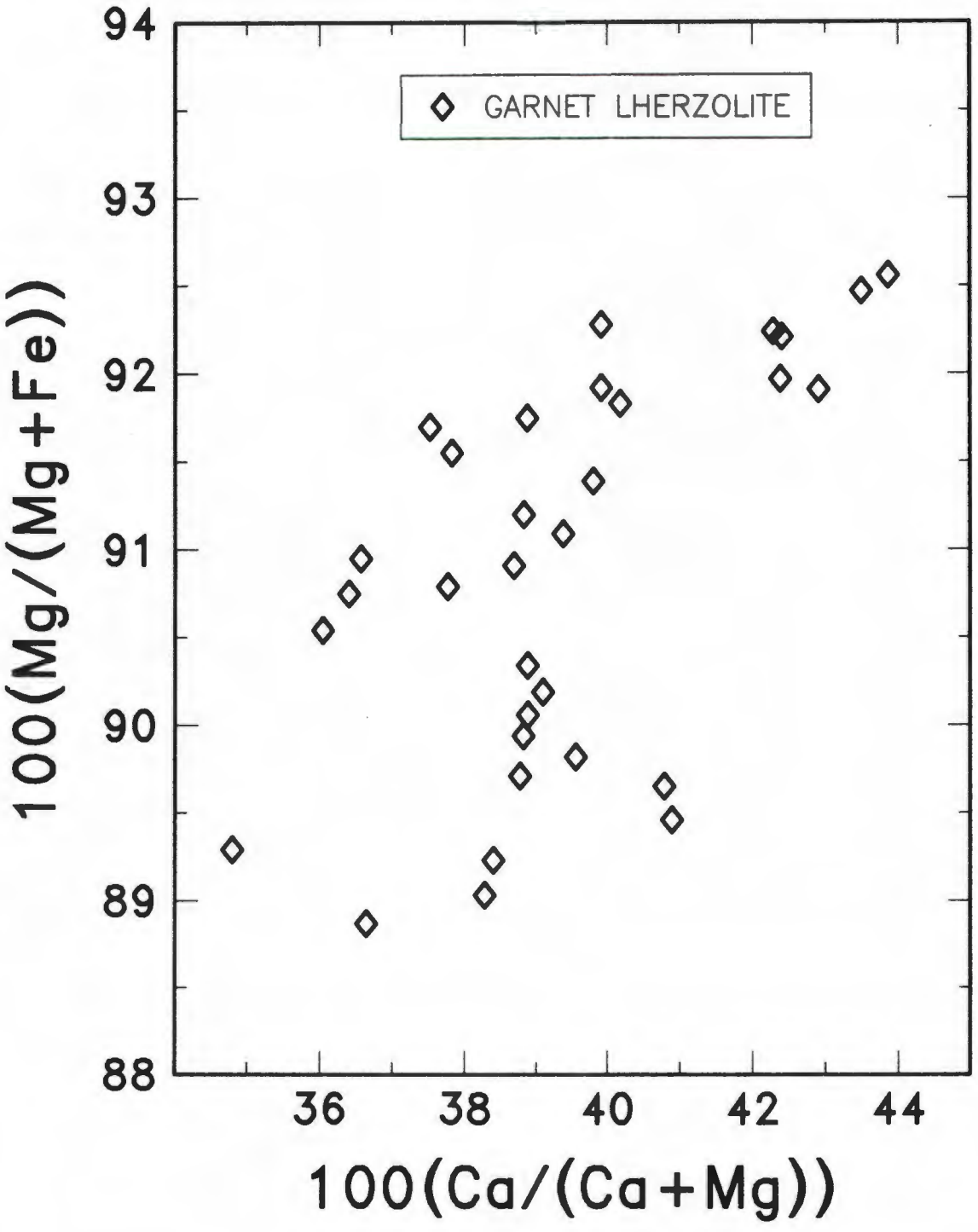

FIGURE 2.13 Ca# versus TiO_2 wt% in clinopyroxene porphyroclasts from garnet lherzolites

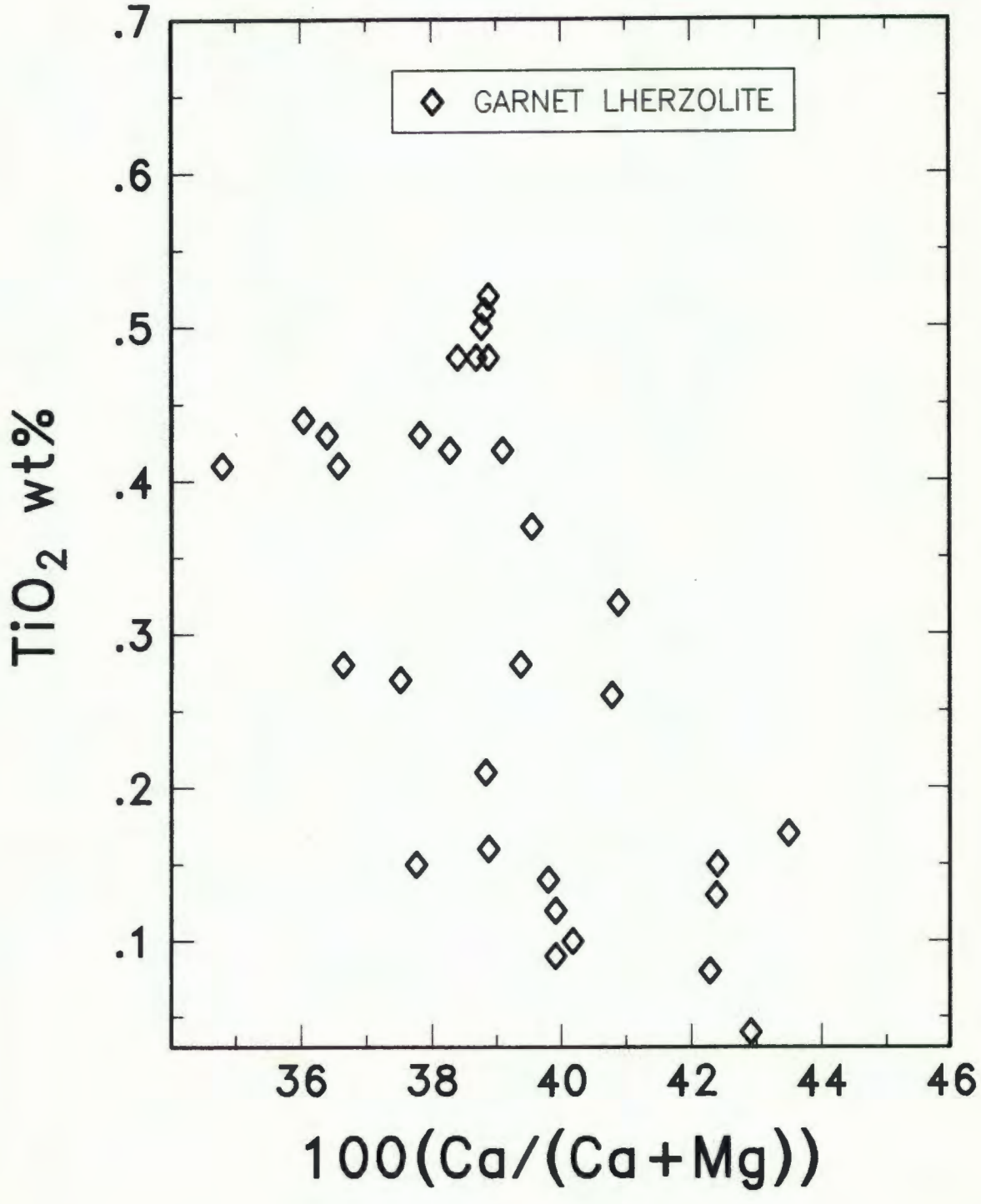

FIGURE 2.14 Ca# versus Na_2O wt% in clinopyroxene porphyroclasts from garnet lherzolites

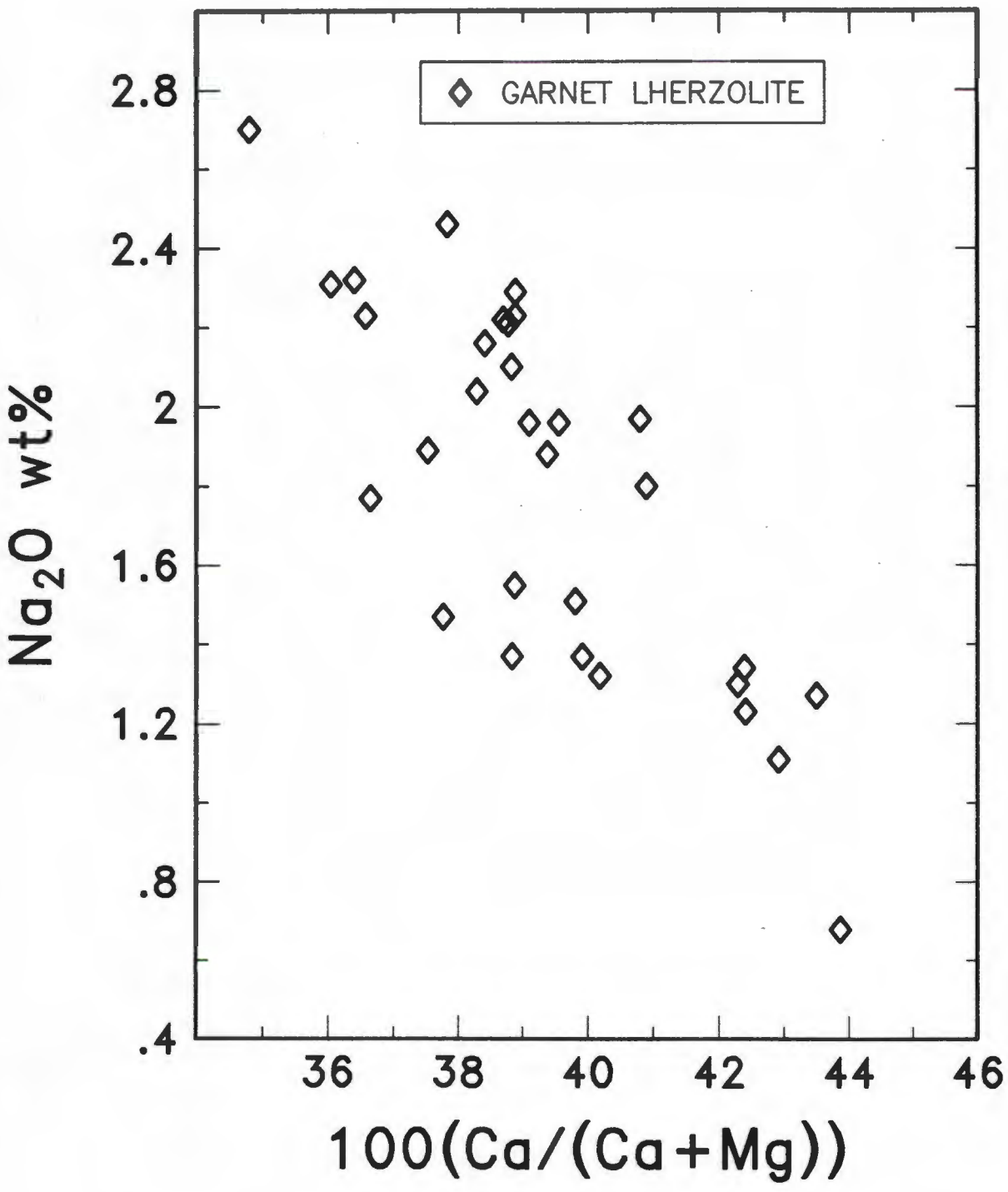

FIGURE 2.15 Ca# versus Al_2O_3 wt% in clinopyroxene porphyroclasts from garnet lherzolites

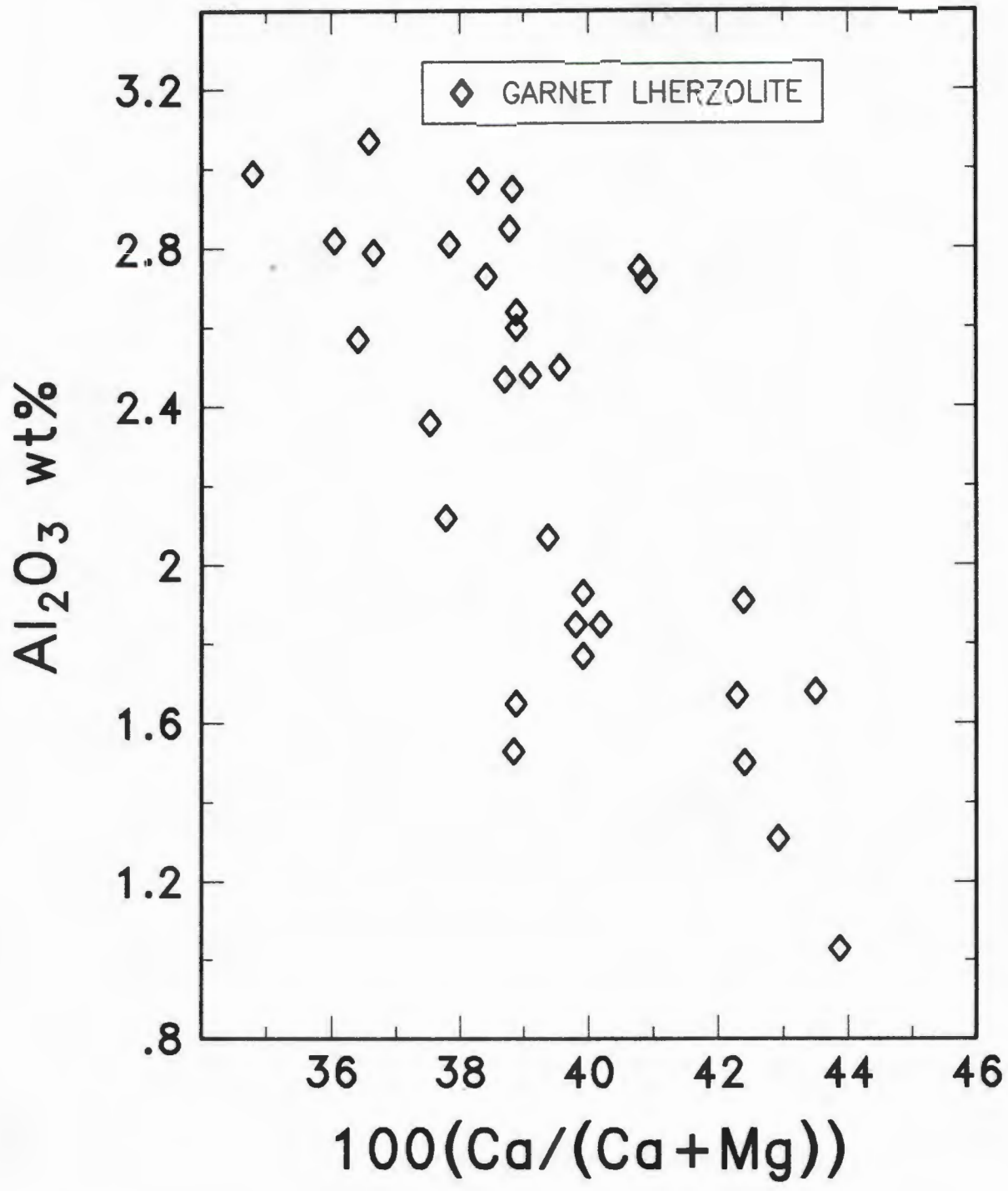

FIGURE 2.16 Na_2O wt% versus TiO_2 wt% in clinopyroxene porphyroclasts from garnet lherzolites

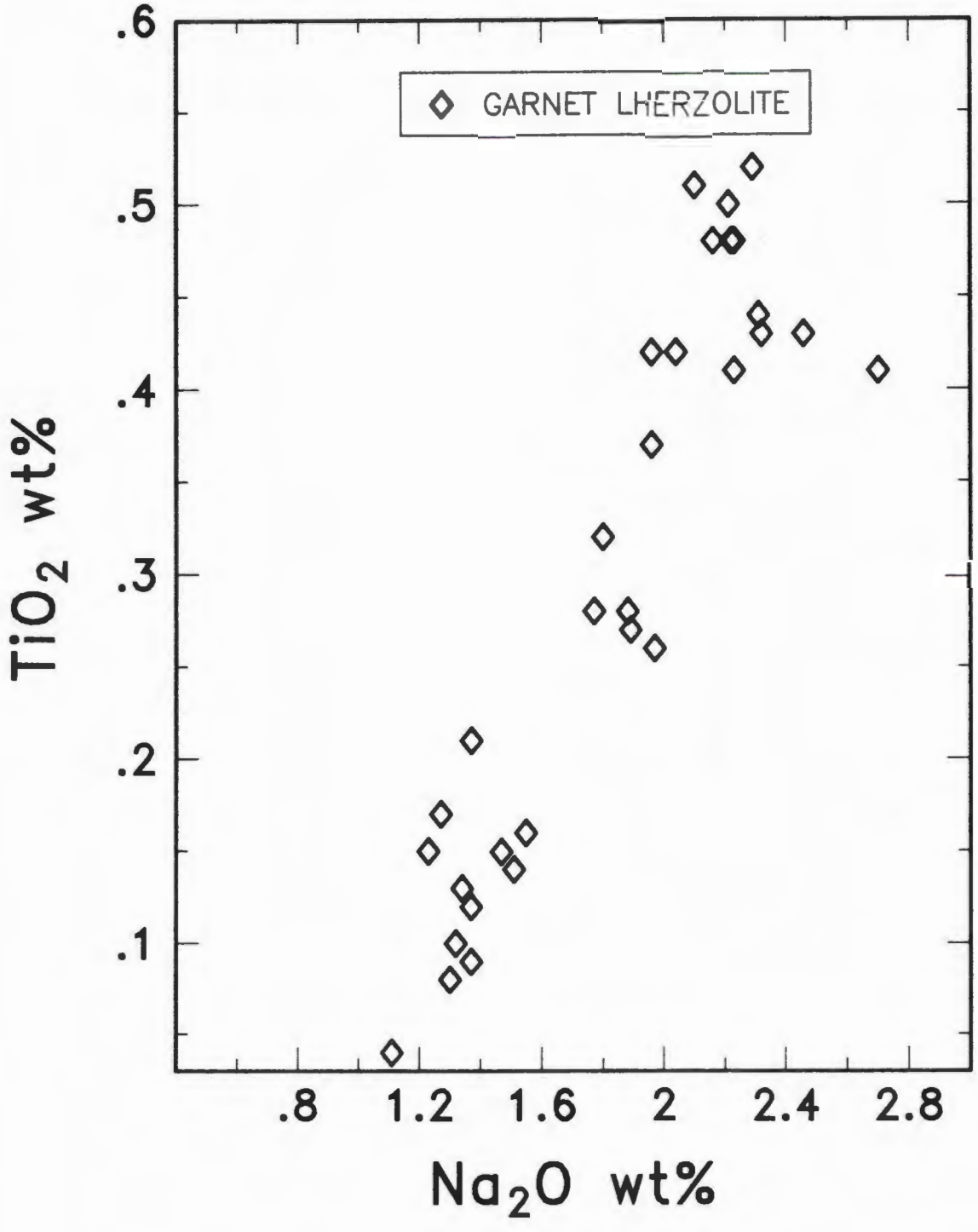

2.6 Discussion

Compositional zoning in the garnet porphyroclasts of high-temperature peridotites has been noted by several authors (Smith and Ehrenberg, 1984; Smith and Boyd, 1986,1987; Sobolev et al., 1986; Smith, 1988). Diffusion coefficients are not well constrained at these temperature and pressure conditions, but diffusion rates in garnet are slower than those in olivine and pyroxene (Smith and Wilson, 1985).

The common feature in all zoned garnets analyzed to date is an increase in TiO_2 concentration from core to rim. Rim enrichments of Na_2O, FeO and P_2O_5 have been observed in some garnet porphyroclasts, but not quantified in all cases. Smith and Boyd (1986) noted that although Cr_2O_3 occasionally decreased from core to rim, some xenoliths had garnets with contrasting Cr gradients approaching a common rim value. Smith (1988) noted that the gradients extended in from rims for radial distances between 100 to 2000 microns, in some cases to crystal centres and in others to apparently homogeneous cores.

Apart from the zonation noted for major and minor elements, Griffin et al. (1989) determined trace element patterns in two garnet peridotites by proton probe analysis. Griffin et al. (1989) noted that the zonation was paralleled by some trace elements as well. The garnet rims are enriched in the incompatible elements Zr, Y and Ga relative to their cores, while compatible elements such as Zn remain constant. Application of diffusion coefficient data indicate that the

zonation must have been produced late in the evolution of these peridotites, since diffusion would homogenize the gradients rapidly at high temperatures. The diffusion coefficients are, however, not well enough constrained to determine an accurate time period. Griffin et al. (1989) have interpreted the profiles as consistent with the formation of Ti-, Zr-, Y-enriched garnet overgrowths, followed by diffusive equilibration between the rim and core over years to hundreds of years.

Green and Gueguen (1983) and Drury and van Roermund (1988a) have reported the presence of sub-micron multiphase inclusions in olivine porphyroclasts in the high-temperature peridotites. Green and Gueguen (1983) reported the presence of sub-micron Cr, Al and C-rich multiphase inclusions, whereas Drury and van Roermund (1988a) reported the presence of sub-micron Fe, Ti-rich and Si, Al, Fe-rich multiphase inclusions. The Cr, Al and C-rich multiphase inclusions have been interpreted as resulting from precipitation during decompression and cooling from intrinsic trace element solid solution in olivine (Green and Gueguen, 1983). In contrast, Drury and van Roermund (1988a) interpreted the Fe, Ti-rich and Si, Al, Fe-rich multiphase inclusions as resulting from fluid infiltration along a crack network shortly before entrainment of the xenoliths, followed by crack healing during xenolith transport in the mantle.

The compositional zonation in the garnet porphyroclasts and the Fe, Ti-rich submicron inclusions in the olivine porphyroclasts indicate that the present major/trace element

compositions of the high-temperature peridotites are not representative of primitive mantle as had been previously suggested (eg. Shimizu and Allegre, 1978). The present compositions of the high-temperature peridotites are instead a reflection of enrichment superimposed on depleted compositions. The effect of the enrichment can be observed by comparing the compositions of the peridotites JJH 35 and JJH 31 which represent the two compositional extremes observed at Jagersfontein. The peridotite JJH 35 does not appear to have been affected by enrichment processes and has low Na_2O and TiO_2 concentrations. It is suggested that this xenolith might be representative of the original protolith prior to the influence of any enrichment events. A model for these peridotites will be considered in Section 6.1.6.

CHAPTER 3

PETROGRAPHY AND MINERAL COMPOSITIONS OF THE MEGACRYST MINERALS

3.1 INTRODUCTION

As noted in Chapter 1, megacrysts are one of the characteristic types of mantle-derived nodules found in kimberlite. Megacrysts, or discrete nodules as they are occasionally termed, are formed predominantly of a single crystal, which is usually 1-20 cm in maximum dimension. Minerals found in this size range in kimberlite pipes include: olivine, orthopyroxene, clinopyroxene, garnet, ilmenite, phlogopite and zircon. The presence and relative abundances of the various megacryst minerals vary between localities. Although some of these minerals are the same species as those in associated ultramafic xenoliths and could theoretically result from disaggregated peridotites, they are usually physically and compositionally distinct.

On the basis of colour, mineral composition and rare host-inclusion relations, it is possible to classify megacrysts into suites of coexisting minerals. Eggler et al. (1979) recognized two separate suites of megacryst minerals in some North American kimberlites, the one Cr-poor and the other Cr-rich. The North American Cr-poor suite is represented by the minerals olivine, orthopyroxene, clinopyroxene, garnet and ilmenite, while the Cr-rich suite is represented by the minerals olivine, orthopyroxene, clinopyroxene and garnet. In general the Cr-poor suite is characterized by higher TiO_2

and lower more variable Mg/(Mg+Fe) than the Cr-rich suite (Eggler et al., 1979). A further Cr-rich variety, the Granny Smith suite, has been noted at some southern African localities (Boyd et al., 1984a). The major component of this suite is an apple-green clinopyroxene (hence the name), which is occasionally intergrown with ilmenite and/or phlogopite. Yet another megacryst suite containing Fe-rich olivine, ilmenite, phlogopite, zircon and Cr-poor (but not subcalcic) clinopyroxene has been recognized at the Monastery kimberlite (Moore, 1987). Megacrysts consisting of two-pyroxene intergrowths in which one of the phases has obviously exsolved from the other have also been found at several southern African localities (Aoki et al., 1980; Meyer and McCallister, 1984). In some cases minor garnet, either as lamellae or blebs, is also present in these intergrowths. These megacrysts may be re-equilibrated versions of the Cr-poor megacryst suite.

In southern Africa the Cr-poor megacryst suite is usually confined to Group 1 kimberlites (Smith, 1984). Notable exceptions are the Cr-poor garnet megacrysts which have been found at some Group 2 localities (Daniels and Gurney, 1989; Read, pers comm.). The Cr-rich megacryst suite, characteristic of many North American localities (Eggler et al., 1979), does not appear to be represented at any southern African localities. Both Cr-rich clinopyroxenes and garnets are found at the Bellsbank and Bobbejaan kimberlites (Gurney, pers. comm.), but it is not certain that they represent a coexisting suite. Cr-rich clinopyroxenes are found at a number of other localities in

southern Africa, but they are not associated with garnet, olivine and orthopyroxene. Some of these Cr-rich clinopyroxenes have been termed the Granny Smith suite, but there are compositional differences between localities (eg. Orapa, Shee and Gurney, 1979; Kimberley, Boyd et al., 1984a) and it is unclear whether they might have a common origin.

There has been considerable debate about the origin of the Cr-poor megacrysts, the principal point of contention being the relationship between the megacrysts and the kimberlite (ie. are the megacrysts xenocrysts or phenocrysts). These arguments will be discussed further in Chapter 6. For the moment it is sufficient to note that the large grain size and lack of aggregation of the Cr-poor megacrysts have led to the commonly accepted view that they are derived from an incompletely consolidated magma.

3.2 HAND SPECIMEN DESCRIPTIONS

As a Group 1 kimberlite, Jagersfontein contains an abundance of Cr-poor megacrysts. The Cr-poor megacryst suite at Jagersfontein is represented by garnet, clinopyroxene, orthopyroxene and olivine. A significant difference between Jagersfontein and most other documented Cr-poor megacryst localities is the absence of ilmenite and ilmenite-silicate intergrowths. At many other localities (eg. Monastery, Lekkerfontein) ilmenite is commonly the most abundant megacryst mineral, occurring as discrete nodules and as primary intergrowths with clinopyroxene, orthopyroxene, garnet, olivine, zircon and phlogopite. No zircon

megacrysts were found associated with the Cr-poor megacryst suite at Jagersfontein either. Phlogopite occurs as large discrete crystals and may be part of the Cr-poor suite, but no analyses were performed on these discrete phlogopites as these were commonly vermiculitized, and no phlogopite inclusions were found in any of the other silicate megacrysts.

Apart from the Cr-poor megacryst suite, a second distinct clinopyroxene megacryst population, the Granny Smith diopsides, is also found at Jagersfontein. Phlogopite and ilmenite are occasionally found associated with these Granny Smith diopsides. A second distinct olivine megacryst population was also noted at Jagersfontein.

The megacryst samples were mostly collected from dumps of oversize heavy mineral concentrate that had been through the primary crusher on the mine. As a result, the average megacryst size at Jagersfontein is about 3 cm, noticeably smaller than those collected from Monastery where the megacrysts are often found in situ in blocks of mined kimberlite. Similar large megacrysts do occur at Jagersfontein and are occasionally found on the floor areas. They cannot be collected effectively however, since the mine has been dormant for several years and is flooded. As the megacrysts at Jagersfontein were collected from heavy mineral concentrate dumps, it was not possible to determine whether any relationship existed betweeen the megacrysts and a particular kimberlite intrusive phase within the diatreme.

Garnet, subcalcic clinopyroxene and Granny Smith diopsides are the most abundant megacrysts at Jagersfontein, with orthopyroxene and olivine less abundant. This is possibly a reflection of sample collection, as the garnet and clinopyroxenes are more easily recognized in the concentrate dumps. It could also reflect the effects of differential weathering at the surface, or differential reaction rates in the kimberlite en route to the surface as olivine and orthopyroxene would be easily serpentinized.

At Jagersfontein, megacrysts containing inclusions of another silicate phase are rare and samples containing more than two phases are very rare indeed. Consequently, during the initial selection process, all those megacrysts which were seen to host coexisting phases were chosen for analysis. Garnet included in subcalcic clinopyroxene and vice versa are the most abundant inclusion relations (Table 4), as might be expected from the individual mineral abundances.

The samples chosen for analyses in this study were all >1 cm, as this is usually considered to be the lower size limit for megacrysts. This discriminates against peridotite minerals that are usually <1 cm. It is important to note that megacryst classification should not be based only on grain size and colour. Although the Cr-poor megacrysts can usually be distinguished in hand specimen from minerals of disaggregated peridotite, there is a tendency to incorrectly classify some eclogites as Cr-poor clinopyroxene megacrysts coexisting with garnet (and vice versa). These can often

TABLE 4

CO-EXISTING MEGACRYST PHASES

HOST	NO.OF SAMPLES	
GARNET		
	CLINOPYROXENE	6
	OLIVINE	3
	ORTHOPYROXENE	1
CLINOPYROXENE		
	GARNET	4
	ORTHOPYROXENE	1
	OLIVINE	1

only be correctly classified on the basis of mineral composition (Dawson and Smith, 1986).

3.2.1 Garnet

The Cr-poor garnet megacrysts at Jagersfontein are a reddish-brown colour. Occasionally remnants of the kelyphitic reaction rim due to interaction between the garnet and the host kimberlite have remained intact.

Seventy-five garnet megacrysts were selected for analysis; 6 of these had clinopyroxene inclusions, 3 had olivine inclusions and 1 had an orthopyroxene inclusion. Garnet was also found as an inclusion in 4 clinopyroxene megacrysts.

Some of the garnet megacrysts for which thin sections were made were found to host polymineralic inclusions. These appear to be similar to those described by Schulze (1985), and to those observed in some of the garnet porphyroclasts in the high-temperature peridotites in this study.

3.2.2 Clinopyroxene

The Cr-poor subcalcic clinopyroxene megacrysts at Jagersfontein are a grey-green colour and often show a whitish alteration product, particularly along fractures.

Twenty-nine clinopyroxene megacrysts were chosen for analysis; 4 of these had garnet inclusions, 1 had an olivine inclusion and 1 had an orthopyroxene inclusion. Cr-poor

clinopyroxene was found as inclusions in 6 garnet megacrysts.

The Granny Smith diopsides are an apple-green colour and are easily distinguished from the Cr-poor clinopyroxenes. Many of these nodules are not megacrysts per se, but are mono-mineralic polycrystalline nodules having grain size <1 cm. Granny Smith diopsides are not found coexisting with garnet, and very rarely with olivine or orthopyroxene (Boyd et al., 1984a). Boyd et al. (1984a) note that ilmenite is usually found in the recrystallized groundmass of the Granny Smith diopsides and is seldom found in the diopside porphyroclasts or in undeformed megacrysts. Very few of the Granny Smith diopsides at Jagersfontein were found to host ilmenite and primary phlogopite was more frequently found as an inclusion than ilmenite.

Forty-one Granny Smith diopsides were selected for analysis.

3.2.3 Olivine

The olivine megacrysts from the Cr-poor suite are a brownish colour and are not easily recognized on the concentrate dumps. They are highly serpentinized along fractures and often recrystallized, suggesting that some so-called dunites could represent recrystallized olivine megacrysts. The olivine neoblasts in the partly recrystallized megacrysts are not in optical continuity with the strained host. Boyd et al. (1984b) suggested that olivine might not form part of

the Cr-poor megacryst suite, but this is not substantiated at Jagersfontein.

Haggerty and Boyd (1975) and Jakob (1977) describe olivine megacrysts from the Monastery kimberlite which have spheroidal kimberlite inclusions. These inclusions are tubular features and have bulk compositions similar to the Quarry kimberlite at Monastery. This type of inclusion was not observed in the olivines at Jagersfontein.

Ten olivine megacrysts were selected for analysis. None of the olivine megacrysts were hosts to coexisting silicate phases, but olivine was found as an inclusion in 1 garnet megacryst.

3.2.4 Orthopyroxene

The Cr-poor orthopyroxene megacrysts at Jagersfontein are a glassy grey-green colour. Differential reaction during emplacement or differential weathering at the surface might be the cause of the low abundance of this megacryst mineral.

Eight orthopyroxene megacrysts were selected for analysis. None of the orthopyroxene megacrysts were hosts to coexisting silicate phases, but orthopyroxene was found as an inclusion in one subcalcic clinopyroxene megacryst and in one garnet megacryst.

3.3 MINERAL COMPOSITIONS

Polished sections were made for a selected small suite of the Jagersfontein megacrysts. These megacrysts appeared to be homogeneous in so far as the electron microprobe could detect. Subsequent analyses were then made on fragments of the megacrysts which were mounted in araldite discs.

Apart from the differences in megacryst abundances between different localities, there are commonly differences in mineral compositions as well (eg. Schulze, 1987). This can be illustrated by comparing the Ca-Mg-Fe ternary plots for the Jagersfontein and Monastery Cr-poor megacrysts (Fig. 3.1). In addition, there appear to be differences in the order of the crystallization sequence of the megacryst assemblage. At localities such as Monastery and Lekkerfontein, olivine, orthopyroxene, clinopyroxene and garnet form the initial high-temperature crystallizing assemblage, while ilmenite becomes part of the assemblage at lower temperatures (eg. Gurney et al., 1979; Robey and Gurney, 1979). At other localities such as Hamilton Branch, ilmenite is part of the initial high-temperature assemblage (Schulze, 1984).

Despite these differences, there are features which are common to the Cr-poor megacryst suite in general. Harte (1983) noted some chemical characteristics which appear to be common to the Cr-poor megacryst suite worldwide:

- A wide but essentially continuous range in Mg/(Mg+Fe) usually exists for each mineral and the more Fe-rich

FIGURE 3.1 Ca–Mg–Fe ternary diagram showing Cr–poor megacrysts from Jagersfontein and fields for the Monastery megacrysts (Gurney et al., 1979)

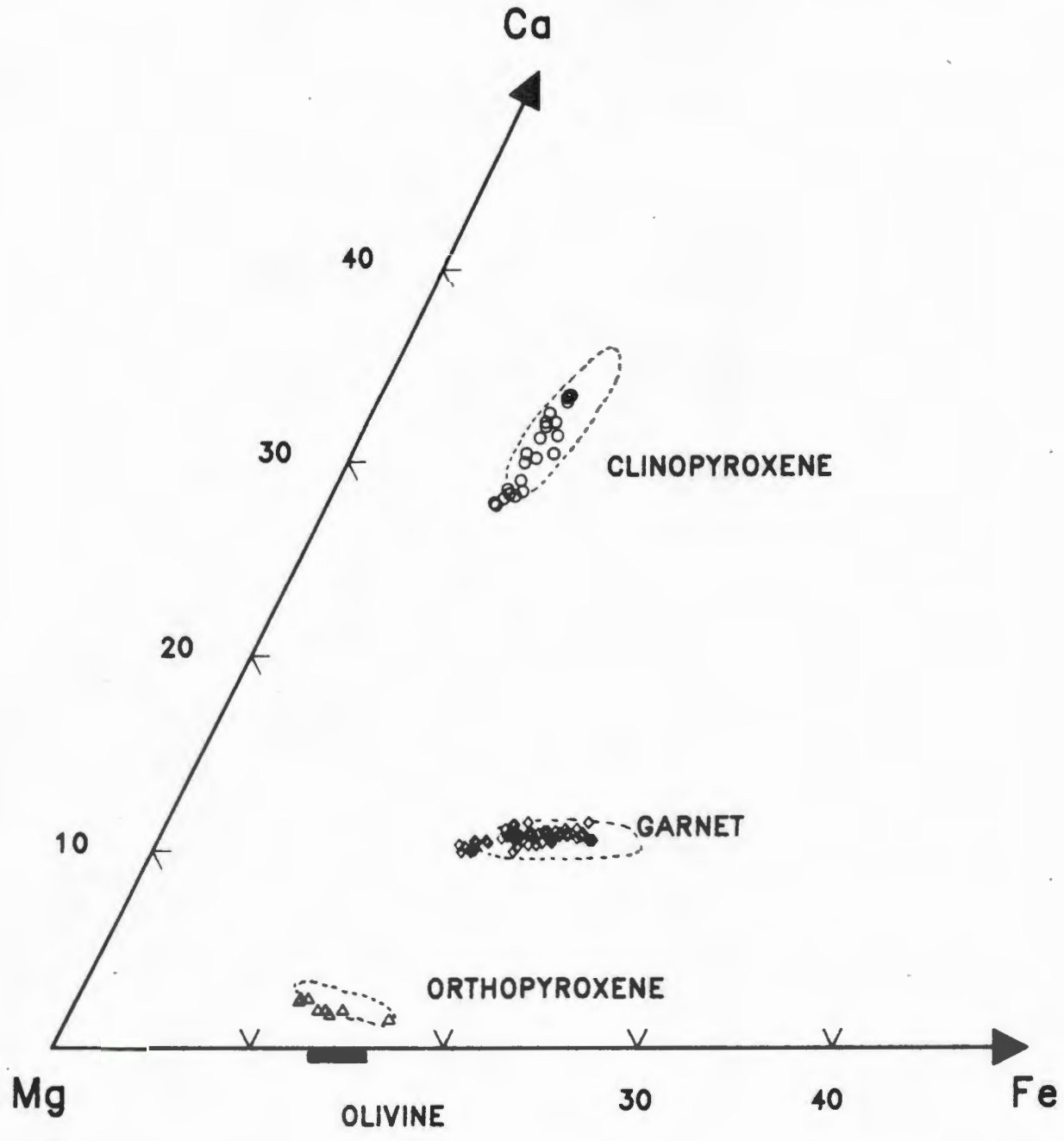

silicates often show inclusions or intergrowths of ilmenite.

- Minor elements such as TiO_2 and Cr_2O_3 in the silicates show some regular variation with Mg/(Mg+Fe).
- Ca/(Ca+Mg) in the clinopyroxenes usually increases regularly with decreasing Mg/(Mg+Fe).

Mineral compositions for the suite of megacrysts are presented in Appendix 4. These minerals are considered representative of the megacryst suite at Jagersfontein, although it is possible that additional samples might extend the compositional range.

3.3.1 Cr-poor garnet

The garnet megacrysts at Jagersfontein are low Cr, high Ti garnets, corresponding to Groups 1 and 2 of the Dawson and Stephens (1975) classification. The effect of Fe enrichment is most pronounced in the garnet megacrysts as the garnet Fe/Mg ratio changes most rapidly during fractionation. The range in Mg#'s from 83 to 75 at Jagersfontein is less than that at Monastery (82 to 68) (Jakob, 1977) and that at Lekkerfontein (81 to 65) (Robey, 1981) reflecting the absence of low-temperature garnet megacrysts with ilmenite intergrowths. The incoming of ilmenite as a liquidus phase occurs at a Mg# of 74 at Monastery (Jakob, 1977) and at a Mg# of 72 at Lekkerfontein (Robey, 1981). Fractional crystallization at Jagersfontein apparently stopped before the commencement of ilmenite crystallization.

The TiO_2 concentration of the garnets at Jagersfontein increases with decreasing Mg# from 0.5 to 1.2 wt% (Fig. 3.2). The earlier megacryst silicate phases at the Monastery kimberlite show an increase in TiO_2 with decreasing Mg# until ilmenite appears as an inclusion phase, whereafter TiO_2 decreases (Jakob, 1977; Gurney et al., 1979). This pattern is not found at Jagersfontein.

The Cr_2O_3 concentration (1.4 to 0.3 wt%) decreases with decreasing Mg# (Fig. 3.3), consistent with a fractionation trend.

The garnet megacrysts display a range in 100(Mg/(Mg+Fe)) ratios (Mg#'s) (83 to 75) at relatively constant 100(Ca/(Ca+Mg)) ratios (Ca#'s). This has been taken as an indication of the buffering of Ca and Mg due to the coprecipitation of orthopyroxene and clinopyroxene (Jakob, 1977). The presence of orthopyroxene prevents Ca enrichment in garnet according to the buffer:

$Ca(Mg,Fe)Si_2O_6+(Mg,Fe)_3Al_2Si_3O_{12} = (Mg,Fe)Si_2O_6+Ca_3Al_2Si_3O_{12}$

Garnets which equilibrate in the presence of clinopyroxene and orthopyroxene have Ca/(Ca+Mg) ratios close to 0.13 (O'Hara and Yoder, 1967). The Jagersfontein garnet megacrysts have Ca/(Ca+Mg) ratios of 0.12-0.15, consistent with crystallization in equilibrium with clinopyroxene and orthopyroxene. Apart from a garnet inclusion in a clinopyroxene megacryst (JJH A79), the garnet megacrysts have a restricted range in CaO concentrations (4.0 to 4.6 wt%) (Fig. 3.4).

The Na_2O concentrations in the garnets are relatively high (0.07 to 0.19 wt%), but do not show any correlation with Mg# (Fig. 3.5).

FIGURE 3.2 Mg# versus TiO_2 wt% in garnet megacrysts from Jagersfontein. Filled symbols are garnets found as inclusions in other silicate megacrysts

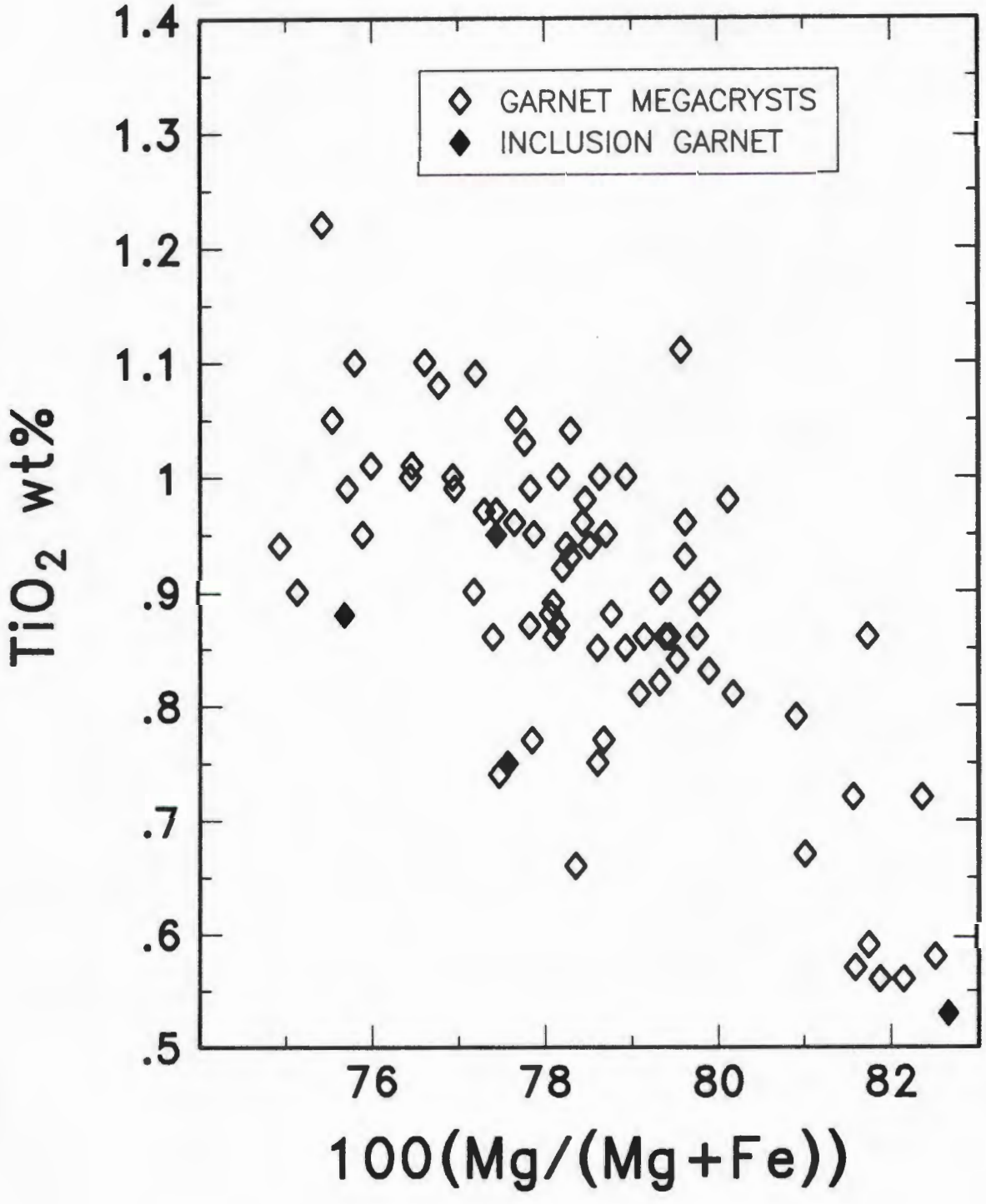

FIGURE 3.3 Mg# versus Cr_2O_3 wt% in garnet megacrysts from Jagersfontein. Filled symbols are garnets found as inclusions in other silicate megacrysts

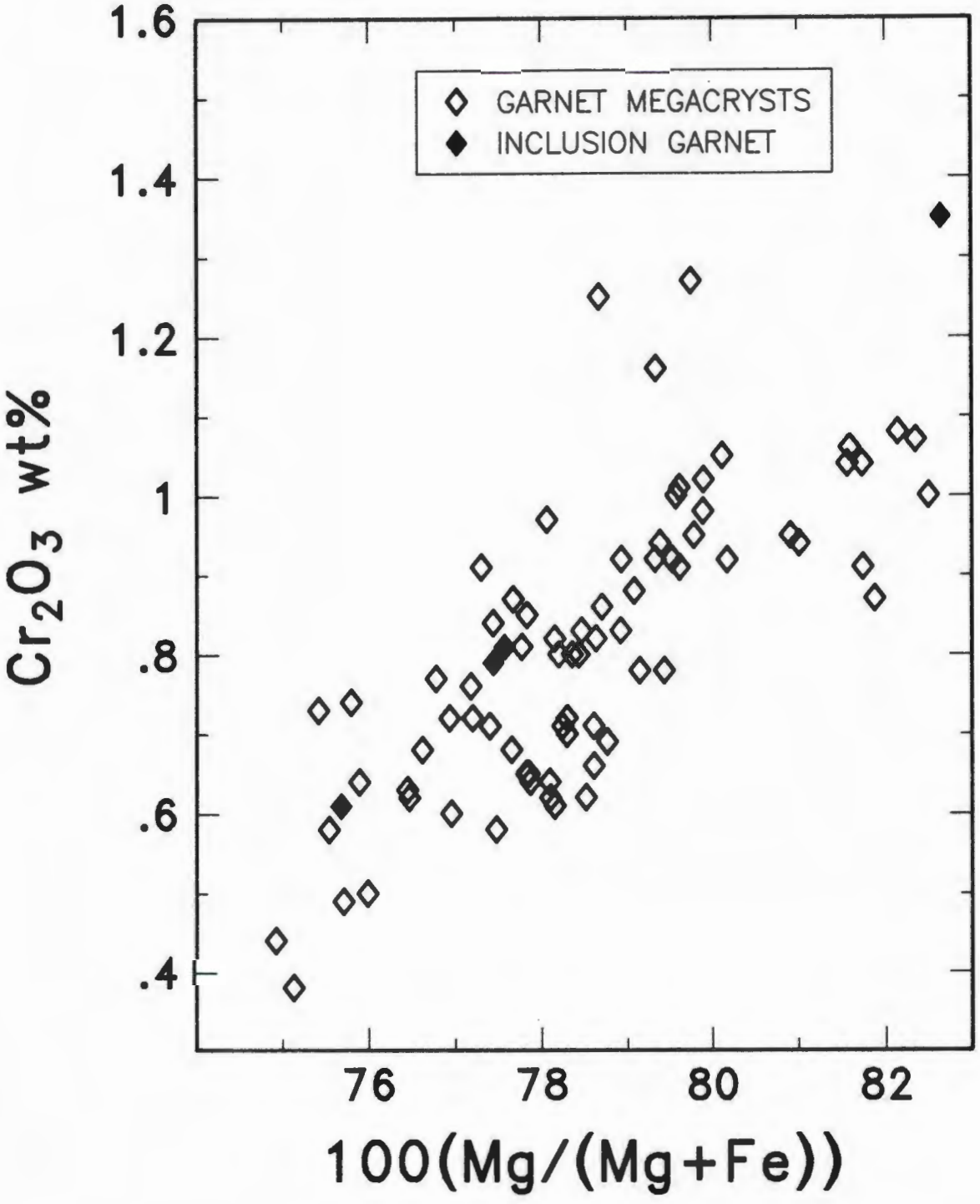

FIGURE 3.4 CaO wt% versus Cr_2O_3 wt% in garnet megacrysts from Jagersfontein. Filled symbols are garnets found as inclusions in other silicate megacrysts

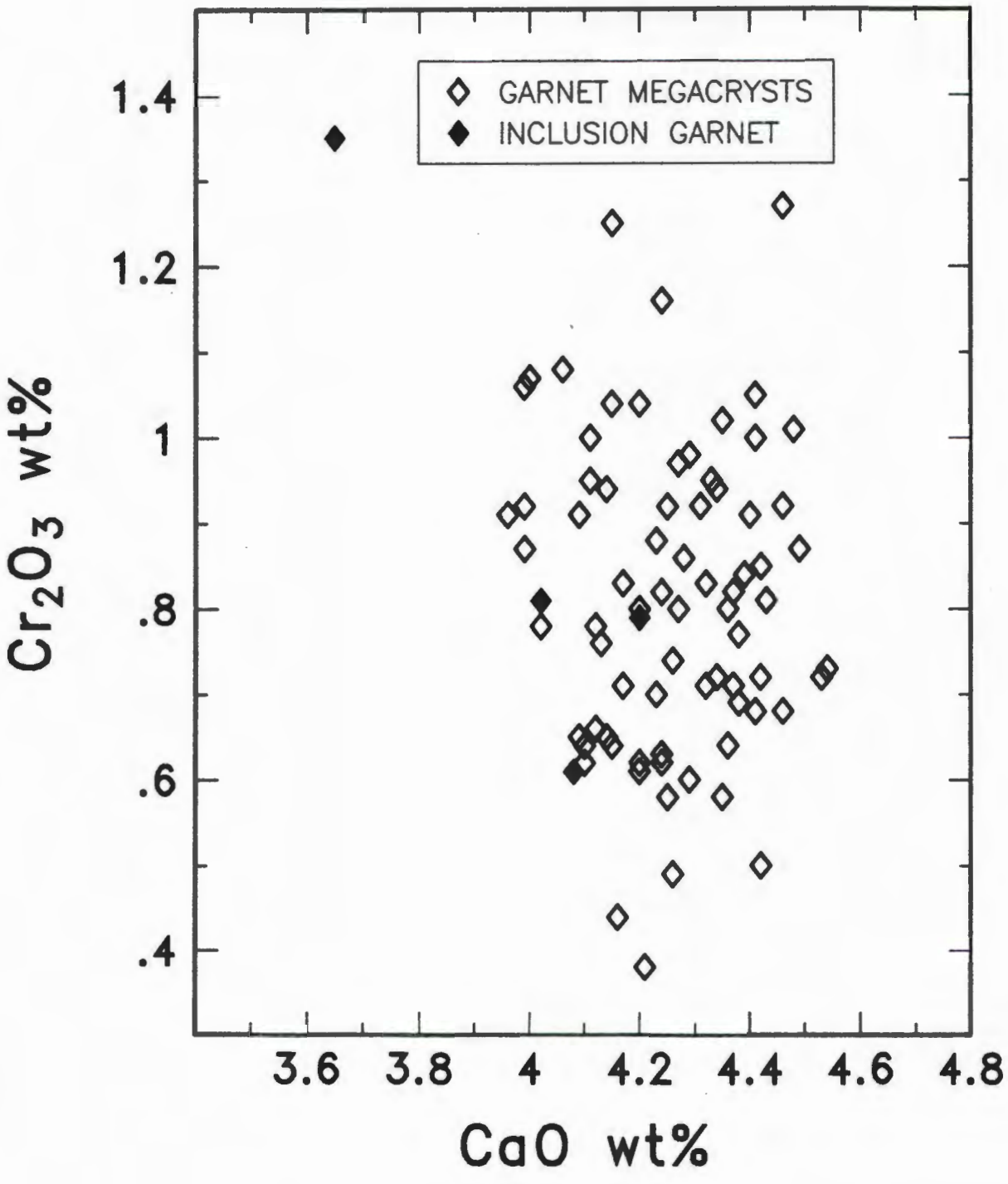

FIGURE 3.5 Na_2O wt% versus Mg# in garnet megacrysts from Jagersfontein. Filled symbols are garnets found as inclusions in other silicate megacrysts

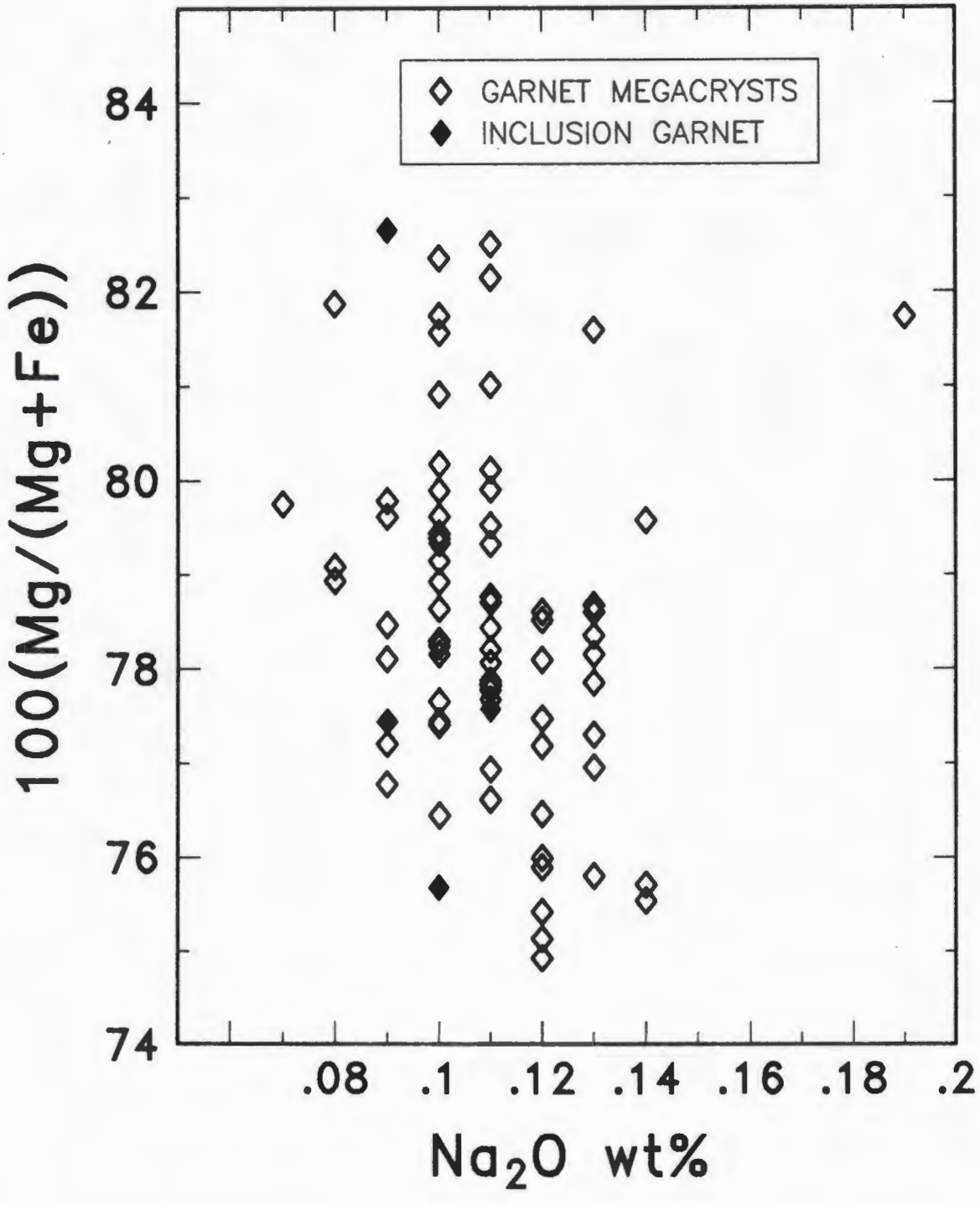

3.3.2 Cr-poor clinopyroxene

The Cr-poor clinopyroxenes display an inverse relationship between Ca# and Mg# (Fig. 3.6). The range in Ca# (28 to 38) is smaller than that observed at Monastery (31 to 43) (Jakob, 1977) and at Lekkerfontein (31 to 44) (Robey, 1981), reflecting the absence of the low-temperature clinopyroxene-ilmenite lamellar intergrowths. The lamellar intergrowths at Monastery are found in clinopyroxenes with a Ca# > 37.5 (Jakob, 1977), and at Lekkerfontein in clinopyroxenes with a Ca# > 38 (Robey, 1981). As was observed in the garnet megacrysts, fractional crystallization apparently stopped before the commencement of ilmenite crystallization.

The Na_2O concentrations (1.4 to 2.6 wt%) increase with increasing Al_2O_3 (2.4 to 4.0 wt%) reflecting increasing jadeite content (Fig. 3.7). The Cr_2O_3 concentrations (0.6 to 1.5 wt%) decrease with decreasing Mg# (Fig. 3.8). The variations in TiO_2 and Cr_2O_3 with Mg# are equivalent to the trends observed in the garnet megacrysts.

One of the subcalcic clinopyroxenes (JJH A64) for which a polished section was made was found to be partly recrystallized. The neoblasts have higher TiO_2 and CaO contents than the undeformed section, but lower Al_2O_3, FeO, MgO and Na_2O contents.

Some of the Cr-poor clinopyroxenes contained spherical immiscible sulphides (eg. Frick, 1973; Haggerty and Boyd, 1975). The morphology of the sulphide inclusions and their relation to growth planes in the clinopyroxenes indicate that they were trapped as drops of immiscible sulphide melt.

FIGURE 3.6 Mg# versus Ca# in clinopyroxene megacrysts from Jagersfontein. Filled symbols are clinopyroxenes found as inclusions in other silicate megacrysts

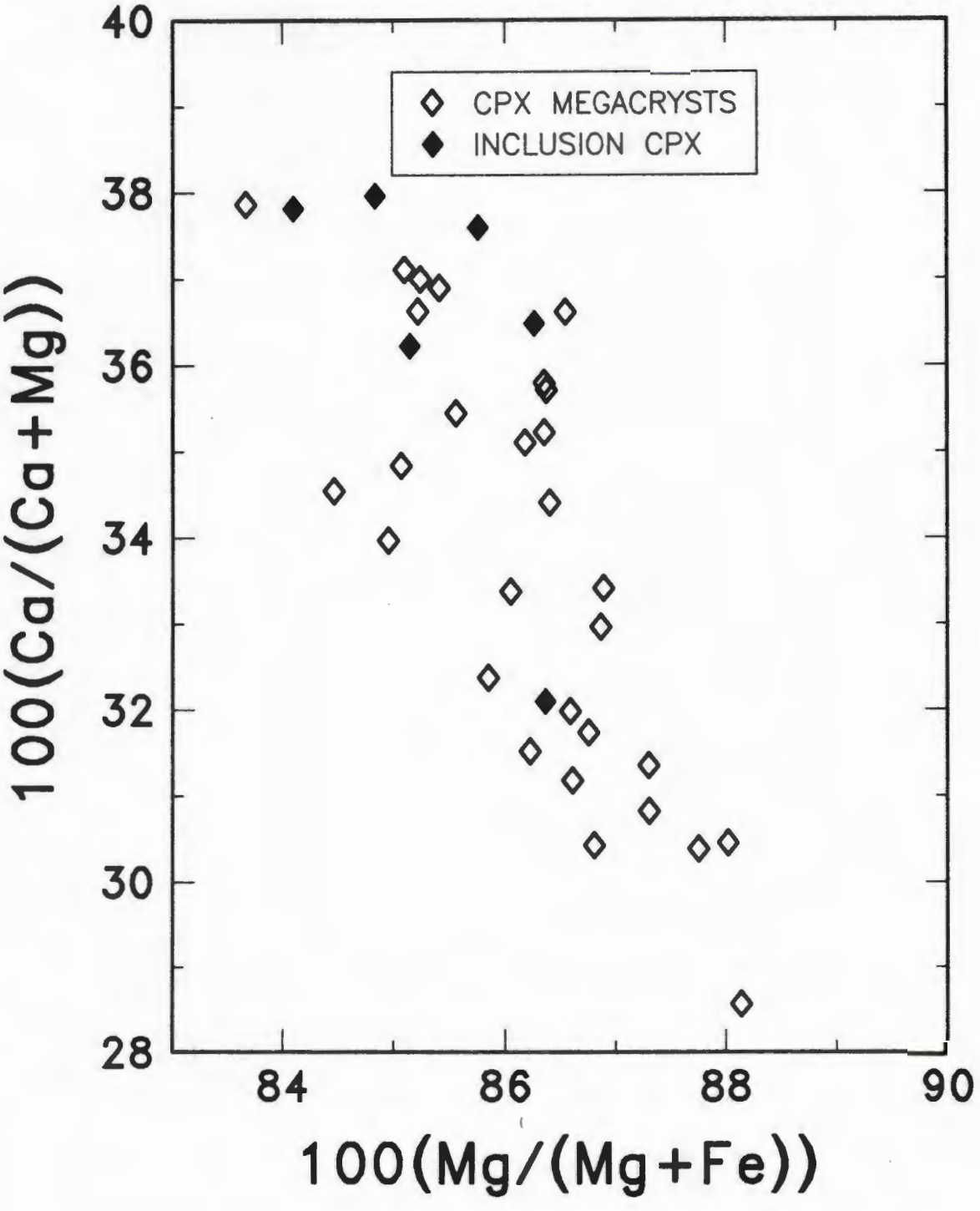

FIGURE 3.7 Atomic prop. of Na versus Al in clinopyroxene megacrysts from Jagersfontein. Filled symbols are clinopyroxenes found as inclusions in other silicate megacrysts

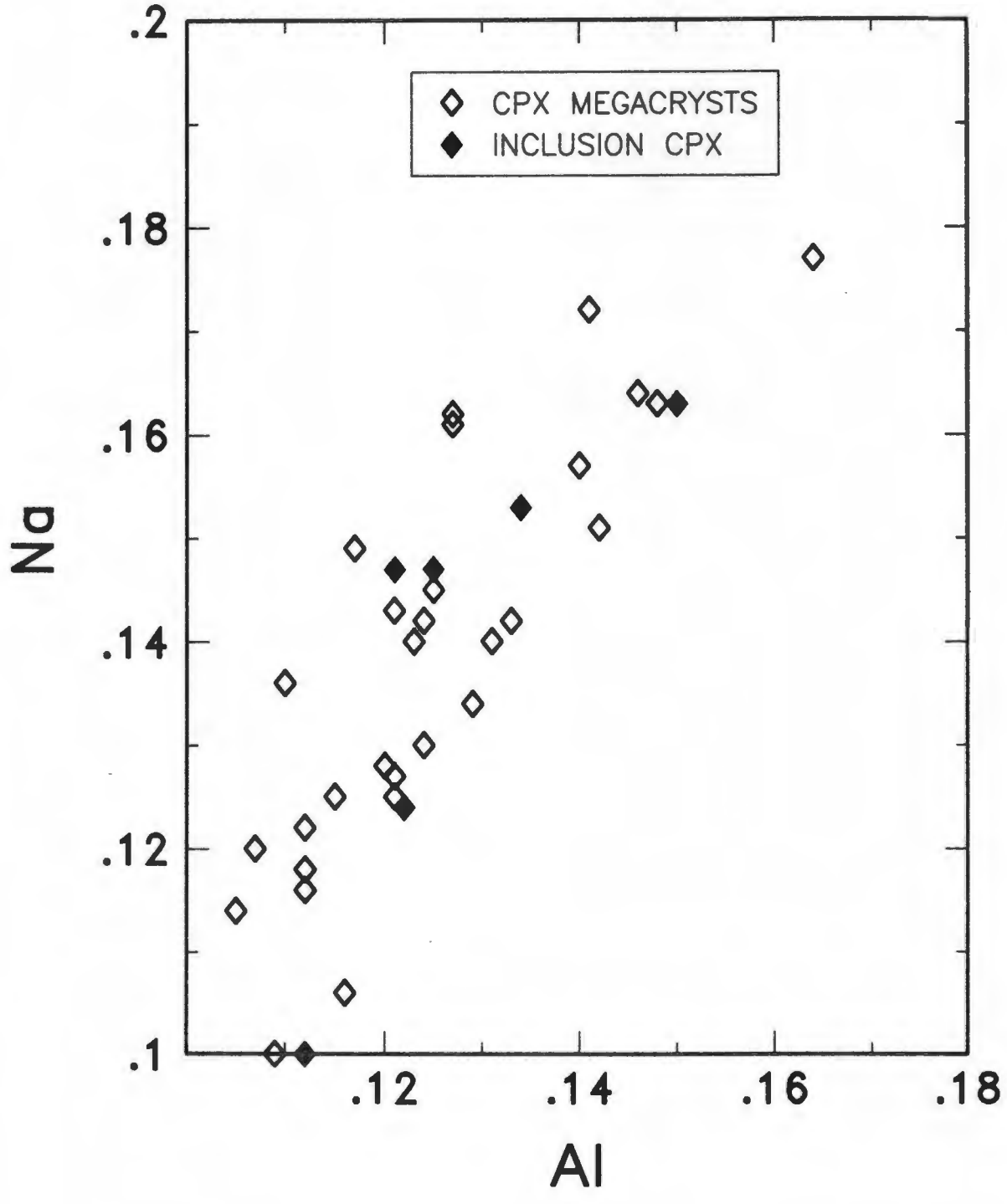

FIGURE 3.8 Mg# versus Cr_2O_3 wt% in clinopyroxene megacrysts from Jagersfontein. Filled symbols are clinopyroxenes found as inclusions in other silicate megacrysts

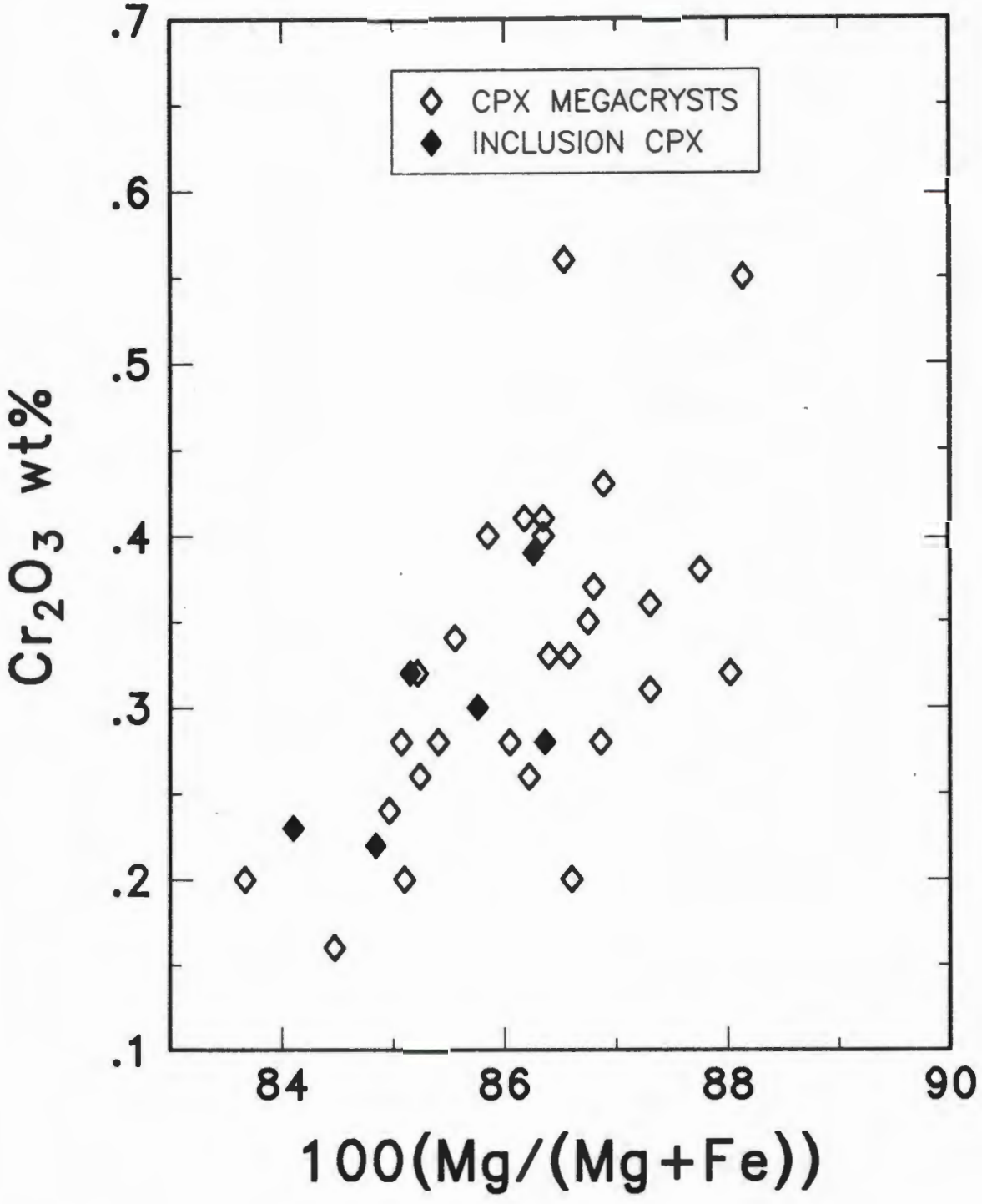

3.3.3 Olivine

The olivine megacrysts in the Cr-poor suite at Jagersfontein have Mg#'s ranging from 88 to 84. This is equivalent to the Mg-rich group of olivine megacrysts at Monastery which have Mg#'s ranging from 88 to 84. On the basis of Fe and Mg partitioning between olivine and liquid, these olivines would be in equilibrium with liquids of Mg#'s from 69 to 61 (Roeder and Emslie, 1970). The Fe-rich group of olivine megacrysts at Monastery (Mg#'s from 78 to 81) has not been found at Jagersfontein.

The Cr_2O_3 and TiO_2 concentrations are usually below detection limit in the olivine megacrysts. The CaO concentrations range from below detection limit (0.03 wt%) to 0.09 wt% and there is a broad decrease of CaO with decreasing Mg#, consistent with an igneous fractionation trend (Fig. 3.9). The Al_2O_3 concentrations range from below detection limit to 0.08 wt%.

The olivine megacrysts have NiO concentrations ranging from 0.19 to 0.34 wt% (Fig. 3.10). Apart from one olivine found as an inclusion in a clinopyroxene megacryst (JJH A66), there appears to be a broad trend of decreasing NiO with decreasing Mg#. It was noted previously that sulphide droplets are occasionally found in the clinopyroxene megacrysts. Although sulphides were not identified in the fragment of JJH A66, it is possible that sulphide fractionation might result in the low NiO concentration in the olivine inclusion.

FIGURE 3.9 Mg# versus CaO wt% in olivine megacrysts from Jagersfontein. Filled symbols are olivines found as inclusions in other silicate megacrysts

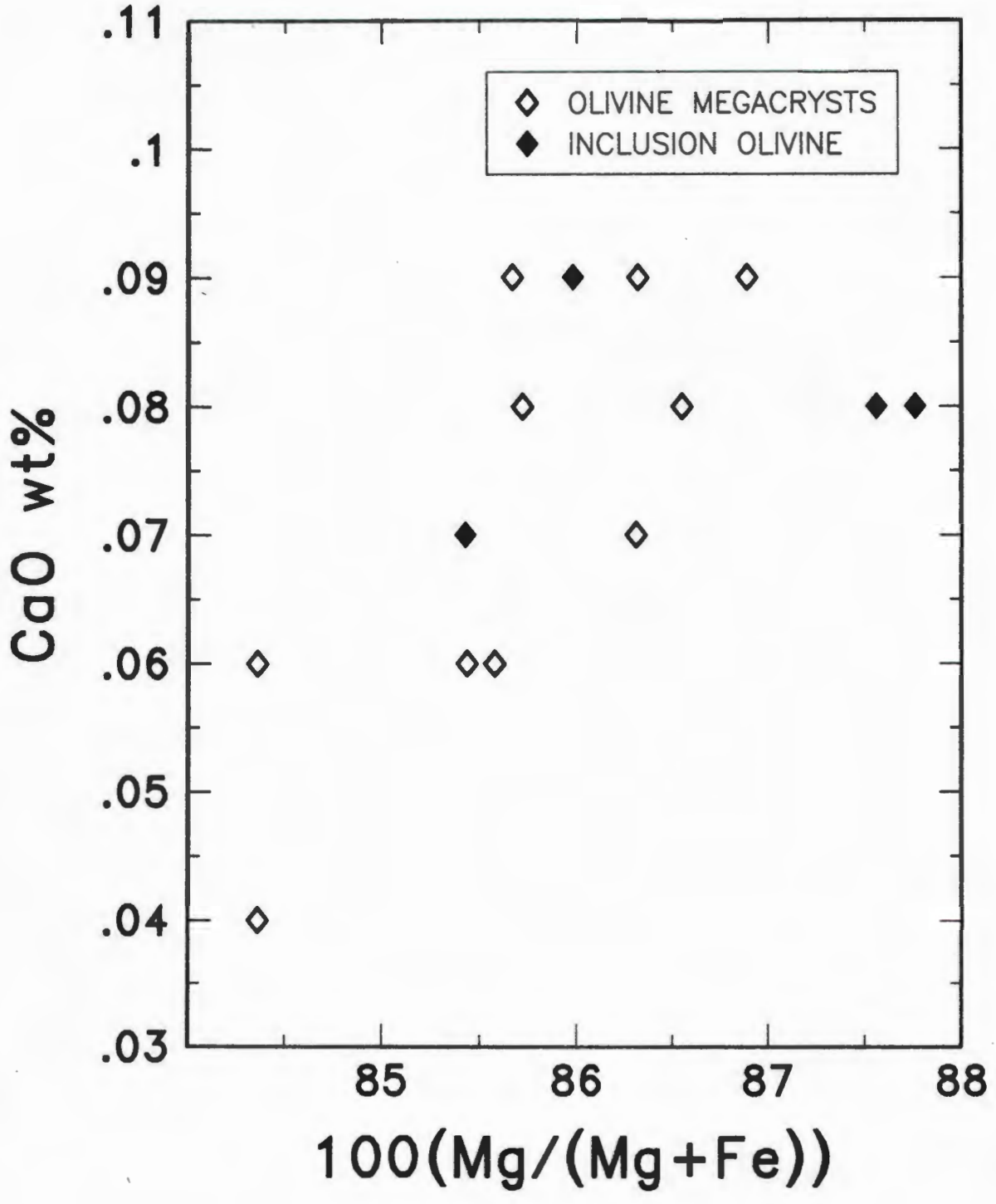

FIGURE 3.10 Mg# versus NiO wt% in olivine megacrysts from Jagersfontein. Filled symbols are olivines found as inclusions in other silicate megacrysts

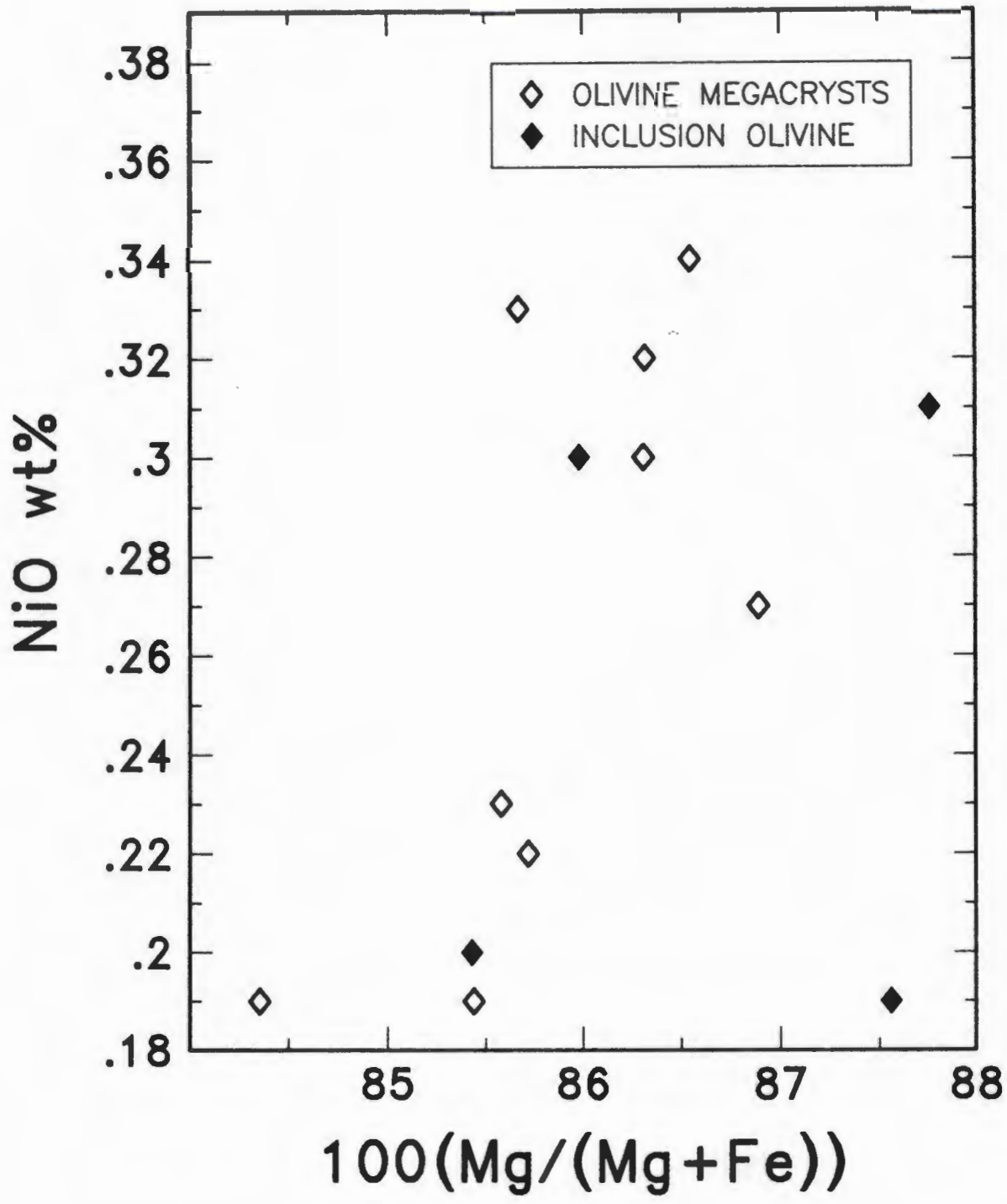

3.3.4 Orthopyroxene

The Cr-poor orthopyroxene megacrysts have Mg#'s of 89 to 83, and define a trend of decreasing Ca# (3.1 to 1.7) with decreasing Mg# (Fig. 3.11), consistent with an igneous fractionation trend, declining temperature and equilibrium with olivine.

The Al_2O_3 concentrations (1.2 to 0.8 wt%) decrease with decreasing CaO (Fig. 3.12) and Na_2O (0.19 to 0.38 wt%).

No correlation of TiO_2 concentration with Mg# was observed in these orthopyroxenes (Fig. 3.13).

FIGURE 3.11 **Mg# versus Ca# in orthopyroxene megacrysts from Jagersfontein. Filled symbols are orthopyroxenes found as inclusions in other silicate megacrysts**

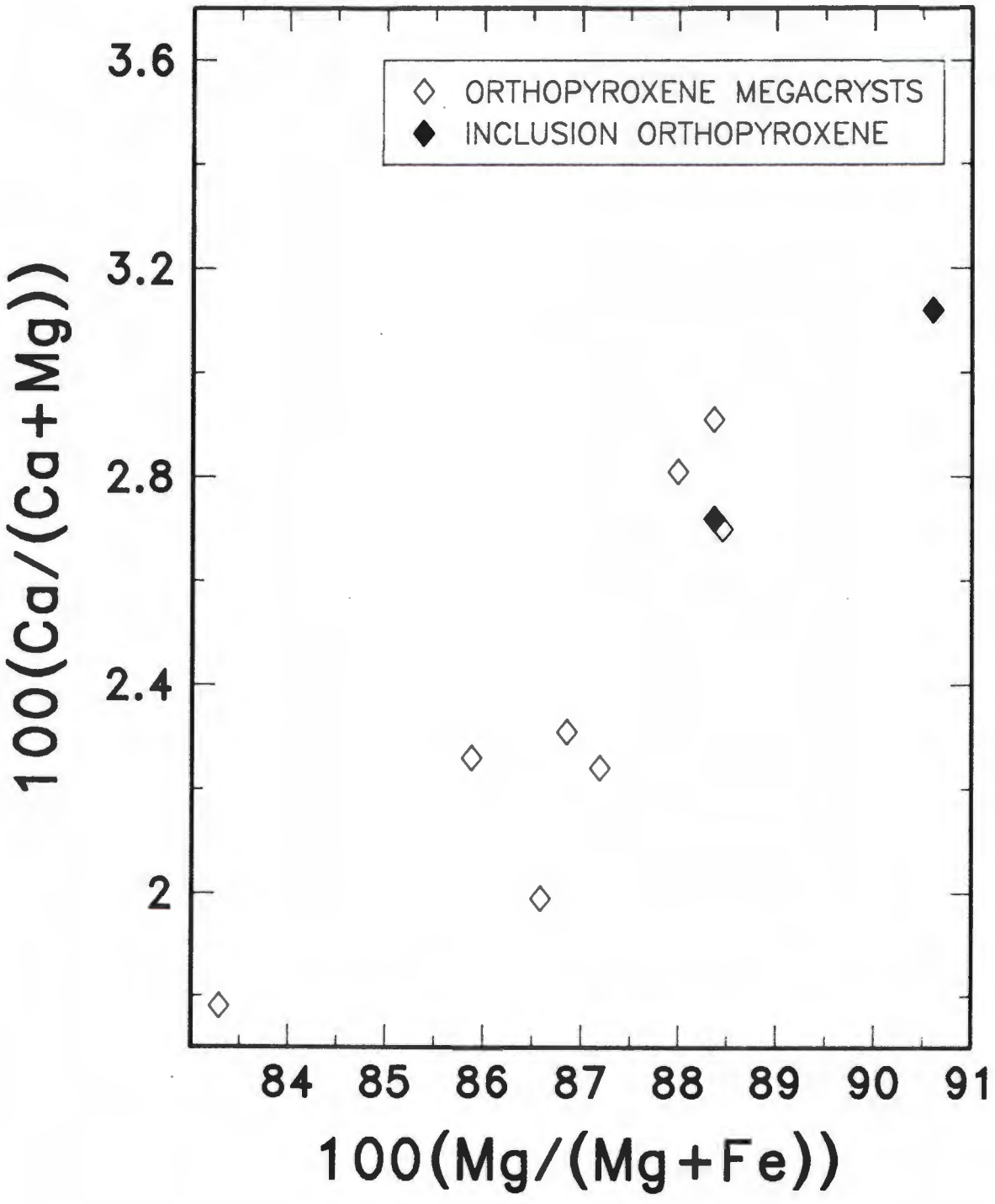

FIGURE 3.12 CaO wt% versus Al_2O_3 wt% in orthopyroxene megacrysts from Jagersfontein. Filled symbols are orthopyroxenes found as inclusions in other silicate megacrysts

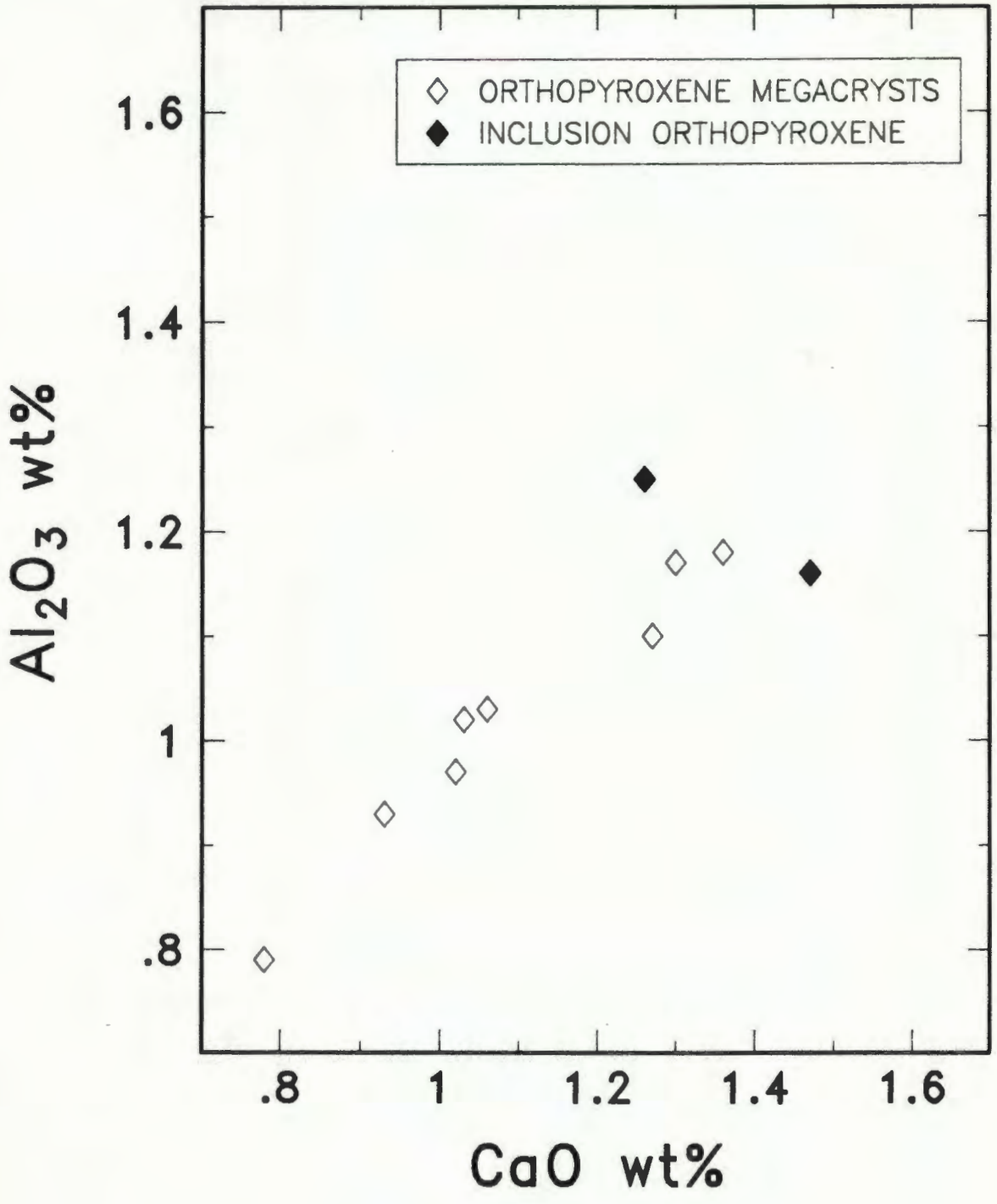

FIGURE 3.13 Mg# versus TiO_2 wt% in orthopyroxene megacrysts from Jagersfontein. Filled symbols are orthopyroxenes found as inclusions in other silicate megacrysts

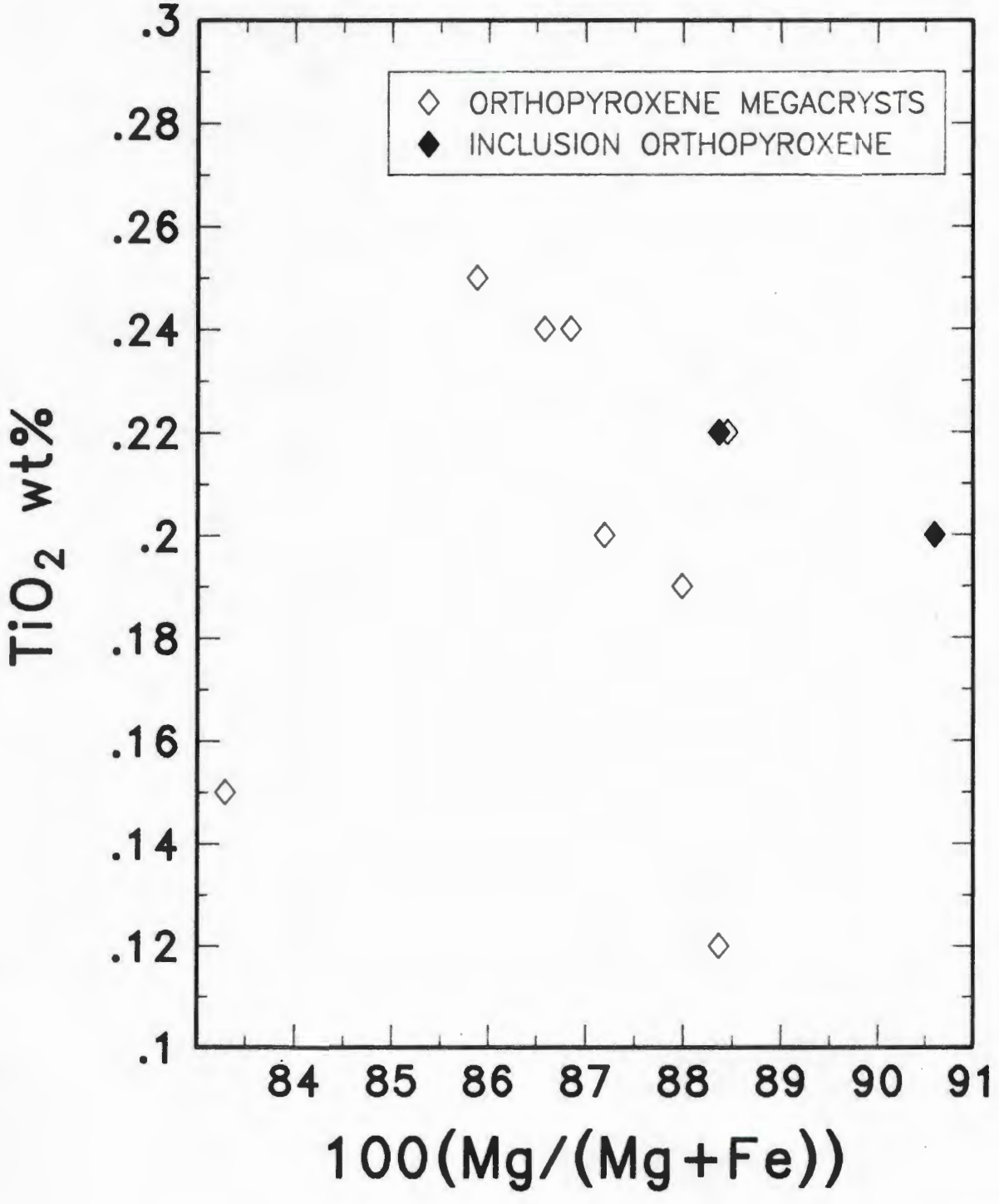

3.3.5 Granny Smith diopsides

The Granny Smith clinopyroxenes are found both as discrete and polycrystalline nodules. These are compositionally indistinguishable. Mazzone et al. (1987) noted compositional differences between sheared and granular Granny Smith megacrysts from Jagersfontein, but this distinction was not observed.

In comparison to the Cr-poor clinopyroxene megacrysts, the Granny Smith diopsides are calcic (Ca#'s > 0.44) and magnesian (Mg#'s > 0.89). In contrast to the igneous fractionation trend observed for the Cr-poor clinopyroxene megacrysts, the Granny Smith clinopyroxenes exhibit no such trend (Fig. 3.14).

The Cr-poor clinopyroxenes and Granny Smith clinopyroxenes have overlapping TiO_2 concentrations, but the Granny Smith clinopyroxenes are richer in Cr_2O_3 (1 to 3.5 wt%) (Fig. 3.15).

The Granny Smith diopsides can be distinguished chemically from the Cr-rich clinopyroxenes of Eggler et al. (1979) by their Na/(Al+Cr) content. The Cr-rich clinopyroxenes have Na < (Al+Cr), whereas the Granny Smith diopsides have Na > (Al+Cr), suggesting the presence of ferric iron (Boyd et al., 1984a) (Fig. 3.16).

Phlogopites in the Granny Smith megacrysts have Mg#'s of 93, TiO_2 concentrations of 0.8-1.3 wt% and Al_2O_3 concentrations of 11.8-12.6 wt%. These values are characteristic of Type 2 micas (Smith et al., 1978).

FIGURE 3.14 Ca# versus Mg# in Granny Smith clinopyroxenes from Jagersfontein

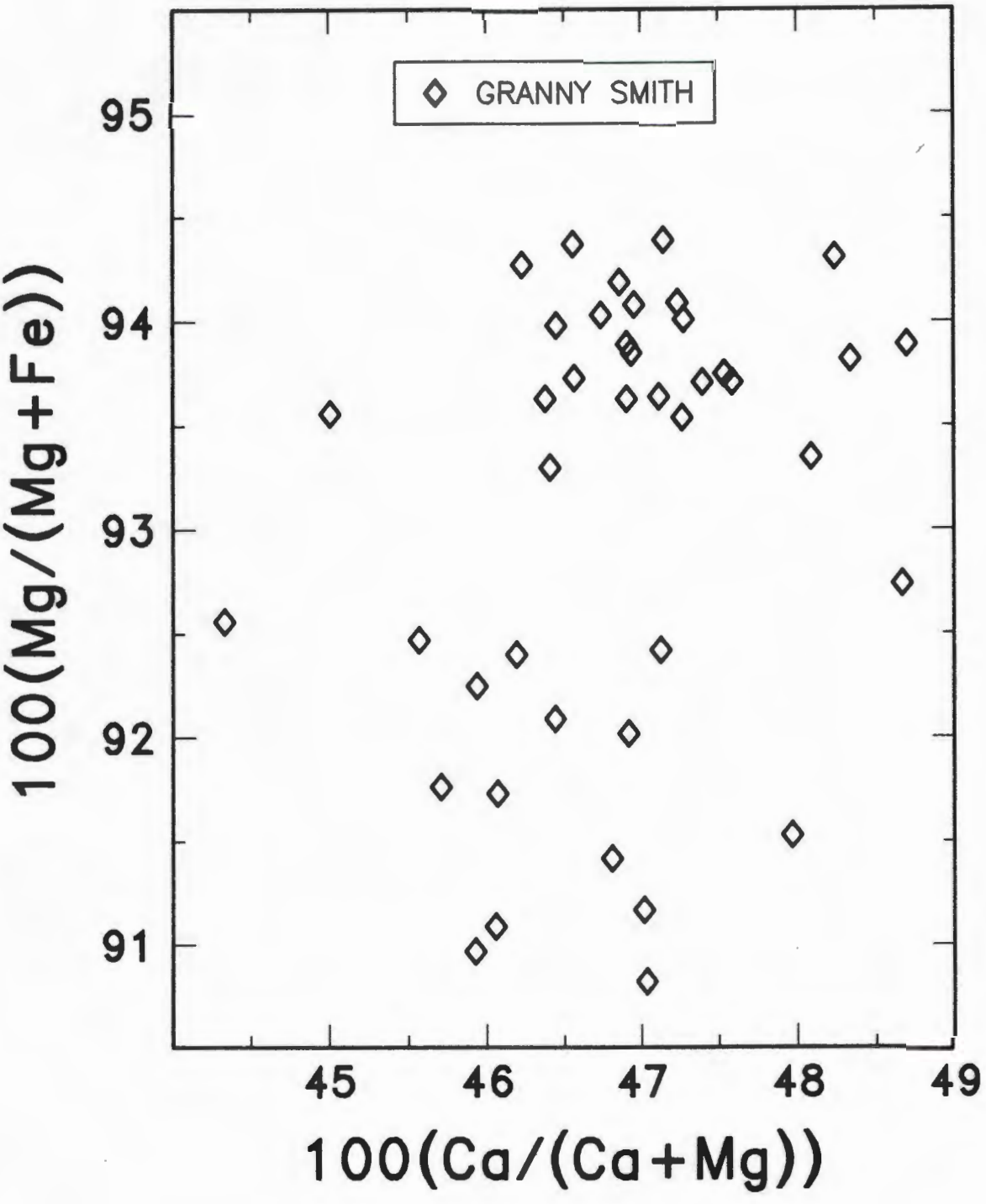

FIGURE 3.15 Cr_2O_3 wt% versus TiO_2 wt% in Granny Smith clinopyroxenes from Jagersfontein

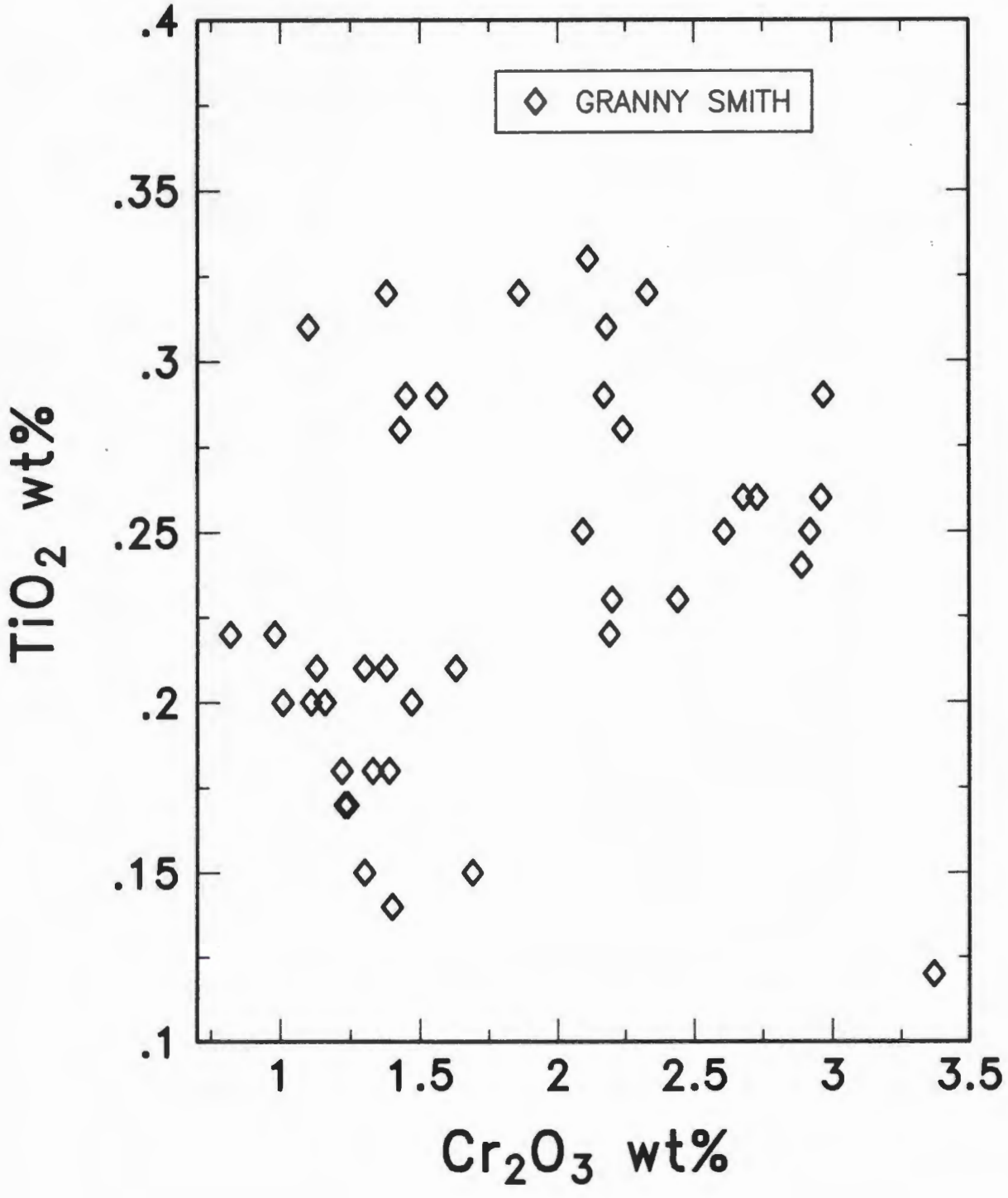

FIGURE 3.16 Atomic prop. Na versus (Al + Cr) in Granny Smith clinopyroxenes from Jagersfontein

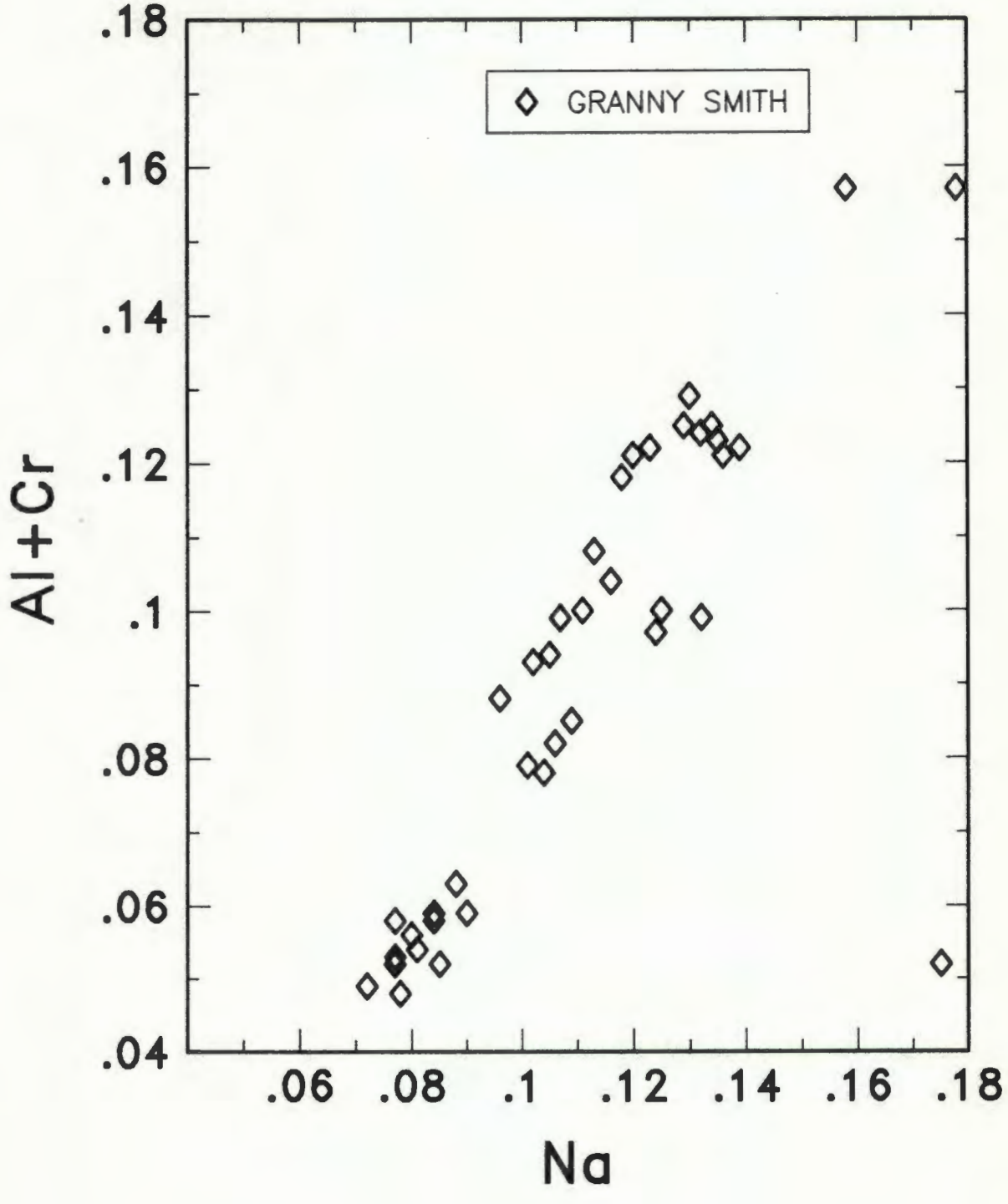

3.3.6 Mg-rich olivine

A second group of olivine megacrysts, compositionally distinct from the olivines in the Cr-poor megacryst suite was found at Jagersfontein. These olivines are also Cr-poor but have Mg#'s ranging from 92 to 95, in comparison to the Mg#'s of the olivines in the Cr-poor megacryst suite which range from 88 to 84.

The NiO concentrations in the Mg-rich olivines are similar to those in the olivines in the Cr-poor megacryst suite and range from 0.24 to 0.34 wt% (Fig. 3.17).

These Mg-rich olivines are compositionally similar to the olivines in the diamondiferous megacrystalline dunites from Udachnaya described by Pokhilenko and Sobolev (1986) and a megacrystalline dunite from Jagersfontein (Nixon et al., 1987). At Jagersfontein, however, they have not been found associated with diamond.

FIGURE 3.17 Mg# versus NiO wt% in Mg-rich olivines from Jagersfontein

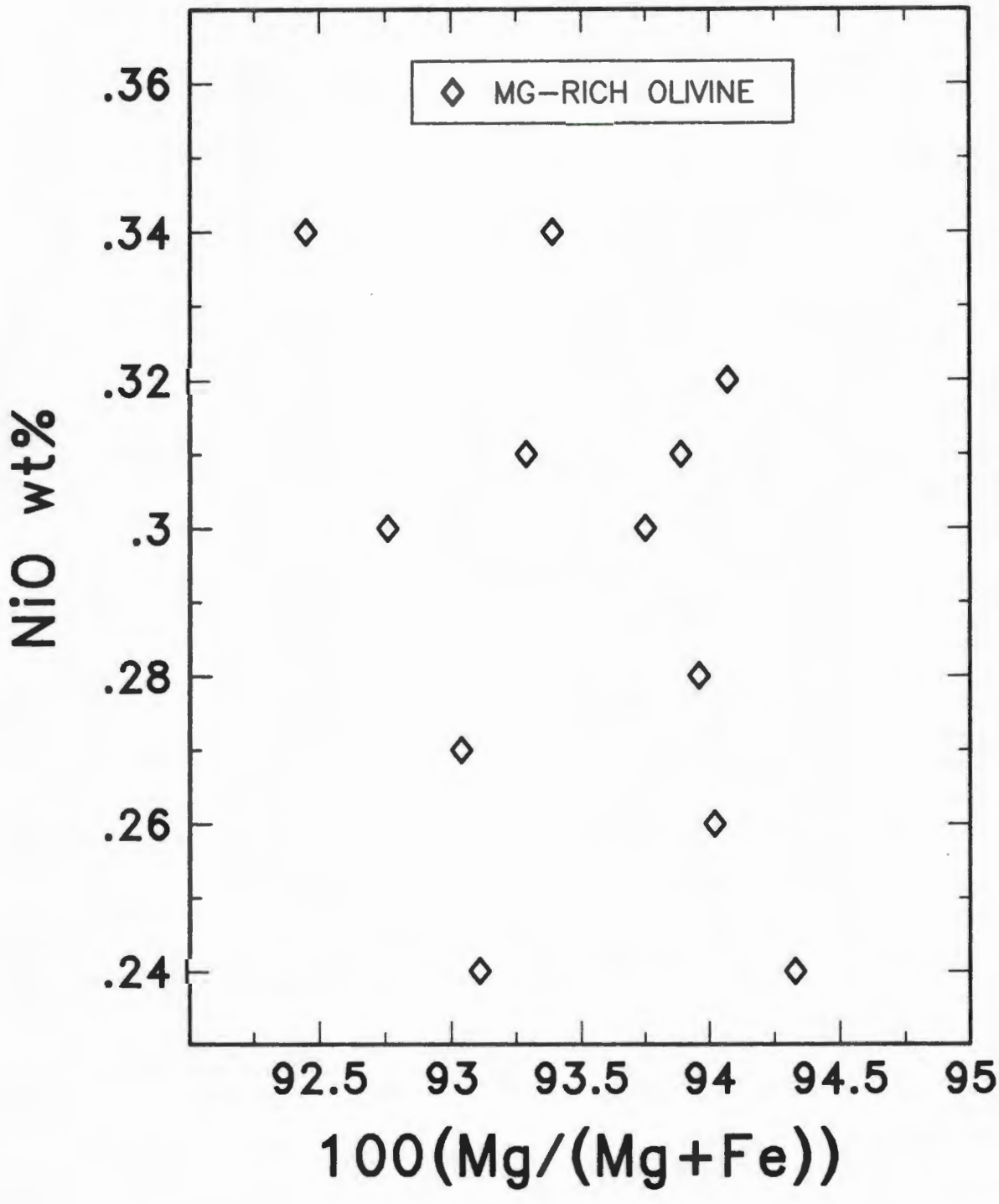

3.4 Discussion

It was initially suggested, on the basis of studies from a number of southern African localities, that the Cr-poor megacrysts and the high-temperature deformed peridotites had similar mineral compositions (Boyd and Nixon, 1973b). Slight differences are however apparent. In particular, the Fe contents of minerals in the megacryst suite are usually higher than those in the corresponding minerals in the high-temperature deformed peridotites. This feature can be well illustrated for the Cr-poor megacrysts and high-temperature peridotites from Jagersfontein on a Ca-Mg-Fe ternary diagram (Fig. 3.18). In addition, the megacryst minerals generally have lower Cr_2O_3 concentrations than the equivalent minerals in the high-temperature peridotites (Fig. 3.19).

Na_2O and TiO_2 concentrations in the high-temperature peridotites generally extend towards the highest values shown by the megacrysts (Fig. 3.20 and 3.21). This is of significance in determining the possible source of the melt responsible for enrichment of the high-temperature peridotites and will be considered further in Chapter 6.

The compositional trends shown by the Cr-poor megacrysts are consistent with fractionation from a magma. Differences in the compositional trends between localities are probably the result of fractionation from a specific magma at each locality. Schulze (1984) noted that the degree of iron enrichment in the fractionating magma was controlled by the fractionating phases. Fractionation of orthopyroxene,

FIGURE 3.18 Ca–Mg–Fe ternary diagram showing Cr-poor megacrysts (open symbols) and high-temperature peridotites (closed symbols) from Jagersfontein

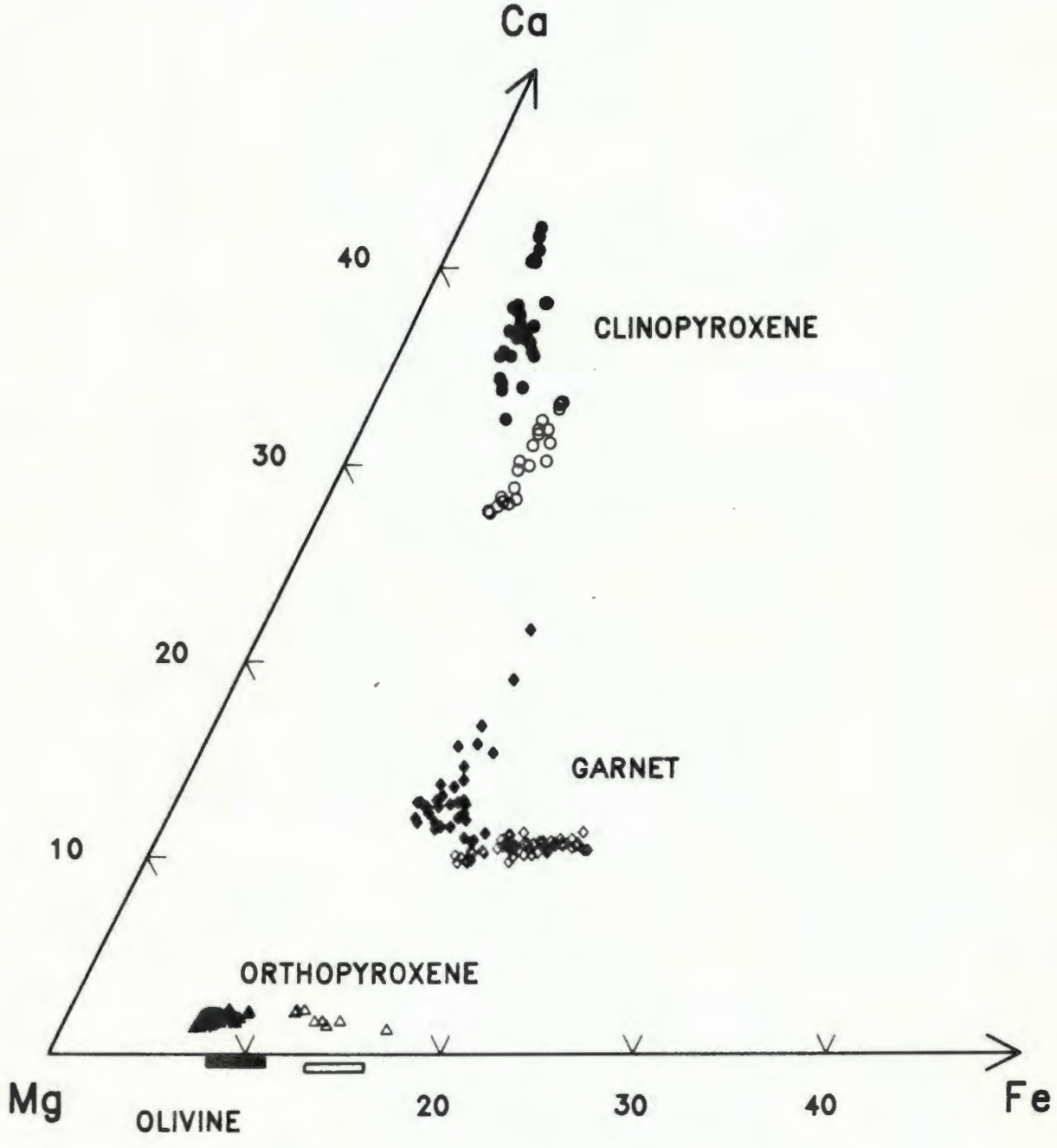

FIGURE 3.19 Mg# versus Cr_2O_3 wt% in garnet porphyroclasts from deformed peridotites and in Cr-poor garnet megacrysts from Jagersfontein

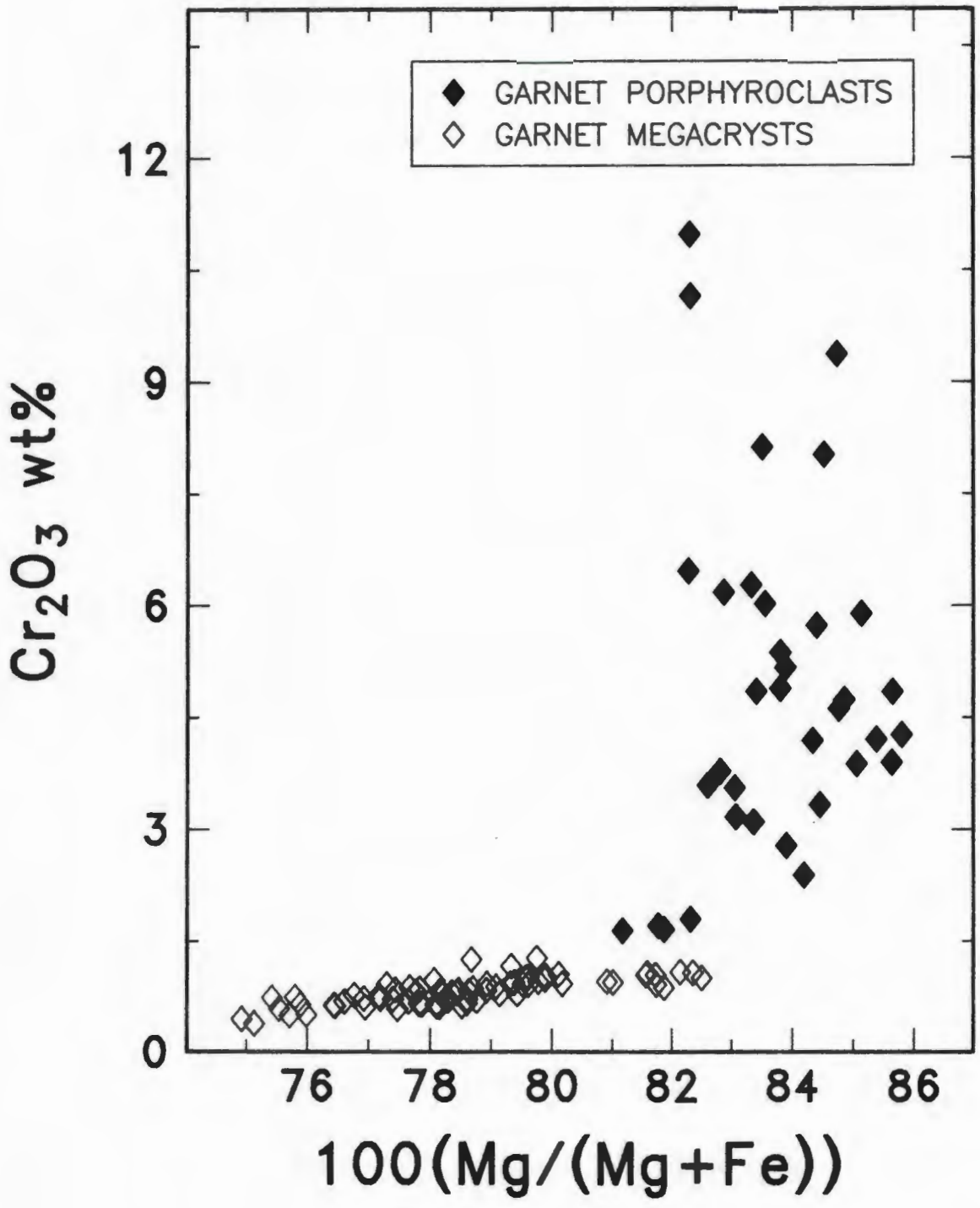

FIGURE 3.20 Mg# versus TiO_2 wt% in garnet porphyroclasts from deformed peridotites and in Cr-poor garnet megacrysts from Jagersfontein

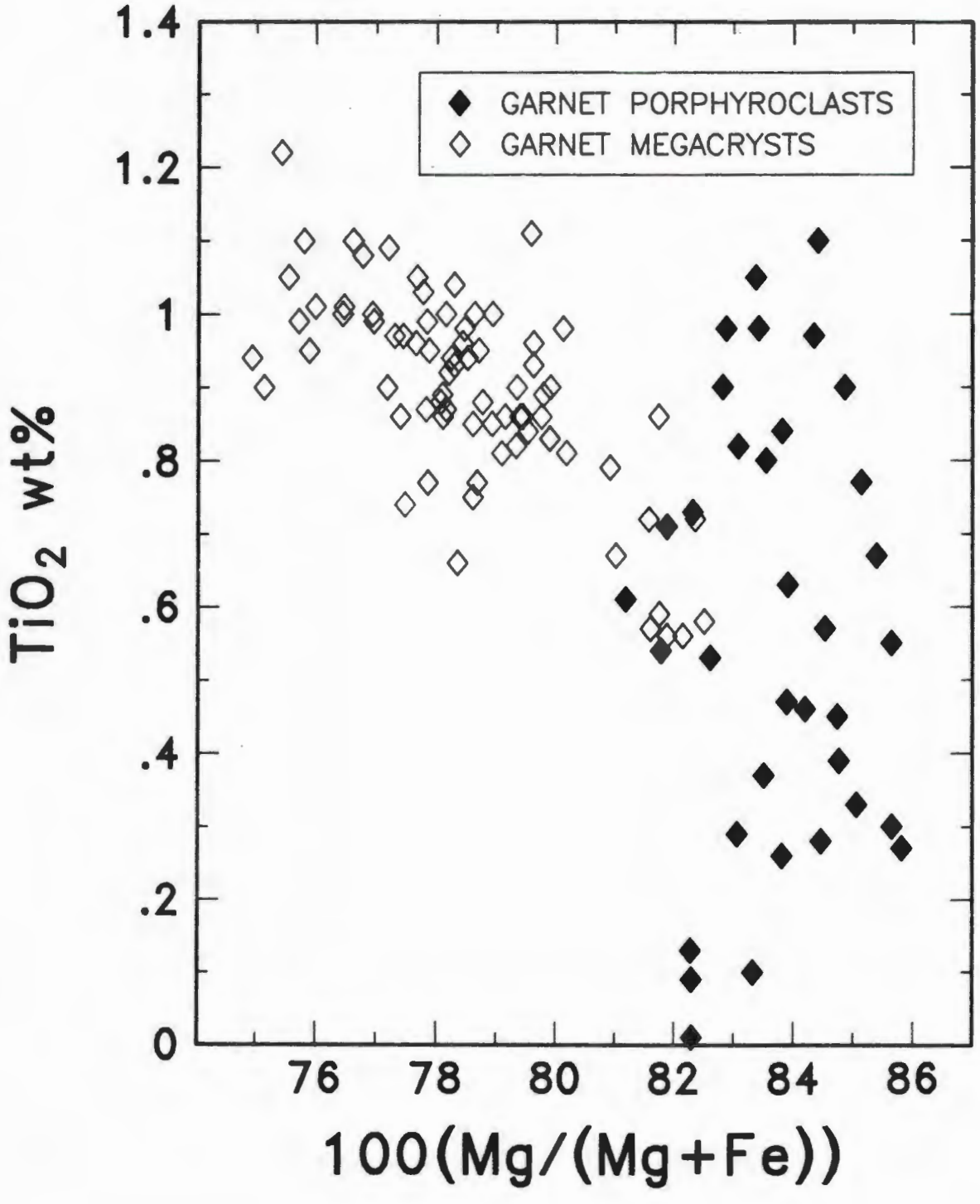

FIGURE 3.21 **Ca# versus Na_2O wt% in clinopyroxene porphyroclasts from deformed peridotites and in Cr-poor clinopyroxene megacrysts from Jagersfontein**

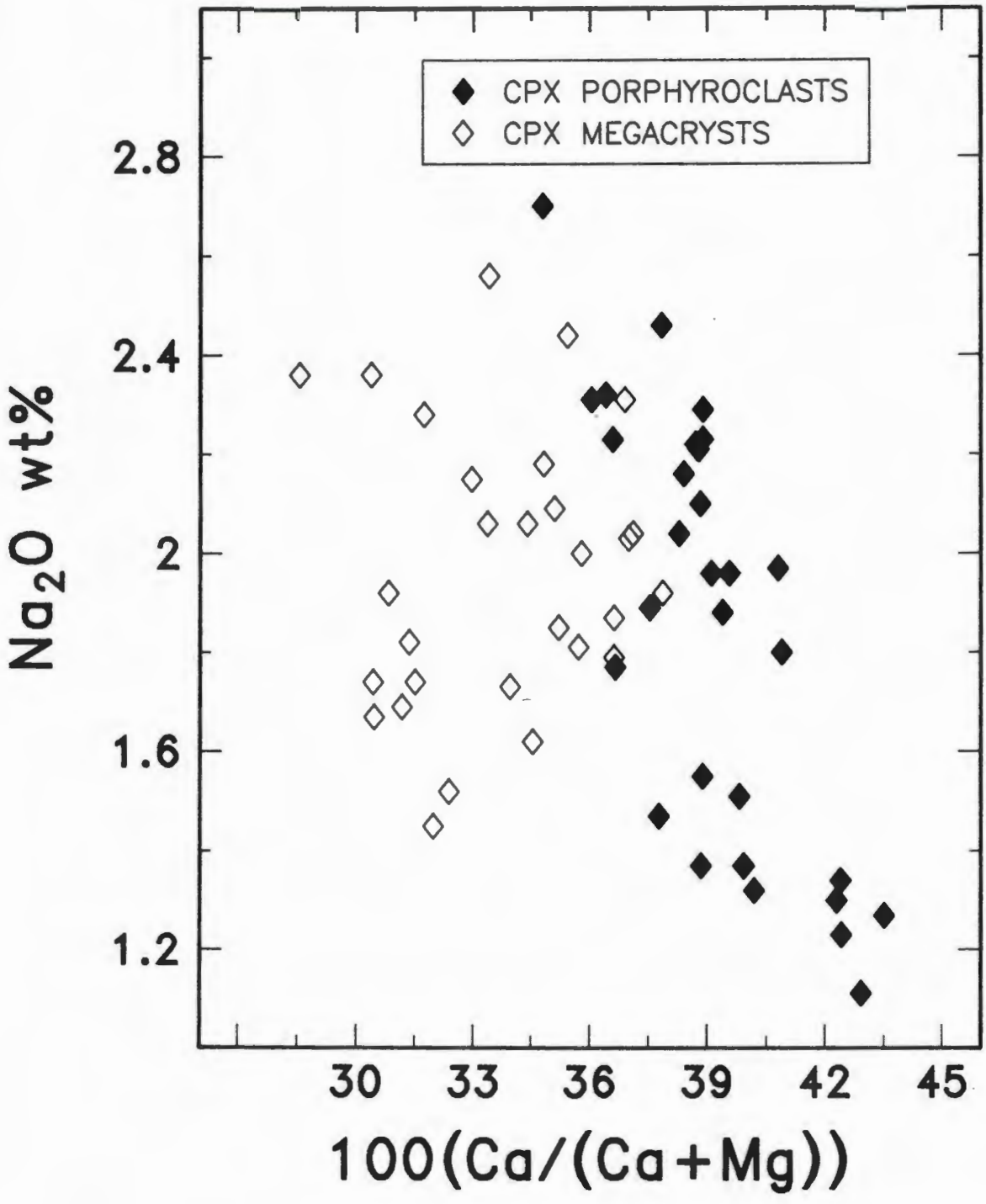

olivine or clinopyroxene (with Fe/Mg K_D's of approximately 0.4, 0.4 and 0.5 respectively), will deplete the liquid in Mg relative to Fe, whereas fractionation of garnet (Fe/Mg K_D = 0.9) will only slightly deplete the liquid in Mg. In contrast, fractionation of ilmenite (Fe/Mg K_D = 4.3) will dramatically decrease the Fe/Mg ratio of the residual liquid. Ilmenite is not found associated with the Cr-poor megacryst suite at Jagersfontein and iron enrichment of the fractionating magma is therefore expected.

A model for the formation of the Cr-poor megacryst suite will be considered in more detail in Chapter 6.

The Granny Smith clinopyroxenes at Jagersfontein are compositionally distinct from the Cr-poor clinopyroxene megacrysts. In addition the compositions of the Granny Smith clinopyroxenes are not consistent with fractionation from a magma. Some mixing (assimilation and fractional crystallization) of the fractionating magma with the lithospheric wallrock might result in the observed compositions. Boyd et al. (1984a) and Jones (1987) have noted the marked compositional similarities between the Granny Smith xenoliths and glimmerites. Glimmerites are not a common feature at Kimberley or Jagersfontein, but it is possible that the Granny Smith megacrysts might represent disaggregated glimmerites.

CHAPTER 4

GEOTHERMOMETRY AND GEOBAROMETRY

4.1 INTRODUCTION

Mineral compositions are influenced to varying degrees by ambient conditions such as pressure and temperature. In an equilibrium mineral assemblage this allows the calculation of the pressure and/or temperature of equilibration, which is then subject to various geological interpretations.

Extensive experimental studies simulating chemical compositions of coexisting peridotite minerals have been carried out in order to evaluate the conditions of equilibration of mantle-derived xenoliths. These experiments are usually performed in simple pure systems such as MAS, CMS and CFMAS (where the acronyms refer to CaO, FeO, MgO, Al_2O_3 and SiO_2). Potentially significant errors are therefore introduced by disregarding the effects of elements such as Cr, Na and Ti which may be components of natural mantle minerals.

In the study of mantle-derived xenoliths the most regularly applied geothermometers utilize either (a) the diopside-enstatite solvus, (b) Fe-Mg exchange between garnet and clinopyroxene or (c) Fe-Mg exchange between garnet and olivine. Of these, the pyroxene solvus geothermometer is considered the most reliable, but its application is restricted to two pyroxene xenoliths. Both the Fe-Mg exchange thermometers lose precision because of the unknown

contribution of Fe^{3+}, but are useful where mineral assemblages do not include both orthopyroxene and clinopyroxene. The geothermometer based on the Fe-Mg exchange reaction between garnet and olivine is particularly applicable to garnet harzburgites. Boyd and Finnerty (1980) noted however, that calculated temperatures of equilibration of garnet lherzolite xenoliths were on average 75-100°C lower, using the Fe-Mg exchange thermometer, than those obtained using the pyroxene solvus thermometer for the same xenolith.

The Al content of orthopyroxene in equilibrium with garnet is to date the only reaction which has proved useful as a geobarometer for mantle xenoliths. Analytical problems with low levels of Al in orthopyroxene and imprecision of the temperature estimate (an overestimation of temperature will cause a pressure overestimation and vice versa) lead to errors in the pressure estimations of all calibrations. Harley (1984) suggested that high pressure errors may be of the order of approximately 10 kbar.

Temperature and pressure estimates obtained by using different calibrations of the above reactions on the same xenolith may disagree by hundreds of degrees and tens of kilobars, so that several sometimes incompatible interpretations regarding mantle stratigraphy or local compositional heterogeneities can be justified from the same xenolith suite. In an attempt to determine which of the calibrations would provide the most applicable results,

several reviewers (Carswell and Gibb, 1980,1987; Mitchell et al., 1980; Finnerty and Boyd, 1984,1987) have evaluated the results obtained by a number of different calibrations.

In their initial evaluation, Carswell and Gibb (1980) concluded that an average of five `best' methods would provide the most reliable temperature estimate. The methods that Carswell and Gibb (op cit.) chose were: the Wells (1977) and Mori and Green (1978) equations for the diopside-enstatite solvus; the Ellis and Green (1979) and Mori and Green (1978) equations for Fe-Mg exchange between garnet and clinopyroxene; and the O'Neill and Wood (1979) equation for Fe-Mg exchange between garnet and olivine.

In contrast, Finnerty and Boyd (1984) considered that such an averaging would produce a less accurate result than a well chosen single calibration. In their evaluation, Finnerty and Boyd (op cit.) tested the accuracy of various geothermobarometers by determining whether the calculated pressure/temperature values of certain xenoliths were in agreement with petrological constraints. In particular, they chose the diamond-graphite univariant reaction (Kennedy and Kennedy, 1976) and the phlogopite stability field (Eggler and Wendlandt, 1979). Finnerty and Boyd (1984) concluded that the combination of Lindsley and Dixon's (1976) pressure uncorrected 20 kbar pyroxene solvus with Macgregor's (1974) Al-enstatite barometer produced calculated pressure/temperature estimates which met the

necessary petrological constraints. Finnerty and Boyd (op cit.) recommended the O'Neill and Wood (1979) calibration as the most reliable geothermometer for garnet harzburgites.

In their revised evaluation, Finnerty and Boyd (1986) still consider the Macgregor (1974) barometer as the most applicable to mantle xenoliths, but they use an empirical fit of the diopside limb of the pyroxene miscibility gap corrected for the pressure effect calibrated by Nickel and Brey (1984) as the most applicable thermometer.

In their revised evaluation, Carswell and Gibb (1987) chose an approach which tested the ability of the different thermometer and barometer calibrations to reproduce the experimental P-T equilibration conditions of `natural' multi-component garnet lherzolite assemblages. They concluded that no single temperature formulation was reliable throughout the P-T range of interest, but that the Nickel and Green (1985) barometer was the most satisfactory pressure formulation.

Recent calibrations which have not been evaluated by the above authors include a thermometer based on the solubility of the enstatite component in coexisting clinopyroxene and orthopyroxene (Bertrand and Mercier, 1985), and a barometer based on aluminium exchange between enstatite and garnet (Bertrand et al., 1986).

There is at present little or no consensus as to which geothermobarometric calibrations to use and at this stage it

is still a case of individual preferences. The choice of preferred thermobarometric pair in this study was based on a combination of requirements. The thermometer and barometer had to take the possible effects of minor elements into consideration as well as fit the petrological constraints determined by Finnerty and Boyd (1984,1987). The thermobarometric pair which appears to best fit these requirements is that of Bertrand and Mercier (1985) versus Nickel and Green (1985).

4.2 GEOTHERMOBAROMETRY OF THE DEFORMED PERIDOTITE XENOLITHS

Estimates of the temperatures and pressures of equilibration of the deformed peridotite xenoliths and J117 were calculated using average values determined for the coexisting minerals (olivine + orthopyroxene + garnet + clinopyroxene) in each xenolith. In the case of the deformed peridotites with garnet zonation, rim compositions were used, as these were considered to be in equilibrium with the surrounding minerals. The mineral compositions are presented in Appendix 3.

Calculations were determined using either the computer program TEMPEST (Finnerty and Boyd, 1984,1987) which solves geothermometers and geobarometers simultaneously, or equations presented in recent journals for those geothermobarometers not on the version of TEMPEST available at U.C.T.

Temperatures and pressures were calculated using the Nickel and Green (1985) (NG85) and Bertrand and Mercier (1985) (BM85) geothermobarometer. This geothermobarometric pair yields estimates in the range 1132-1361 ^{o}C and 48-54 kbar (Fig. 4.1 and Appendix 5). It appears that the xenoliths were sampled from essentially a single depth (corresponding to 160-180 km) even though they show a large range in temperature. This is identical to the pressure range determined by Nickel and Green (1985) for a collection of high-temperature peridotite xenoliths from various southern African localities.

The coarse xenolith (J117) yields a temperature estimate of 1332 ^{o}C which is close to the highest temperature of equilibration of the deformed peridotites. The xenoliths plot in the diamond stability field and deviate to the high-temperature side of the steady state continental geotherm calculated by Pollack and Chapman (1977) for a heatflow of 40 mW/m^{2}. Evidence for recent changes in equilibration conditions of the high-temperature peridotites is shown by a clinopyroxene inclusion in a garnet porphyroclast. This clinopyroxene inclusion yields a temperature of 1193 ^{o}C, which is 75 ^{o}C lower than the temperature calculated for clinopyroxene porphyroclasts in the same garnet lherzolite (JJH 34). A correlation between the degree of deformation and the temperature of equilibration is also apparent; the lowest temperature xenoliths have porphyroclastic textures, while the higher temperature xenoliths have mosaic-porphyroclastic textures (Table 5).

FIGURE 4.1 Temperatures (BM85) and pressures (NG85) of garnet lherzolites from Jagersfontein. Dashed lines indicate the graphite/diamond stability field of Kennedy and Kennedy (1976) and the 40mW/m^2 conductive geotherm of Pollack and Chapman (1977)

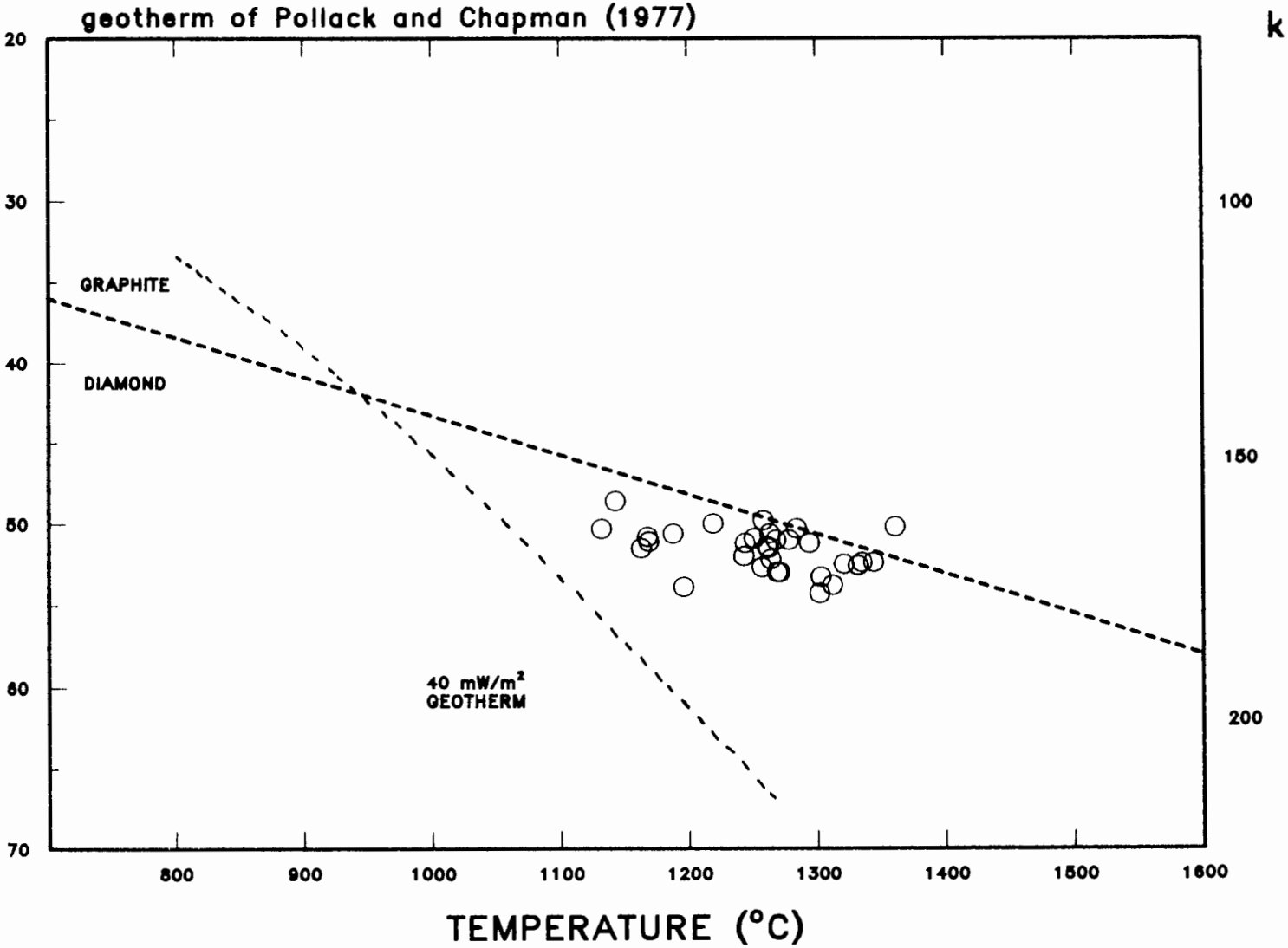

TABLE 5

TEXTURES AND TEMPERATURES OF THE PERIDOTITE XENOLITHS

SAMPLE NO.	TEXTURE	T (°C) (BM85)	P (kbar) (NG85)
JJH 35	PORPHYROCLASTIC	1132	50.3
JJH 1	PORPHYROCLASTIC	1143	48.6
JJH 14	PORPHYROCLASTIC	1163	51.5
JJH 17	PORPHYROCLASTIC	1168	50.8
JJH 33	PORPHYROCLASTIC	1169	51.1
JJH 28	PORPHYROCLASTIC	1188	50.6
JJG 1729	PORPHYROCLASTIC	1196	53.9
JJH 26	MOSAIC	1219	50.0
JJH 20	FLUIDAL MOSAIC	1243	52.0
JJH 2	FLUIDAL MOSAIC	1244	51.2
JJH 10	MOSAIC	1251	50.9
JJH 8	MOSAIC	1257	52.7
JJH 38	MOSAIC	1258	49.8
JJH 13	MOSAIC	1261	51.4
JJH 4	FLUIDAL MOSAIC	1262	51.5
JJH 3	MOSAIC	1263	50.6
JJH 32	MOSAIC	1264	52.2
JJH 34	LAMINAR MOSAIC	1268	51.0
JJH 18	FLUIDAL MOSAIC	1269	53.0
JJG 1710	FLUIDAL MOSAIC	1271	53.0
JJH 37	MOSAIC	1278	51.0
JJG 1798	MOSAIC	1284	50.3
JJG 1753	MOSAIC	1294	51.2
JJH 36	MOSAIC	1302	54.3
JJH 15	MOSAIC	1303	53.3
JJH 11	MOSAIC	1312	53.8
JJH 12	MOSAIC	1321	52.5
J 117	COARSE	1332	52.6
JJH 7	MOSAIC	1335	52.4
JJG 1713	MOSAIC	1344	52.4
JJH 31	MOSAIC	1361	50.2

MOSAIC = MOSAIC PORPHYROCLASTIC
FLUIDAL MOSAIC = FLUIDAL MOSAIC PORPHYROCLASTIC
LAMINAR MOSAIC = LAMINAR MOSAIC PORPHYROCLASTIC

BM85 - Bertrand and Mercier, 1985
NG85 - Nickel and Green, 1985

Temperatures of equilibration of the garnet harzburgites were obtained using a thermometer based on the Fe/Mg exchange between garnet and olivine. In order to compare the relative temperatures and pressures of the garnet lherzolites and garnet harzburgites, estimates of temperatures and pressures of equilibration should be determined for all the xenoliths with a single geothermobarometric pair. As the harzburgites have no clinopyroxene the O'Neill and Wood (1979) (OW79) versus Nickel and Green (1985) geothermobarometer (Fig. 4.2 and Appendix 5) was chosen. This calibration, excluding one anomalous sample, yields a broad P-T range with temperatures of 1058-1336 ^{o}C and pressures of 41-59 kbar. This greater range in temperature, but particularly pressure, is possibly associated with the uncertainty introduced by assuming there is no Fe^{3+}. It could also be a reflection of disequilibrium indicated by the garnet zonation. The anomalous sample (JJG 1729) has an exceptionally low calculated temperature and pressure of equilibration (745^{o}C, 28 kbar). No correlation between temperature of equilibration and degree of deformation is apparent for this geothermobarometric pair (Table 6).

In order to compare the deformed peridotites from Jagersfontein with data from Finnerty and Boyd (1987), temperatures and pressures were also calculated using the Finnerty and Boyd (1986) (FB86) versus Macgregor (1974) (MC74) geothermobarometer. This geothermobarometric pair yields estimates in the range 1109-1405 ^{o}C and 53-65 kbar (Fig. 4.3 and Appendix 5). These calculated temperatures

FIGURE 4.2 Temperatures (OW79) and pressures (NG85) of garnet lherzolites and garnet harzburgites from Jagersfontein. Dashed lines as in Fig.4.1

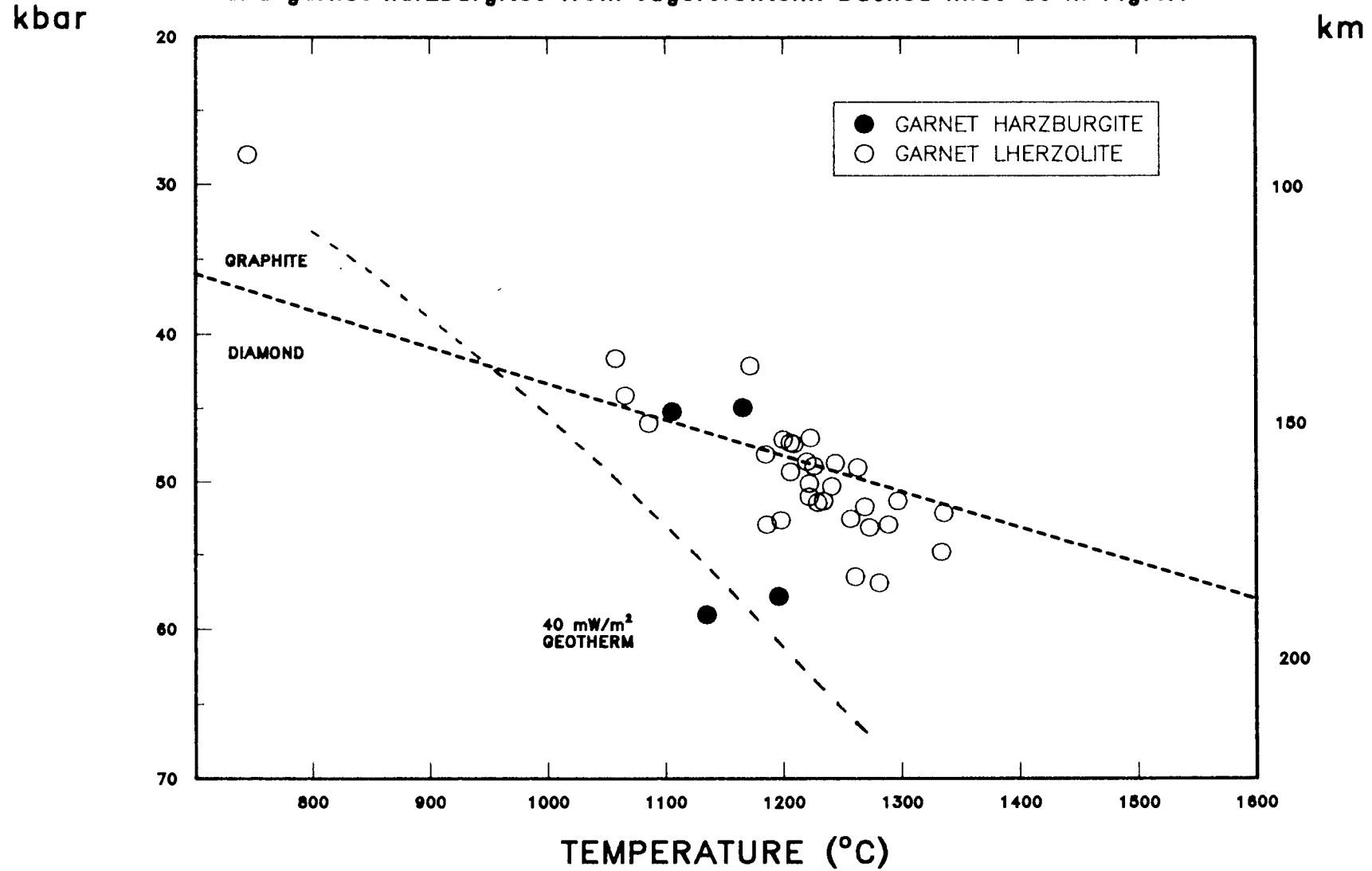

TABLE 6

TEXTURES AND TEMPERATURES OF THE PERIDOTITE XENOLITHS

SAMPLE NO.	TEXTURE	T (°C) (OW79)	P (kbar) (NG85)
JJG 1729	PORPHYROCLASTIC	745	28.0
JJH 4	FLUIDAL MOSAIC	1058	41.6
JJH 28	PORPHYROCLASTIC	1066	44.1
JJH 1	PORPHYROCLASTIC	1086	46.0
JJH 29	MOSAIC	1106	45.2
JJH 6	PORPHYROCLASTIC	1135	59.0
JJH 19	MOSAIC	1166	44.9
JJH 31	MOSAIC	1172	42.1
JJH 35	PORPHYROCLASTIC	1179	52.9
JJH 26	MOSAIC	1185	48.1
JJH 9	PORPHYROCLASTIC	1196	57.8
JJH 33	PORPHYROCLASTIC	1198	52.6
JJH 37	MOSAIC	1200	47.1
JJH 2	FLUIDAL MOSAIC	1206	49.3
JJG 1798	MOSAIC	1206	47.3
JJH 38	MOSAIC	1209	47.4
JJH 3	MOSAIC	1220	48.6
JJH 20	FLUIDAL MOSAIC	1222	51.0
JJH 32	MOSAIC	1222	50.1
JJH 7	MOSAIC	1223	47.0
JJH 34	LAMINAR MOSAIC	1226	48.9
JJH 8	MOSAIC	1229	51.4
JJH 18	FLUIDAL MOSAIC	1234	51.3
JJH 11	MOSAIC	1241	50.3
JJG 1753	MOSAIC	1244	48.7
JJH 36	MOSAIC	1257	52.5
JJH 14	PORPHYROCLASTIC	1261	56.5
J 117	COARSE	1263	49.0
JJH 13	MOSAIC	1269	51.7
JJG 1710	FLUIDAL MOSAIC	1273	53.1
JJH 17	PORPHYROCLASTIC	1281	56.9
JJH 10	MOSAIC	1289	52.9
JJH 12	MOSAIC	1297	51.3
JJH 15	MOSAIC	1334	54.8
JJG 1713	MOSAIC	1336	52.1

MOSAIC = MOSAIC PORPHYROCLASTIC
FLUIDAL MOSAIC = FLUIDAL MOSAIC PORPHYROCLASTIC
LAMINAR MOSAIC = LAMINAR MOSAIC PORPHYROCLASTIC

OW79 - O'Neill and Wood, 1979
NG85 - Nickel and Green, 1985

FIGURE 4.3 Temperatures (FB86) and pressures (MC74) of garnet lherzolites from Jagersfontein. Dashed lines as in Fig.4.1

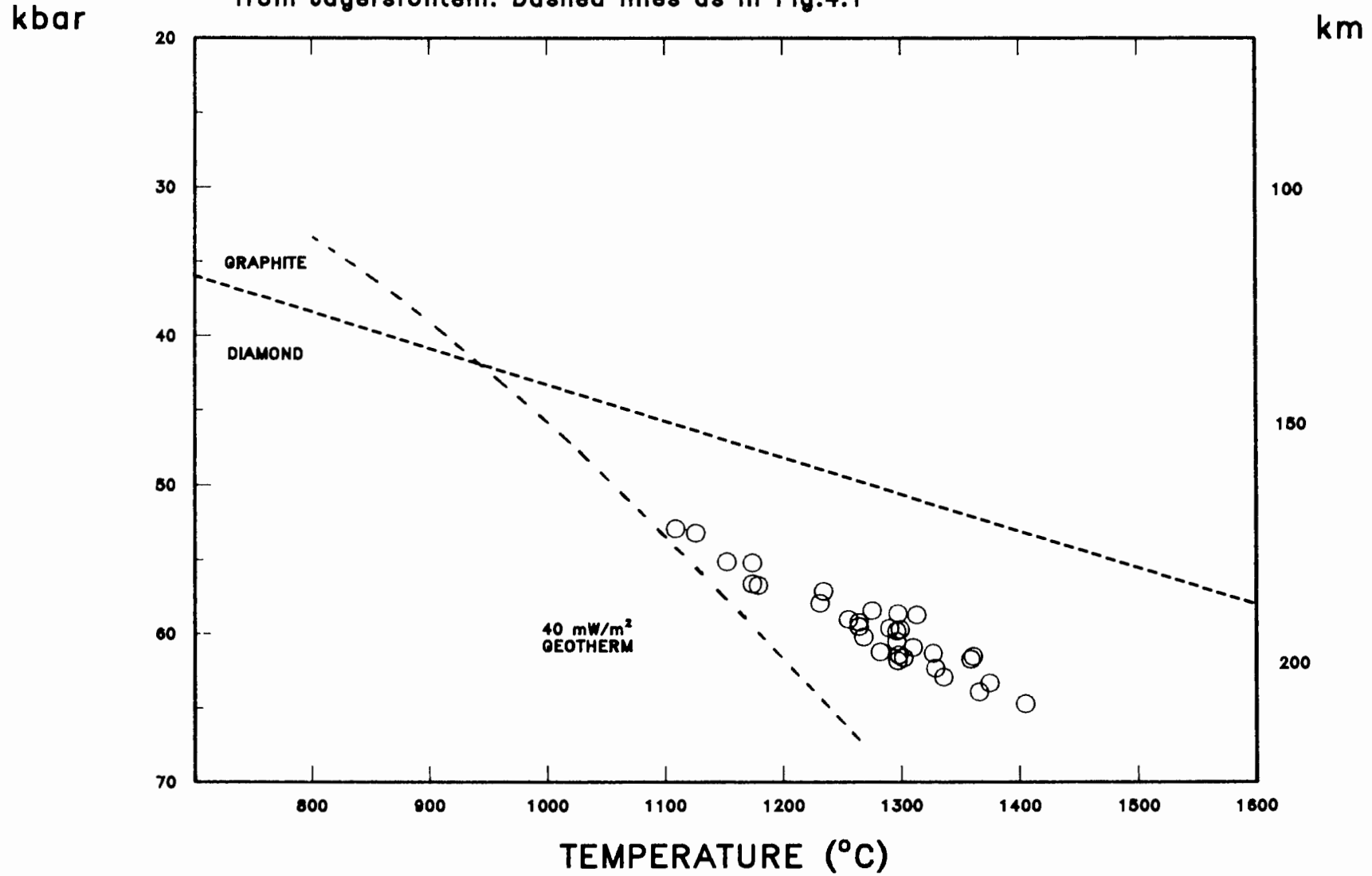

are very similar to those obtained using the Bertrand and Mercier (1985) thermometer (Fig. 4.4). The xenoliths all plot in the diamond stability field and are displaced to the high-temperature side of the steady state continental geotherm calculated by Pollack and Chapman (1977) for a heatflow of 40 mW/m^2. A similar correlation between the temperature of equilibration and the degree of deformation obtained for the Bertrand and Mercier (1986) calibration is shown by the Finnerty and Boyd (1986) calibration (Table 7).

Using the Finnerty and Boyd (1986) versus Macgregor (1974) geothermobarometric pair the xenoliths define a trend of increasing temperature of equilibration with increasing depth of equilibration. This illustrates the importance of the calibration of the geobarometer. Using the preferred Nickel and Green (1985) barometer the high-temperature xenoliths indicate a more restricted depth of equilibration and there is no correlation between this depth and the equilibration temperature. Apart from the differences in range of equilibration pressures, the pressures obtained using the Nickel and Green (1985) barometer are also 5-10 kbar lower than those of the Macgregor (1974) calculations. This is a result of the combined effects of the absence of Fe, Ca, Cr and Na in the Macgregor (1974) calculation, which cause pressures to be overestimated (Carswell and Gibb, 1987).

FIGURE 4.4 Temperatures of equilibration calculated for garnet lherzolites from Jagersfontein with FB87 and BM85 thermometers

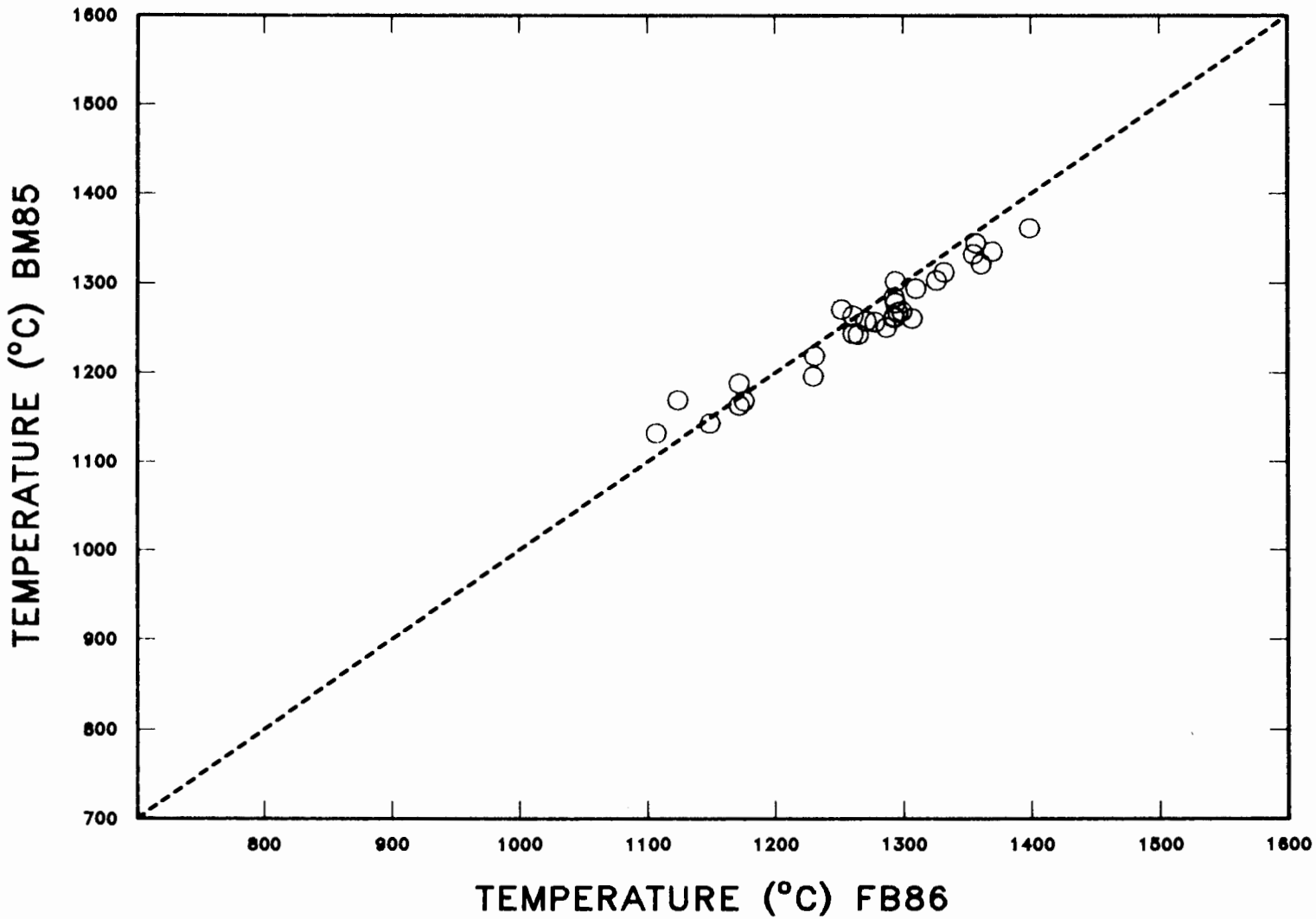

TABLE 7

TEXTURES AND TEMPERATURES OF THE PERIDOTITE XENOLITHS

SAMPLE NO.	TEXTURE	T (°C) (FB86)	P (kbar) (MC74)
JJH 35	PORPHYROCLASTIC	1109	52.9
JJH 33	PORPHYROCLASTIC	1126	53.2
JJH 1	PORPHYROCLASTIC	1152	55.1
JJH 14	PORPHYROCLASTIC	1174	56.6
JJH 28	PORPHYROCLASTIC	1174	55.2
JJH 17	PORPHYROCLASTIC	1179	56.7
JJG 1729	PORPHYROCLASTIC	1231	57.9
JJH 26	MOSAIC	1234	57.1
JJG 1710	FLUIDAL MOSAIC	1255	59.0
JJH 32	MOSAIC	1264	59.2
JJH 2	FLUIDAL MOSAIC	1264	59.5
JJH 20	FLUIDAL MOSAIC	1268	60.2
JJH 38	MOSAIC	1275	58.4
JJH 8	MOSAIC	1282	61.2
JJH 10	MOSAIC	1290	59.6
JJH 4	FLUIDAL MOSAIC	1296	60.5
JJH 3	MOSAIC	1296	59.8
JJH 36	MOSAIC	1297	61.8
JJH 37	MOSAIC	1297	58.6
JJG 1798	MOSAIC	1298	61.4
JJH 34	LAMINAR MOSAIC	1299	59.7
JJH 18	FLUIDAL MOSAIC	1302	61.6
JJH 13	MOSAIC	1310	60.9
JJG 1753	MOSAIC	1313	58.7
JJH 30	MOSAIC	1327	61.3
JJH 15	MOSAIC	1329	62.3
JJH 11	MOSAIC	1336	62.9
J 117	COARSE	1359	61.7
JJG 1713	MOSAIC	1361	61.5
JJH 12	MOSAIC	1366	63.9
JJH 7	MOSAIC	1375	63.3
JJH 31	MOSAIC	1405	64.7

MOSAIC = MOSAIC PORPHYROCLASTIC
FLUIDAL MOSAIC = FLUIDAL MOSAIC PORPHYROCLASTIC
LAMINAR MOSAIC = LAMINAR MOSAIC PORPHYROCLASTIC

FB86 - Finnerty and Boyd, 1986
MC74 - MacGregor, 1974

4.3 GEOTHERMOBAROMETRY OF THE MEGACRYST SUITE

Application of geothermometric calculations to the megacryst suite is limited by the fact that the nodules of the megacryst suite are usually monomineralic crystals. Before the geothermometers can be validly used, it is essential to define which of the megacrysts were coexisting phases in equilibrium in the mantle. Some megacryst suites define such simple compositional trends that the coexisting phases can be inferred with confidence (eg. Jakob, 1977). Direct confirmatory evidence of these interpretations can be obtained from rare examples of megacrysts that host other mineral inclusions.

Mineral compositions indicate that equilibrium conditions have been established between the coprecipitating silicate phases at Jagersfontein. It should therefore be possible to obtain a rough estimate of the range of temperatures and pressures of equilibration of the megacrysts by inferring equilibrium between the appropriate high, intermediate and low temperature megacrysts which do not host coexisting phases.

Results of a comparative study on the deformed peridotites, which showed that the temperatures obtained using the Boyd and Nixon (1973a), Lindsley and Dixon (1976, 20 kbar) (LD76) and Bertrand and Mercier (1986) thermometers were essentially equivalent in this temperature range, suggest that comparisons between these equilibration temperatures may be valid.

Temperatures of equilibration of the Cr-poor orthopyroxene megacrysts were calculated using the Ca/(Ca+Mg) thermometer of Boyd and Nixon (1973a), an empirical thermometer calibrated from coexisting Cr-poor orthopyroxenes and clinopyroxenes in Lesotho xenoliths. These temperatures range from 1190 to 1340 ^{o}C. The temperature estimates calculated using the Lindsley and Dixon (1976, 20 kbar) calibration indicate that the discrete subcalcic clinopyroxene megacrysts crystallized over a temperature range of 1314 to 1442 ^{o}C. This range does not extend to temperatures as low as those found in the Monastery suite (Jakob, 1977) where the clinopyroxene-ilmenite lamellar intergrowths crystallize at lower temperatures.

Subcalcic clinopyroxenes with garnet inclusions yield equilibration temperatures of 1316-1471 ^{o}C, while garnet megacrysts with subcalcic clinopyroxene inclusions yield equilibration temperatures of 1297-1413 ^{o}C.

It cannot be demonstrated that Granny Smith diopside megacrysts equilibrate in the presence of either orthopyroxene or garnet. This brings into question the validity of temperature estimation as neither the diopside solvus nor Fe-Mg exchange between clinopyroxene and garnet can be shown to be applicable. It is perhaps worth noting that the diopsides have a limited range of calcic compositions that would correspond to a small range of temperatures (at approximately 1000^{o}C) if the diopside solvus were applicable.

Pressure calculations using the Nickel and Green (1985) barometer require orthopyroxene to coexist with garnet. Only one garnet megacryst with coexisting orthopyroxene was found. Tie-lines were drawn parallel to this coexisting pair from high, intermediate and low temperature discrete orthopyroxene megacrysts to garnets and these `mineral pairs' were then assumed to be in equilibrium. Pressure estimates obtained for these megacrysts are essentially isobaric at 52±1 kbar. Since the megacryst garnets are very similar with respect to most major elements, except Mg/Fe, it is unlikely that this assignment of equilibrium pairs introduces large errors into the calculation. The isobaric crystallization of the orthopyroxene megacrysts can be expected from the linear variation of Al_2O_3 with Ca/(Ca+Mg) (Fig. 3.12).

4.4 DISCUSSION

The most frequent application of the pressure and temperature estimates obtained for mantle xenoliths is in the construction of `paleogeotherms'. Irving (1976) stressed that the process of magma generation involves perturbation of the regional mantle geotherm. Any `geotherm' estimated from mantle xenoliths, which might have been influenced by magma generation, can therefore only be meaningful for the highly complex pressure-temperature regime associated with that zone, and cannot be equated with the steady state geotherm in unmodified regions of the mantle. Comparison of the calculated temperature/pressure

estimates for the mantle-derived xenoliths with the steady-state geotherm should therefore indicate any modification in ambient temperature/pressure which might be associated with the kimberlite generation.

Low-temperature peridotite xenoliths from southern African kimberlites plot close to the steady-state geotherm calculated for a continental shield with a heatflow of 40 mW/m^2 (Pollack and Chapman, 1977). The position of the high-temperature peridotites relative to the conductive geotherm is, however, controversial. Finnerty (in press) has shown that based on present interpretations, three scenarios have been advocated: (1) an inflection toward a lower thermal gradient at greater depth (Bertrand et al., 1986); (2) an uninflected geotherm (Carswell and Gibb, 1987) and (3) an inflection to a higher thermal gradient at greater depth (Finnerty and Boyd, 1987). Finnerty (in press) noted that the 'inflections' produced in (1) and (2) were based on erroneous pressure calculations and that the 'inflection' produced in (3) was more likely to represent conditions in the mantle. This 'inflection' is ascribed to a temperature perturbation associated with either the uprise of mantle diapirs/plumes associated with the generation of kimberlite, or in terms of local magma chambers.

The favoured pressure-temperature calibration in this study, (BM85 vs NG85), produces an 'inflection' in which the high-temperature peridotites deviate from the geotherm towards higher temperatures at almost constant depth (Fig. 4.1).

As noted by Gurney et al. (1979) for the Monastery Cr-poor megacrysts, the processes that produce the megacryst mineral suite are most probably igneous. The volume of megacryst minerals in the mantle is probably not very high, certainly a thick layer would be a geophysical marker that has not been noted. The individuality of the megacryst suites at different localities also argues in favour of localized events rather than a pervasive layer throughout the mantle. The results obtained from the BM85 versus NG85 thermobarometer are consistent with a localized thermal perturbation. Use of the pressure-temperature calibration favoured by Finnerty (op cit) (FB86 vs MC74) results in a similar range in temperature, but pressures increase with increasing temperature. This increase of pressure nevertheless still reflects a relatively restricted depth interval.

The depth at which the temperature perturbation associated with the high-temperature deformed peridotites occurs, varies with geographical locality but not with age of the intrusion (MacGregor and Basu, 1974; MacGregor, 1975; Boyd and Nixon, 1979; Mitchell, 1984; Boyd and Gurney, 1986). MacGregor (1975) and Boyd and Gurney (1986) noted that this depth was systematically greater for xenoliths erupted within the boundaries of the Kaapvaal craton than for those erupted in areas peripheral to the craton. They suggested that the regular variation in depth of origin of the high-temperature peridotites might reflect a boundary in physical and perhaps chemical properties in the mantle. Possible critical boundary layers in the upper mantle in this depth

range include the lithosphere-asthenosphere boundary and the peridotite solidus in the presence of volatiles (Wyllie, 1987).

Since they can yield such disparate results, the geothermobarometric calculations do not yield absolute pressures and temperatures. Whatever methods are chosen however, the relative temperatures and pressures of equilibration of the Cr-poor megacrysts and the deformed peridotites at Jagersfontein (Fig. 4.5) show certain common features. There is a wide range of temperature estimates, with the range in temperatures shown by the Cr-poor megacrysts extending to much higher values than those calculated for the deformed peridotites and both appear to have equilibrated in the same pressure (depth) interval in the mantle. This suggests a close spatial association between the Cr-poor megacrysts and the high-temperature peridotites, which in the case of the favoured methods of calculation of equilibration conditions is essentially isobaric.

FIGURE 4.5 Temperatures (BM85) and pressures (NG85) of peridotites and Cr-poor megacrysts from Jagersfontein. Temperatures for megacrysts indicated with arrows and pressure with a bar. Dashed lines as in 4.1

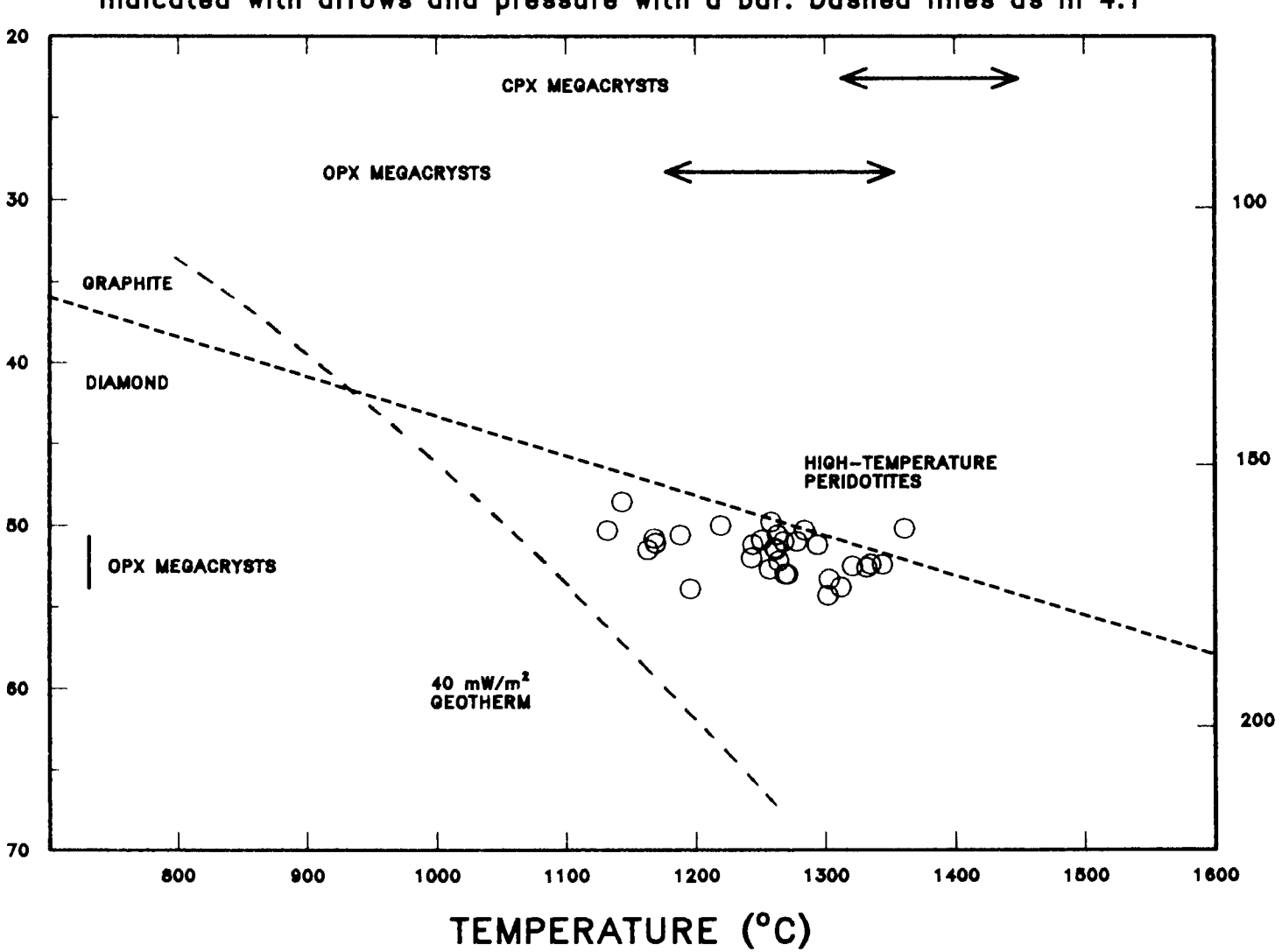

CHAPTER 5

TRACE ELEMENTS AND RADIOGENIC ISOTOPE DATA

5.1 INTRODUCTION

Isotopic studies on peridotite xenoliths from southern Africa have concentrated largely on the coarse low-temperature, deformed low-temperature and modally metasomatized varieties from Kimberley and Matsoku (Barrett, 1975; Shimizu, 1975a; Kramers, 1977,1979; Menzies and Murthy, 1980; Erlank et al., 1982,1987; Richardson et al., 1985). These studies have indicated a wide array of Nd and Sr isotope ratios, evidence of both ancient and recent enrichment in the subcontinental mantle.

Isotopic studies on the high-temperature peridotites have been restricted to a small number of samples from Thaba Putsoa and Premier (Shimizu, 1975a; O'Nions et al., 1978; Basu and Tatsumoto, 1980; Allegre et al., 1982; Richardson et al., 1985). These studies have indicated ratios similar to mid-ocean ridge basalts (MORB) or ocean island basalts (OIB), but very little combined Nd-Sr isotope data have been determined.

Similarly, relatively few isotopic measurements have been determined for the megacryst minerals. Most previous studies encompassed samples from a number of localities (Barrett, 1975; Kramers et al., 1981), and until the work of Jones (1987) little attempt had been made to compare megacrysts from one locality. Previously published data

also lacked major element characterization of the megacryst minerals.

5.1.1 Sample selection

No whole rock analyses were performed in this study because previous studies of peridotite xenoliths (eg. Richardson et al., 1985; Zindler and Jagoutz, 1988) have demonstrated that whole rock $^{87}Sr/^{86}Sr$ and $^{143}Nd/^{144}Nd$ ratios are influenced by the host kimberlite. Analyses were restricted to clinopyroxene and garnet mineral separates because these minerals contain the bulk of the trace elements. These mineral separates were carefully scrutinized for possible contamination before selection for analysis (see Appendix 6 for sample preparation).

Isotopic studies of the high-temperature peridotites should provide information on their lithospheric or asthenospheric origin. In addition, evidence of the enrichment observed in the major elements might be observed in the isotope ratios. Seven high-temperature peridotites, representing the compositional range found at Jagersfontein, were selected for isotopic analysis (Table 8).

Isotopic studies of megacryst minerals are important in determining relationships with their host kimberlite and in characterizing their source. Four Cr-poor clinopyroxenes, three Cr-poor garnets and three Granny Smith megacrysts, representing the compositional range observed in the

TABLE 8

Samples selected for isotope analysis

HIGH-TEMPERATURE PERIDOTITES

Sample	Clinopyroxene Ca#
JJH 35	43.87
JJG 1729	40.90
JJH 26	40.80
JJH 10	39.10
JJG 1753	38.29
JJG 1713	36.58
JJH 12	36.41

CR-POOR CLINOPYROXENE MEGACRYSTS

Sample	Clinopyroxene Ca#
JJH A59	31.35
JJG 1859	34.54
JJH A83	36.99
JJH A95	37.86

CR-POOR GARNET MEGACRYSTS

Sample	Garnet Mg#
JJH B38	77.87
JJH B87	78.10
JJH B53	78.32

GRANNY SMITH CLINOPYROXENES

Sample	Clinopyroxene Ca#
JJG 1869	46.23
JJH A10	46.86
JJH A90	48.70

megacrysts at Jagersfontein, were selected for isotopic analysis (Table 8).

5.2 Sr, Nd AND Sm CONCENTRATIONS

The Sr, Nd and Sm concentrations were measured by isotope dilution mass spectrometry. The samples were all small (see Appendix 7 for sample weights) and measurements were not always successful, necessitating repeat dissolutions for some xenoliths. In most cases there was close agreement between repeat dissolutions, but inhomogeneities were also noted. Concentrations and isotope ratios are presented in Appendix 7.

5.2.1 High-temperature peridotites

The clinopyroxene separates have Sr concentrations which range from 76.5 to 113 ppm, Nd concentrations which range from 2.48 to 6.13 ppm and Sm concentrations which range from 0.26 to 1.69 ppm. This range is exaggerated by the low concentrations of these elements in JJH 35.

No correlation between equilibration temperature and these trace element concentrations was observed, except that JJH 35 has the lowest concentrations and the lowest temperature of equilibration. The clinopyroxene separates are enriched in Nd relative to Sm, with JJH 35 showing the greatest relative enrichment (Fig. 5.1).

FIGURE 5.1 Nd and Sm concentrations in clinopyroxenes from high-temperature peridotites from Jagersfontein. Normalized to chondritic values of Evensen et al. (1978)

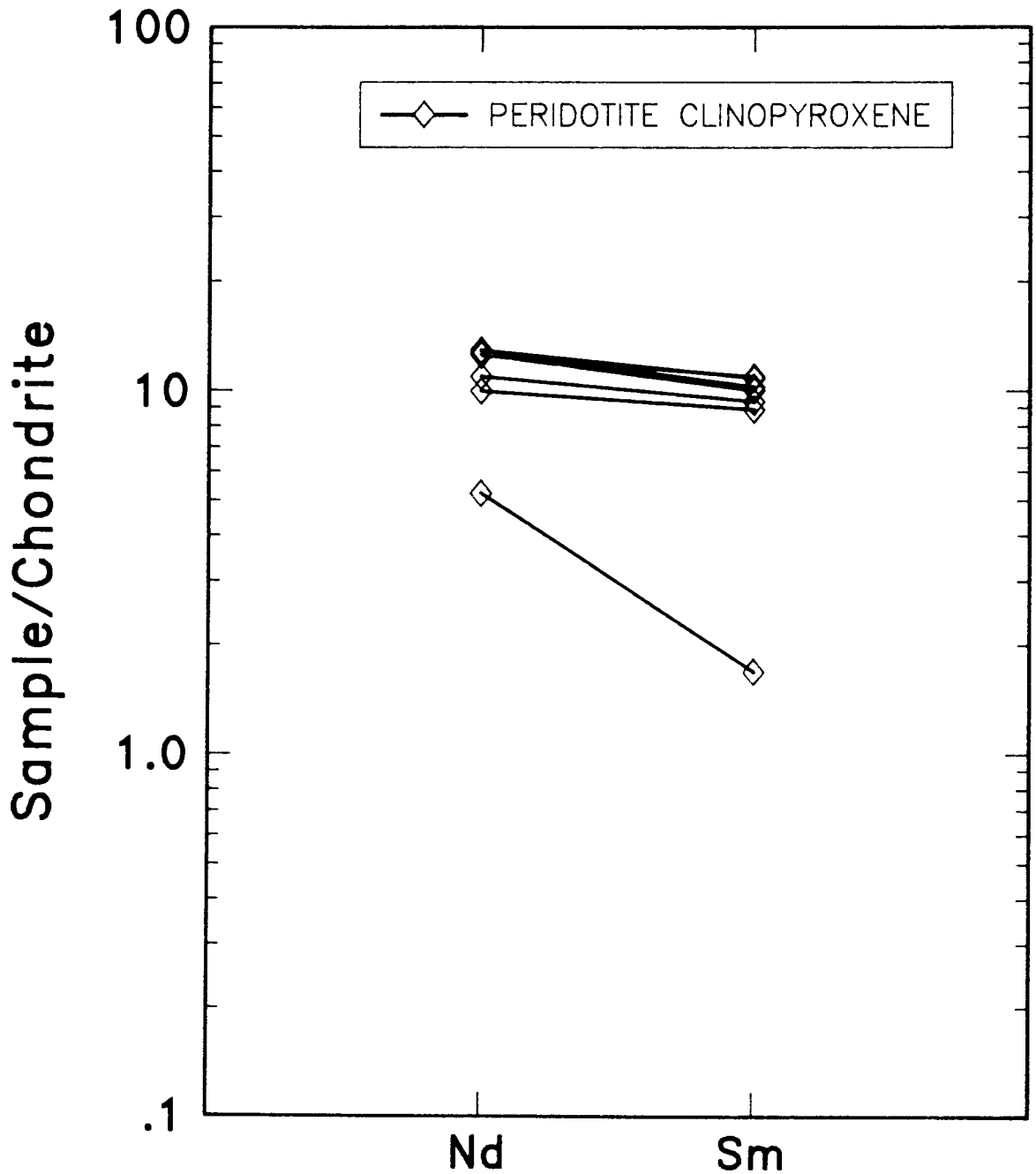

The garnet separates have Sr concentrations which range from 0.35 to 0.89 ppm, Nd concentrations which range from 0.59 to 1.36 ppm and Sm concentrations which range from 0.30 to 1.22 ppm. JJH 35 again has the lowest Sr and Sm concentrations, but not the lowest Nd concentration. The garnet separates are enriched in Sm relative to Nd, the least relative enrichment being shown by JJH 35 (Fig. 5.2).

5.2.2 Megacryst minerals

The Cr-poor clinopyroxene megacrysts have Sr concentrations which range from 76.9 to 106 ppm, Nd concentrations which range from 4.50 to 8.14 ppm and Sm concentrations which range from 1.37 to 2.05 ppm. These clinopyroxene megacrysts show an increase in REE concentration with increasing degree of fractionation and are enriched in Nd relative to Sm (Fig. 5.3).

The Cr-poor garnet megacrysts have Sr concentrations which range from 0.96 to 1.54 ppm, Nd concentrations which range from 0.93 to 1.02 ppm and Sm concentrations which range from 0.75 to 0.94 ppm. Both Nd and Sm concentrations were only measured successfully in JJH B38 and this sample shows an enrichment of Sm relative to Nd (Fig. 5.3).

The Granny Smith clinopyroxenes have higher Sr, Nd and Sm concentrations than the Cr-poor clinopyroxenes. They have Sr concentrations which range from 122 to 201 ppm, Nd concentrations which range from 5.71 to 13.7 ppm and Sm concentrations which range from 1.79 to 3.62 ppm.

FIGURE 5.2 Nd and Sm concentrations in garnets from high-temperature peridotites from Jagersfontein. Normalized to chondritic values of Evensen et al. (1978)

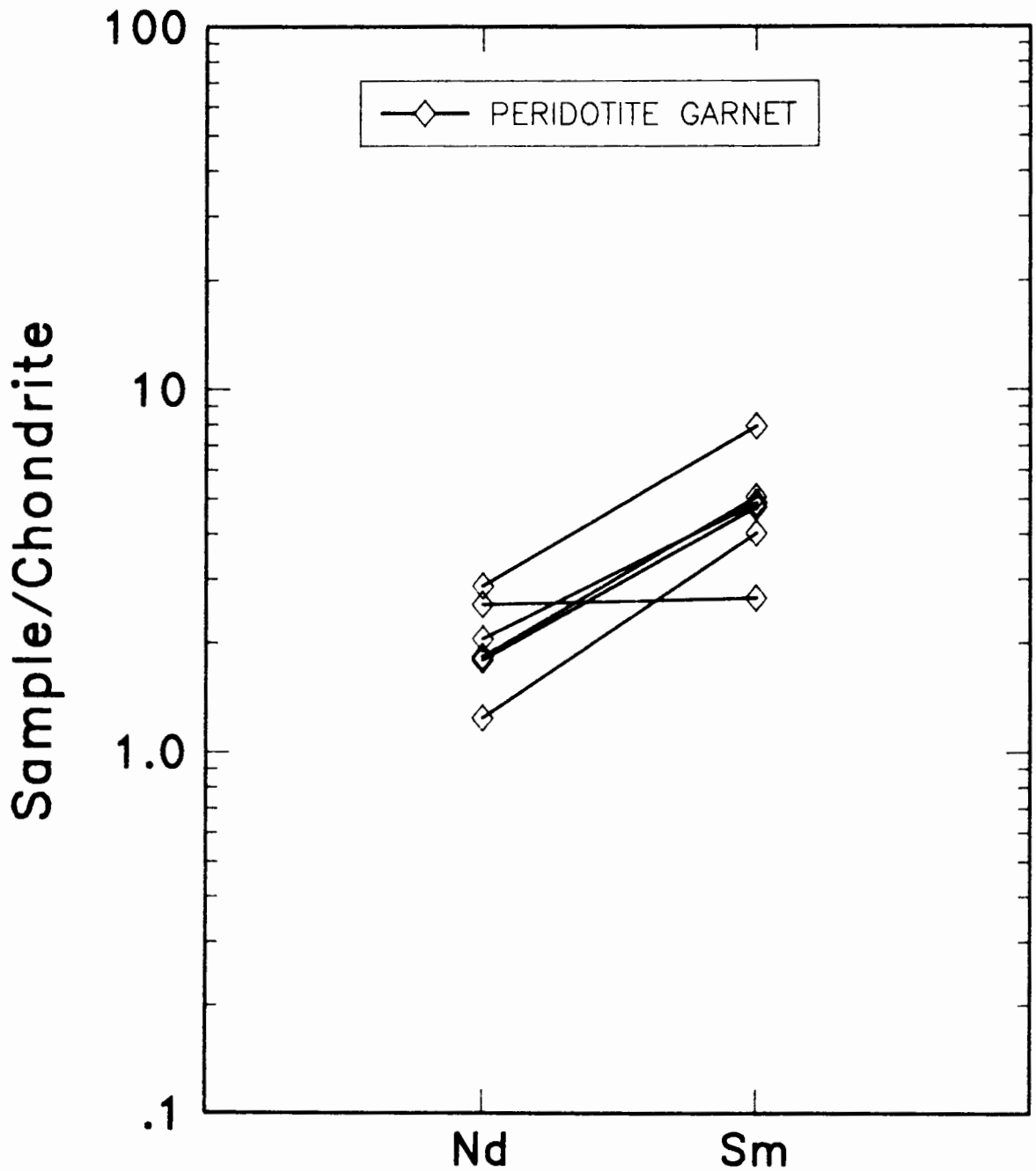

FIGURE 5.3 **Nd and Sm concentrations in megacrysts from Jagersfontein. Normalized to chondritic values of Evensen et al. (1978)**

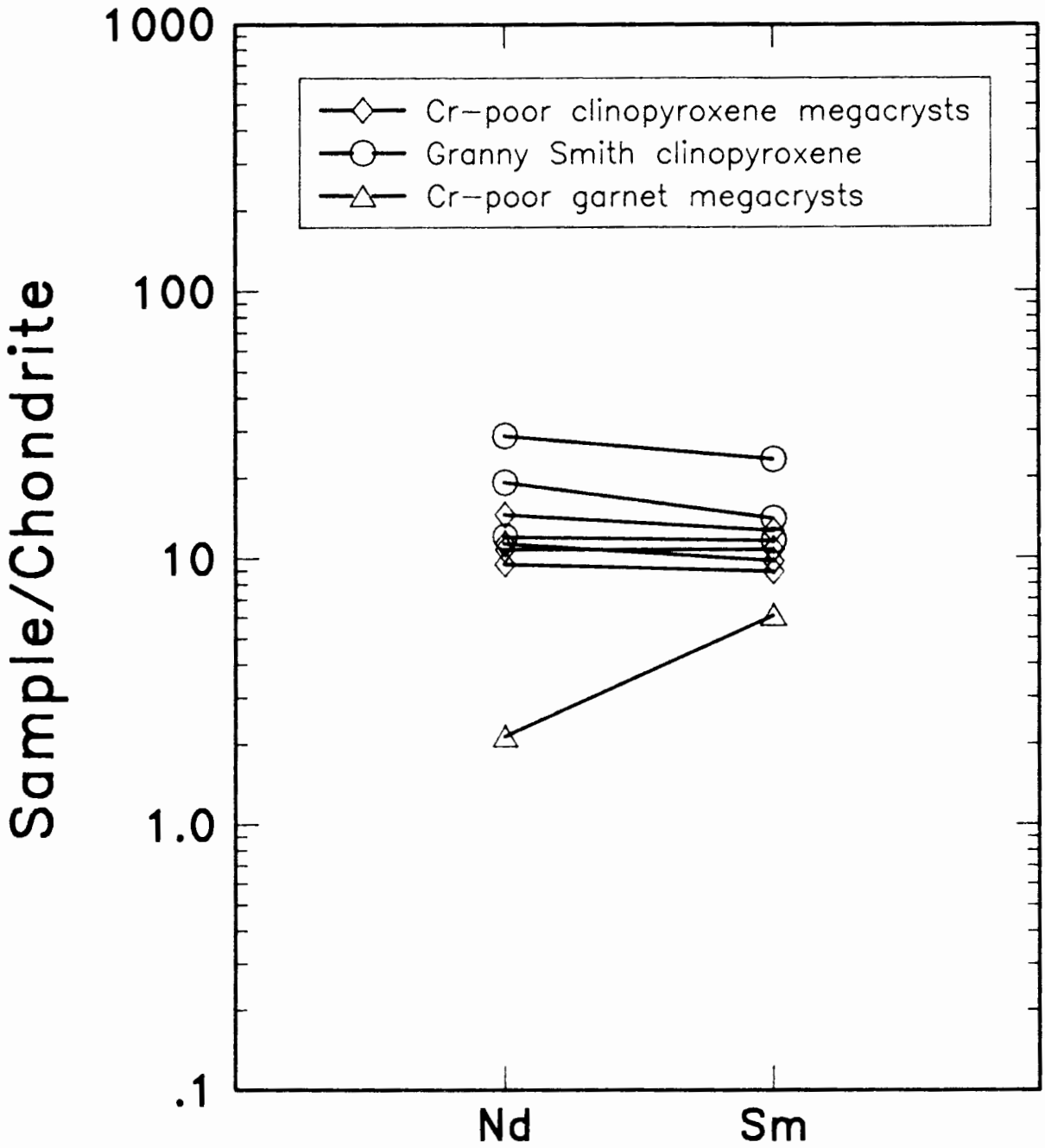

Enrichment of Nd relative to Sm was also observed in these clinopyroxenes (Fig. 5.3).

5.3 Sr ISOTOPE DATA

Blocking temperatures in the Rb-Sr system are considerably lower than the temperatures at which these high-temperature peridotites and Cr-poor megacrysts have equilibrated and therefore no age information beyond that of kimberlite emplacement is expected. Rb concentrations of both garnet and clinopyroxene are very low and no successful measurements were made during this study. As a result of these low concentrations however, the present day clinopyroxene Sr isotopic measurements are essentially initial ratios. Rb/Sr ratios in garnet may however be significant and might necessitate an age correction. The $^{87}Sr/^{86}Sr$ ratios of the co-existing garnet and clinopyroxene should be equivalent for internal isotopic equilibrium.

5.3.1 High-temperature peridotites

The $^{87}Sr/^{86}Sr$ ratios in the peridotitic clinopyroxenes range from .70243 to .70310. No correlation between the Sr concentration and Sr isotopic ratio was observed in these clinopyroxenes (Fig. 5.4). A similar range in Sr isotopic ratio (.70243 to .70309) was noted by Allegre et al. (1982) for clinopyroxene separates from high-temperature peridotites from Thaba Putsoa, northern Lesotho.

FIGURE 5.4 Variation in Sr concentration with $^{87}Sr/^{86}Sr$ in clinopyroxenes from high-temperature peridotites, Cr-poor megacrysts and Granny Smith nodules

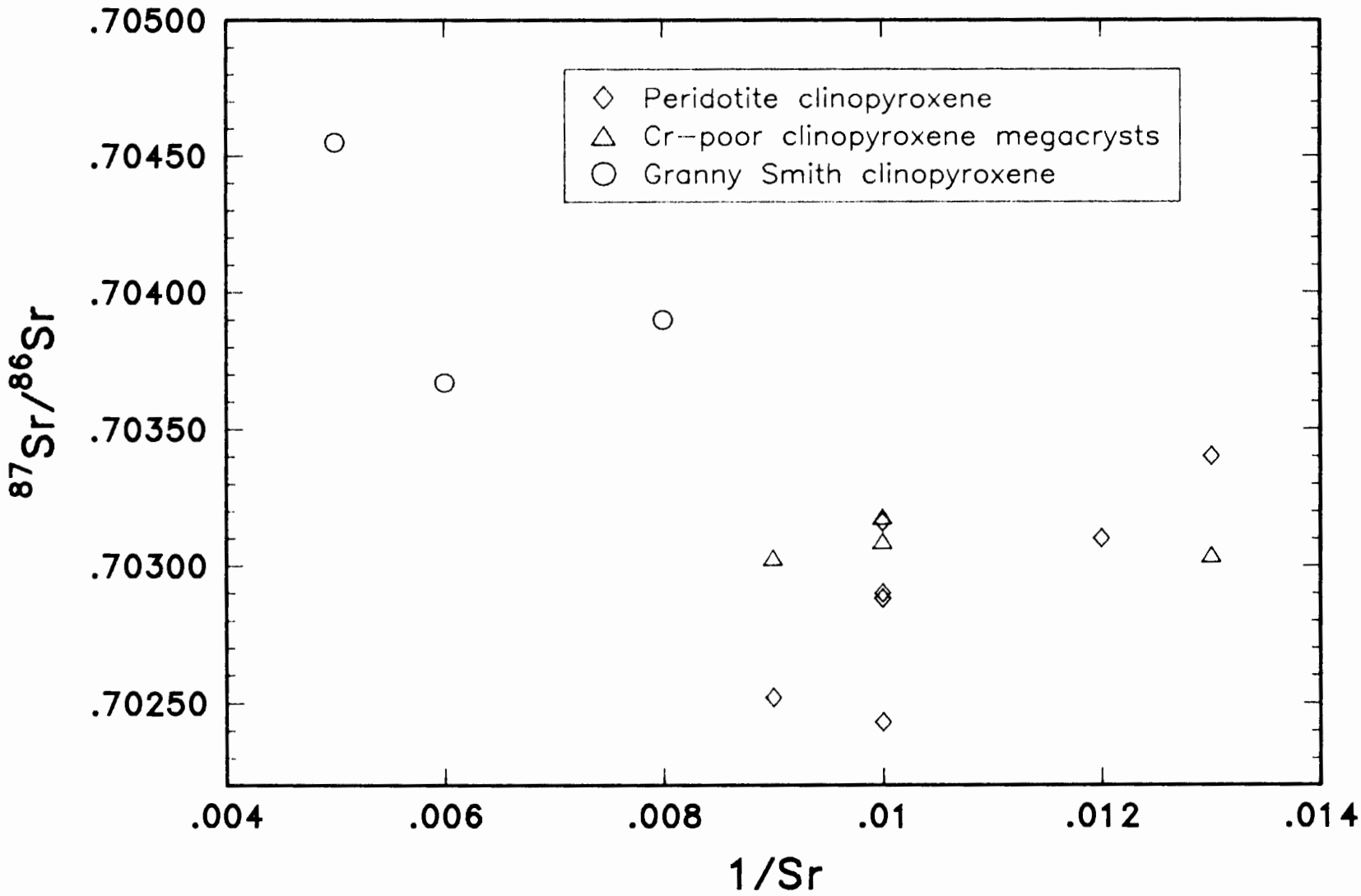

Only one of the Sr isotopic measurements for the garnet separates was successful. This sample (JJG 1753) had an $^{87}Sr/^{86}Sr$ ratio of .70395$\pm$4, notably higher than that of the clinopyroxene (.70288$\pm$3) in the same xenolith. As the Rb/Sr ratio of the garnet is not known the possible effect of an age correction on this ratio must be considered. Richardson et al. (1985) noted the presence of a Sr-rich colourless secondary mineral along garnet fractures which resulted in high Sr isotopic ratios. If this mineral had escaped detection during handpicking of this sample it might be an alternate explanation for the high garnet $^{87}Sr/^{86}Sr$ ratio.

5.3.2 Megacryst minerals

The $^{87}Sr/^{86}Sr$ ratios of the Cr-poor clinopyroxene megacrysts range from .70303 to .70325. The Sr isotopic ratios from repeat dissolutions were generally within error, but one sample yielded two distinct ratios.

This range in initial Sr ratios from a single locality is not consistent with fractionation from a single magma. In addition, the absence of a systematic correlation between the Sr concentrations and the Sr isotopic ratios (Fig. 5.4) does not support mixing processes during megacryst crystallization. The range in Sr isotopic ratios might therefore be due to very localized interaction between the megacryst and the lithospheric wallrock.

Lack of evidence for mixing during megacryst crystallization was also noted by Smith (1984) who demonstrated that both a

high-temperature Cr-poor clinopyroxene and a low-temperature Cr-poor clinopyroxene intergrown with ilmenite from Monastery had the same $^{87}Sr/^{86}Sr$ ratio.

The $^{87}Sr/^{86}Sr$ ratios in the Cr-poor garnet megacrysts range from .70383 to .70535. These ratios are much higher than those in the clinopyroxenes as was noted for the peridotite garnet separates.

The Granny Smith clinopyroxenes have $^{87}Sr/^{86}Sr$ ratios which range from .70361 to .7045. No correlation between Sr concentration and Sr isotopic ratio was noted in these samples either (Fig. 5.4).

5.4 Nd ISOTOPE DATA

Blocking temperatures in the Sm-Nd system are also considerably lower than the temperatures at which these high-temperature peridotites and Cr-poor megacrysts have equilibrated and therefore no age information beyond that of kimberlite emplacement is expected. The $^{143}Nd/^{144}Nd$ ratios of the garnet and clinopyroxene (corrected for age of emplacement) should therefore be equivalent for internal isotopic equilibrium.

5.4.1 High-temperature peridotites

The $^{143}Nd/^{144}Nd$ ratios of the clinopyroxene separates range from .51266 to .51323. The cause of the discrepancy in isotope ratios between the two dissolutions of JJH 35 is

FIGURE 5.5 Variation in Nd concentration with $^{143}Nd/^{144}Nd$ in clinopyroxenes from high-temperature peridotites, Cr-poor megacrysts and Granny Smith nodules

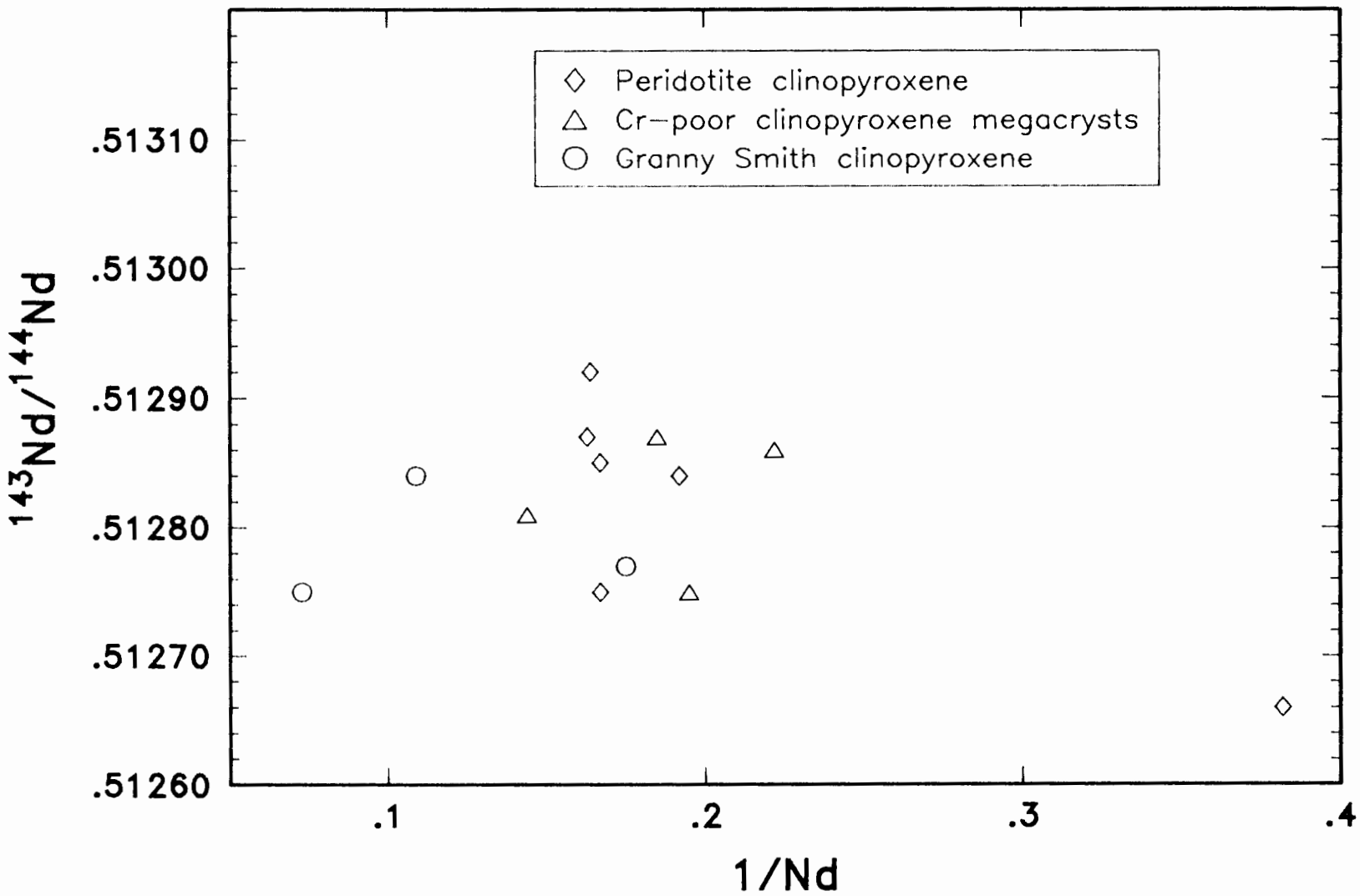

unknown. No correlation between Nd concentration and Nd isotopic ratio was observed in these samples (Fig. 5.5).

The $^{143}Nd/^{144}Nd$ ratios of the garnet separates range from .51287 to .51345. No correlation between Nd concentration and Nd isotopic ratio was observed in these samples either.

Two point Sm-Nd mineral ages could be calculated for five of the peridotites (Fig. 5.6). These ages were:

JJH 10 = 152 $\pm$ 39 m.y.

JJH 26 = 72 $\pm$ 13 m.y.

JJH 35 = 238 $\pm$ 67 m.y.

JJG 1729 = 71 $\pm$ 20 m.y.

JJG 1753 = 99 $\pm$ 17 m.y.

Assigned errors are derived from the maximum and minimum slopes allowed by 2 sigma measurement errors. Apart from two samples these ages are within error of the age of kimberlite emplacement. JJH 10 and JJH 35 yield ages which are older than the age of kimberlite emplacement. As noted previously however, two distinct Nd isotopic ratios were measured on two separate dissolutions of JJH 35. Use of the other Nd isotope ratio with that of the garnet separate indicates inter-mineral isotopic disequilibrium and suggests enrichment of trace elements without re-equilibration of isotopic ratios prior to kimberlite emplacement.

5.4.2 Megacryst minerals

The Cr-poor clinopyroxene megacrysts have $^{143}Nd/^{144}Nd$ ratios which range from .51275 to .51297. No correlation between

FIGURE 5.6 $^{147}Sm/^{144}Nd$ versus $^{143}Nd/^{144}Nd$ in clinopyroxene and garnet separates from high-temperature peridotites from Jagersfontein

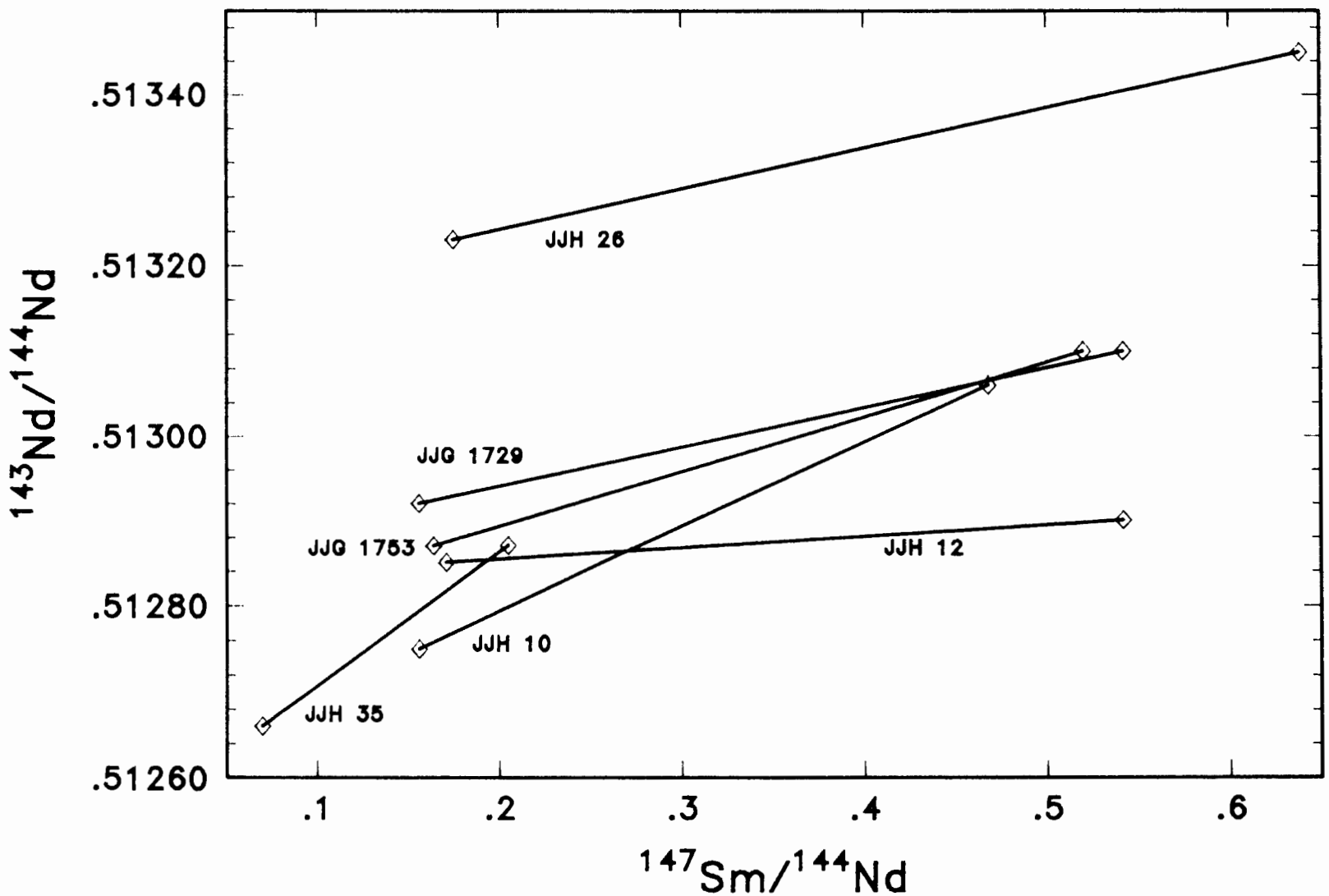

Nd concentration and Nd isotopic ratio was observed in these samples (Fig. 5.5)

The Cr-poor garnet megacrysts have $^{143}Nd/^{144}Nd$ ratios which range from .51305 to .51350. Correction of these ratios to 85 m.y. (the age of kimberlite emplacement) results in a change in the isotopic ratio of .0003 for the garnet and .0001 for the clinopyroxene megacrysts.

Two point Sm-Nd mineral ages calculated between two of the clinopyroxene megacrysts and the garnet megacryst yield similar ages (98 ± 19 m.y.) which are equivalent to the age of kimberlite emplacement. A Sm-Nd mineral age calculation between a third clinopyroxene and the garnet megacryst yields an age of 148 ± 17 m.y. which is distinctly older than the age of kimberlite emplacement (Fig. 5.7). Assigned errors are derived from the maximum and minimum slopes allowed by 2 sigma measurement errors. None of these clinopyroxenes and the garnet were from coexisting samples, but if they had been in equilibrium at the time of kimberlite emplacement an age equivalent to that of kimberlite would be expected. It is possible that localized interaction with the lithospheric wallrock, as suggested to explain the range in Sr isotopic ratios, might have influenced the Nd isotopic ratios as well.

The Granny Smith clinopyroxenes have $^{143}Nd/^{144}Nd$ ratios which range from .51275 to .51284. This range is similar to that observed for the Cr-poor clinopyroxenes.

FIGURE 5.7 $^{147}Sm/^{144}Nd$ versus $^{143}Nd/^{144}Nd$ in Cr-poor clinopyroxene and garnet megacrysts from Jagersfontein

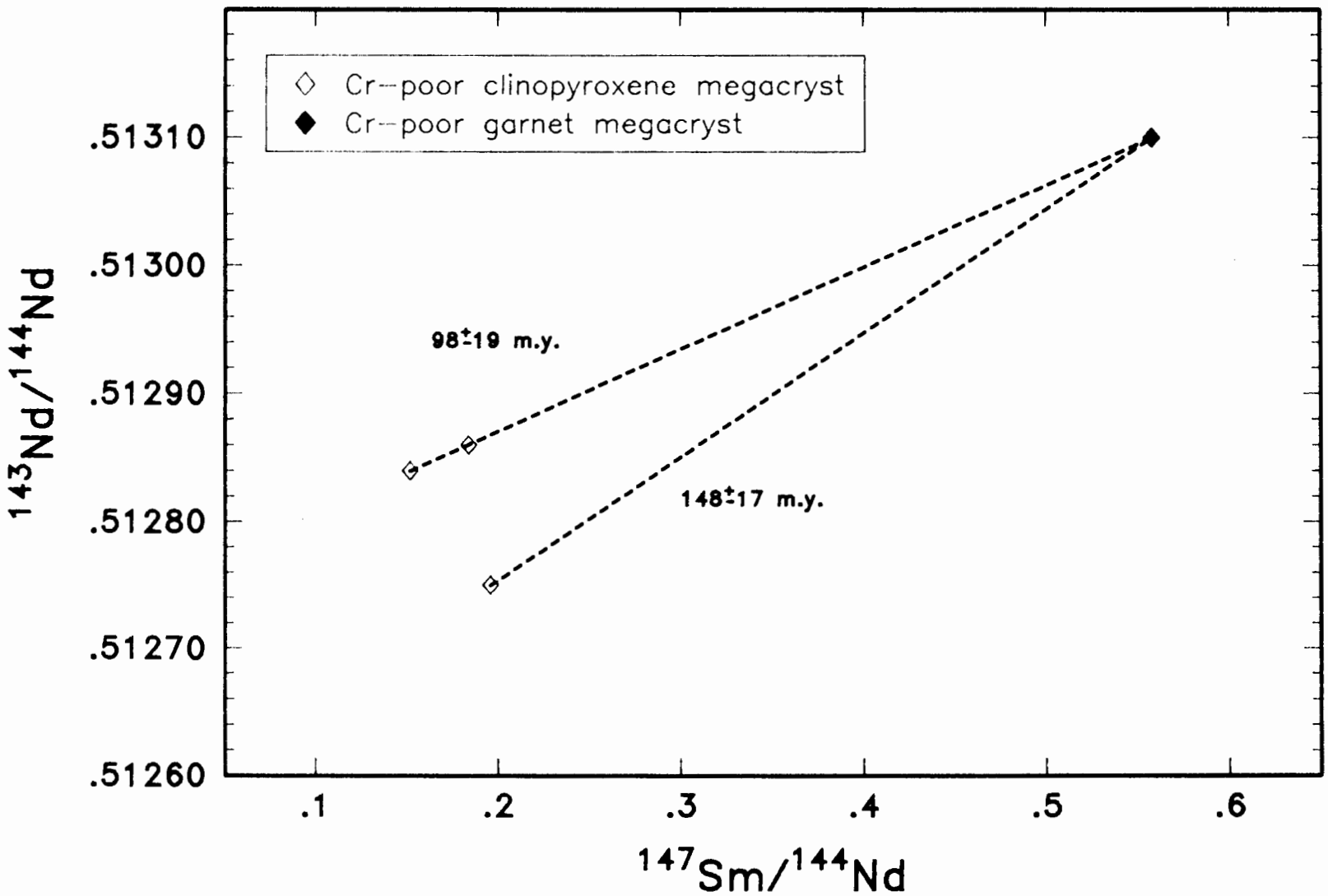

5.5 COMBINED Nd-Sr ISOTOPE DATA

The $^{143}Nd/^{144}Nd$ and $^{87}Sr/^{86}Sr$ isotopic measurements of mantle-derived xenoliths are typically described relative to an estimate for the bulk earth. $^{87}Sr/^{86}Sr$ ratios lower than bulk earth and $^{143}Nd/^{144}Nd$ ratios higher than bulk earth are described as `depleted', whereas $^{87}Sr/^{86}Sr$ ratios higher and $^{143}Nd/^{144}Nd$ ratios lower than bulk earth are described as `enriched'. In addition the ratios are usually compared to the `mantle array' defined by mid-ocean ridge basalt (MORB) and some ocean island basalts (OIB).

Models for plate tectonic reconstruction suggest a possible correlation between South Atlantic hotspots and southern African kimberlites (Crough et al., 1980). According to Morgan's (1983) palaeotrack calculations, the Jagersfontein kimberlite cannot be correlated with any presently known hotspot traces. The isotopic ratios from Bouvet are, however, representative of possible hotspot magmas. Le Roex (1987) noted the following values for MORB and OIB in the Southern Ocean:

	$^{87}Sr/^{86}Sr$	$^{143}Nd/^{144}Nd$
N-MORB	.70246-.70297	.51302-.51312
T-MORB	.70291-.70371	.51284-.51301
P-MORB	.70356-.70364	.51286-.51295
BOUVET	.70365-.70376	.51282-.51285

5.5.1 High-temperature peridotites

On a $^{143}Nd/^{144}Nd$ versus $^{87}Sr/^{86}Sr$ diagram the clinopyroxene separates plot to the left of the `mantle array' in the `depleted' quadrant, indicating enrichment in Nd/Sm relative to Rb/Sr. The clinopyroxene separates show a general negative correlation between Nd and Sr isotopic ratios.

The Sr isotopic ratios are similar to those observed in Southern Ocean N-MORB, although the Nd isotopic ratios are lower. Only one sample (JJH 26) has a Nd isotopic ratio which is higher than that for Southern Ocean N-MORB. Two clinopyroxene separates from high-temperature peridotites from Jagersfontein analyzed by Winterburn (1987) have similar ratios to those determined in this study (Fig. 5.8).

Mantle-derived xenoliths with equivalent isotopic signatures to the high-temperature peridotites at Jagersfontein have been found in oceanic peridotites (eg. Roden et al., 1984) and in continental regions that have experienced recent extension (eg. Menzies et al., 1985).

In contrast, the clinopyroxene separates from metasomatized peridotites from Kimberley (Menzies and Murthy, 1980) have `enriched' signatures. These metasomatized peridotites are considered to form part of the old, cold lithospheric keel beneath southern Africa where they have had the opportunity to develop their distinctive isotopic signatures. These clinopyroxenes extend the `mantle array' to lower Nd and higher Sr isotopic ratios (Fig. 5.9). The high-temperature

FIGURE 5.8 $^{87}Sr/^{86}Sr$ versus $^{143}Nd/^{144}Nd$ in clinopyroxenes from high-temperature peridotites from Jagersfontein. Filled symbols are data from Winterburn (1987)

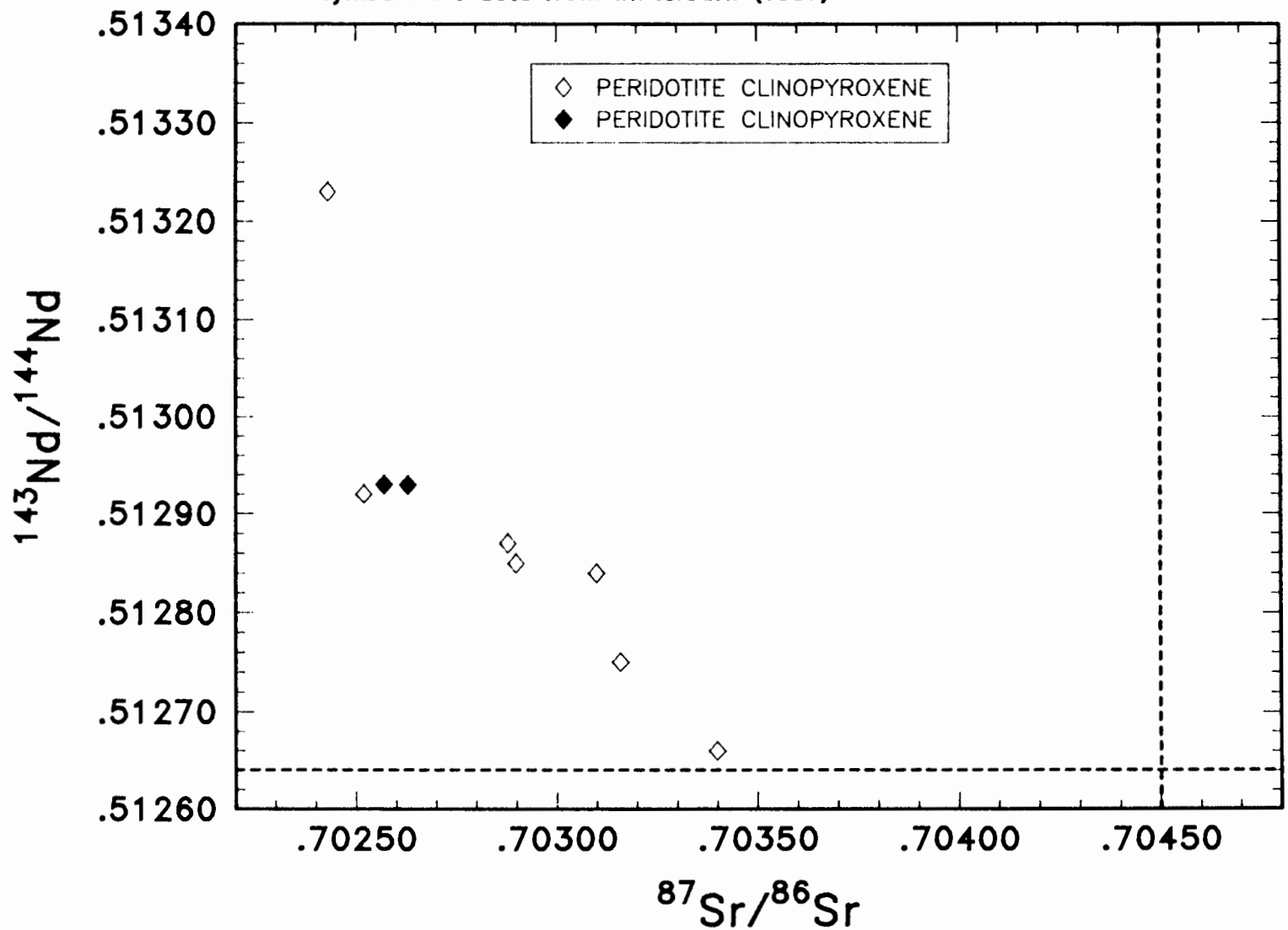

FIGURE 5.9 $^{87}Sr/^{86}Sr$ versus $^{143}Nd/^{144}Nd$ in clinopyroxenes from peridotites. Jagersfontein data are for high-temperature peridotites (symbols as in Fig.5.8) and Kimberley data are for low-temperature peridotites (Menzies and Murthy, 1980)

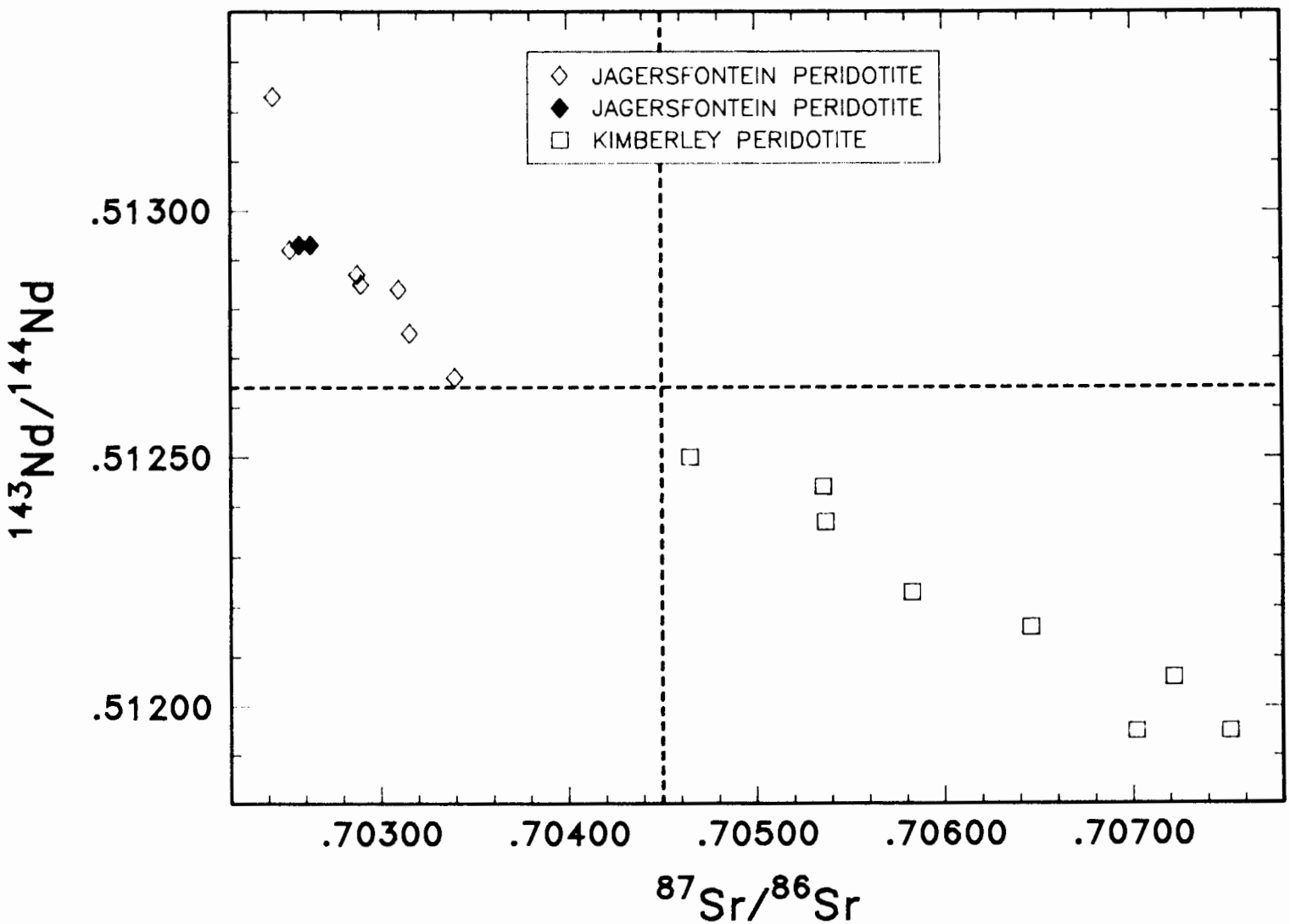

peridotites have isotopic ratios similar to residues of younger basalt extraction and it is suggested that they indicate post-Archaean underplating of the base of the lithosphere.

5.5.2 Megacryst minerals

On a $^{143}Nd/^{144}Nd$ versus $^{87}Sr/^{86}Sr$ diagram the clinopyroxene megacrysts also plot to the left of the 'mantle array' in the 'depleted' mantle quadrant. The Cr-poor clinopyroxene megacrysts from Jagersfontein have similar isotopic ratios to those from other southern African localities (Fig. 5.10), suggesting a similar source for all Cr-poor megacrysts.

The Sr isotopic ratios of the Cr-poor clinopyroxenes are similar to those from Southern Ocean T-MORB, although the Nd isotopic ratios extend to lower values.

The Cr-poor clinopyroxene megacrysts and clinopyroxene separates from the high-temperature peridotites at Jagersfontein have similar Sr and Nd isotopic ratios (Fig. 5.11), although some of the high-temperature peridotites appear to be more depleted.

The Granny Smith clinopyroxenes from Jagersfontein have similar isotopic compositions to those observed in Granny Smith clinopyroxenes from Kimberley by Jones ((1987) (Fig. 5.12).

FIGURE 5.10 $^{87}Sr/^{86}Sr$ versus $^{143}Nd/^{144}Nd$ in Cr-poor clinopyroxene megacrysts from Jagersfontein (filled symbol is from Smith, pers. comm.) and other southern African localities (Kramers et al., 1981 and Jones, 1987)

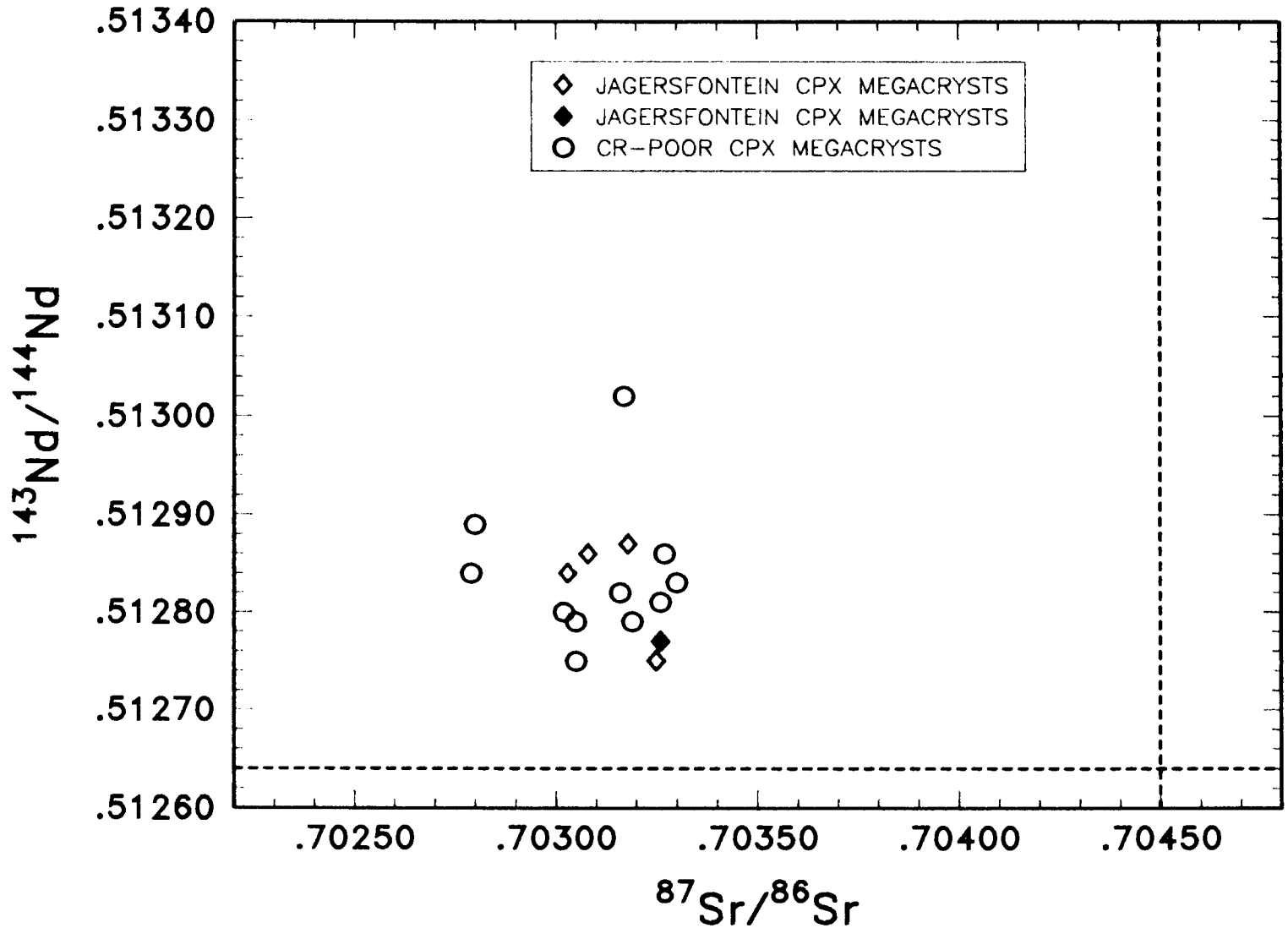

FIGURE 5.11 $^{87}Sr/^{86}Sr$ versus $^{143}Nd/^{144}Nd$ in clinopyroxenes from high-temperature peridotites and Cr-poor megacrysts from Jagersfontein. Filled symbols are data from Winterburn (1987) and Smith (pers. comm.)

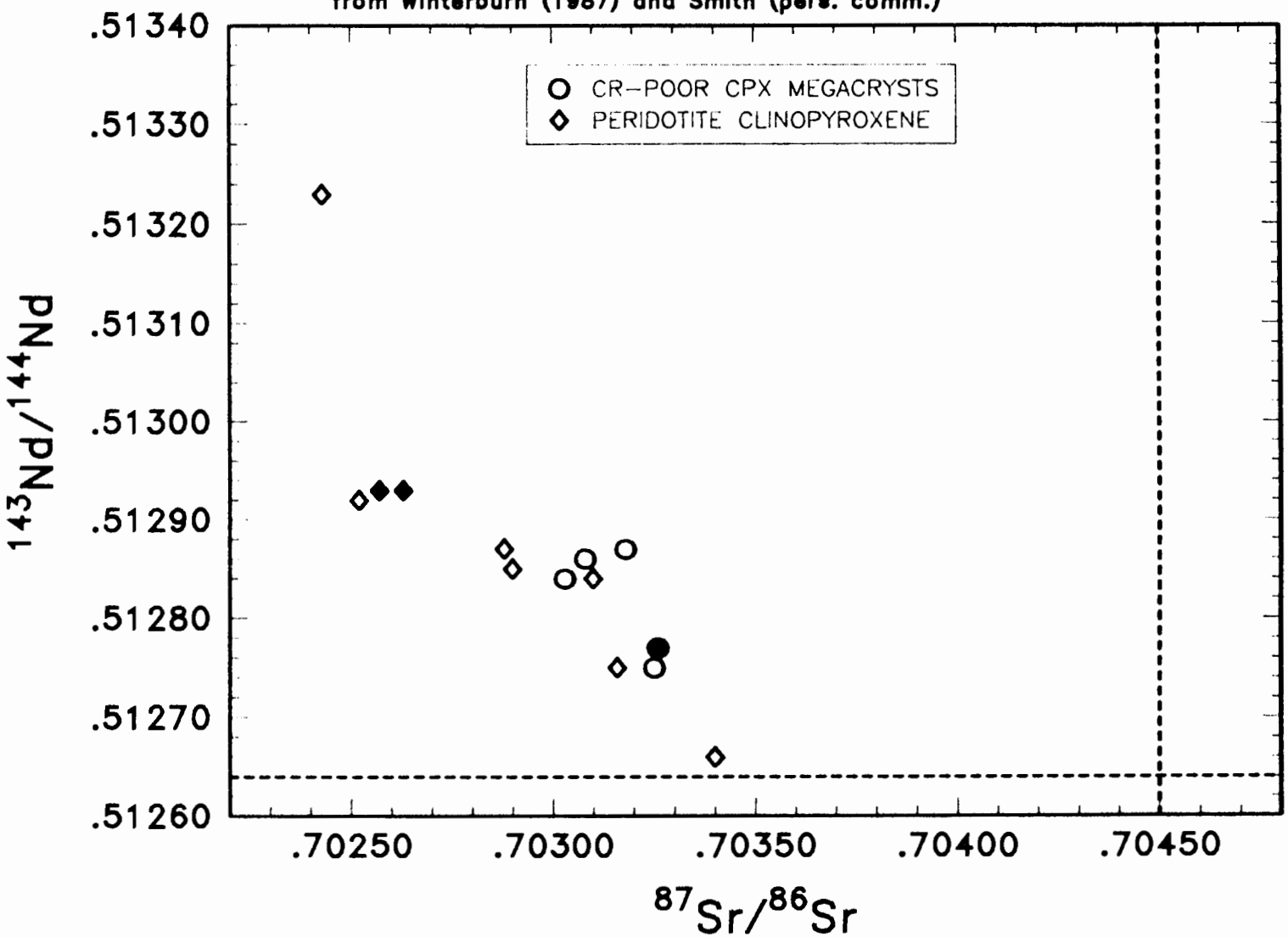

FIGURE 5.12 $^{87}Sr/^{86}Sr$ versus $^{143}Nd/^{144}Nd$ in Granny Smith clinopyroxenes from Jagersfontein and Kimberley. Data from Kimberley are from Jones (1987)

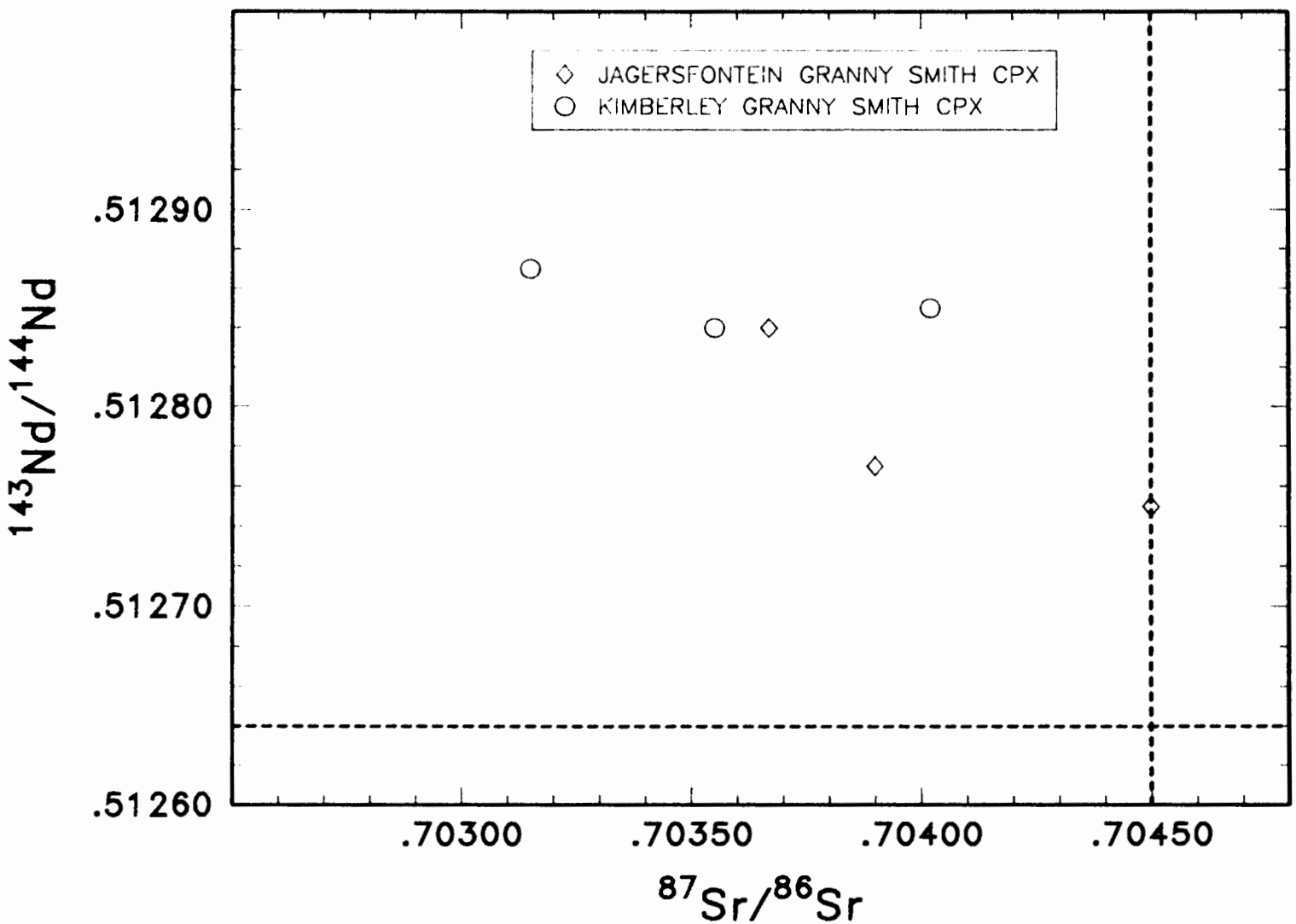

At Jagersfontein, the Granny Smith clinopyroxenes have similar Nd isotopic ratios to the Cr-poor clinopyroxenes, but higher Sr isotopic ratios (Fig. 5.13). Both the Granny Smith and Cr-poor clinopyroxenes have Sr isotopic ratios which are more depleted than that of their host kimberlite (JAG K9, from Smith (1984)), but have similar Nd isotopic ratios.

FIGURE 5.13 $^{87}Sr/^{86}Sr$ versus $^{143}Nd/^{144}Nd$ in Cr-poor clinopyroxene megacrysts and Granny Smith clinopyroxenes from Jagersfontein at 85 m.y. Filled symbols from Smith (1984)

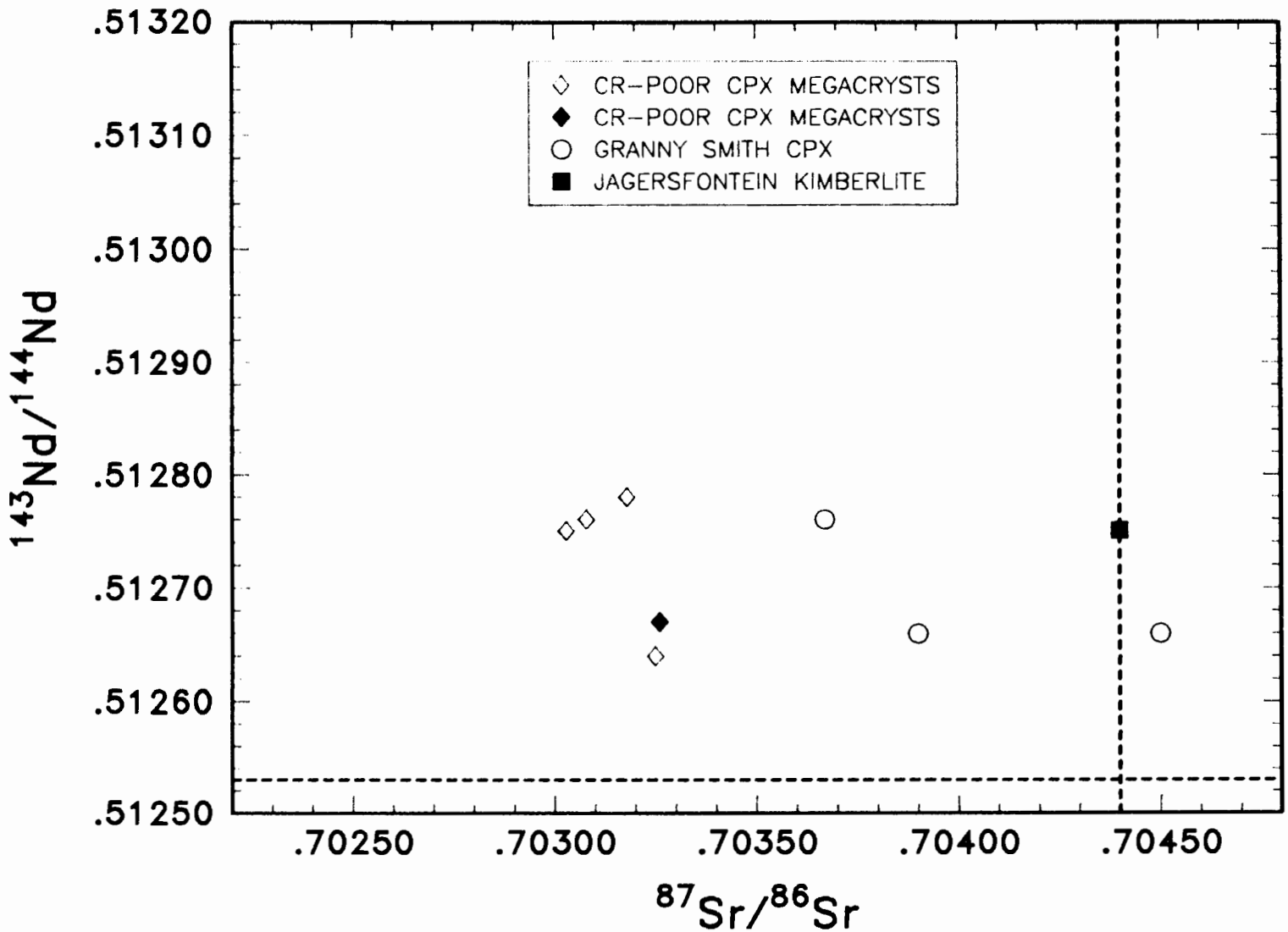

5.6 DISCUSSION

5.6.1. Kimberlite-megacryst association - REE evidence

It is theoretically possible to calculate the REE content of the parental megacryst magma using crystal/liquid distribution coefficients. Distribution coefficients are however, not well constrained for the appropriate conditions in the mantle. Irving (1978) noted that crystal-liquid REE distribution coefficients for clinopyroxene-liquid vary by a factor of four within the basaltic system. Calculated REE abundances would therefore be a function of the distribution coefficients chosen. Kramers et al. (1981) chose a different approach and estimated the distribution coefficients from known REE concentrations in kimberlites and clinopyroxene megacrysts by assuming that the kimberlites represented the parental magma composition.

Nixon et al. (1981) noted that a sample of Jagersfontein kimberlite had an exceptionally low total REE abundance, whereas data from Smith et al. (1985b) indicate a wide range in REE abundances for four different Jagersfontein kimberlite samples. The REE abundances of kimberlites are strongly influenced by their modal mineralogy and it is therefore impossible to single out a representative sample. In addition, considering the hybrid nature of the kimberlite as found at the surface, its composition is not necessarily representative of that of its source. The approach by Kramers et al. (1981) does therefore not appear to be satisfactory.

Sm and Nd concentrations were measured in the Cr-poor clinopyroxene megacrysts. The Cr-poor clinopyroxene megacrysts are LREE enriched and there appears to be a gross trend of increasing REE with decreasing equilibration temperature (Jones, 1987). Jones (1987) measured a more complete spectrum of REE concentrations in Cr-poor clinopyroxene megacrysts and suggested that their parental magma was similar to alkali basalt. Jones (1987) suggested that this magma subsequently fractionationed and interacted with lithospheric wallrock resulting in the kimberlite as seen at the surface. Kimberlites, however, have high MgO contents (20-30%) and these compositions are not consistent with initial fractionation of the megacryst suite.

In contrast to the observations for the Cr-poor megacrysts from kimberlite, Ehrenberg (1982b) noted that the megacrystalline nodules from The Thumb had a LREE enriched parent magma similar to that of the host minette.

5.6.2 Kimberlite-megacryst association - isotopic evidence:

Smith et al. (1986) noted that the Cr-poor clinopyroxene megacrysts from widely separated southern African localities had a restricted range in $^{87}Sr/^{86}Sr$ ratios (.7028-.7032), suggesting a widespread homogeneous source. In contrast, kimberlites have a wide range in $^{87}Sr/^{86}Sr$ ratios and at any particular locality the kimberlite and Cr-poor megacrysts do not appear to be in Sr isotopic equilibrium (Kramers, 1979; Smith, 1984; Jones, 1987).

The initial $^{87}Sr/^{86}Sr$ ratios of three kimberlite samples from Jagersfontein, analyzed by Smith (1984), range from .7044 to .7055. These ratios are higher than those obtained for the Cr-poor clinopyroxene megacrysts (.70303 to .70325) from Jagersfontein. In comparison, the initial Nd isotopic ratio of a single sample of Jagersfontein kimberlite (.51275) is similar to that obtained for the Cr-poor clinopyroxene megacrysts (.51265 to .51287).

Smith (1984) suggested that it was unlikely that the higher $^{87}Sr/^{86}Sr$ ratios in the kimberlite were due to alteration, but that isotopic modification of the kimberlite in the mantle subsequent to megacryst crystallization was possible.

Considering the hybrid nature of the kimberlite as seen at the surface, a megacryst magma-proto-kimberlite consanguinity might still be justifiable. It is suggested that the proto-kimberlite magma is the result of melting in a rising mantle plume (hotspot) and that its initial characteristics are those of its OIB-type source. These characteristics are observed in the Cr-poor megacrysts. The kimberlite is part of the same igneous event but has experienced significant interaction with, and assimilation of, lithospheric wallrocks during its ascent.

Smith et al. (1987) noted that the $^{206}Pb/^{204}Pb$ ratios of Cr-poor clinopyroxenes (19.3 to 20.6) were more radiogenic than kimberlite and similar to those of some OIB. This is

consistent with the suggestion above that the Cr-poor megacryst magma has a similar source to OIB.

5.6.3 Relationship between Cr-poor clinopyroxene megacrysts and Granny Smith megacrysts

The Cr-poor and Granny Smith clinopyroxenes from Jagersfontein are not in Sr isotopic equilibrium. The Granny Smith clinopyroxenes have higher $^{87}Sr/^{86}Sr$ ratios, intermediate between those of the Cr-poor clinopyroxenes and the kimberlite. The Nd isotopic compositions of the Cr-poor clinopyroxenes, the Granny Smith clinopyroxenes and the kimberlite are, however, similar. This suggests that the Granny Smith clinopyroxenes might also be crystallization products of the kimberlite magma, but at shallower depths (in the phlogopite stability field) and after mixing with lithospheric wall-rock. This would be similar to an assimilation-fractional crystallization model. Alternatively they might be the products of a previous magma which had suffered `heat death' in the lithosphere.

5.6.4 High-temperature peridotites - REE evidence:

The Nd and Sm concentrations measured in this study are similar to those obtained by Shimizu (1975b). Shimizu (op cit.) noted that the garnets had LREE concentrations 1-2 x chondrite and HREE concentrations 10-16 x chondrite. The clinopyroxenes had LREE concentrations 10 x chondrite and HREE concentrations equivalent to chondrite. Using these data and assuming modal proportions of 10% garnet and 10%

clinopyroxene, he calculated a whole-rock REE pattern which was similar to chondrite. Whole-rock REE content is, however, a function of mineralogy and choice of modal proportions is important. The chondritic whole-rock pattern might be a purely coincidental result of the choice of modal proportions in combination with the measured REE abundances.

The REE abundances in the garnets and clinopyroxenes from the high-temperature peridotites at Jagersfontein are similar to those of the Cr-poor garnet and clinopyroxene megacrysts.

CHAPTER 6

SYNTHESIS

6.1 REVIEW OF PETROGENETIC MODELS FOR THE HIGH-TEMPERATURE PERIDOTITES

Any petrogenetic model developed for the high-temperature peridotites must take the following features into account: their geographical distribution, textures, compositional evolution, temperatures and pressures of equilibration and isotopic composition. In the following sections, the effect of these factors on the development of petrogenetic models for the high-temperature peridotites will be discussed.

6.1.1. Geographical Distribution

In southern Africa the high-temperature peridotites are found at localities both on and off the Kaapvaal craton, as well as in both Precambrian (eg. Premier, Danchin, 1979) and Cretaceous (eg. Jagersfontein) kimberlites. High-temperature peridotites are, however, not found at all kimberlite localities. They appear to be restricted to the Group 1 kimberlites, although even within this grouping their presence is sporadic. The high-temperature peridotites are not as widespread as the Cr-poor megacrysts, nor are they as common. As far as has been observed, however, the high-temperature peridotites are not found where Cr-poor megacrysts are absent.

6.1.2 Relationship between temperature and texture

Boyd and Nixon (1972) first recognized a possible relationship between, on the one hand, depth of origin and temperature of equilibration estimated by pyroxene geothermobarometry and, on the other hand, textures observed in xenoliths from kimberlites in Lesotho. Subsequent work at other localities has shown that a simple division into low-temperature coarse and high-temperature deformed categories is not always valid.

Deformed peridotites with mineral compositions similar to those of coarse peridotites have been found in the Matsoku and Kimberley pipes (Cox et al., 1973; Dawson et al., 1975; Harte et al., 1975; Boyd and Nixon, 1978), and some coarse peridotites have mineral compositions reflecting high temperatures of equilibration (Boyd and Nixon, 1979). Low-temperature deformed and high-temperature deformed peridotites have, however, not been found at the same locality.

At Jagersfontein, the high-temperature peridotites were mostly deformed and only one coarse high-temperature peridotite was found. This is in general true of high-temperature peridotites at any locality; coarse high-temperature peridotites are not a common occurrence.

6.1.3. Deformation

Boyd (1973) and Nixon and Boyd (1973a) noted that coarse peridotites showed dT/dP similar to geophysical estimates for a shield geotherm, but that the deformed peridotites from Lesotho defined an inflected limb. They suggested that the inflection of the geothermal gradient, as reflected by the high calculated temperatures of equilibration of deformed peridotites from Lesotho kimberlites, was due to shear heating at the base of the lithosphere resulting from plate motion during break-up of Gondwanaland. Nixon and Boyd (op cit.) interpreted the textures of the high-temperature xenoliths as being due to plastic deformation occurring over millions of years.

In evaluating the model of Nixon and Boyd (op cit.), Green and Gueguen (1974) and Mercier and Carter (1975) examined the stress and strain rates, as well as conditions of viscosity which would be consistent with creep in the asthenosphere caused by plate motion. They concluded that shear heating would be inadequate to produce a thermal anomaly. The same conclusion was reached by Boullier and Nicolas (1975) who noted, on the basis of textural studies, that the flow textures in the deformed rocks required strain rates beyond those expected for plate movement. As an alternative model to that proposed by Nixon and Boyd (1973a), Green and Gueguen (1974) suggested that the deformation might be due to shearing occurring around the outermost regions of a rising diapir.

In contrast to the diapiric model, Parmentier and Turcotte (1974) suggested that the shape of the geotherm was the result of transient heating of the moving lithosphere, induced by a mantle plume.

In a re-evaluation of their model, Green and Gueguen (1983) noted that the stresses implied by the olivine microstructures in deformed xenoliths required a reassessment of their earlier dismissal of shear heating as a significant process. Green and Gueguen (1983) retained their basic diapiric model, suggesting that the upward transport provided the heat source for melting as well as the chemical discontinuity between deformed and undeformed xenoliths. Their model accounted for shear heating effects during more rapid deformation associated with the coalescence of the magma and/or its initial upward acceleration.

In a study of the microstructural features of the high-temperature peridotites, Goetze (1975) noted that the bimodal olivine texture represented a transient condition of syntectonic recrystallization. Using the experimental calibration of piezometers based on dislocations and substructures, Goetze (op cit.) concluded that the deformation took place in a matter of minutes or days under a differential stress of 2-3 kbars. Gueguen and Nicolas (1980) noted that although the stress estimates of Goetze (1975) were not accurate, the deformed xenoliths had experienced stresses of at least 500 bars, substantially

above the 10-100 bars ascribed to the asthenosphere by geophysical methods.

In accord with Goetze (1975), Mercier (1979) noted that the bimodal textures indicated a short-lived deformation event (hours), and ascribed the deformation to late events occurring immediately prior to sampling by the kimberlite and related to its intrusion mechanism through the upper mantle. Similarly, Gueguen and Nicolas (1980) noted that strain rates were high and that shearing was probably restricted to a narrow zone.

The deformed peridotites at Jagersfontein yield high calculated temperatures of equilibration and, according to the observations noted above, would be expected to show evidence of annealing if present in the mantle under these conditions for any length of time. The preservation of the fluidal and laminar-mosaic-porphyroclastic textures observed in the high-temperature peridotites from Jagersfontein, therefore indicates that this deformation must be a late-stage event in their evolution. Kimberlite eruption must follow directly (within hours) after deformation of the peridotite xenoliths before any annealing can occur.

Although diapirs or mantle plumes provide possible mechanisms for kimberlite ascent through the asthenosphere, they are not feasible mechanisms for ascent through the rigid lithosphere. Spera (1987) noted that of the three major alternatives for magma migration through the lithosphere ((1) porous flow, (2) diapirism and (3)

fracture), only fracture was viable for the mobilization of significant volumes of magma through the lithosphere. Diapiric ascent and melt percolation mechanisms would not drive magma upward at high enough rates.

Artyushkov and Sobolev (1984) suggested a diapir-crack model for kimberlite eruption. In this model the magma rises diapirically through the asthenosphere and is then transported by crack propagation through the lithosphere. Artyushkov and Sobolev (1984) and Spera (1984) suggested that translithospheric ascent velocities would be of the order of 10-30 m/s (ie. 36-108 km/hr). This would be sufficient to transport the high-temperature xenoliths to the surface before much post-deformation annealing during eruption could occur. Pressures calculated for the high-temperature peridotites from Jagersfontein indicate equilibration at depths of approximately 160-180 km. Ascent velocities of the order of 10-30 m/s would therefore transport the xenoliths to the surface in less than 5 hours.

6.1.4 Compositional evolution

As an alternative to the models presented by Nixon and Boyd (1973a) and Green and Gueguen (1974), Gurney and Harte (1980) suggested that the high-temperature peridotites formed the immediate envelope to an intruding, Cr-poor megacryst-precipitating magma, and were formed from coarse low-temperature peridotites. The textural and compositional features of the high-temperature peridotites were

interpreted as being due to magma intrusion, with the distinctive chemical characteristics resulting from metasomatic exchange between the magma and the thermally metamorphosed wallrock.

Ehrenberg (1979) proposed a similar model for sheared garnet lherzolites from The Thumb, a minette intrusion on the Colorado Plateau. He suggested that the sheared lherzolites were the products of deformation and Fe,Ti metasomatism of coarse lherzolites during the intrusion of the magma from which the megacrystalline group of nodules crystallized. In comparison with the high-temperature deformed peridotites from kimberlites, the sheared garnet lherzolites from The Thumb show evidence of grain growth subsequent to deformation. The megacrystalline nodules also contain optically visible exsolution lamellae, suggesting a significantly longer interval between crystallization of the megacrysts and eruption of the minette than is observed in the kimberlite samples.

Dawson (1980) proposed that the deformed high-temperature peridotites were not in equilibrium, but had been subjected to a certain amount of infiltration metasomatism.

Subsequent detailed electron microprobe and proton probe studies have shown that the garnet porphyroclasts in the high-temperature peridotites can be clearly zoned (Smith and Ehrenberg, 1984; Smith and Boyd, 1986,1987; Sobolev et al., 1986; Smith, 1988; Griffin et al., 1989). The rims of zoned garnet porphyroclasts are enriched in TiO_2, Na_2O, FeO,

Zr, Y and Ga relative to their cores. This enrichment has been suggested to be due to interaction with an Fe,Ti-rich melt.

A possible source of this Fe,Ti-rich melt is the Cr-poor megacryst magma. The Cr-poor garnet megacrysts at Jagersfontein have similar TiO_2 and Na_2O concentrations to those in the most enriched garnet porphyroclasts (Fig. 6.1). The garnet porphyroclasts and garnet megacrysts would therefore have been in equilibrium with melt of similar composition. It has already been shown, on the basis of temperatures and pressures of equilibration, that the Cr-poor megacrysts and high-temperature peridotites have a close spatial association. The magma responsible for the formation of the Cr-poor megacrysts is therefore very likely to be the melt responsible for the enrichment of the high-temperature peridotites. This melt would have infiltrated along the grain boundary margins and diffused through the grains.

In addition, minerals in the deformed high-temperature peridotites at Jagersfontein show a general increase in Na_2O, TiO_2, Al_2O_3 and to a lesser extent FeO with increasing temperature of equilibration (Fig. 6.2). This relative enrichment is possibly the result of proximity to the emplaced megacryst magma. The peridotites closest to the megacryst magma would show greater enrichment than those at a distance.

FIGURE 6.1 Na_2O wt% versus TiO_2 wt% in garnet porphyroclasts from deformed peridotites and in Cr-poor garnet megacrysts

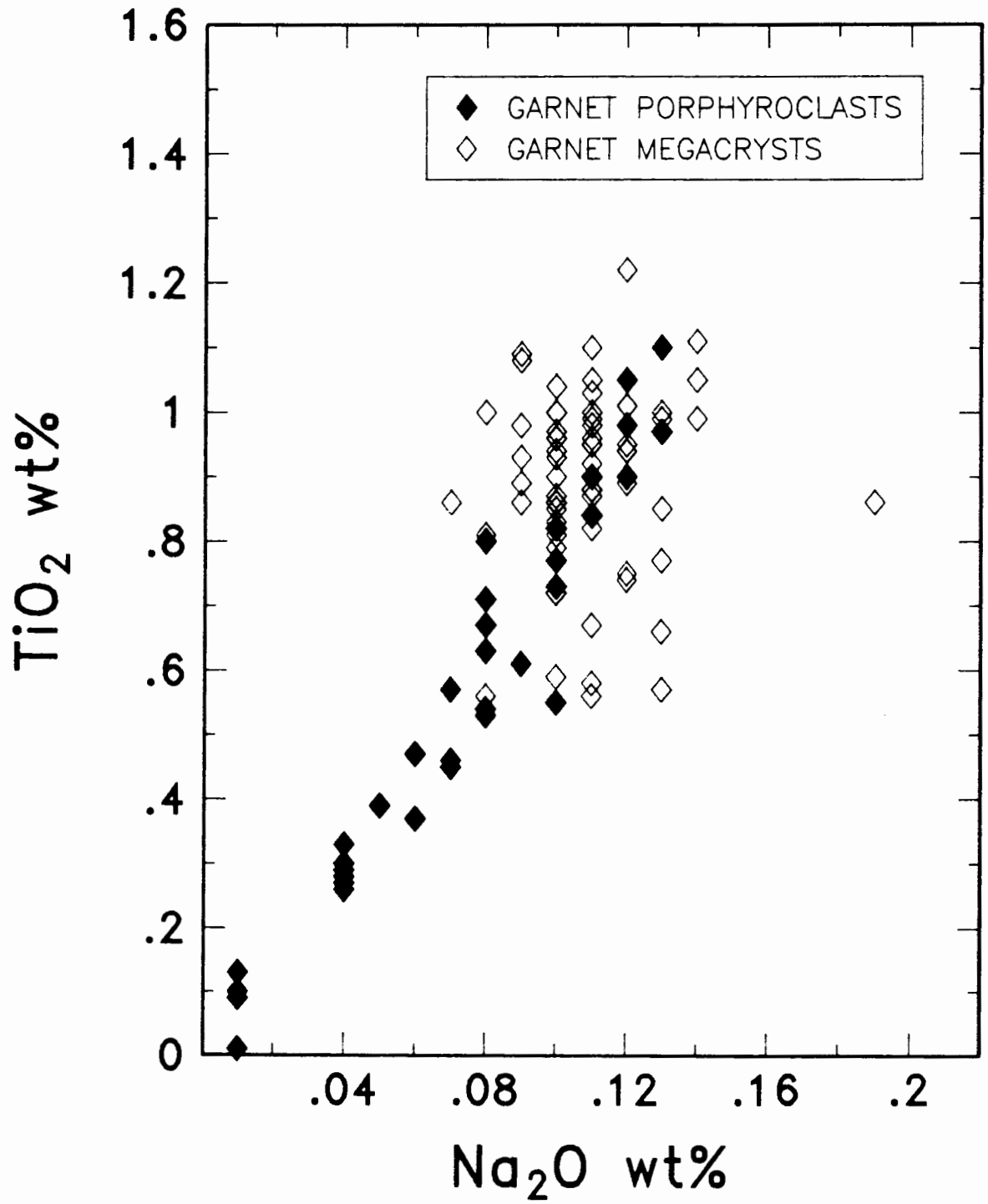

FIGURE 6.2 Increase in TiO_2 wt% in garnet porphyroclasts with temperature (BM85) in deformed peridotites from Jagersfontein

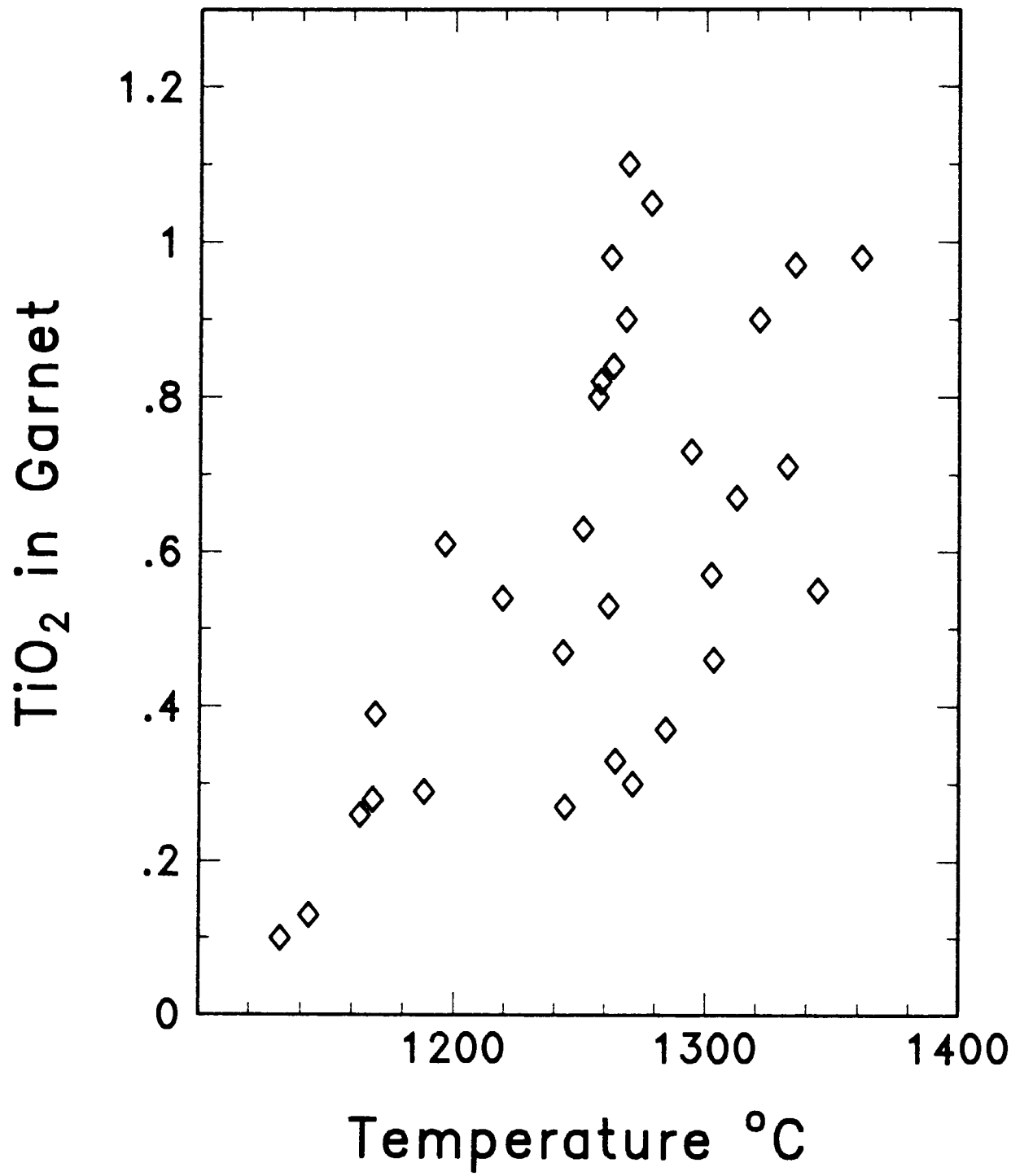

Further evidence of the enrichment of the high-temperature peridotites at Jagersfontein is provided by a clinopyroxene inclusion in a garnet porphyroclast. This clinopyroxene has lower Na_2O, TiO_2 and FeO, and higher CaO concentrations than the clinopyroxene porphyroclasts in the same xenolith. Diffusion rates within garnet are slower than those in olivine and the pyroxenes. By virtue of its inclusion in a garnet porphyroclast, the clinopyroxene has therefore been shielded from the effects of enrichment. Its composition provides constraints on the pre-enrichment clinopyroxene composition. The clinopyroxene inclusion has an equilibration temperature which is 75°C lower than that of the clinopyroxene porphyroclasts in the same xenolith. This provides important evidence for recent changes in the equilibration conditions of the high-temperature peridotites.

The high-temperature peridotite showing the least enrichment (JJH 35) might therefore be most representative of the original depleted protolith. This peridotite has a relatively low calculated temperature of equilibration (1132°C) and low concentrations of Na_2O and TiO_2. The asthenosphere is considered to have a potential temperature of 1280°C (White and McKenzie, 1989). As it is cool and chemically depleted, JJH 35 cannot represent material from the convecting asthenosphere and must be part of the subcontinental lithosphere. If this peridotite is representative of the immediately pre-enrichment composition of material which becomes the high-temperature peridotites, it provides evidence that these xenoliths are not

representative of primitive fertile mantle or convecting asthenosphere, but rather that they are the result of enrichment of a depleted protolith. What then is the origin of this depleted protolith?

Low-temperature peridotites differ in several aspects from the high-temperature peridotites (Table 9). Although Gurney and Harte (1980) suggested that the high-temperature peridotites were the result of metasomatism of low-temperature coarse peridotites, they subsequently noted that on the basis of modal abundances (Harte and Gurney, 1982), the low-temperature peridotites at Jagersfontein could not represent the coarse protoliths for the high-temperature peridotites.

O'Hara et al. (1975) and Richardson et al. (1984) have suggested that the low-temperature peridotites which form the bulk of the Kaapvaal craton might be high-pressure residues of komatiite formation. Whether or not this is true does not detract from the evidence, of modal abundances and compositions, that the high-temperature peridotites require a different origin. Boyd (1987) noted that the olivine in high-temperature peridotites had forsterite contents similar to those of olivines in Cr-diopside spinel lherzolites in alkaline basalts and abyssal peridotites. These forsterite contents are consistent with an origin as residues of melting processes that involve the formation of basalt. As a result, Boyd and Mertzman (1987) and Kesson and Ringwood (1988) suggested a subducted origin for the high-temperature peridotites. The isotopic signatures of

TABLE 9

GENERALIZED FEATURES OF LOW AND HIGH-TEMPERATURE PERIDOTITES

	LOW-TEMPERATURE	HIGH-TEMPERATURE
MODES		
Olivine	62	73
Orthopyroxene	31	17
Clinopyroxene	5	7
Garnet	2	3
COMPOSITION		
Olivine Mg#	92-94	89-92
Clinopyroxene Ca#	> 43	< 43
Whole rock REE	LREE enriched	chondritic
Isotopes	enriched	depleted
TEMPERATURE	< 1100°C	> 1100°C

Data from Harte (1983) and Boyd and Mertzman (1987).

the high-temperature peridotites are not, however, consistent with a formation during oceanic lithosphere subduction related to the formation of the Namaqua-Natal mobile belt as has been suggested by Boyd and Mertzman (1987).

If the depleted protolith is simply a residue of basalt formation, it does not seem necessary to resort to a subducted origin for the high-temperature peridotites. White and McKenzie (1989) have demonstrated that the generation of continental flood basalts can be related to the thermal anomaly created by a nearby mantle plume. They noted that a mantle plume can generate a mushroomed-shaped region beneath the lithosphere 2000 km in diameter, with temperatures raised 100-200^{o}C above normal. White and McKenzie (1989) suggested that if the continental lithosphere rifted across the thermal anomaly created by the hotspot, passively upwelling asthenosphere would generate large quantities of partial melt. This melt might penetrate to the surface and produce voluminous basaltic flows.

The depleted protolith of the high-temperature peridotites at Jagersfontein is likely to be residue(s) associated with partial melting events in the asthenosphere. This protolith would represent depleted asthenospheric material which had underplated the base of the lithosphere subsequent to the initial stabilization of the lithosphere during the Archaean. The protolith might possibly be associated with the formation of the Karoo basalts. An association with the Karoo basalts is not, however, necessary and the protolith

could represent the residue after any post-Archaean partial melting event.

6.1.5 Isotopic composition

Richardson et al. (1985) suggested that the trace element and isotopic systematics of the high-temperature peridotites did not require a complex origin involving diffusive introduction of a basaltic or protokimberlitic component from megacryst magmas. They suggested that the more frequent occurrence of this peridotite type in kimberlites near the margins of and off the Archaean craton suggested that it may be derived from asthenospheric MORB type sources abutting the subcontinental lithosphere. Localities, with high-temperature peridotites, such as Frank Smith (Boyd, 1974) and Premier (Danchin and Boyd, 1976; Danchin, 1979) are, however, not close to craton margins.

In addition, major element data from this study show that the high-temperature peridotites are formed by enrichment of an initially depleted protolith. The high-temperature peridotites would therefore not be direct samples from the convecting asthenosphere. The protolith is, however, suggested to be the residue of asthenospheric partial melting and might retain some features of its MORB type source.

6.1.6 A model for the high-temperature peridotites

The model suggested here is a refinement of the `metasomatic aureole' model of Gurney and Harte (1980). It is now recognized that typical coarse low-temperature peridotite does not fit the requirements of the pre-enrichment protolith for the high-temperature peridotites.

The depleted protolith of the high-temperature peridotites would appear to be similar in composition to oceanic peridotites. The deformed high-temperature peridotites can not be considered representative of primitive mantle. Both the textural and compositional features presently observed in the high-temperature peridotites are late-stage events in their evolution. Interaction with the Cr-poor megacryst magma is considered to be essential to the enrichment that is presently observed in the high-temperature peridotites.

6.2 REVIEW OF CR-POOR MEGACRYST FORMATION MODELS

The Cr-poor megacrysts have similar high temperatures and pressures of equilibration to the high-temperature peridotites, suggesting a spatial association in the upper mantle. In addition, interaction with the megacryst magma might have resulted in the enrichment observed in the high-temperature peridotites. It is therefore important to determine the petrogenesis of the Cr-poor megacrysts, particularly their association with the host kimberlite.

6.2.1 Geographical distribution

In contrast to the high-temperature peridotites, Cr-poor megacrysts are a ubiquitous feature of Group 1 kimberlites. This is the first line of evidence for a close association between the Cr-poor megacrysts and their host kimberlite. A similar but less strong link is also observed between the Cr-poor megacrysts and the high-temperature peridotites.

6.2.2 Relationship to host kimberlite

The large grain size and lack of aggregation of the Cr-poor megacrysts have led to the commonly accepted view that they crystallized from a liquid. Controversy still exists, however, over whether or not the megacrysts are phenocrysts in a proto-kimberlitic liquid (Mitchell, 1973; Eggler et al., 1979; Gurney et al., 1979; Garrison and Taylor, 1980) or xenocrysts (Boyd and Nixon, 1973a; Pasteris et al., 1979).

The high-temperature crystallization of the megacryst magma is revealed by the absence of optically visible exsolution features. The presence of submicroscopic pigeonite exsolution, indicative of rapid cooling at low pressures, in the subcalcic clinopyroxene megacrysts (McCallister and Nord, 1981), supports rapid eruption of the megacrysts while still at high temperature. These time constraints imply that kimberlite eruption should follow almost immediately (within hours) after megacryst formation. This again

supports a close association between the Cr-poor megacrysts and their host kimberlite.

6.2.3 Depth of origin

In order to account for the wide range in composition and calculated equilibration temperatures of the Cr-poor megacryst suite, Boyd and Nixon (1973a) and Nixon and Boyd (1973b) suggested that megacrysts were dispersed in magmas existing over a large vertical range, with the magma showing decreasing temperature and Mg/(Mg+Fe) with decreasing depth.

In contrast, Gurney et al. (1979) found no evidence for differences in pressure of formation despite large temperature variations, and suggested that the wide temperature range shown by the Cr-poor megacryst suite reflected differentiation at essentially constant pressure in a magma body of limited extent. Harte and Gurney (1981) suggested that the Cr-poor megacryst magma originated in the asthenosphere and moved upwards into a region where temperatures on a normal shield geotherm were the same or below those of the lowest temperature megacrysts. At this level (within the lithosphere), the upward flow was restricted leading to the formation of a magma body of limited size and intricate form. Simultaneous crystallization of the high-temperature undifferentiated magma in the central magma body and low-temperature differentiated magma in the outer apophyses would then take place.

Temperature-pressure estimates indicating constant pressure crystallization were also noted by Ehrenberg (1979) for megacrystalline nodules from The Thumb minette.

The horizontal and vertical dimensions of the area in which the Cr-poor megacrysts crystallized however still remain a matter of dispute.

6.2.4 Compositional evolution

Eggler and Wendlandt (1979) demonstrated experimentally that liquid of kimberlitic composition would coexist with garnet-olivine-orthopyroxene-clinopyroxene±(magnesite-phlogopite) at pressures of 50-60 kbar and suggested that megacrysts were cognate to kimberlite magma. Similarly, Brey et al. (1983) predicted that partial melts generated at depths greater than 120 km would be kimberlitic, highly magnesian and in equilibrium with mineral phases typical of megacryst assemblages.

Harte (1983), however, showed that calculated trace element data for a megacryst magma was close to that of a basanite, and noted that the maximum Mg# of .9 in megacryst olivines was compatible with that expected for picritic-basaltic primary magmas. Similarly, Jones (1987) showed that liquids modelled to be in equilibrium with Cr-poor megacrysts had similar REE patterns to primitive alkali basalts and that the REE were distinctly less fractionated than those of the host kimberlite. In contrast, Irving (1986) noted that an

ilmenite megacryst from Monastery crystallized from a liquid more enriched in LREE than the present host kimberlite.

This discrepancy between interpretations for the source of the Cr-poor megacrysts will be considered in section 6.2.6.

6.2.5 Isotopic composition

Cr-poor megacrysts and their host kimberlites at the surface are not in Sr isotopic equilibrium (Smith, 1984; Jones, 1987). Smith (1984) and Jones (1987) do, however, concede that a partial relationship is possible if the kimberlite is contaminated subsequent to megacryst formation and has a composite origin. Considering the hybrid nature of the kimberlite at the surface, some contamination by assimilation is a certainty (eg. Kirkley, 1987), and a model for proto-kimberlite-megacryst consanguinity (as presented in section 6.2.6) seems entirely justifiable.

6.2.6 A model for megacryst formation

As noted previously various features of the Cr-poor megacrysts, such as their ubiquitous association with Group 1 kimberlites and the requirement that they are transported to the surface soon after formation, suggest a close association between the megacrysts and their host kimberlite. In contrast, the trace element and isotopic compositions of Cr-poor megacrysts suggest a parent magma which is similar in composition to within-plate alkali

basalt or OIB. It is suggested that this apparent discrepancy can be easily resolved.

The Cr-poor megacrysts have crystallized as the result of impingement of a mantle plume (hotspot) on the base of the subcontinental lithosphere. In accord with the model of Wyllie (1989) this mantle plume is forced to diverge when it reaches the lithosphere-asthenosphere boundary. The melt penetrates the lithosphere in the form of small dykes or veins and will start to crystallize and evolve volatile-rich fluids upon reaching the solidus. The evolution of the fluid enhances the propagation of cracks through the lithosphere and preconditions the lithosphere for the eventual eruption of the kimberlite. In this sense, the Cr-poor megacrysts therefore represent the proto-kimberlite magma. The host kimberlite as seen at the surface has been subjected to fractionation, interaction with and assimilation of lithospheric wallrock and near-surface alteration and is not representative of its mantle source.

An important feature of this model is that the megacrysts are considered to be a localized feature rather than a continuous layer in the mantle. This is consistent with the differences in mineral components and compositional trends observed between different localitites and with the geothermobarometric evidence that they represent a 'thermal perturbation' of the steady-state geotherm.

The above observation is similar to that of Hunter and Taylor (1984) who noted that the kimberlite which reaches

the surface is hybrid and that megacrysts would therefore not be phenocrysts sensu stricto, they suggest the term cognate xenocrysts.

6.3 DISCUSSION

Petrogenetic models for the high-temperature peridotites and Cr-poor megacrysts have been considered in the previous sections. It is necessary to put these into perspective in terms of other mantle features.

6.3.1 Lithosphere-asthenosphere boundary

The preceding reviews indicate that a particularly controversial aspect of the petrogenesis of the high-temperature deformed peridotites is their lithospheric or asthenospheric origin. This is of interest, because if the high-temperature peridotites were asthenospheric they might provide an independent means of determining the thickness of the continental lithosphere.

The continental lithosphere is defined, in geophysical terms, as that portion of the upper mantle that moves as a coherent mechanical unit with a velocity similar to the surface crustal plate. The thickness of the continental lithosphere is principally controlled by its age. Jordan (1978,1988) has suggested the presence of a thermal boundary layer, the tectosphere, extending to depths of up to 400 km beneath the Archaean cratons.

Ballard and Pollack (1987) noted that heat flow in the interior of the Kaapvaal craton was typically about 40 mW/m^2, increasing to about 60 mW/m^2 at the boundary between the craton and the surrounding Proterozoic mobile belts and to about 70 mW/m^2 with increasing distance from the craton. Ballard and Pollack (op cit) demonstrated that various parameters could influence this contrast in surface heat flow. They developed models which were dependent on: the thickness of the lithospheric root beneath the Archaean craton which diverted the heat into the surrounding mobile belts, the contrast in crustal heat production beneath the craton and the mobile belts, the relative contribution of the heat produced in the crust and the thickness of the mobile belt lithosphere. The models developed by Ballard and Pollack (1987) are consistent with a cratonic root beneath southern Africa extending to depths of 200 to 400 km.

Translation of the geophysical definition of the lithosphere into geochemical terms remains controversial. In addition, as noted by Bailey (1987), the geochemical nature of the asthenosphere still needs to be unequivocally defined. Bailey (1987) further observed that at present the ascription of a rock to the asthenosphere, on the basis of selected trace elements and isotope ratios, is a convoluted way of saying it has some attributes of MORB. The asthenosphere is convecting and will therefore not preserve chemical heterogeneities to the extent possible in the rigid sub-continental lithosphere.

The high-temperature peridotites and Cr-poor megacrysts at Jagersfontein both yield a wide range of equilibration temperatures over essentially the same restricted depth interval. This depth of equilibration is possibly an indication of a physical barrier in the upper mantle. As noted previously, the lithosphere-asthenosphere boundary is a critical level in the mantle, where the mantle flow changes from convective (ductile) to static (brittle). This change in rheology is sufficient to stall mantle plumes/diapirs with the formation of magma chambers and the transition from a mechanism of diapiric uprise to crack propagation (Wyllie, 1987).

It is therefore suggested that the depth of equilibration indicated by the high-temperature peridotites represents the position of the lithosphere-asthenosphere boundary beneath Jagersfontein. The ambient temperature of the mantle at this depth (assuming a conductive geotherm) would be approximately equal to, or lower than, that of the lowest temperature calculated for the high-temperature peridotites at Jagersfontein. It was also previously noted (p. 163) that the compositional features of the least enriched high-temperature peridotite suggested that it could not represent part of the convecting asthenosphere. The high-temperature peridotites are therefore suggested to represent samples of the base of the lithosphere. Interaction between the high-temperature asthenospheric megacryst magma and the cooler lithospheric wallrocks has produced a range of temperature in the high-temperature peridotites reflecting proximity to the site of intrusion of the megacryst magma.

6.3.2 Composite xenoliths

Although it is proposed here that the composition of the high-temperature peridotites is the result of veining and wallrock enrichment, composite peridotite/megacryst xenoliths have not been found.

Composite peridotite/pyroxenite xenoliths are occasionally found in alkali basalts. In these xenoliths it is possible to determine the mineralogic and compositional changes in the wallrocks adjacent to the veins which might be the product of interaction with silicate melts. Observations made on these composite peridotite/pyroxenite xenoliths have led to the conclusion that the host Mg-rich peridotite is altered to more Fe, Ti and alkali-rich compositions adjacent to pyroxenite veins by infiltration of the vein forming fluids (eg. Wilshire et al., 1980; Kempton et al., 1984; Menzies et al., 1985).

The ubiquitous association of megacrysts (tschermakitic clinopyroxene, aluminous orthopyroxene, kaersutitic amphibole etc.) and veined Cr-diopside xenoliths in alkali basalts and the compositional similarities between the megacrysts and the Al-augite xenoliths has been noted by several researchers (Irving, 1974, 1980; Wilshire and Shervais, 1975). Wilshire et al. (1980) suggested that this was best explained by disruption of the vein systems to produce the megacryst assemblage. Menzies et al. (1985) also noted a similarity between vein minerals and megacryst

for both isotopes and REE, adding support to the contention that the megacrysts represent disrupted veins and that the veins are pegmatites or apophyses that formed close to conduits of basanitic magma. Vein assemblages and structural relationships analogous to those seen in the xenoliths from alkali basalts are also observed in alpine peridotite massifs.

Composite xenoliths are also found at the Matsoku kimberlite, northern Lesotho, where the host rocks have the modal and textural characteristics of Mg-rich coarse common peridotites, but the minerals are enriched in FeO and TiO_2 without evidence of modal metasomatism. Harte et al. (1987) noted that similarities between the Matsoku pyroxenite sheets and the Al-augite dykes in spinel peridotites included: richness in clinopyroxene, minerals with relatively high TiO_2 and Al/(Al+Cr), and the presence of minerals associated with modal metasomatism in the adjacent peridotites. Harte et al. (op cit.) noted that despite the intrusive appearance of the pyroxenite sheets, the extreme variability of their compositions did not indicate that they commonly represented liquid compositions. This departure from expected liquid compositions is also seen in the Al-augite pyroxenite dykes in spinel peridotites from alkali basalts, and a variety of crystal/liquid segregation processes have been put forward as explanations (eg. Wilshire et al., 1980; Irving, 1980).

These composite xenoliths do not support the idea of deformation associated with conduit formation because the

peridotites hosting the veins are coarse-grained. Pike and Schwarzman (1977) noted that a pyroxenite intrusive contact (ie the conduit) crosscut and therefore postdated deformation in a peridotite and Harte et al. (1987) noted that the pyroxenite sheets at Matsoku were not associated with deformation. Conduit formation would therefore appear not to be a viable mechanism for the high strain rates required to produce the fluidal textures seen in the high-temperature deformed peridotites. The porphyroclastic peridotites at Matsoku do, however, show evidence of significant annealing subsequent to deformation and this could have erased evidence of deformation adjacent to the veins. The high-temperature peridotites, in contrast, are transported to the surface soon after deformation. In addition, the composite xenoliths entrained by alkali basalts are spinel lherzolites and are of shallower origin than the high-temperature peridotites. At these shallower depths, intrusion of magma might result in fractures which are subsequently infilled to form veins, whereas at greater depth, intrusion of magma might be associated with plastic deformation.

6.3.3 Distribution of Cr-poor megacrysts and high-temperature peridotites

If there is an association between the Cr-poor megacrysts and the high-temperature peridotites it might be expected that they should both be found at the same locality. This is, however, not always the case and possible explanations need to be considered.

Although the Kimberley pipes (Kampfersdam, Bultfontein, De Beers) do not appear to contain any high-temperature deformed garnet lherzolites, they do contain a suite of metasomatized dunites (Dawson et al., 1981; Boyd et al., 1983). These dunites are commonly deformed and show similar FeO, TiO_2 and Na_2O enrichment to that observed at Jagersfontein. These authors have suggested that the kimberlitic magma was the source of the metasomatic fluids. The possibility that the enrichment might be associated with the megacryst magma must also be considered. Smith and Boyd (1986) have also described TiO_2 zonation in the garnet porphyroclasts of a low-temperature (1100^{o}C) deformed peridotite from Bultfontein and this trait in the Bultfontein xenoliths might be more common than present data indicate.

High-temperature peridotites are very rare at Monastery, the type locality for Cr-poor megacrysts, but phlogopite garnet peridotites are common. A single example of a lamellar clinopyroxene-ilmenite megacryst in a phlogopite peridotite has been found at Monastery (Moore, pers. comm.). Intrusion of the megacryst magma at Monastery does not appear to be associated with high-temperatures, but might be associated with modal metasomatism of the coarse low-temperature peridotites. This is consistent with the process suggested by Harte (1987), in which a progression from non-modal metasomatism to modal metasomatism may be associated with the progressive evolution of the intrusive magma and its more intimate penetration of the host rocks.

It is important to note that high-temperature peridotites have not been recovered from a locality which does not contain Cr-poor megacrysts.

6.3.4 Source of the kimberlite/megacryst magma

Kimberlites are petrographically complex and variations in texture, xenolith and xenocryst content, content and proportions of macrocrysts, and mineralogy of the matrix all combine to give a wide range of chemical compositions (Dawson, 1987). Kimberlites are particularly notable for their high incompatible element abundances. Eggler and Wendlandt (1979) demonstrated that kimberlites might be produced by the eutectic-like melting of phlogopite magnesite peridotite at pressures of 40-50 kbar at 1000-1300^{o}C. Kramers et al. (1981) suggested that kimberlite could be derived by small degrees of melting of `ordinary' mantle, whereas Nixon et al. (1981) suggested metasomatic enrichment of the source before melting.

Kimberlites have been subdivided on the basis of geochemical and petrographic differences into Group I (basaltic) and Group II (micaceous) varieties. Smith (1983) suggested that the Group I kimberlites were derived from partial melting in the asthenosphere in view of similarities between Sr, Nd and Pb isotopic signatures and those from ocean island basalts (OIB); while Group II kimberlites with high Sr and low Nd and Pb were derived from the subcontinental lithosphere. A zone of oceanic basalts with anomalous isotopic compositions

encircling the globe at ~30°S was noted by Hart (1984) and termed the DUPAL anomaly. Le Roex (1986) subsequently noted that South Atlantic hotspots (OIB's) falling within the DUPAL anomaly had similar characteristics to Group II kimberlites, while those outside the DUPAL anomaly were similar to Group I. Le Roex (1986) suggested that this implied that the source region for Group II kimberlites might also be located in the asthenosphere. Plate tectonic reconstruction models (eg. Crough et al., 1980) are also consistent with possible correlations between South Atlantic hotspots and southern African kimberlites.

Isotopic constraints indicate that OIB's were derived from mantle sources with a time-integrated depletion in Rb and Nd relative to Sr and Sm respectively (O'Nions et al., 1977), whereas they are strongly enriched in incompatible elements. A similar 'decoupling' of isotopic ratios and trace element abundances is seen in the Group 1 kimberlites. Based on current knowledge of partition coefficients, the incompatible element enrichment observed in OIB cannot easily be generated by simple partial melting of depleted source regions consistent with their low $^{87}Sr/^{86}Sr$ and high $^{143}Nd/^{144}Nd$ ratios. This 'decoupling' of isotopic ratios and trace element abundances suggests that there have been comparatively recent (< .2 b.y.) enrichment events in the mantle. Weaver et al. (1987) noted that four main hypotheses had been advocated to explain these anomalous features:

1] Upwelling of primordial or near-primordial mantle across the mesosphere-asthenosphere boundary (Schilling, 1973;

Sun and Hanson, 1975; Dupre and Allegre, 1980; Allegre, 1982)

2] Subducted ocean crust which has had a considerable residence time at the mesosphere-asthenosphere boundary (Hofmann and White, 1982; Ringwood, 1982; Vollmer, 1983; White, 1985)

3] Delaminated subcontinental mantle resident in the deep asthenosphere (McKenzie and O'Nions, 1983; Cohen et al., 1984)

4] Contamination of a mantle source by recycled continental crustal material (Hawkesworth et al., 1979; Cohen and O'Nions, 1982; White, 1985)

The Jagersfontein kimberlite is a Group 1 kimberlite (Smith, 1983) and has similar isotopic characteristics to non-DUPAL hotspots. The Group 1 kimberlites are therefore likely to have formed by decompression melting of a rising mantle plume (hotspot) from the same source as the non-DUPAL OIBs. The differences in trace element concentrations between the non-DUPAL OIBs and Group 1 kimberlites can be partly explained by different degrees of partial melting of the same source. In contrast to the OIB the kimberlite would be formed by smaller degrees of partial melting at a greater depth due to the greater thickness of the Archaean lithosphere. None of the presently known non-DUPAL hotspots in the South Atlantic, however have palaeotracks which suggest a close association with the Jagersfontein kimberlite. Although the confirmatory evidence of a possible hotspot origin is lacking, it does not necessarily preclude a hotspot origin for the Jagersfontein kimberlite.

6.3.5 The subcontinental mantle beneath Jagersfontein

The study of a large selection of mantle-derived xenoliths from a single locality enables the development of possible palaeo-stratigraphic models.

With the exception of one high-temperature coarse peridotite (discussed in this study), the coarse peridotite suite at Jagersfontein has been further subdivided according to temperatures and pressures of equilibration. Winterburn and Harte (1987) have described medium temperature (1050 >T >900^{o}C, 37 >P >33 kbar) and low temperature (T <900^{o}C, P <34 kbar) groups. In contrast to the high-temperature peridotites, these two groups commonly show modal metasomatism. The metasomatic minerals include phlogopite, amphibole, Cr-spinel, Cr-diopside, ilmenite and rutile (Field et al., 1989; Winterburn and Harte, 1987). Haggerty (1983) has also reported the presence of lindsleyite and mathiasite (LIMA) in the heavy mineral concentrate at Jagersfontein. Field et al. (1989) noted that the Jagersfontein xenoliths were dominated by disseminated metasomatism in comparison to Kimberley where both veined and disseminated metasomatized xenoliths are found (eg. Erlank et al., 1987). This coarse peridotite suite is suggested to represent the old, cold lithospheric keel which has remained isolated from mantle convection and been variously affected by metasomatic processes since its stabilization, possibly during the Archaean.

In contrast, the protolith for the high-temperature peridotites is suggested to be coarse low-temperature peridotite which has more recently stabilized as part of the base of the lithospheric keel. This depleted peridotite is enriched just prior to kimberlite eruption by interaction with the Cr-poor megacryst magma.

ACKNOWLEDGEMENTS

Financial support for the period of this study was received from the CSIR-FRD and a Ph.D. studentship from Prof. J.J. Gurney.

As my thesis supervisor, John Gurney proved to be a constant source of enthusiasm. His patience and encouragement over the last period of this study was greatly appreciated. As Head of Department, Tony Erlank must be thanked for encouraging me to continue with post-graduate studies.

I was fortunate to be given the opportunity to analyze samples at both the Max Planck Institute for Cosmochemistry, in Mainz, West Germany and the Bernard Price Institute for Geophysics, in Johannesburg. Emil Jagoutz and Craig Smith are thanked for making all the necessary arrangements.

At the MPI, Craig, Dieter, Emil and Jutta provided invaluable assistance in unravelling the intracacies of isotope analysis. Similarly, thanks must go to the staff and students at the BPI, especially Craig, Janet, Alastair, Moose, Trevor and Ingeborg.

Special thanks are due to Dieter and Gabi Schier and Craig and Meryl Smith for their incredible hospitality during my stay in Mainz, and to Michelle, Jenny, Annalie and Peter for their hospitality and friendship during my visits to Johannesburg.

In their special areas of expertise, thanks are due to Dick Rickard and Anton le Roex for instruction in use of the electron microprobe, to Dave Hill and Andy Duncan for instruction in computing techniques, to David Wilson for thin section preparation, to Patrick Sieas for maintaining the xerox facility and to Bruce Cairns for keeping the whole show on the road. Special thanks must also go to Lynn and Susie for their endless capacity for morale boosting.

To all ex- and present inmates of `Joe's Garage' and `507' - thanks for putting up with my endless cups of coffee, for providing inspiration by handing in your theses and for encouraging me to hand in mine! Special thanks are due to fellow members of the Kimberlite Research Group, Rory, Melissa, Marshall, Stuart and Leon for many hours of discussion, help and advice - I look forward to our next field trip together.

Lastly, thanks must go to my family who have put up with all my years of `studying' - I hope I eventually manage to put it all to good use!

REFERENCES

ALLEGRE C.J. 1982. Chemical geodynamics. Tectonophysics 81, 109-132.

ALLEGRE C.J., SHIMIZU N. and ROUSSEAU D. 1982. History of the continental lithosphere recorded by ultramafic xenoliths. Nature 296, 732-735.

ANDERSON D.L. and BASS J.D. 1984. Mineralogy and composition of the upper mantle. Geophysical Research Letters 11, 637-640.

AOKI K.I., FUJIMAKI H. and KITAMURA M. 1980. Exsolved garnet-bearing pyroxene megacrysts from some South African kimberlites. Lithos 13, 269-279.

ARTYUSHKOV E.V. and SOBOLEV S.V. 1984. Physics of the kimberlite magmatism. In: Kornprobst J. ed., Kimberlites 11A: Kimberlites and related rocks, pp 309-322. Elsevier Science Publishers.

AVE LALLEMANT H.G., MERCIER J-C.C., CARTER N.L. and ROSS J.V. 1980. Rheology of the upper mantle: inferences from peridotite xenoliths. Tectonophysics 70, 85-113.

BAILEY D.K. 1987. Mantle metasomatism - perspective and prospect. In: Fitton J.G. and Upton B.G.J. eds., Alkaline Igneous Rocks. Geological Society Special Publication 30, 1-13.

BALLARD S. and POLLACK H.N. 1987. Diversion of heat by Archean cratons: a model for southern Africa. Earth and Planetary Science Letters 85, 253-264.

BARRETT D.R. 1975. The genesis of kimberlites and associated rocks: Strontium isotopic evidence. Physics and Chemistry of the Earth 9, 637-653.

BASU A.R. and TATSUMOTO M. 1980. Nd isotopes in selected mantle-derived rocks and minerals and their implication for mantle evolution. Contributions to Mineralogy and Petrology 75, 43-54.

BERTRAND P. and MERCIER J-C.C. 1985. The mutual solubility of coexisting ortho and clinopyroxene: toward an absolute geothermometer for the natural system? Earth and Planetary Science Letters 76, 109-122.

BERTRAND P., SOTIN C., MERCIER J-C.C and TAKAHASHI E. 1986. From the simplest chemical system to the natural one: garnet peridotite barometry. Contributions to Mineralogy and Petrology 93, 168-178.

BOULLIER A.M. and NICOLAS A. 1975. Classification of textures and fabrics of peridotite xenoliths from South African kimberlites. Physics and Chemistry of the Earth 9, 467-476.

BOYD F.R. 1973. A pyroxene geotherm. Geochimica et Cosmochimica Acta 37, 2533-2546.

BOYD F.R. 1974. Ultramafic nodules from the Frank Smith kimberlite pipe, South Africa. Carnegie Institution of Washington Yearbook 73, 285-294.

BOYD F.R. 1987. High- and low-temperature garnet peridotite xenoliths and their possible relation to the lithosphere-asthenosphere boundary beneath southern Africa. In: Nixon P.H. ed., Mantle Xenoliths, pp 403-412. J.Wiley & Sons, New York.

BOYD F.R. and FINNERTY A.A. 1980. Conditions of origin of natural diamonds of peridotite affinity. Journal of Geophysical Research 85(B12), 6911-6918.

BOYD F.R. and GURNEY J.J. 1986. Diamonds and the African lithosphere. Science 232, 472-477.

BOYD F.R. and McCALLISTER R.H. 1976. Densities of fertile and sterile garnet peridotites. Geophysical Research Letters 3, 509-512.

BOYD F.R. and MERTZMAN S.A. 1987. Composition and structure of the Kaapvaal lithosphere, southern Africa. In: Mysen B.O. ed., Magmatic Processes: Physiochemical Principles, pp 13-24. Special Publication No.1, The Geochemical Society, University Park, PA.

BOYD F.R. and NIXON P.H. 1972. Ultramafic nodules from the Thaba Putsoa kimberlite pipe. Carnegie Institution of Washington Yearbook 71, 363-373.

BOYD F.R. and NIXON P.H. 1973a. Origin of the ilmenite-silicate nodules in kimberlites from Lesotho and South Africa. In: Nixon P.H. ed., Lesotho Kimberlites, pp 254-268. Lesotho National Development Corporation, Maseru.

BOYD F.R. and NIXON P.H. 1973b. Structure of the upper mantle beneath Lesotho. Carnegie Institution of Washington Yearbook 72, 431-445.

BOYD F.R. and NIXON P.H. 1975. Origins of ultramafic nodules from some kimberlites of northern Lesotho and the Monastery mine, South Africa. Physics and Chemistry of the Earth 9, 431-454.

BOYD F.R. and NIXON P.H. 1978. Ultramafic nodules from the Kimberley pipes, South Africa. Geochimica et Cosmochimica Acta 42, 1367-1382.

BOYD F.R. and NIXON P.H. 1979. Garnet lherzolite xenoliths from the kimberlites of East Griqualand, South Africa. Carnegie Institution of Washington Yearbook 78, 488-492.

BOYD F.R., JONES R.A. and NIXON P.H. 1983. Mantle metasomatism: the Kimberley dunites. Carnegie Institution of Washington Yearbook 82, 330-336.

BOYD F.R., DAWSON J.B. and SMITH J.V. 1984a. Granny Smith diopside megacrysts from the kimberlites of the Kimberley area and Jagersfontein, South Africa. Geochimica et Cosmochimica Acta 48, 381-384.

BOYD F.R., NIXON P.H. and BOCTOR N.Z. 1984b. Rapidly crystallized garnet pyroxenite xenoliths possibly related to discrete nodules. Contributions to Mineralogy and Petrology 86, 119-130.

BREY G., BRICE W.R., ELLIS D.J., GREEN D.H., HARRIS K.L. and RYABCHIKOV I.D. 1983. Pyroxene-carbonate reactions in the upper mantle. Earth and Planetary Science Letters 62, 63-74.

CARSWELL D.A. 1975. Primary and secondary phlogopites and clinopyroxenes in garnet lherzolite xenoliths. Physics and Chemistry of the Earth 9, 417-429.

CARSWELL D.A. and GIBB F.G.F. 1980. Geothermobarometry of garnet lherzolite nodules with special reference to those from the kimberlites of northern Lesotho. Contributions to Mineralogy and Petrology 74, 403-416.

CARSWELL D.A. and GIBB F.G.F. 1987. Evaluation of mineral thermometers and barometers applicable to garnet lherzolite assemblages. Contributions to Mineralogy and Petrology 95, 499-511.

CARTER N.L. 1975. Steady state flow of rocks. Reviews of Geophysics and Space Physics 14, 301-360.

COHEN R.S. and O'NIONS R.K. 1982. Identification of recycled continental material in the mantle from Sr, Nd and Pb isotope investigations. Earth and Planetary Science Letters 61, 73-84.

COHEN R.S., O'NIONS R.K. and DAWSON J.B. 1984. Isotope geochemistry of xenoliths from East Africa: implications for development of mantle reservoirs and their interaction. Earth and Planetary Science Letters 68, 209-220.

COX K.G., GURNEY J.J. and HARTE B. 1973. Xenoliths from the Matsoku pipe. In: Nixon P.H. ed., Lesotho Kimberlites, pp 76-100. Lesotho National Development Corporation, Maseru.

CROUGH S.T., MORGAN W.J. and HARGRAVES R.B. 1980. Kimberlites: Their relation to mantle hotspots. Earth and Planetary Science Letters 50, 260-274.

DANCHIN R.V. 1979. Mineral and bulk chemistry of garnet lherzolite and garnet harzburgite xenoliths from the Premier Mine, South Africa. In: Boyd F.R. and Meyer H.O.A. eds., The Mantle Sample: Inclusions in kimberlites and other volcanics, pp 104-126. American Geophysical Union, Washington.

DANCHIN R.V. and BOYD F.R. 1976. Ultramafic nodules from the Premier kimberlite pipe, South Africa. Carnegie Institution of Washington Yearbook 75, 531-538.

DANIELS L.R.M. and GURNEY J.J. 1989. The chemistry of concentrate minerals and diamond inclusions of the Dokolwayo kimberlite, Swaziland. In: Kimberlites and related rocks, Volume 2: Their mantle/crust setting, diamonds and diamond exploration. Geological Society of Australia Special Publication 14, pp 1012-1021. Blackwell.

DAWSON J.B. 1980. Kimberlites and their xenoliths. Springer-Verlag, Berlin, New York. 250 pp.

DAWSON J.B. 1987. The kimberlite clan: relationship with olivine and leucite lamproites and inferences for upper-mantle metasomatism. In: Fitton J.G. and Upton B.G.J. eds., Alkaline Igneous Rocks. Geological Society Special Publication 30, 95-101.

DAWSON J.B. and SMITH J.V. 1986. Relationships between eclogites and certain megacrysts from the Jagersfontein kimberlite, South Africa. Lithos 19, 325-330.

DAWSON J.B. and STEPHENS W.E. 1975. Statistical classification of garnets from kimberlite and associated xenoliths. Journal of Geology 83, 589-607.

DAWSON J.B., GURNEY J.J. and LAWLESS P.J. 1975. Palaeogeothermal gradients derived from xenoliths in kimberlite. Nature 257, 299-300.

DAWSON J.B., HERVIG R.L. and SMITH J.V. 1981. Fertile, iron-rich dunite xenoliths from the Bultfontein kimberlite, South Africa. Fortschritte der Mineralogie 59, 303-324.

DRURY M.R. and VAN ROERMUND H.L.M. 1988a. Metasomatic origin for Fe-Ti-rich multiphase inclusions in olivine from kimberlite xenoliths. Geology 16, 1035-1038.

DRURY M.R. and VAN ROERMUND H.L.M. 1988b. Fluid assisted recrystallization in upper mantle peridotites from kimberlites. Journal of Petrology 30, 133-152.

DUPRE B. and ALLEGRE C.J. 1980. Pb-Sr-Nd isotopic correlation and the chemistry of the North Atlantic mantle. Nature 286, 17-22.

EGGLER D.H. and WENDLANDT R.F. 1979. Experimental studies on the relationship between kimberlite magmas and partial melting of peridotite. In: Boyd F.R. and Meyer H.O.A. eds., Kimberlites, Diatremes and Diamonds, pp 330-338. American Geophysical Union, Washington.

EGGLER D.H., McCALLUM M.E. and SMITH C.B. 1979. Megacryst assemblages in kimberlite from northern Colorado and southern Wyoming: petrology, geothermometry-barometry and areal distribution. In: Boyd F.R. and Meyer H.O.A. eds., The Mantle Sample, pp 213-226. American Geophysical Union, Washington.

EHRENBERG S.N. 1979. Garnetiferous ultramafic inclusions in minette from the Navajo volcanic field. In: Boyd F.R. and Meyer H.O.A. eds., The Mantle Sample, pp 330-344. American Geophysical Union, Washington.

EHRENBERG S.N. 1982a. Petrogenesis of garnet lherzolite and megacrystalline nodules from The Thumb, Navajo volcanic field. Journal of Petrology 23, 507-547.

EHRENBERG S.N. 1982b. Rare earth element geochemistry of garnet lherzolite megacrystalline nodules from minette of Colorado Plateau province. Earth and Planetary Science Letters 57, 191-210.

ELLIS D.G. and GREEN D.H. 1979. An experimental study of the effect of Ca upon garnet-clinopyroxene Fe-Mg exchange equilibria. Contributions to Mineralogy and Petrology 71, 13-22.

ERLANK A.J., ALLSOPP H.L., HAWKESWORTH C.J. and MENZIES M.A. 1982. Chemical and isotopic characterization of upper mantle metasomatism in the peridotite nodules from Bultfontein. Terra Cognita 2, 261-263.

ERLANK A.J., WATERS F.G., HAWKESWORTH C.J., HAGGERTY S.E., ALLSOPP H.L., RICKARD R.S. and MENZIES M.A. 1987. Evidence for mantle metasomatism in peridotite nodules from the Kimberley pipes, South Africa. In: Menzies M.A. and Hawkesworth C.J. eds., Mantle Metasomatism, pp 221-311. Academic Press Geology Series.

EVENSEN N.M., HAMILTON P.J. and O'NIONS R.K. 1978. Rare-earth abundances in chondritic meteorites. Geochimica et Cosmochimica Acta 42, 1199-1212.

FIELD S.W., HAGGERTY S.E. and ERLANK A.J. 1989. Subcontinental metasomatism in the region of Jagersfontein, South Africa. In: Kimberlites and Related Rocks, Volume 2: Their mantle/crust setting, diamonds and diamond exploration. Geological Society of Australia Special Publication 14, pp 771-783. Blackwell.

FINNERTY A.A. (in press). Xenolith-derived geotherms: whither the inflection?

FINNERTY A.A. and BOYD F.R. 1984. Evaluation of thermobarometers for garnet peridotites. Geochimica et Cosmochimica Acta 48, 15-27.

FINNERTY A.A. and BOYD F.R. 1986. Thermometer as presented in Finnerty A.A. and Boyd F.R. (1987).

FINNERTY A.A. and BOYD F.R. 1987. Thermobarometry for garnet peridotites: basis for the determination of thermal and compositional structure of the upper mantle. In: Nixon P.H. ed., Mantle Xenoliths, pp 381-402. J.Wiley & Sons, New York.

FRICK C. 1973. The sulphides in griquaite and garnet-peridotite xenoliths in kimberlite. Contributions to Mineralogy and Petrology 39, 1-16.

GARRISON J.R.(Jnr) and TAYLOR L.A. 1980. Megacrysts and xenoliths in kimberlite, Elliott County, Kentucky: A mantle sample from beneath the Permian Appalachian Plateau. Contributions to Mineralogy and Petrology 75, 27-42.

GOETZE C. 1975. Sheared lherzolites: from the point of view of rock mechanics. Geology 3, 172-173.

GREEN H.W. and GUEGUEN Y. 1974. Origin of kimberlites by diapiric upwelling in the upper mantle. Nature 249, 617-620.

GREEN H.W. and GUEGUEN Y. 1983. Deformation of peridotite in the mantle and extraction by kimberlite: a case history documented by fluid and solid precipitates in olivine. Tectonophysics 92, 71-92.

GRIFFIN W.L., SMITH D., BOYD F.R., COUSENS D.R., RYAN C.G., SIE S.H. and SUTER G.F. (1989). Trace-element zoning in garnets from sheared mantle xenoliths. Geochimica et Cosmochimica Acta 53, 561-567.

GUEGUEN Y. and NICOLAS A. 1980. Deformation of mantle rocks. Annual Reviews in Earth and Planetary Science 8, 119-144.

GURNEY J.J. and HARTE B. 1980. Chemical variations in upper mantle nodules from southern African kimberlites. Philosophical Transactions of the Royal Society of London A297, 273-293.

GURNEY J.J., JAKOB W.R.O. and DAWSON J.B. 1979. Megacrysts from the Monastery kimberlite pipe, South Africa. In: Boyd F.R. and Meyer H.O.A. eds., The Mantle Sample, pp 227-243. American Geophysical Union, Washington.

HAGGERTY S.E. 1983. The mineral chemistry of new titanates from the Jagersfontein kimberlite, South Africa: Implications for metasomatism in the upper mantle. Geochimica et Cosmochimica Acta 47, 1833-1854.

HAGGERTY S.E. and BOYD F.R. 1975. Kimberlite in an olivine megacryst from Monastery. Long Abstracts, Kimberlite Symposium, London.

HARLEY S.L. 1984. Comparison of the garnet-orthopyroxene geobarometer with recent experimental studies and applications to natural assemblages. Journal of Petrology 25, 697-712.

HART S.R. 1984. A large-scale isotope anomaly in the Southern Hemisphere mantle. Nature 309, 753-757.

HARTE B. 1977. Rock nomenclature with particular relation to deformation and recrystallization textures in olivine-bearing xenoliths. Journal of Petrology 85, 279-288.

HARTE B. 1983. Mantle peridotites and processes - the kimberlite sample. In: Hawkesworth C.J. and Norry M.J. eds., Continental basalts and mantle xenoliths, pp 46-99. Shiva Publishing Limited, Cheshire.

HARTE B. 1987. Metasomatic events recorded in mantle nodules. In: Nixon P.H. ed., Mantle Xenoliths, pp 625-640. J. Wiley & Sons, New York.

HARTE B. and GURNEY J.J. 1981. The mode of formation of chromium-poor megacryst suites from kimberlites. Journal of Geology 89, 749-753.

HARTE B. and GURNEY J.J. 1982. Compositional features of peridotite nodules from the Jagersfontein kimberlite pipe, South Africa. Terra Cognita 2, 256-257.

HARTE B., COX K.G. and GURNEY J.J. 1975. Petrography and geological history of the upper mantle xenoliths from the Matsoku kimberlite pipe. Physics and Chemistry of the Earth 9, 477-506.

HARTE B., WINTERBURN P.A. and GURNEY J.J. 1987. Metasomatic and enrichment phenomena in garnet peridotite facies mantle xenoliths from the Matsoku kimberlite pipe, Lesotho. In: Menzies M.A. and Hawkesworth C.J. eds., Mantle Metasomatism, pp 145-220. Academic Press Geology Series.

HAWKESWORTH C.J., NORRY M.J., RODDICK J.C. and VOLLMER R. 1979. $^{143}Nd/^{144}Nd$ and $^{87}Sr/^{86}Sr$ ratios from the Azores and their significance in LIL-element enriched mantle. Nature 280, 28-31.

HENOC J., HEINRICH K.F.J. and MYKLEBUST R.L. 1973. A rigorous correction procedure for quantitative electron probe microanalysis. U.S.Bureau of Standards, Technical Note 769, U.S.Govt. Printing Office, Washington.

HERVIG R.L., SMITH J.V. and DAWSON J.B. 1986. Lherzolite xenoliths in kimberlites and basalts: petrogenetic and crystallochemical significance of some minor and trace elements in olivine, pyroxenes, garnet and spinel. Transactions of the Royal Society of Edinburgh: Earth Sciences 77, 181-201.

HOFMANN A.W. and WHITE W.M. 1982. Mantle plumes from ancient oceanic crust. Earth and Planetary Science Letters 57, 421-436.

HUNTER R.H. and TAYLOR L.A. 1982. Instability of garnet from the mantle: Glass as evidence of metasomatic melting. Geology 10, 617-620.

HUNTER R.H. and TAYLOR L.A. 1984. Magma-mixing in the low velocity zone: kimberlitic megacrysts from Fayette County, Pennsylvania. American Mineralogist 69, 16-29.

IRVING A.J. 1974. Megacrysts from the Newer Basalts and other basaltic rocks of southeastern Australia. Geological Society of America Bulletin 85, 1503-1514.

IRVING A.J. 1976. On the validity of palaeogeotherms determined from xenolith suites in basalts and kimberlites. American Mineralogist 61, 638-642.

IRVING A.J. 1978. A review of experimental studies of crystal/liquid trace element partitioning. Geochimica et Cosmochimica Acta 42, 743-747.

IRVING A.J. 1980. Petrology and geochemistry of composite ultramafic xenoliths in alkali basalts and implications for magmatic processes within the mantle. American Journal of Science 280, 389-426.

IRVING A.J. 1986. Polybaric magma mixing in alkali basalts and kimberlites: Evidence from corundum, zircon and ilmenite megacrysts. 4IKC, Geological Society of Australia Abstracts 16, 262-264.

JAGOUTZ E. and WANKE H. 1986. Sr and Nd isotopic systematics of Shergotty meteorite. Geochimica et Cosmochimica Acta 50, 939-953.

JAKOB W.R.O. 1977. Geochemical aspects of the megacryst suite from the Monastery kimberlite pipe. Unpublished M.Sc., University of Cape Town.

JOHNSTON J.L. 1973. Petrology and geochemistry of ultramafic xenoliths from the Jagersfontein mine, OFS, South Africa. Abstracts volume, First International Kimberlite Conference, pp 181-183.

JONES R.A. 1987. Strontium and neodymium isotopic and rare earth element evidence for the genesis of megacrysts in kimberlites of southern Africa. In: Nixon P.H. ed., Mantle Xenoliths, pp 711-724. J.Wiley & Sons, New York.

JORDAN T.H. 1978. Composition and development of the continental tectosphere. Nature 274, 544-548.

JORDAN T.H. 1979. Mineralogies, densities and seismic velocities of garnet lherzolites and their geophysical implications. In: Boyd F.R. and Meyer H.O.A. eds., The Mantle Sample, pp 1-14. American Geophysical Union, Washington.

JORDAN T.H. 1988. Structure and formation of the continental tectosphere. Journal of Petrology 29, 11-37.

KEMPTON P.D., MENZIES M.A. and DUNGAN M.A. 1984. Petrography, petrology and geochemistry of xenoliths and megacrysts from the Geronimo volcanic field, southeastern Arizona. In: Kornprobst J. ed., Kimberlites IIB: The mantle and crust-mantle relationships, pp 71-84. Elsevier Science Publishers.

KENNEDY C.S. and KENNEDY G.C. 1976. The equilibrium boundary between graphite and diamond. Journal of Geophysical Research 81, 2467-2470.

KESSON S.E. and RINGWOOD A.E. 1988. Slab-mantle interactions II: Sheared and refertilized garnet peridotite xenoliths - samples from Wadati-Benioff zones? Chemical Geology 70, 52.

KIRKLEY M.B. 1987. Aspects of the geochemistry of kimberlite carbonates. Unpublished Ph.D., University of Cape Town.

KRAMERS J.D. 1977. Lead and strontium isotopes in Cretaceous kimberlites and mantle-derived xenoliths from southern Africa. Earth and Planetary Science Letters 34, 419-431.

KRAMERS J.D. 1979. Lead, Uranium, Strontium, Potassium and Rubidium in inclusion-bearing diamonds and mantle-derived xenoliths from southern Africa. Earth and Planetary Science Letters 42, 58-70.

KRAMERS J.D. and SMITH C.B. 1983. A feasibility study of U-Pb and Pb-Pb dating of kimberlites using groundmass mineral fractions and whole rock samples. Isotope Geoscience 1, 23-35.

KRAMERS J.D., SMITH C.B., LOCK N.P., HARMON R.S. and BOYD F.R. 1981. Can kimberlites be generated from ordinary mantle? Nature 291, 53-56.

LE ROEX A.P. 1986. Geochemical correlations between southern African kimberlites and South Atlantic hotspots. Nature 324, 243-245.

LE ROEX A.P. 1987. Source regions of mid-ocean ridge basalts: Evidence for enrichment processes. In: Menzies M.A. and Hawkesworth C.J. eds., Mantle Metasomatism, pp 389-422. Academic Press, London.

LINDSLEY D.H. and DIXON S.A. 1976. Diopside-enstatite equilibria at 850 ^{o}C to 1400 ^{o}C, 5 to 35 kbars. American Journal of Science 276, 1285-1301.

MacGREGOR I.D. 1974. The system MgO-Al_2O_3-SiO_2: Solubility of Al_2O_3 in enstatite for spinel and garnet peridotite compositions. American Mineralogist 59, 110-119.

MacGREGOR I.D. 1975. Petrologic and thermal structure of the upper mantle beneath South Africa in the Cretaceous. Physics and Chemistry of the Earth 9, 455-466.

MacGREGOR I.D. and BASU A.R. 1974. Thermal structure of the lithosphere: a petrologic model. Science 185, 1007-1011.

MAZZONE P., McLANAHAN A. and HAGGERTY S.E. 1987. Clinopyroxene megacrysts from the Jagersfontein kimberlite. EOS 68, 444.

McCALLISTER R.H. and NORD G.L.(Jnr) 1981. Subcalcic diopsides from kimberlites: Chemistry, exsolution microstructures and thermal history. Contributions to Mineralogy and Petrology 78, 118-125.

McKENZIE D. and O'NIONS R.K. 1983. Mantle reservoirs and ocean island basalts. Nature 301, 229-231.

MERCIER J-C.C. 1979. Peridotite xenoliths and the dynamics of kimberlite intrusion. In: Boyd F.R. and Meyer H.O.A. eds., The Mantle Sample, pp 197-212. American Geophysical Union, Washington.

MERCIER J-C.C. and CARTER N.L. 1975. Pyroxene geotherms. Journal of Geophysical Research 80, 3349-3362.

MENZIES M.A. and MURTHY V.R. 1980. Enriched mantle: Nd and Sr isotopes in diopsides from kimberlite nodules. Nature 283, 634-636.

MENZIES M.A., KEMPTON P. and DUNGAN M. 1985. Interaction of continental lithosphere and asthenospheric melts below the Geronimo volcanic field, Arizona, U.S.A. Journal of Petrology 26, 663-693.

MEYER H.O.A. and McCALLISTER R.H. 1984. Two-pyroxene megacrysts from South African kimberlites. In: Kornprobst J. ed., Kimberlites 11B: The mantle sample and crust-mantle relationships, pp 133-144. Elsevier Science Publishers.

MITCHELL R.H. 1973. Magnesian ilmenite and its role in kimberlite petrogenesis. Journal of Geology 81, 301-311.

MITCHELL R.H. 1984. Garnet lherzolites from the Hanaus-1 and Louwrensia kimberlites of Namibia. Contributions to Mineralogy and Petrology 86, 178-188.

MITCHELL R.H., CARSWELL D.A. and CLARKE D.B. 1980. Geological implications and validity of calculated equilibration conditions for ultramafic xenoliths from the Pipe 200 kimberlite, northern Lesotho. Contributions to Mineralogy and Petrology 72, 205-217.

MOORE R.O. 1987. A study of the kimberlites, diamonds and associated rocks and minerals from the Monastery Mine, South Africa. Unpublished Ph.D., University of Cape Town.

MORGAN W.J. 1983. Hotspot tracks and the early rifting of the Atlantic. Tectonophysics 94, 123-139.

MORI T. and GREEN D.H. 1978. Laboratory duplication of phase equilibria observed in natural garnet lherzolites. Journal of Geology 86, 83-97.

NICKEL K.G. and BREY G.P. 1984. Subsolidus orthopyroxene-clinopyroxene systematics in the system CaO-MgO-SiO_2 to 60 kb: a re-evaluation of the regular solution model. Contributions to Mineralogy and Petrology 87, 35-42.

NICKEL K.G. and GREEN D.H. 1985. Empirical geothermobarometry for garnet peridotites and implications for the nature of the lithosphere, kimberlites and diamonds. Earth and Planetary Science Letters 73, 158-170.

NICOLAS A. 1978. Stress estimates from structural studies in some mantle peridotites. Philosophical Transactions of the Royal Society of London A288, 49-57.

NICOLAS A., BOUDIER F. and BOULLIER A.M. 1973. Mechanisms of flow in naturally and experimentally deformed peridotites. American Journal of Science 273, 853-876.

NIXON P.H. and BOYD F.R. 1973a. Petrogenesis of the granular and sheared ultrabasic nodule suite in kimberlites. In: Nixon P.H. ed., Lesotho Kimberlites, pp 48-56. Lesotho National Development Corporation, Maseru.

NIXON P.H. and BOYD F.R. 1973b. The discrete nodule association in kimberlites from northern Lesotho. In: Nixon P.H. ed., Lesotho Kimberlites, pp 67-76. Lesotho National Development Corporation, Maseru.

NIXON P.H., ROGERS N.W., GIBSON I.L. and GREY A. 1981. Depleted and fertile mantle xenoliths from southern African kimberlites. Annual Reviews in Earth and Planetary Science 9, 285-309.

NIXON P.H., VAN CALSTEREN P.W.C., BOYD F.R. and HAWKESWORTH C.J. 1987. Harzburgites with garnets of diamond facies from southern African kimberlites. In: Nixon, P.H. ed., Mantle Xenoliths, pp. 523-533. J. Wiley & Sons.

O'HARA M.J. and YODER H.S. 1967. Formation and fractionation of basic magmas at high pressures. Scottish Journal of Geology 3, 67-117.

O'HARA M.J., SAUNDERS M.J. and MERCY E.L.P. 1975. Garnet-peridotite, primary ultrabasic magma and eclogite: interpretation of the upper mantle processes in kimberlites. Physics and Chemistry of the Earth 9, 571-604.

O'NEILL H.St.C. and WOOD B.J. 1979. An empirical study of Fe-Mg partitioning between olivine and garnet and its calibration as a geothermometer. Contributions to Mineralogy and Petrology 70, 59-70.

O'NIONS R.K., HAMILTON P.J. and EVENSEN N.M. 1977. Variations in $^{143}Nd/^{144}Nd$ and $^{87}Sr/^{86}Sr$ ratios in oceanic basalts. Earth and Planetary Science Letters 34, 13-22.

O'NIONS R.K., CARTER S.R., EVENSEN N.M. and HAMILTON P.J. 1978. Sr and Nd isotope study of ultramafic xenoliths: evolution of sub-cratonic mantle. EOS 59, 399.

PARMENTIER E.M. and TURCOTTE D.L. 1974. An explanation of the pyroxene geotherm based on plume convection in the upper mantle. Earth and Planetary Science Letters 24, 209-212.

PASTERIS J.D., BOYD F.R. and NIXON P.H. 1979. The ilmenite association at the Frank Smith mine, R.S.A. In: Boyd F.R. and Meyer H.O.A. eds., The Mantle Sample, pp 256-278. American Geophysical Union, Washington.

PIKE J.E.N. and SCHWARZMAN E.C. 1977. Classification of textures in ultramafic xenoliths. Journal of Geology 85, 49-61.

POKHILENKO N.P. and SOBOLEV N.V. 1986. Xenoliths of diamondiferous peridotites from Udachnaya kimberlite pipe, Yakutia. 4IKC, Geological Society of Australia Abstracts 16, 309-311.

POLLACK H.N. and CHAPMAN D.S. 1977. On the regional variation of heatflow, geotherms and lithospheric thickness. Tectonophysics 38, 279-296.

RICHARDSON S.H., GURNEY J.J., ERLANK A.J. and HARRIS J.W. 1984. Origin of diamonds in old enriched mantle. Nature 310, 198-202.

RICHARDSON S.H., ERLANK A.J. and HART S.R. 1985. Kimberlite-borne garnet peridotite xenoliths from old enriched subcontinental lithosphere. Earth and Planetary Science Letters 75, 116-128.

RINGWOOD A.E. 1982. Phase transformations and differentiation in subducted lithosphere: Implications for mantle dynamics, basalt petrogenesis and crustal evolution. Journal of Geology 90, 611-643.

ROBEY J.vA. and GURNEY J.J. 1979. Megacrysts from the Lekkerfontein kimberlite, North Central Cape, R.S.A. Kimberlite Symposium II, Cambridge.

ROBEY J.vA. 1981. Kimberlites of the Central Cape Province, R.S.A. Unpublished Ph.D., University of Cape Town.

RODEN M.K., HART S.R., FREY F.A. and MELSON W.G. 1984. Sr, Nd and Pb isotopic and REE geochemistry of St. Paul's Rocks: the metamorphic and metasomatic development of an alkali basalt mantle source. Contributions to Mineralogy and Petrology 85, 379-400.

ROEDER P.L. and EMSLIE R.F. 1970. Olivine-liquid equilibrium. Contributions to Mineralogy and Petrology 29, 275-289.

SCHANDL E.S. and CLARKE D.B. 1982. Metasomatism in the mantle beneath Pipe 200, northern Lesotho. Terra Cognita 2, 265-266.

SCHILLING J.G. 1973. Icelandic mantle plume: Geochemical evidence along the Reykjanes Ridge. Nature 242, 565-571.

SCHULZE D.J. 1984. Cr-poor megacrysts from the Hamilton Branch kimberlite, Elliott County, Kentucky. In: Kornprobst J. ed., Kimberlites IIB: The mantle and crust-mantle relationships, pp 97-108. Elsevier Science Publishers.

SCHULZE D.J. 1985. Evidence for primary kimberlitic liquids in megacrysts from kimberlites in Kentucky, U.S.A. Journal of Geology 93, 75-79.

SCHULZE D.J. 1987. Megacrysts from alkalic volcanic rocks. In: Nixon P.H. ed., Mantle Xenoliths, pp 433-451. J.Wiley & Sons, New York.

SHEE S.R. and GURNEY J.J. 1979. The mineralogy of xenoliths from Orapa, Botswana. In: Boyd F.R. and Meyer H.O.A. eds., The Mantle Sample, pp 37-49. American Geophysical Union, Washington.

SHIMIZU N. 1975a. Geochemistry of ultramafic inclusions from Salt Lake Crater, Hawaii, and from southern African kimberlites. Physics and Chemistry of the Earth 9, 655-669.

SHIMIZU N. 1975b. Rare earth elements in garnets and clinopyroxenes from garnet lherzolite nodules in kimberlites. Earth and Planetary Science Letters 25, 26-32.

SHIMIZU N. and ALLEGRE C.J. 1978. Geochemistry of transition elements in garnet lherzolite xenoliths in kimberlites. Contributions to Mineralogy and Petrology 67, 41-50.

SMITH C.B. 1983. Pb, Sr and Nd isotopic evidence for sources of southern African Cretaceous kimberlites. Nature 304, 51-54.

SMITH C.B. 1984. Rubidium-strontium, uranium-lead and samarium-neodymium isotopic studies of kimberlite and selected mantle-derived xenoliths. Unpublished Ph.D., University of the Witwatersrand.

SMITH C.B., ALLSOPP H.L., KRAMERS J.D, HUTCHINSON G. and RODDICK J.C. 1985a. Emplacement ages of Jurassic-Cretaceous South African kimberlites by the Rb-Sr method on phlogopite and whole-rock samples. Transactions of the Geological Society of South Africa 88, 249-266.

SMITH C.B., GURNEY J.J., SKINNER E.M.W., CLEMENT C.R. and EBRAHIM N. 1985b. Geochemical character of southern African kimberlites: A new approach based on isotopic constraints. Transactions of the Geological Society of South Africa 88, 267-280.

SMITH C.B., ALLSOPP H.L., KRAMERS, J.D., GURNEY J.J. and JAGOUTZ E. 1986. Isotopic and geochemical studies of kimberlite and included xenoliths. 4IKC, Geological Society of Australia Abstracts 16, 329-331.

SMITH C.B., KRAMERS J.D. and JAGOUTZ E. 1987. Subcalcic megacrysts in kimberlite: Deep lithosphere or asthenosphere origins? Terra Cognita 7, 620-621.

SMITH D. 1988. Implications of zoned garnets for the evolution of sheared lherzolites: examples from northern Lesotho and the Colorado Plateau. Journal of Geophysical Research 93(B5), 4895-4905.

SMITH D. and BOYD F.R. 1986. Compositional heterogeneities in minerals in peridotite nodules. 4IKC, Geological Society of Australia Abstracts 16, 335-337.

SMITH D. and BOYD F.R. 1987. Compositional heterogeneities in a high-temperature lherzolite nodule and implications for mantle processes. In: Nixon P.H. ed., Mantle Xenoliths, pp 551-561. J.Wiley & Sons, New York.

SMITH D. and EHRENBERG S.N. 1984. Zoned minerals in garnet peridotite nodules from the Colorado Plateau: implications for mantle metasomatism and kinetics. Contributions to Mineralogy and Petrology 86, 274-285.

SMITH D. and WILSON C.R. 1985. Garnet-olivine equilibration during cooling in the mantle. American Mineralogist 70, 30-39.

SMITH J.V., BRENNESHOLTZ R. and DAWSON J.B. 1978. Chemistry of micas from kimberlites and xenoliths - 1. Micaceous kimberlites. Geochimica et Cosmochimica Acta 42, 959-971.

SOBOLEV N.V. LAURENT'EV YU G., POKHILENKO N.P. and USOVA L.V. 1973. Chrome-rich garnets from the kimberlites of Yakutia and their parageneses. Contributions to Mineralogy and Petrology 40, 39-52.

SOBOLEV N.V., POKHILENKO N.P., CARSWELL D.A. and RODIONOV A.S. 1986. Sheared lherzolites from kimberlites of Yakutia. 4IKC, Geological Society of Australia Abstracts 16, 338-339.

SPERA F.J. 1984. Carbon dioxide in petrogenesis III: role of volatiles in the ascent of alkaline magma with special reference to xenolith-bearing mafic lavas. Contributions to Mineralogy and Petrology 88, 217-232.

SPERA F.J. 1987. Dynamics of translithospheric migration of metasomatic fluid and alkaline magma. In: Menzies M.A. and Hawkwesworth C.J. eds., Mantle Metasomatism, pp 1-20. Academic Press, London.

STRECKEISEN A. 1976. To each plutonic rock its proper name. Earth Science Reviews 12, 1-33.

SUN S.-S. and HANSON G.N. 1975. Evolution of the mantle: Geochemical evidence from alkali basalt. Geology 3, 297-302.

TAKAHASHI E. 1986. Melting of dry peridotite KLB-1 up to 14 GPa: Implications on the origin of peridotite upper mantle. Journal of Geophysical Research 91, 9367-9382.

VOLLMER R. 1983. Earth degassing, mantle metasomatism and isotopic evolution of the mantle. Geology 11, 452-454.

WEAVER B.L., WOOD D.A., TARNEY J. and JORON J.L. 1987. Geochemistry of ocean island basalts from the South Atlantic: Ascencion, Bouvet, St Helena, Gough and Tristan da Cunha. In: Fitton J.G. and Upton B.G.J. eds., Alkaline Igneous Rocks. Geological Society Special Publication 30, 253-367.

WELLS P.A. 1977. Pyroxene thermometry, in simple and complex systems. Contributions to Mineralogy and Petrology 62, 129-139.

WHITE R. and McKENZIE D. 1989. Magmatism at rift zones: The generation of volcanic continental margins and flood basalts. Journal of Geophysical Research 94, 7685-7729.

WHITE W.M. 1985. Sources of oceanic basalts: Radiogenic isotope evidence. Geology 13, 115-118.

WILLIAMS A.F. 1932. The genesis of the diamond. Ernest Benn Limited, London. 636p.

WILSHIRE H.G. and SHERVAIS J.W. 1975. Al-augite amd Cr-diopside ultramafic xenoliths in basaltic rocks from western United States. Physics and Chemistry of the Earth 9, 257-272.

WILSHIRE H.G., PIKE J.E.N., MEYER C.E. and SCHWARZMAN E.L. 1980. Amphibole-rich veins in lherzolite xenoliths, Dish Hill and Deadman Lake, California. American Journal of Science 280, 576-593.

WINTERBURN P.A. 1987. Geochemical studies of peridotite xenoliths from southern African kimberlites. Unpublished Ph.D., University of Edinburgh.

WINTERBURN P.A. and HARTE B. 1987. Metasomatism in coarse peridotite nodules from the Jagersfontein kimberlite pipe. Terra Cognita 7, 395-396.

WYLLIE P.J. 1987. Metasomatism and fluid generation in mantle xenoliths: experimental. In: Nixon P.H. ed., Mantle Xenoliths, pp 609-621. J.Wiley & Sons, New York.

ZINDLER A. and JAGOUTZ E. 1988. Mantle cryptology. Geochimica et Cosmochimica Acta 52, 319-333.

APPENDIX 1

PERIDOTITE XENOLITHS

SAMPLE	DESCRIPTION
JJH 1	PORPHYROCLASTIC GARNET LHERZOLITE
JJH 2	FLUIDAL MOSAIC-PORPHYROCLASTIC GARNET LHERZOLITE
JJH 3	MOSAIC-PORPHYROCLASTIC GARNET LHERZOLITE
JJH 4	FLUIDAL MOSAIC-PORPHYROCLASTIC GARNET LHERZOLITE
JJH 6	PORPHYROCLASTIC GARNET HARZBURGITE
JJH 7	MOSAIC-PORPHYROCLASTIC GARNET LHERZOLITE
JJH 8	MOSAIC-PORPHYROCLASTIC GARNET LHERZOLITE
JJH 9	PORPHYROCLASTIC GARNET HARZBURGITE
JJH 10	MOSAIC-PORPHYROCLASTIC GARNET LHERZOLITE
JJH 11	MOSAIC-PORPHYROCLASTIC GARNET LHERZOLITE
JJH 12	MOSAIC-PORPHYROCLASTIC GARNET LHERZOLITE
JJH 13	MOSAIC-PORPHYROCLASTIC GARNET LHERZOLITE
JJH 14	PORPHYROCLASTIC GARNET LHERZOLITE
JJH 15	MOSAIC-PORPHYROCLASTIC GARNET LHERZOLITE
JJH 17	PORPHYROCLASTIC GARNET LHERZOLITE
JJH 18	FLUIDAL MOSAIC-PORPHYROCLASTIC GARNET LHERZOLITE
JJH 19	MOSAIC-PORPHYROCLASTIC GARNET HARZBURGITE
JJH 20	FLUIDAL MOSAIC-PORPHYROCLASTIC GARNET LHERZOLITE
JJH 26	MOSAIC-PORPHYROCLASTIC GARNET LHERZOLITE
JJH 28	PORPHYROCLASTIC GARNET LHERZOLITE
JJH 29	MOSAIC-PORPHYROCLASTIC GARNET HARZBURGITE
JJH 30	MOSAIC-PORPHYROCLASTIC GARNET LHERZOLITE
JJH 31	MOSAIC-PORPHYROCLASTIC GARNET LHERZOLITE
JJH 32	MOSAIC-PORPHYROCLASTIC GARNET LHERZOLITE
JJH 33	PORPHYROCLASTIC GARNET LHERZOLITE
JJH 34	LAMINAR MOSAIC-PORPHYROCLASTIC GARNET LHERZOLITE
JJH 35	PORPHYROCLASTIC GARNET LHERZOLITE
JJH 36	MOSAIC-PORPHYROCLASTIC GARNET LHERZOLITE
JJH 37	MOSAIC-PORPHYROCLASTIC GARNET LHERZOLITE
JJH 38	MOSAIC-PORPHYROCLASTIC GARNET LHERZOLITE
JJG 1710	FLUIDAL MOSAIC-PORPHYROCLASTIC GARNET LHERZOLITE
JJG 1713	MOSAIC-PORPHYROCLASTIC GARNET LHERZOLITE
JJG 1729	PORPHYROCLASTIC GARNET LHERZOLITE
JJG 1753	MOSAIC-PORPHYROCLASTIC GARNET LHERZOLITE
JJG 1798	MOSAIC-PORPHYROCLASTIC GARNET LHERZOLITE
J 117	COARSE GARNET LHERZOLITE

APPENDIX 2

ANALYTICAL CONDITIONS-ELECTRON MICROPROBE

Major element mineral analyses were obtained on a Cameca/Camebax electron microprobe at the University of Cape Town.

The following instrumental conditions were used:

Beam current: 40nA
Accelerating voltage: 15kV
Beam size: 5 microns
Counting time: 10 seconds
Analyzing crystals: TLAP for Na, Mg, Si and Al
LIF200 for Fe, Mn and Ni
PET for Ca, K, Ti and Cr

Standards:	Garnet	Pyroxene	Olivine
Si	K-P	DIOP	M-OL
Ti	RUT	RUT	RUT
Al	K-P	K-P	K-P
Cr	CHRO	CHRO	CHRO
Fe	K-P	K-P	M-OL
Mn	RHOD	RHOD	RHOD
Mg	K-P	DIOP	M-OL
Ca	K-P	DIOP	K-P
Na	K-H	K-H	
K		K-H	
Ni			NISI

Reduction of all data was performed on-line. Raw counts were corrected for dead time and background, nominal concentrations were calculated from the standard K-factors. These nominal concentrations were then corrected using ZAF correction factors (modified after Henoc et al., 1973).

APPENDIX 3

MINERAL ANALYSES - PERIDOTITES

An average composition from approximately 10-15 analyses per mineral was calculated for each of the primary mineral phases in the peridotites. For those garnets showing obvious compositional zoning, core and rim compositions are given rather than averages. Where neoblasts were noted to have different compositions to the porphyroclasts these are also noted, as well as a few analyses of the spongy borders to the clinopyroxene porphyroclasts.

The following abbreviations are used in the tables:

Olivine: Fo = 100Mg/(Mg+Fe)

Fa = 100Fe/(Mg+Fe)

Orthopyroxene,Clinopyroxene and Garnet:

Ca = 100Ca/(Ca+Mg+Fe)

Mg = 100Mg/(Ca+Mg+Fe)

Fe = 100Fe/(Ca+Mg+Fe)

M = 100Mg/(Mg+Fe)

C = 100Ca/(Ca+Mg)

In all cases: ND = not detected

\- = not analyzed

TABLE NO: 1

OLIVINE COMPOSITIONS - PERIDOTITE NODULES

	1	2	3	4	5	6	7	8	9	10
SiO_2	40.81	41.01	40.69	40.89	40.95	41.22	40.55	40.55	39.96	41.21
TiO_2	ND	ND	ND	ND	ND	ND	ND	ND	ND	ND
Al_2O_3	ND	ND	ND	ND	ND	ND	ND	ND	ND	ND
Cr_2O_3	.06	.05	.05	.05	.06	.05	.06	.07	.05	.04
FeO	8.80	7.60	8.84	8.23	8.16	8.72	8.99	8.84	9.26	8.07
MnO	.13	.09	.12	.13	.11	.11	.12	.12	.12	.10
MgO	50.09	50.50	49.24	49.92	49.90	49.75	49.79	49.43	49.39	50.00
CaO	.05	.08	.06	.07	.07	.06	.07	.08	.10	.07
Na_2O	-	-	-	-	-	-	-	-	-	-
K_2O	-	-	-	-	-	-	-	-	-	-
NiO	.28	.35	.38	.36	.33	.35	.31	.34	.34	.36
TOTAL	100.24	99.70	99.40	99.67	99.60	100.28	99.91	99.45	99.24	99.87

** ATOMIC PROPORTIONS BASED ON SELECTED NO. OF OXYGENS **

OXYGEN	4	4	4	4	4	4	4	4	4	4
SI	.995	.999	1.000	1.000	1.001	1.003	.993	.997	.988	1.004
TI	-	-	-	-	-	-	-	-	-	-
AL	-	-	-	-	-	-	-	-	-	-
CR	.001	.001	.001	.001	.001	.001	.001	.001	.001	.001
FE2+	.179	.155	.182	.168	.167	.177	.184	.182	.191	.164
MN	.003	.002	.002	.003	.002	.002	.002	.002	.003	.002
MG	1.819	1.834	1.804	1.819	1.818	1.804	1.817	1.811	1.819	1.815
CA	.001	.002	.002	.002	.002	.002	.002	.002	.003	.002
NA	-	-	-	-	-	-	-	-	-	-
K	-	-	-	-	-	-	-	-	-	-
NI	.005	.007	.008	.007	.006	.007	.006	.007	.007	.007
SUM	3.004	3.000	2.999	3.000	2.998	2.996	3.006	3.002	3.012	2.995
	FO 91.03	FO 92.21	FO 90.85	FO 91.53	FO 91.59	FO 91.04	FO 90.80	FO 90.88	FO 90.48	FO 91.69
	FA 8.97	FA 7.79	FA 9.15	FA 8.47	FA 8.41	FA 8.96	FA 9.20	FA 9.12	FA 9.52	FA 8.31

**** SAMPLE DIRECTORY ****

SAMPLE NO.	DESCRIPTION	SAMPLE NO.	DESCRIPTION
1	JJH 1	6	JJH 7
2	JJH 2	7	JJH 8
3	JJH 3	8	JJH 9
4	JJH 4	9	JJH 10
5	JJH 6	10	JJH 11

TABLE NO: 1

OLIVINE COMPOSITIONS - PERIDOTITE NODULES

	11	12	13	14	15	16	17	18	19	20
SiO_2	40.26	40.25	40.66	40.05	40.56	40.78	41.28	40.72	40.41	40.89
TiO_2	ND	ND	ND	ND	ND	ND	ND	ND	ND	ND
Al_2O_3	ND	ND	ND	ND	ND	ND	ND	ND	ND	ND
Cr_2O_3	.06	.04	.05	.04	ND	.06	.07	.05	ND	.04
FeO	8.75	9.96	8.76	9.37	8.70	8.52	7.88	8.75	10.03	8.35
MnO	.10	.10	.10	.11	.11	.09	.11	.09	.13	.12
MgO	50.11	48.88	49.38	49.71	49.79	49.89	50.28	49.78	48.50	49.51
CaO	.07	.07	.06	.07	.08	.08	.05	.06	.08	.07
Na_2O	-	-	-	-	-	-	-	-	-	-
K_2O	-	-	-	-	-	-	-	-	-	-
NiO	.30	.36	.35	.30	.37	.35	.37	.33	.40	.36
TOTAL	99.67	99.68	99.38	99.67	99.64	99.79	100.06	99.80	99.58	99.36

** ATOMIC PROPORTIONS BASED ON SELECTED NO. OF OXYGENS **

OXYGEN	4	4	4	4	4	4	4	4	4	4
SI	.988	.993	.999	.986	.995	.997	1.003	.997	.997	1.003
TI	-	-	-	-	-	-	-	-	-	-
AL	-	-	-	-	-	-	-	-	-	-
CR	.001	.001	.001	.001	-	.001	.001	.001	-	.001
FE2+	.180	.205	.180	.193	.178	.174	.160	.179	.207	.171
MN	.002	.002	.002	.002	.002	.002	.002	.002	.003	.002
MG	1.832	1.796	1.809	1.823	1.820	1.818	1.821	1.816	1.784	1.810
CA	.002	.002	.002	.002	.002	.002	.001	.002	.002	.002
NA	-	-	-	-	-	-	-	-	-	-
K	-	-	-	-	-	-	-	-	-	-
NI	.006	.007	.007	.006	.007	.007	.007	.006	.008	.007
SUM	3.011	3.007	3.000	3.013	3.005	3.002	2.996	3.003	3.002	2.996
	FO 91.08	FO 89.74	FO 90.95	FO 90.43	FO 91.07	FO 91.25	FO 91.92	FO 91.02	FO 89.60	FO 91.35
	FA 8.92	FA 10.26	FA 9.05	FA 9.57	FA 8.93	FA 8.75	FA 8.08	FA 8.98	FA 10.40	FA 8.65

**** SAMPLE DIRECTORY ****

SAMPLE NO.	DESCRIPTION	SAMPLE NO.	DESCRIPTION
11	JJH 12	16	JJH 18
12	JJH 13	17	JJH 19
13	JJH 14	18	JJH 20
14	JJH 15	19	JJH 26
15	JJH 17	20	JJH 28

TABLE NO: 1

OLIVINE COMPOSITIONS - PERIDOTITE NODULES

	21	22	23	24	25	26	27	28	29	30
SiO_2	40.80	41.06	40.61	41.28	40.71	40.47	40.69	40.69	40.02	40.47
TiO_2	ND	ND	ND	ND	ND	ND	ND	ND	ND	ND
Al_2O_3	ND	ND	ND	ND	ND	ND	ND	ND	ND	ND
Cr_2O_3	.12	.07	.07	ND	ND	ND	ND	ND	ND	ND
FeO	7.63	7.54	9.26	8.04	7.89	9.55	8.55	8.32	9.16	9.27
MnO	.12	.08	.11	.09	.10	.10	.12	.11	.12	.11
MgO	49.84	50.07	48.86	49.48	49.44	48.96	49.49	49.65	49.27	48.76
CaO	.07	.06	.07	.05	.06	.09	.07	.08	.05	.07
Na_2O	-	-	-	-	-	-	-	-	-	-
K_2O	-	-	-	-	-	-	-	-	-	-
NiO	.34	.32	.36	.35	.36	.32	.30	.37	.36	.41
TOTAL	98.94	99.22	99.36	99.32	98.59	99.52	99.25	99.25	99.01	99.12

** ATOMIC PROPORTIONS BASED ON SELECTED NO. OF OXYGENS **

OXYGEN	4	4	4	4	4	4	4	4	4	4
SI	1.002	1.004	1.001	1.010	1.004	.997	1.000	.999	.990	1.000
TI	-	-	-	-	-	-	-	-	-	-
AL	-	-	-	-	-	-	-	-	-	-
CR	.002	.001	.001	-	-	-	-	-	-	-
FE2+	.157	.154	.191	.165	.163	.197	.176	.171	.190	.192
MN	.002	.002	.002	.002	.002	.002	.002	.002	.003	.002
MG	1.824	1.825	1.794	1.804	1.817	1.797	1.813	1.817	1.817	1.795
CA	.002	.002	.002	.001	.002	.002	.002	.002	.001	.002
NA	-	-	-	-	-	-	-	-	-	-
K	-	-	-	-	-	-	-	-	-	-
NI	.007	.006	.007	.007	.007	.006	.006	.007	.007	.008
SUM	2.997	2.995	2.998	2.990	2.996	3.003	3.000	3.000	3.009	3.000
	FO 92.09	FO 92.21	FO 90.39	FO 91.64	FO 91.78	FO 90.13	FO 91.16	FO 91.40	FO 90.55	FO 90.36
	FA 7.91	FA 7.79	FA 9.61	FA 8.36	FA 8.22	FA 9.87	FA 8.84	FA 8.60	FA 9.45	FA 9.64

**** SAMPLE DIRECTORY ****

SAMPLE NO.	DESCRIPTION	SAMPLE NO.	DESCRIPTION
21	JJH 29	26	JJH 34
22	JJH 30	27	JJH 35
23	JJH 31	28	JJH 36
24	JJH 32	29	JJH 37
25	JJH 33	30	JJH 38

TABLE NO: 1

OLIVINE COMPOSITIONS - PERIDOTITE NODULES

	31	32	33	34	35	36
SiO_2	41.21	41.02	40.70	40.72	40.64	40.21
TiO_2	ND	.05	ND	ND	ND	ND
Al_2O_3	ND	ND	ND	ND	ND	ND
Cr_2O_3	ND	.07	.09	.04	.10	ND
FeO	7.86	8.26	7.49	10.00	8.60	10.54
MnO	.11	.11	.12	.11	.10	.13
MgO	49.52	49.12	50.18	48.10	49.06	48.36
CaO	.05	.07	.04	.07	.07	.08
Na_2O	-	-	-	-	-	-
K_2O	-	-	-	-	-	-
NiO	.41	.38	.41	.38	.36	.38
TOTAL	99.19	99.09	99.05	99.44	98.95	99.73

** ATOMIC PROPORTIONS BASED ON SELECTED NO. OF OXYGENS **

OXYGEN	4	4	4	4	4	4
SI	1.009	1.008	.998	1.005	1.002	.994
TI	-	.001	-	-	-	-
AL	-	-	-	-	-	-
CR	-	.001	.002	.001	.002	-
FE2+	.161	.170	.154	.206	.177	.218
MN	.002	.002	.002	.002	.002	.003
MG	1.808	1.799	1.835	1.770	1.803	1.781
CA	.001	.002	.001	.002	.002	.002
NA	-	-	-	-	-	-
K	-	-	-	-	-	-
NI	.008	.008	.008	.008	.007	.008
SUM	2.990	2.990	3.000	2.994	2.996	3.006
	FO 91.82	FO 91.38	FO 92.27	FO 89.55	FO 91.04	FO 89.10
	FA 8.18	FA 8.62	FA 7.73	FA 10.45	FA 8.96	FA 10.90

**** SAMPLE DIRECTORY ****

SAMPLE NO.	DESCRIPTION	SAMPLE NO.	DESCRIPTION
31	JJG 1710	36	J 117
32	JJG 1713		
33	JJG 1729		
34	JJG 1753		
35	JJG 1798		

TABLE NO: 2

ORTHOPYROXENE COMPOSITIONS - PERIDOTITE NODULES

	1	2	3	4	5	6	7	8	9	10
SiO_2	57.12	56.42	57.60	57.49	57.34	57.67	57.25	57.81	57.50	57.59
TiO_2	ND	ND	.05	.21	.24	ND	ND	.20	.15	ND
Al_2O_3	.73	.86	.88	.98	.94	.54	.59	1.07	.85	.59
Cr_2O_3	.35	.46	.35	.34	.34	.34	.35	.38	.41	.36
FeO	5.36	5.21	4.68	5.34	5.44	5.07	5.19	5.20	5.33	5.23
MnO	.12	.14	.11	.13	.12	.12	.13	.12	.12	.13
MgO	34.77	34.84	34.52	33.98	33.59	35.03	34.80	34.48	34.39	35.06
CaO	.89	.95	1.08	1.01	1.00	.96	1.13	1.07	.96	.96
Na_2O	.12	.13	.19	.29	.30	ND	ND	.35	.24	.04
K_2O	ND	ND	ND	ND	ND	ND	ND	ND	ND	ND
TOTAL	99.48	99.03	99.47	99.78	99.32	99.76	99.47	100.69	99.96	99.98

** ATOMIC PROPORTIONS BASED ON SELECTED NO. OF OXYGENS **

OXYGEN	6	6	6	6	6	6	6	6	6	6
SI	1.976	1.963	1.986	1.982	1.987	1.985	1.980	1.975	1.979	1.980
TI	-	-	.001	.005	.006	-	-	.005	.004	-
AL	.030	.035	.036	.040	.038	.022	.024	.043	.034	.024
CR	.010	.013	.010	.009	.009	.009	.010	.010	.011	.010
FE2+	.155	.152	.135	.154	.158	.146	.150	.149	.153	.150
MN	.004	.004	.003	.004	.004	.003	.004	.003	.003	.004
MG	1.793	1.806	1.774	1.746	1.734	1.797	1.793	1.756	1.764	1.797
CA	.033	.035	.040	.037	.037	.035	.042	.039	.035	.035
NA	.008	.009	.013	.019	.020	-	-	.023	.016	.003
K	-	-	-	-	-	-	-	-	-	-
SUM	4.008	4.018	3.997	3.998	3.994	4.000	4.004	4.005	4.002	4.004
	CA 1.67	CA 1.78	CA 2.05	CA 1.93	CA 1.92	CA 1.79	CA 2.11	CA 2.02	CA 1.81	CA 1.78
	MG 90.51	MG 90.62	MG 91.03	MG 90.13	MG 89.90	MG 90.83	MG 90.33	MG 90.34	MG 90.33	MG 90.63
	FE 7.83	FE 7.60	FE 6.93	FE 7.95	FE 8.17	FE 7.38	FE 7.56	FE 7.65	FE 7.86	FE 7.59
	M: 92.04	M: 92.26	M: 92.93	M: 91.90	M: 91.67	M: 92.49	M: 92.28	M: 92.20	M: 92.00	M: 92.28
	C: 1.81	C: 1.92	C: 2.20	C: 2.09	C: 2.10	C: 1.93	C: 2.28	C: 2.18	C: 1.97	C: 1.93

**** SAMPLE DIRECTORY ****

SAMPLE NO.	DESCRIPTION	SAMPLE NO.	DESCRIPTION
1	JJH 1	6	JJH 6
2	JJH 1 NEOBLAST	7	JJH 6 NEOBLAST
3	JJH 2	8	JJH 7
4	JJH 3	9	JJH 8
5	JJH 4	10	JJH 9

TABLE NO: 2

ORTHOPYROXENE COMPOSITIONS - PERIDOTITE NODULES

	11	12	13	14	15	16	17	18	19	20
SiO_2	57.24	57.10	57.31	57.73	57.38	56.65	58.19	57.18	58.23	57.20
TiO_2	ND	.20	.22	.13	.21	.23	.10	.09	.06	.22
Al_2O_3	.76	.97	1.04	.95	1.00	.97	.73	.96	.74	.90
Cr_2O_3	.33	.24	.25	.36	.39	.26	.28	.24	.24	.42
FeO	5.21	5.56	5.92	4.84	5.16	5.93	5.21	5.48	5.13	5.16
MnO	.11	.12	.11	.12	.12	.14	.12	.10	.12	.11
MgO	34.82	33.96	33.84	34.96	34.23	33.81	34.93	34.07	35.00	34.16
CaO	1.11	1.01	1.26	1.02	1.08	.98	.87	1.19	.86	.97
Na_2O	.05	.27	.28	.26	.35	.28	.13	.22	.14	.29
K_2O	ND	ND	ND	ND	ND	ND	ND	ND	ND	ND
TOTAL	99.65	99.44	100.24	100.38	99.93	99.26	100.57	99.54	100.53	99.44

** ATOMIC PROPORTIONS BASED ON SELECTED NO. OF OXYGENS **

OXYGEN	6	6	6	6	6	6	6	6	6	6
SI	1.976	1.978	1.974	1.975	1.976	1.971	1.987	1.978	1.988	1.978
TI	-	.005	.006	.003	.005	.006	.003	.002	.002	.006
AL	.031	.040	.042	.038	.041	.040	.029	.039	.030	.037
CR	.009	.007	.007	.010	.011	.007	.008	.007	.006	.011
FE2+	.150	.161	.171	.138	.149	.173	.149	.159	.146	.149
MN	.003	.004	.003	.003	.004	.004	.003	.003	.003	.003
MG	1.791	1.753	1.737	1.783	1.757	1.753	1.777	1.757	1.781	1.761
CA	.041	.037	.047	.037	.040	.037	.032	.044	.031	.036
NA	.003	.018	.019	.017	.023	.019	.009	.015	.009	.019
K	-	-	-	-	-	-	-	-	-	-
SUM	4.006	4.003	4.005	4.006	4.005	4.009	3.997	4.004	3.997	4.002
	CA 2.07	CA 1.92	CA 2.38	CA 1.91	CA 2.05	CA 1.86	CA 1.63	CA 2.25	CA 1.61	CA 1.85
	MG 90.34	MG 89.83	MG 88.89	MG 91.02	MG 90.31	MG 89.34	MG 90.78	MG 89.66	MG 90.92	MG 90.48
	FE 7.59	FE 8.25	FE 8.73	FE 7.07	FE 7.64	FE 8.79	FE 7.60	FE 8.09	FE 7.48	FE 7.67
	M: 92.25	M: 91.59	M: 91.06	M: 92.79	M: 92.20	M: 91.04	M: 92.28	M: 91.72	M: 92.40	M: 92.19
	C: 2.24	C: 2.09	C: 2.61	C: 2.05	C: 2.22	C: 2.04	C: 1.76	C: 2.45	C: 1.74	C: 2.00

**** SAMPLE DIRECTORY ****

SAMPLE NO.	DESCRIPTION	SAMPLE NO.	DESCRIPTION
11	JJH 9 NEOBLAST	16	JJH 13
12	JJH 10	17	JJH 14
13	JJH 10 NEOBLAST	18	JJH 15
14	JJH 11	19	JJH 17
15	JJH 12	20	JJH 18

TABLE NO: 2

ORTHOPYROXENE COMPOSITIONS - PERIDOTITE NODULES

	21	22	23	24	25	26	27	28	29	30
SiO_2	57.38	56.90	57.61	57.48	57.75	57.10	57.85	57.64	58.36	57.62
TiO_2	.18	.19	.10	.12	.13	.18	.07	.17	.09	.14
Al_2O_3	1.00	1.07	.86	.95	.91	1.06	.80	.93	.85	1.01
Cr_2O_3	.40	.45	.35	.35	.14	.18	.23	.24	.59	.63
FeO	4.68	4.83	5.30	5.44	5.93	5.86	4.84	4.85	4.65	4.60
MnO	.11	.10	.14	.17	.14	.09	.10	.08	.10	.11
MgO	34.45	34.23	34.61	34.58	34.27	33.71	34.79	34.14	34.43	34.38
CaO	1.00	1.17	1.04	1.11	.88	1.43	.86	1.20	.74	.82
Na_2O	.31	.37	.19	.21	.21	.22	.14	.16	.26	.25
K_2O	ND	ND	ND	ND	ND	ND	ND	ND	ND	ND
TOTAL	99.52	99.32	100.21	100.42	100.37	99.84	99.69	99.42	100.08	99.57

** ATOMIC PROPORTIONS BASED ON SELECTED NO. OF OXYGENS **

OXYGEN	6	6	6	6	6	6	6	6	6	6
SI	1.979	1.970	1.978	1.972	1.983	1.974	1.989	1.989	1.996	1.984
TI	.005	.005	.003	.003	.003	.005	.002	.004	.002	.004
AL	.041	.044	.035	.038	.037	.043	.032	.038	.034	.041
CR	.011	.012	.010	.009	.004	.005	.006	.007	.016	.017
FE2+	.135	.140	.152	.156	.170	.169	.139	.140	.133	.132
MN	.003	.003	.004	.005	.004	.003	.003	.002	.003	.003
MG	1.770	1.767	1.771	1.768	1.753	1.737	1.782	1.755	1.755	1.764
CA	.037	.043	.038	.041	.032	.053	.032	.044	.027	.030
NA	.021	.025	.013	.014	.014	.015	.009	.011	.017	.017
K	-	-	-	-	-	-	-	-	-	-
SUM	4.002	4.009	4.004	4.008	4.001	4.005	3.995	3.990	3.985	3.992
	CA 1.90	CA 2.23	CA 1.95	CA 2.08	CA 1.65	CA 2.70	CA 1.62	CA 2.29	CA 1.42	CA 1.57
	MG 91.15	MG 90.60	MG 90.29	MG 89.98	MG 89.64	MG 88.65	MG 91.25	MG 90.50	MG 91.64	MG 91.56
	FE 6.95	FE 7.17	FE 7.76	FE 7.94	FE 8.70	FE 8.65	FE 7.12	FE 7.21	FE 6.95	FE 6.87
	M: 92.92	M: 92.66	M: 92.09	M: 91.89	M: 91.15	M: 91.11	M: 92.76	M: 92.62	M: 92.95	M: 93.02
	C: 2.04	C: 2.40	C: 2.11	C: 2.26	C: 1.81	C: 2.96	C: 1.75	C: 2.46	C: 1.52	C: 1.69

**** SAMPLE DIRECTORY ****

SAMPLE NO.	DESCRIPTION	SAMPLE NO.	DESCRIPTION
21	JJH 19	26	JJH 26 NEOBLAST
22	JJH 19 NEOBLAST	27	JJH 28
23	JJH 20	28	JJH 28 NEOBLAST
24	JJH 20 NEOBLAST	29	JJH 29
25	JJH 26	30	JJH 29 NEOBLAST

TABLE NO: 2

ORTHOPYROXENE COMPOSITIONS - PERIDOTITE NODULES

	31	32	33	34	35	36	37	38	39	40
SiO_2	58.77	58.29	58.65	57.99	57.59	58.63	57.63	57.85	58.88	57.23
TiO_2	.19	.22	.17	.07	.08	.11	.23	ND	.11	.23
Al_2O_3	1.01	1.11	1.10	.90	.74	.85	1.00	.70	.87	1.06
Cr_2O_3	.43	.44	.50	.29	.31	.30	.27	.31	.51	.28
FeO	4.51	4.53	5.40	4.90	4.76	4.80	5.84	5.08	4.99	5.54
MnO	.08	.08	.10	.12	.14	.16	.11	.13	.10	.10
MgO	34.06	34.06	33.23	34.39	34.66	34.91	34.42	35.10	33.83	33.93
CaO	.94	1.05	1.05	1.05	.83	.84	.99	.87	1.10	.99
Na_2O	.34	.33	.42	.18	.15	.16	.29	.07	.21	.30
K_2O	ND	ND	ND	ND	ND	ND	ND	ND	ND	ND
TOTAL	100.34	100.12	100.63	99.90	99.27	100.77	100.79	100.13	100.61	99.67

** ATOMIC PROPORTIONS BASED ON SELECTED NO. OF OXYGENS **

OXYGEN	6	6	6	6	6	6	6	6	6	6
SI	2.003	1.993	2.002	1.991	1.988	1.993	1.972	1.983	2.006	1.977
TI	.005	.006	.004	.002	.002	.003	.006	-	.003	.006
AL	.041	.045	.044	.036	.030	.034	.040	.028	.035	.043
CR	.012	.012	.013	.008	.008	.008	.007	.008	.014	.008
FE2+	.129	.130	.154	.141	.137	.136	.167	.146	.142	.160
MN	.002	.002	.003	.003	.004	.005	.003	.004	.003	.003
MG	1.730	1.736	1.691	1.759	1.784	1.768	1.756	1.794	1.717	1.747
CA	.034	.038	.038	.039	.031	.031	.036	.032	.040	.037
NA	.022	.022	.028	.012	.010	.011	.019	.005	.014	.020
K	-	-	-	-	-	-	-	-	-	-
SUM	3.978	3.984	3.979	3.992	3.995	3.989	4.008	4.000	3.974	4.002
	CA 1.81	CA 2.02	CA 2.04	CA 1.99	CA 1.57	CA 1.58	CA 1.85	CA 1.62	CA 2.11	CA 1.89
	MG 91.40	MG 91.17	MG 89.77	MG 90.75	MG 91.38	MG 91.37	MG 89.61	MG 90.99	MG 90.40	MG 89.88
	FE 6.79	FE 6.80	FE 8.19	FE 7.26	FE 7.04	FE 7.05	FE 8.53	FE 7.39	FE 7.48	FE 8.24
	M: 93.08	M: 93.05	M: 91.64	M: 92.60	M: 92.84	M: 92.84	M: 91.31	M: 92.49	M: 92.36	M: 91.61
	C: 1.95	C: 2.17	C: 2.22	C: 2.15	C: 1.69	C: 1.70	C: 2.03	C: 1.75	C: 2.28	C: 2.05

**** SAMPLE DIRECTORY ****

SAMPLE NO.	DESCRIPTION	SAMPLE NO.	DESCRIPTION
31	JJH 30	36	JJH 33 NEOBLAST
32	JJH 30 NEOBLAST	37	JJH 34
33	JJH 31	38	JJH 35
34	JJH 32	39	JJH 36
35	JJH 33	40	JJH 37

TABLE NO: 2

ORTHOPYROXENE COMPOSITIONS - PERIDOTITE NODULES

	41	42	43	44	45	46	47	48	49	50
SiO_2	56.98	58.15	57.27	58.22	58.00	57.95	57.41	57.45	57.95	57.62
TiO_2	.30	.18	.22	.06	.08	.19	.23	.10	.22	.23
Al_2O_3	1.19	.99	1.15	.88	1.30	1.13	1.25	.85	1.12	1.39
Cr_2O_3	.29	.28	.28	.36	.47	.37	.36	.57	.17	.15
FeO	5.53	5.75	5.79	4.76	4.88	4.81	4.95	4.53	6.06	6.16
MnO	.12	.09	.07	.13	.15	.10	ND	.12	.12	.09
MgO	33.42	33.59	33.29	34.67	34.63	34.15	34.36	34.81	33.19	32.94
CaO	1.06	.98	1.12	1.04	1.26	1.08	1.13	.72	1.08	1.16
Na_2O	.31	.30	.23	.18	.22	.32	.29	.24	.28	.21
K_2O	ND	ND	ND	ND	ND	ND	ND	ND	ND	ND
TOTAL	99.21	100.32	99.43	100.31	101.00	100.11	100.00	99.40	100.20	99.96

** ATOMIC PROPORTIONS BASED ON SELECTED NO. OF OXYGENS **

OXYGEN	6	6	6	6	6	6	6	6	6	6
SI	1.978	1.994	1.984	1.990	1.973	1.986	1.972	1.981	1.993	1.987
TI	.008	.005	.006	.002	.002	.005	.006	.003	.006	.006
AL	.049	.040	.047	.035	.052	.046	.051	.035	.045	.056
CR	.008	.008	.008	.010	.013	.010	.010	.016	.005	.004
FE2+	.161	.165	.168	.136	.139	.138	.142	.131	.174	.178
MN	.004	.003	.002	.004	.004	.003	-	.004	.003	.003
MG	1.729	1.717	1.719	1.766	1.756	1.744	1.759	1.789	1.701	1.693
CA	.039	.036	.042	.038	.046	.040	.042	.027	.040	.043
NA	.021	.020	.015	.012	.015	.021	.019	.016	.019	.014
K	-	-	-	-	-	-	-	-	-	-
SUM	3.996	3.987	3.991	3.992	4.000	3.992	4.002	4.000	3.986	3.984
	CA 2.04	CA 1.88	CA 2.16	CA 1.96	CA 2.37	CA 2.06	CA 2.14	CA 1.37	CA 2.08	CA 2.24
	MG 89.63	MG 89.52	MG 89.14	MG 91.02	MG 90.48	MG 90.76	MG 90.54	MG 91.92	MG 88.82	MG 88.48
	FE 8.32	FE 8.60	FE 8.70	FE 7.01	FE 7.15	FE 7.17	FE 7.32	FE 6.71	FE 9.10	FE 9.28
	M: 91.50	M: 91.24	M: 91.11	M: 92.85	M: 92.67	M: 92.67	M: 92.52	M: 93.19	M: 90.71	M: 90.50
	C: 2.23	C: 2.05	C: 2.36	C: 2.11	C: 2.55	C: 2.22	C: 2.31	C: 1.47	C: 2.29	C: 2.47

**** SAMPLE DIRECTORY ****

SAMPLE NO.	DESCRIPTION	SAMPLE NO.	DESCRIPTION
41	JJH 37 NEOBLAST	46	JJG 1713
42	JJH 38	47	JJG 1713 NEOBLAST
43	JJH 38 NEOBLAST	48	JJG 1729
44	JJG 1710	49	JJG 1753
45	JJG 1710 NEOBLAST	50	JJG 1753 NEOBLAST

TABLE NO: 2

ORTHOPYROXENE COMPOSITIONS - PERIDOTITE NODULES

	51	52
SiO_2	57.16	57.54
TiO_2	.11	.14
Al_2O_3	.90	1.11
Cr_2O_3	.44	.15
FeO	5.11	6.19
MnO	.11	.12
MgO	34.74	33.72
CaO	1.11	1.15
Na_2O	.25	.25
K_2O	ND	ND
TOTAL	99.94	100.38

** ATOMIC PROPORTIONS BASED ON SELECTED NO. OF OXYGENS **

OXYGEN	6	6
SI	1.969	1.979
TI	.003	.004
AL	.037	.045
CR	.012	.004
FE2+	.147	.178
MN	.003	.003
MG	1.783	1.728
CA	.041	.042
NA	.017	.017
K	-	-
SUM	4.012	4.001

CA 2.08	CA 2.17
MG 90.46	MG 88.69
FE 7.47	FE 9.14
M: 92.38	M: 90.66
C: 2.25	C: 2.39

**** SAMPLE DIRECTORY ****

SAMPLE NO.	DESCRIPTION	SAMPLE NO.	DESCRIPTION
51	JJG 1798		
52	J 117		

TABLE NO: 3

GARNET COMPOSITIONS - PERIDOTITE NODULES

	1	2	3	4	5	6	7	8	9	10
SiO_2	41.04	41.30	41.11	41.17	40.21	41.49	41.29	40.30	41.59	41.92
TiO_2	.13	.27	.84	.98	.09	.97	.80	ND	.63	.67
Al_2O_3	18.11	20.26	19.02	18.80	15.03	19.51	18.36	15.33	21.25	20.25
Cr_2O_3	6.47	4.27	4.89	4.85	10.98	4.19	6.02	10.15	2.78	4.21
FeO	7.61	6.34	7.27	7.41	6.91	7.02	7.19	7.09	7.21	6.59
MnO	.35	.26	.30	.32	.31	.30	.31	.33	.26	.25
MgO	19.82	21.50	21.11	20.91	18.02	21.20	20.47	18.50	21.08	21.59
CaO	6.06	5.10	5.09	5.11	8.38	4.64	5.53	7.34	4.56	4.71
Na_2O	ND	.04	.11	.12	ND	.13	.08	ND	.08	.08
K_2O	-	-	-	-	-	-	-	-	-	-
TOTAL	99.60	99.34	99.74	99.67	99.94	99.45	100.05	99.06	99.44	100.27

** ATOMIC PROPORTIONS BASED ON SELECTED NO. OF OXYGENS **

OXYGEN	12	12	12	12	12	12	12	12	12	12
SI	2.991	2.968	2.967	2.976	2.978	2.986	2.982	2.996	2.977	2.982
TI	.007	.015	.046	.053	.005	.053	.043	-	.034	.036
AL	1.556	1.716	1.618	1.602	1.312	1.655	1.563	1.343	1.793	1.698
CR	.373	.243	.279	.277	.643	.238	.344	.597	.157	.237
FE2+	.464	.381	.439	.448	.428	.423	.434	.441	.432	.392
MN	.022	.016	.018	.020	.019	.018	.019	.021	.016	.015
MG	2.153	2.303	2.271	2.252	1.989	2.274	2.203	2.050	2.249	2.289
CA	.473	.393	.394	.396	.665	.358	.428	.585	.350	.359
NA	-	.006	.015	.017	-	.018	.011	-	.011	.011
K	-	-	-	-	-	-	-	-	-	-
SUM	8.039	8.040	8.047	8.040	8.040	8.023	8.027	8.034	8.019	8.020
	CA 15.32	CA 12.77	CA 12.69	CA 12.78	CA 21.58	CA 11.72	CA 13.96	CA 19.01	CA 11.54	CA 11.81
	MG 69.67	MG 74.85	MG 73.17	MG 72.75	MG 64.54	MG 74.45	MG 71.87	MG 66.65	MG 74.21	MG 75.29
	FE 15.01	FE 12.39	FE 14.14	FE 14.47	FE 13.89	FE 13.83	FE 14.17	FE 14.33	FE 14.24	FE 12.90
	M: 82.27	M: 85.80	M: 83.80	M: 83.41	M: 82.29	M: 84.33	M: 83.53	M: 82.30	M: 83.90	M: 85.38

**** SAMPLE DIRECTORY ****

SAMPLE NO.	DESCRIPTION	SAMPLE NO.	DESCRIPTION
1	JJH 1	6	JJH 7
2	JJH 2	7	JJH 8
3	JJH 3	8	JJH 9
4	JJH 4	9	JJH 10
5	JJH 6	10	JJH 11 RIM

TABLE NO: 3

GARNET COMPOSITIONS - PERIDOTITE NODULES

	11	12	13	14	15	16	17	18	19	20
SiO_2	41.84	41.52	41.97	41.18	41.27	41.66	41.82	41.44	42.09	41.54
TiO_2	.32	.90	.53	.12	.26	.46	.28	1.10	.77	.09
Al_2O_3	19.91	19.15	20.74	20.36	19.47	21.48	21.09	18.49	18.83	19.10
Cr_2O_3	4.72	4.74	3.59	3.73	5.37	2.39	3.33	5.73	5.89	6.39
FeO	6.35	6.82	7.78	7.76	6.96	7.14	6.92	6.88	6.44	6.36
MnO	.29	.26	.31	.25	.31	.24	.29	.30	.24	.29
MgO	21.15	21.43	20.72	20.49	20.21	21.34	21.09	20.89	20.69	20.70
CaO	4.85	4.88	4.69	5.20	5.78	4.54	5.00	5.24	4.87	4.74
Na_2O	.05	.12	.08	.05	.04	.07	.04	.13	.10	.05
K_2O	-	-	-	-	-	-	-	-	-	-
TOTAL	99.48	99.82	100.41	99.14	99.67	99.32	99.86	100.20	99.92	99.26

** ATOMIC PROPORTIONS BASED ON SELECTED NO. OF OXYGENS **

OXYGEN	12	12	12	12	12	12	12	12	12	12
SI	3.001	2.982	2.990	2.980	2.981	2.980	2.984	2.979	3.018	3.001
TI	.017	.049	.028	.007	.014	.025	.015	.059	.042	.005
AL	1.683	1.621	1.742	1.737	1.657	1.811	1.774	1.567	1.591	1.626
CR	.268	.269	.202	.213	.307	.135	.188	.326	.334	.365
FE2+	.381	.410	.464	.470	.420	.427	.413	.414	.386	.384
MN	.018	.016	.019	.015	.019	.015	.018	.018	.015	.018
MG	2.261	2.294	2.200	2.210	2.175	2.275	2.243	2.238	2.211	2.229
CA	.373	.376	.358	.403	.447	.348	.382	.404	.374	.367
NA	.007	.017	.011	.007	.006	.010	.006	.018	.014	.007
K	-	-	-	-	-	-	-	-	-	-
SUM	8.009	8.033	8.015	8.042	8.026	8.026	8.023	8.024	7.985	8.002
	CA 12.37	CA 12.20	CA 11.85	CA 13.08	CA 14.70	CA 11.41	CA 12.58	CA 13.21	CA 12.59	CA 12.31
	MG 75.00	MG 74.50	MG 72.81	MG 71.69	MG 71.49	MG 74.59	MG 73.82	MG 73.25	MG 74.41	MG 74.79
	FE 12.64	FE 13.30	FE 15.34	FE 15.24	FE 13.82	FE 14.00	FE 13.59	FE 13.54	FE 13.00	FE 12.90
	M: 85.58	M: 84.85	M: 82.60	M: 82.47	M: 83.80	M: 84.19	M: 84.45	M: 84.40	M: 85.13	M: 85.29

**** SAMPLE DIRECTORY ****

SAMPLE NO.	DESCRIPTION	SAMPLE NO.	DESCRIPTION
11	JJH 11 CORE	16	JJH 15
12	JJH 12	17	JJH 17
13	JJH 13 RIM	18	JJH 18
14	JJH 13 CORE	19	JJH 19 RIM
15	JJH 14	20	JJH 19 CORE

TABLE NO: 3

GARNET COMPOSITIONS - PERIDOTITE NODULES

	21	22	23	24	25	26	27	28	29	30
SiO_2	41.40	42.30	42.40	40.73	41.85	42.32	42.00	41.24	40.93	41.87
TiO_2	.47	.54	.29	.45	.98	.33	.39	.90	.10	.57
Al_2O_3	19.41	21.93	21.20	16.61	17.93	20.74	19.84	20.13	19.22	16.86
Cr_2O_3	5.17	1.71	3.56	9.37	6.18	3.88	4.62	3.78	6.27	8.03
FeO	7.06	8.22	7.25	6.47	7.50	6.52	6.53	7.63	6.94	6.52
MnO	.28	.28	.29	.31	.30	.22	.28	.30	.30	.25
MgO	20.62	20.69	19.93	20.14	20.36	20.81	20.38	20.63	19.46	19.98
CaO	5.37	4.29	4.94	4.92	4.99	4.83	5.34	4.81	6.10	6.11
Na_2O	.06	.08	.04	.07	.12	.04	.05	.11	ND	.07
K_2O	-	-	-	-	-	-	-	-	-	-
TOTAL	99.84	100.04	99.90	99.07	100.21	99.69	99.43	99.53	99.33	100.26

** ATOMIC PROPORTIONS BASED ON SELECTED NO. OF OXYGENS **

OXYGEN	12	12	12	12	12	12	12	12	12	12
SI	2.981	3.006	3.023	2.987	3.016	3.018	3.018	2.971	2.976	3.027
TI	.025	.029	.016	.025	.053	.018	.021	.049	.005	.031
AL	1.648	1.837	1.782	1.436	1.523	1.743	1.681	1.710	1.647	1.437
CR	.294	.096	.201	.543	.352	.219	.263	.215	.360	.459
FE2+	.425	.489	.432	.397	.452	.389	.392	.460	.422	.394
MN	.017	.017	.018	.019	.018	.013	.017	.018	.018	.015
MG	2.213	2.192	2.118	2.201	2.186	2.212	2.183	2.215	2.109	2.153
CA	.414	.327	.377	.387	.385	.369	.411	.371	.475	.473
NA	.008	.011	.006	.010	.017	.006	.007	.015	-	.010
K	-	-	-	-	-	-	-	-	-	-
SUM	8.027	8.003	7.972	8.004	8.002	7.986	7.993	8.025	8.015	7.999
	CA 13.57	CA 10.87	CA 12.89	CA 12.95	CA 12.74	CA 12.43	CA 13.77	CA 12.19	CA 15.81	CA 15.67
	MG 72.50	MG 72.88	MG 72.34	MG 73.75	MG 72.31	MG 74.48	MG 73.09	MG 72.72	MG 70.15	MG 71.28
	FE 13.93	FE 16.25	FE 14.77	FE 13.30	FE 14.95	FE 13.09	FE 13.14	FE 15.09	FE 14.04	FE 13.05
	M: 83.88	M: 81.77	M: 83.05	M: 84.73	M: 82.87	M: 85.05	M: 84.76	M: 82.81	M: 83.32	M: 84.52

**** SAMPLE DIRECTORY ****

SAMPLE NO.	DESCRIPTION	SAMPLE NO.	DESCRIPTION
21	JJH 20	26	JJH 32
22	JJH 26	27	JJH 33
23	JJH 28	28	JJH 34
24	JJH 29	29	JJH 35
25	JJH 31	30	JJH 36

TABLE NO: 3

GARNET COMPOSITIONS - PERIDOTITE NODULES

	31	32	33	34	35	36	37	38	39	40
SiO_2	41.83	41.60	41.75	41.83	41.96	41.97	42.62	41.63	41.99	41.39
TiO_2	1.05	.67	.82	.70	.30	.55	.34	.61	.73	.37
Al_2O_3	20.80	20.60	20.31	19.89	19.94	20.24	20.84	22.01	21.98	17.01
Cr_2O_3	3.10	3.67	3.17	3.60	4.85	3.90	3.89	1.64	1.80	8.13
FeO	7.53	7.14	7.53	7.45	6.32	6.32	6.58	8.38	7.98	6.85
MnO	.31	.28	.30	.29	.26	.27	.27	.29	.27	.23
MgO	21.17	20.55	20.74	20.44	21.16	21.13	20.11	20.27	20.84	19.45
CaO	4.59	4.64	4.74	4.72	5.08	4.70	4.73	4.38	4.34	6.49
Na_2O	.12	.12	.10	.07	.04	.10	.05	.09	.10	.06
K_2O	-	-	-	-	-	-	-	-	-	-
TOTAL	100.50	99.27	99.46	98.99	99.91	99.18	99.43	99.30	100.03	99.98

** ATOMIC PROPORTIONS BASED ON SELECTED NO. OF OXYGENS **

OXYGEN	12	12	12	12	12	12	12	12	12	12
SI	2.973	2.991	2.999	3.020	2.999	3.010	3.044	2.986	2.985	3.011
TI	.056	.036	.044	.038	.016	.030	.018	.033	.039	.020
AL	1.743	1.746	1.720	1.693	1.680	1.711	1.754	1.861	1.842	1.458
CR	.174	.209	.180	.205	.274	.221	.220	.093	.101	.468
FE2+	.448	.429	.452	.450	.378	.379	.393	.503	.474	.417
MN	.019	.017	.018	.018	.016	.016	.016	.018	.016	.014
MG	2.242	2.202	2.221	2.199	2.254	2.259	2.140	2.167	2.208	2.108
CA	.350	.357	.365	.365	.389	.361	.362	.337	.331	.506
NA	.017	.017	.014	.010	.006	.014	.007	.013	.014	.008
K	-	-	-	-	-	-	-	-	-	-
SUM	8.021	8.004	8.013	7.998	8.011	8.001	7.954	8.010	8.011	8.010
	CA 11.50	CA 11.96	CA 12.01	CA 12.11	CA 12.88	CA 12.04	CA 12.50	CA 11.20	CA 10.97	CA 16.69
	MG 73.77	MG 73.67	MG 73.10	MG 72.96	MG 74.61	MG 75.31	MG 73.93	MG 72.08	MG 73.28	MG 69.56
	FE 14.73	FE 14.36	FE 14.89	FE 14.92	FE 12.51	FE 12.64	FE 13.57	FE 16.72	FE 15.75	FE 13.75
	M: 83.36	M: 83.68	M: 83.07	M: 83.02	M: 85.65	M: 85.63	M: 84.49	M: 81.17	M: 82.31	M: 83.50

**** SAMPLE DIRECTORY ****

SAMPLE NO.	DESCRIPTION	SAMPLE NO.	DESCRIPTION
31	JJH 37 RIM	36	JJG 1713 RIM
32	JJH 37 CORE	37	JJG 1713 CORE
33	JJH 38 RIM	38	JJG 1729
34	JJH 38 CORE	39	JJG 1753
35	JJG 1710	40	JJG 1798

TABLE NO: 3

GARNET COMPOSITIONS - PERIDOTITE NODULES

	41
SiO_2	41.96
TiO_2	.71
Al_2O_3	21.91
Cr_2O_3	1.66
FeO	8.20
MnO	.28
MgO	20.78
CaO	4.24
Na_2O	.08
K_2O	-
TOTAL	99.82

** ATOMIC PROPORTIONS BASED ON SELECTED NO. OF OXYGENS **

OXYGEN	12
SI	2.990
TI	.038
AL	1.841
CR	.094
FE2+	.489
MN	.017
MG	2.207
CA	.324
NA	.011
K	-
SUM	8.010

CA 10.72
MG 73.09
FE 16.19

M: 81.87

**** SAMPLE DIRECTORY ****

SAMPLE NO.	DESCRIPTION	SAMPLE NO.	DESCRIPTION
41	J117		

TABLE NO: 4

CLINOPYROXENE COMPOSITIONS - PERIDOTITE NODULES

	1	2	3	4	5	6	7	8	9	10
SiO_2	54.76	54.82	54.86	54.61	55.35	54.66	55.01	54.65	53.91	55.07
TiO_2	.04	.09	.48	.52	.44	.65	.28	.42	.43	.27
Al_2O_3	1.31	1.77	2.60	2.64	2.82	3.14	2.07	2.48	1.62	2.36
Cr_2O_3	1.25	1.16	1.33	1.41	1.43	1.59	1.62	.94	.88	1.36
FeO	2.93	2.91	3.48	3.56	3.56	3.55	3.27	3.62	3.59	3.11
MnO	.09	.11	.10	.11	.12	.10	.12	.10	.14	.11
MgO	18.69	19.51	18.27	18.09	19.12	17.66	18.77	18.68	19.43	19.28
CaO	19.55	18.03	16.17	16.01	14.99	16.80	16.96	16.68	18.56	16.11
Na_2O	1.11	1.37	2.23	2.29	2.31	2.43	1.88	1.96	.95	1.89
K_2O	.04	.04	ND	ND	ND	ND	.04	ND	ND	ND
TOTAL	99.77	99.81	99.53	99.25	100.15	100.59	100.02	99.54	99.52	99.57

** ATOMIC PROPORTIONS BASED ON SELECTED NO. OF OXYGENS **

OXYGEN	6	6	6	6	6	6	6	6	6	6
SI	1.982	1.975	1.979	1.977	1.978	1.958	1.978	1.973	1.957	1.980
TI	.001	.002	.013	.014	.012	.018	.008	.011	.012	.007
AL	.056	.075	.111	.113	.119	.133	.088	.106	.069	.100
CR	.036	.033	.038	.040	.040	.045	.046	.027	.025	.039
FE2+	.089	.088	.105	.108	.106	.106	.098	.109	.109	.094
MN	.003	.003	.003	.003	.004	.003	.004	.003	.004	.003
MG	1.008	1.047	.982	.976	1.018	.943	1.006	1.005	1.051	1.033
CA	.758	.696	.625	.621	.574	.645	.653	.645	.722	.621
NA	.078	.096	.156	.161	.160	.169	.131	.137	.067	.132
K	.002	.002	-	-	-	-	.002	-	-	-
SUM	4.011	4.017	4.012	4.013	4.011	4.020	4.014	4.018	4.017	4.009
	CA 40.87	CA 38.01	CA 36.50	CA 36.43	CA 33.79	CA 38.07	CA 37.18	CA 36.67	CA 38.36	CA 35.52
	MG 54.35	MG 57.20	MG 57.37	MG 57.25	MG 59.95	MG 55.66	MG 57.23	MG 57.12	MG 55.85	MG 59.13
	FE 4.78	FE 4.79	FE 6.13	FE 6.32	FE 6.26	FE 6.28	FE 5.59	FE 6.21	FE 5.79	FE 5.35
	M: 91.91	M: 92.28	M: 90.34	M: 90.05	M: 90.54	M: 89.86	M: 91.09	M: 90.19	M: 90.61	M: 91.70
	C: 42.92	C: 39.92	C: 38.89	C: 38.89	C: 36.05	C: 40.62	C: 39.38	C: 39.10	C: 40.72	C: 37.53

**** SAMPLE DIRECTORY ****

SAMPLE NO.	DESCRIPTION	SAMPLE NO.	DESCRIPTION
1	JJH 1	6	JJH 7 BORDER
2	JJH 2	7	JJH 8
3	JJH 3	8	JJH 10
4	JJH 4	9	JJH 10 BORDER
5	JJH 7	10	JJH 11

TABLE NO: 4

CLINOPYROXENE COMPOSITIONS - PERIDOTITE NODULES

	11	12	13	14	15	16	17	18	19	20
SiO_2	55.10	54.36	55.17	54.92	55.30	54.73	54.79	55.26	55.20	56.27
TiO_2	.43	.48	.15	.15	.08	.48	.14	.26	.13	.43
Al_2O_3	2.57	2.73	1.50	2.12	1.67	2.47	1.85	2.75	1.91	2.81
Cr_2O_3	1.47	1.02	1.08	.77	1.01	1.62	1.26	.73	1.03	1.72
FeO	3.48	3.98	2.85	3.57	2.83	3.29	3.23	3.66	2.85	3.00
MnO	.11	.12	.10	.13	.10	.14	.12	.09	.10	.11
MgO	19.15	18.50	18.93	19.76	18.87	18.47	19.24	17.80	18.31	18.23
CaO	15.25	16.05	19.39	16.68	19.23	16.22	17.70	17.06	18.74	15.43
Na_2O	2.32	2.16	1.23	1.47	1.30	2.22	1.51	1.97	1.34	2.46
K_2O	ND	ND	ND	ND	ND	ND	ND	ND	ND	ND
TOTAL	99.89	99.41	100.41	99.58	100.40	99.65	99.85	99.59	99.62	100.47

** ATOMIC PROPORTIONS BASED ON SELECTED NO. OF OXYGENS **

OXYGEN	6	6	6	6	6	6	6	6	6	6
SI	1.976	1.967	1.980	1.978	1.983	1.973	1.975	1.991	1.991	1.999
TI	.012	.013	.004	.004	.002	.013	.004	.007	.004	.011
AL	.109	.116	.063	.090	.071	.105	.079	.117	.081	.118
CR	.042	.029	.031	.022	.029	.046	.036	.021	.029	.048
FE2+	.104	.120	.086	.108	.085	.099	.097	.110	.086	.089
MN	.003	.004	.003	.004	.003	.004	.004	.003	.003	.003
MG	1.024	.998	1.013	1.061	1.008	.993	1.033	.956	.984	.965
CA	.586	.622	.746	.644	.739	.627	.684	.659	.724	.587
NA	.161	.152	.086	.103	.090	.155	.106	.138	.094	.169
K	-	-	-	-	-	-	-	-	-	-
SUM	4.018	4.023	4.012	4.013	4.011	4.016	4.017	4.002	3.997	3.991
	CA 34.19	CA 35.76	CA 40.44	CA 35.53	CA 40.33	CA 36.47	CA 37.67	CA 38.19	CA 40.36	CA 35.78
	MG 59.72	MG 57.32	MG 54.92	MG 58.54	MG 55.04	MG 57.76	MG 56.96	MG 55.42	MG 54.85	MG 58.79
	FE 6.09	FE 6.92	FE 4.64	FE 5.93	FE 4.63	FE 5.77	FE 5.37	FE 6.39	FE 4.79	FE 5.43
	M: 90.75	M: 89.23	M: 92.21	M: 90.79	M: 92.24	M: 90.91	M: 91.39	M: 89.66	M: 91.97	M: 91.55
	C: 36.41	C: 38.41	C: 42.41	C: 37.77	C: 42.29	C: 38.70	C: 39.81	C: 40.80	C: 42.39	C: 37.83

**** SAMPLE DIRECTORY ****

SAMPLE NO.	DESCRIPTION	SAMPLE NO.	DESCRIPTION
11	JJH 12	16	JJH 18
12	JJH 13	17	JJH 20
13	JJH 14	18	JJH 26
14	JJH 15	19	JJH 28
15	JJH 17	20	JJH 30

TABLE NO: 4

CLINOPYROXENE COMPOSITIONS - PERIDOTITE NODULES

	21	22	23	24	25	26	27	28	29	30
SiO_2	56.13	56.38	55.76	55.12	54.93	55.43	55.03	54.92	55.04	54.01
TiO_2	.42	.41	.41	.12	.12	.17	.50	.36	ND	.16
Al_2O_3	1.21	2.99	.99	1.93	.49	1.68	2.85	2.80	1.03	.74
Cr_2O_3	2.19	1.95	2.72	1.09	1.15	1.31	1.17	1.34	.96	.95
FeO	2.70	3.95	3.39	2.99	2.74	2.60	3.73	3.40	2.70	2.31
MnO	.10	.13	.16	.12	.11	.10	.11	.11	.11	ND
MgO	18.21	18.48	17.94	19.09	18.49	17.91	18.24	17.49	18.85	17.30
CaO	18.41	13.72	17.63	17.64	20.70	19.18	16.07	17.30	20.49	23.76
Na_2O	1.53	2.70	1.72	1.37	.72	1.27	2.21	2.18	.68	.45
K_2O	ND	ND	ND	.04	ND	ND	ND	ND	.05	ND
TOTAL	100.91	100.72	100.73	99.51	99.46	99.66	99.92	99.91	99.92	99.70

** ATOMIC PROPORTIONS BASED ON SELECTED NO. OF OXYGENS **

OXYGEN	6	6	6	6	6	6	6	6	6	6
SI	2.001	1.999	1.999	1.987	1.996	1.999	1.977	1.978	1.988	1.972
TI	.011	.011	.011	.003	.003	.005	.014	.010	-	.004
AL	.051	.125	.042	.082	.021	.071	.121	.119	.044	.032
CR	.062	.055	.077	.031	.033	.037	.033	.038	.027	.027
FE2+	.080	.117	.102	.090	.083	.078	.112	.102	.082	.071
MN	.003	.004	.005	.004	.003	.003	.003	.003	.003	-
MG	.967	.976	.958	1.026	1.001	.963	.977	.939	1.015	.941
CA	.703	.521	.677	.681	.806	.741	.619	.668	.793	.930
NA	.106	.186	.120	.096	.051	.089	.154	.152	.048	.032
K	-	-	-	.002	-	-	-	-	.002	-
SUM	3.985	3.994	3.991	4.002	3.999	3.987	4.010	4.010	4.001	4.010
	CA 40.16	CA 32.28	CA 38.98	CA 37.91	CA 42.63	CA 41.59	CA 36.23	CA 39.07	CA 41.97	CA 47.88
	MG 55.25	MG 60.47	MG 55.17	MG 57.07	MG 52.96	MG 54.01	MG 57.20	MG 54.94	MG 53.71	MG 48.49
	FE 4.60	FE 7.25	FE 5.85	FE 5.02	FE 4.40	FE 4.40	FE 6.56	FE 5.99	FE 4.32	FE 3.63
	M: 92.32	M: 89.29	M: 90.41	M: 91.92	M: 92.32	M: 92.47	M: 89.71	M: 90.16	M: 92.56	M: 93.03
	C: 42.09	C: 34.80	C: 41.40	C: 39.92	C: 44.60	C: 43.50	C: 38.78	C: 41.56	C: 43.87	C: 49.68

**** SAMPLE DIRECTORY ****

SAMPLE NO.	DESCRIPTION	SAMPLE NO.	DESCRIPTION
21	JJH 30 BORDER	26	JJH 33
22	JJH 31	27	JJH 34
23	JJH 31 BORDER	28	JJH 34 INC IN GNT
24	JJH 32	29	JJH 35
25	JJH 32 BORDER	30	JJH 35 BORDER

TABLE NO: 4

CLINOPYROXENE COMPOSITIONS - PERIDOTITE NODULES

	31	32	33	34	35	36	37	38	39	40
SiO_2	55.89	54.80	55.84	55.98	55.37	54.49	54.29	54.36	55.73	54.77
TiO_2	.16	.51	.37	.10	.41	.52	.32	.25	.42	.67
Al_2O_3	1.65	2.95	2.50	1.85	3.07	1.86	2.72	1.01	2.97	1.43
Cr_2O_3	1.67	1.12	.88	1.31	1.42	1.69	.67	.67	.68	.81
FeO	3.06	3.61	3.70	3.02	3.29	3.03	3.82	3.70	4.04	4.05
MnO	.11	.11	.12	.12	.10	.10	.12	.13	.12	.14
MgO	19.10	18.12	18.32	19.06	18.55	17.59	18.20	18.75	18.40	17.70
CaO	16.90	16.00	16.68	17.81	14.88	18.87	17.52	19.27	15.88	19.70
Na_2O	1.55	2.10	1.96	1.32	2.23	1.50	1.80	1.08	2.04	1.20
K_2O	.04	.04	ND	.04	ND	ND	ND	ND	ND	ND
TOTAL	100.13	99.36	100.38	100.61	99.33	99.66	99.47	99.23	100.29	100.48

** ATOMIC PROPORTIONS BASED ON SELECTED NO. OF OXYGENS **

OXYGEN	6	6	6	6	6	6	6	6	6	6
SI	2.000	1.978	1.995	1.995	1.989	1.975	1.967	1.982	1.990	1.977
TI	.004	.014	.010	.003	.011	.014	.009	.007	.011	.018
AL	.070	.126	.105	.078	.130	.079	.116	.043	.125	.061
CR	.047	.032	.025	.037	.040	.048	.019	.019	.019	.023
FE2+	.092	.109	.111	.090	.099	.092	.116	.113	.121	.122
MN	.003	.003	.004	.004	.003	.003	.004	.004	.004	.004
MG	1.019	.975	.975	1.012	.993	.950	.983	1.019	.979	.952
CA	.648	.619	.638	.680	.573	.733	.680	.753	.608	.762
NA	.108	.147	.136	.091	.155	.105	.126	.076	.141	.084
K	.002	.002	-	.002	-	-	-	-	-	-
SUM	3.992	4.004	3.999	3.991	3.993	4.000	4.020	4.018	3.998	4.005
	CA 36.86	CA 36.35	CA 37.03	CA 38.16	CA 34.41	CA 41.29	CA 38.24	CA 39.95	CA 35.59	CA 41.49
	MG 57.94	MG 57.25	MG 56.56	MG 56.79	MG 59.66	MG 53.53	MG 55.25	MG 54.06	MG 57.35	MG 51.85
	FE 5.21	FE 6.40	FE 6.41	FE 5.05	FE 5.94	FE 5.17	FE 6.51	FE 5.99	FE 7.07	FE 6.66
	M: 91.75	M: 89.94	M: 89.82	M: 91.83	M: 90.95	M: 91.19	M: 89.46	M: 90.03	M: 89.03	M: 88.62
	C: 38.88	C: 38.83	C: 39.56	C: 40.18	C: 36.58	C: 43.54	C: 40.90	C: 42.49	C: 38.29	C: 44.45

**** SAMPLE DIRECTORY ****

SAMPLE NO.	DESCRIPTION	SAMPLE NO.	DESCRIPTION
31	JJH 36	36	JJG 1713 BORDER
32	JJH 37	37	JJG 1729
33	JJH 38	38	JJG 1729 BORDER
34	JJG 1710	39	JJG 1753
35	JJG 1713	40	JJG 1753 BORDER

TABLE NO: 4

CLINOPYROXENE COMPOSITIONS - PERIDOTITE NODULES

	41	42
SiO_2	55.36	55.39
TiO_2	.21	.28
Al_2O_3	1.53	2.79
Cr_2O_3	.94	.59
FeO	3.33	4.26
MnO	.08	.13
MgO	19.37	19.09
CaO	17.11	15.36
Na_2O	1.37	1.77
K_2O	ND	ND
TOTAL	99.31	99.67

** ATOMIC PROPORTIONS BASED ON SELECTED NO. OF OXYGENS **

OXYGEN	6	6
SI	1.998	1.988
TI	.006	.008
AL	.065	.118
CR	.027	.017
FE2+	.101	.128
MN	.002	.004
MG	1.042	1.021
CA	.662	.591
NA	.096	.123
K	-	-
SUM	3.998	3.998

CA 36.68	CA 33.95
MG 57.75	MG 58.70
FE 5.57	FE 7.35
M: 91.20	M: 88.87
C: 38.84	C: 36.65

**** SAMPLE DIRECTORY ****

SAMPLE NO.	DESCRIPTION	SAMPLE NO.	DESCRIPTION
41	JJG 1798		
42	J 117		

APPENDIX 4

MINERAL ANALYSES - MEGACRYSTS

An average composition was calculated for each of those megacrysts for which probe-sections were made. The remaining compositions are for single grains mounted in araldite discs.

The following abbreviations are used in the tables:

Olivine: Fo = 100Mg/(Mg+Fe)

Fa = 100Fe/(Mg+Fe)

Orthopyroxene, clinopyroxene and garnet:

Ca = 100Ca/(Ca+Mg+Fe)

Mg = 100Mg/(Ca+Mg+Fe)

Fe = 100Fe/(Ca+Mg+Fe)

M = 100Mg/(Mg+Fe)

C = 100Ca/(Ca+Mg)

In all cases: ND = not detected

\- = not analyzed

TABLE NO: 1

CR-POOR CLINOPYROXENE MEGACRYSTS

	1	2	3	4	5	6	7	8	9	10
SiO_2	54.05	55.19	54.53	55.16	54.06	55.28	55.88	55.62	55.61	55.50
TiO_2	.40	.30	.28	.30	.34	.32	.34	.38	.35	.27
Al_2O_3	3.30	2.77	2.64	3.47	2.91	2.54	2.89	2.95	2.85	2.88
Cr_2O_3	.34	.28	.20	.38	.33	.26	.41	.32	.41	.36
FeO	5.65	5.48	5.82	5.09	5.46	5.98	5.58	5.73	5.38	5.44
MnO	.11	.12	.14	.19	.13	.17	.08	.12	.13	.14
MgO	18.78	20.33	21.10	20.46	19.46	21.00	19.52	18.54	19.10	20.99
CaO	14.34	13.90	13.29	12.42	14.19	13.44	14.68	14.90	14.44	13.33
Na_2O	2.44	2.15	1.69	2.36	2.06	1.74	2.09	1.87	1.85	1.82
K_2O	ND	ND	ND	ND	ND	.04	ND	.04	ND	ND
TOTAL	99.42	100.53	99.70	99.84	98.95	100.77	101.48	100.47	100.13	100.74

** ATOMIC PROPORTIONS BASED ON SELECTED NO. OF OXYGENS **

OXYGEN	6	6	6	6	6	6	6	6	6	6
SI	1.960	1.971	1.963	1.972	1.965	1.970	1.979	1.990	1.991	1.971
TI	.011	.008	.008	.008	.009	.009	.009	.010	.009	.007
AL	.141	.117	.112	.146	.125	.107	.121	.124	.120	.121
CR	.010	.008	.006	.011	.009	.007	.011	.009	.012	.010
FE2+	.171	.164	.175	.152	.166	.178	.165	.171	.161	.162
MN	.003	.004	.004	.006	.004	.005	.002	.004	.004	.004
MG	1.015	1.082	1.132	1.090	1.054	1.115	1.030	.988	1.019	1.111
CA	.557	.532	.513	.476	.553	.513	.557	.571	.554	.507
NA	.172	.149	.118	.164	.145	.120	.143	.130	.128	.125
K	-	-	-	-	-	.002	-	.002	-	-
SUM	4.040	4.034	4.030	4.024	4.031	4.026	4.018	3.999	3.998	4.019
	CA 31.96	CA 29.92	CA 28.17	CA 27.69	CA 31.17	CA 28.40	CA 31.79	CA 32.99	CA 31.94	CA 28.50
	MG 58.21	MG 60.87	MG 62.20	MG 63.45	MG 59.46	MG 61.73	MG 58.78	MG 57.10	MG 58.77	MG 62.42
	FE 9.83	FE 9.21	FE 9.63	FE 8.86	FE 9.36	FE 9.86	FE 9.43	FE 9.90	FE 9.29	FE 9.08
	M: 85.56	M: 86.86	M: 86.60	M: 87.75	M: 86.40	M: 86.22	M: 86.18	M: 85.22	M: 86.35	M: 87.30
	C: 35.44	C: 32.96	C: 31.17	C: 30.38	C: 34.39	C: 31.51	C: 35.09	C: 36.62	C: 35.21	C: 31.35

**** SAMPLE DIRECTORY ****

SAMPLE NO.	DESCRIPTION	SAMPLE NO.	DESCRIPTION
1	JJH A4	6	JJH A12
2	JJH A5	7	JJH A39
3	JJH A6	8	JJH A56
4	JJH A7	9	JJH A58
5	JJH A8	10	JJH A59

TABLE NO: 1

CR-POOR CLINOPYROXENE MEGACRYSTS

	11	12	13	14	15	16	17	18	19	20
SiO_2	54.66	54.85	55.16	55.63	55.47	55.64	54.52	54.76	54.90	55.20
TiO_2	.29	.38	.42	.32	.31	.33	.34	.26	.50	.40
Al_2O_3	3.05	2.85	2.55	2.60	3.90	3.38	2.89	2.66	2.92	2.72
Cr_2O_3	.31	.63	.24	.33	.43	.28	.40	.32	.20	.56
FeO	5.41	5.30	6.33	5.78	5.11	5.89	5.39	5.24	5.82	5.23
MnO	.19	.15	.08	.13	.10	.09	.08	.12	.11	.14
MgO	20.87	18.85	20.06	20.92	19.00	18.83	19.14	21.61	18.65	18.87
CaO	12.93	14.56	14.35	13.68	13.26	14.00	14.84	13.16	15.30	15.16
Na_2O	1.92	1.81	1.73	1.45	2.56	2.18	2.00	1.67	2.04	1.79
K_2O	ND	ND	ND	ND	ND	ND	ND	ND	ND	ND
TOTAL	99.64	99.39	100.93	100.85	100.15	100.63	99.61	99.81	100.45	100.08

** ATOMIC PROPORTIONS BASED ON SELECTED NO. OF OXYGENS **

OXYGEN	6	6	6	6	6	6	6	6	6	6
SI	1.964	1.982	1.969	1.976	1.979	1.984	1.970	1.963	1.971	1.982
TI	.008	.010	.011	.009	.008	.009	.009	.007	.014	.011
AL	.129	.121	.107	.109	.164	.142	.123	.112	.124	.115
CR	.009	.018	.007	.009	.012	.008	.011	.009	.006	.016
FE2+	.163	.160	.189	.172	.152	.176	.163	.157	.175	.157
MN	.006	.005	.002	.004	.003	.003	.002	.004	.003	.004
MG	1.117	1.015	1.067	1.107	1.010	1.001	1.031	1.154	.998	1.010
CA	.498	.564	.549	.521	.507	.535	.574	.505	.589	.583
NA	.134	.127	.120	.100	.177	.151	.140	.116	.142	.125
K	-	-	-	-	-	-	-	-	-	-
SUM	4.027	4.002	4.023	4.007	4.013	4.008	4.024	4.028	4.022	4.004
	CA 28.00	CA 32.42	CA 30.41	CA 28.93	CA 30.36	CA 31.26	CA 32.50	CA 27.82	CA 33.42	CA 33.33
	MG 62.86	MG 58.37	MG 59.12	MG 61.53	MG 60.51	MG 58.48	MG 58.29	MG 63.54	MG 56.66	MG 57.70
	FE 9.14	FE 9.21	FE 10.47	FE 9.54	FE 9.13	FE 10.26	FE 9.21	FE 8.65	FE 9.92	FE 8.97
	M: 87.30	M: 86.37	M: 84.96	M: 86.58	M: 86.89	M: 85.07	M: 86.35	M: 88.02	M: 85.10	M: 86.54
	C: 30.82	C: 35.71	C: 33.96	C: 31.98	C: 33.41	C: 34.83	C: 35.79	C: 30.45	C: 37.10	C: 36.61

**** SAMPLE DIRECTORY ****

SAMPLE NO.	DESCRIPTION	SAMPLE NO.	DESCRIPTION
11	JJH A61	16	JJH A69
12	JJH A62	17	JJH A70
13	JJH A64	18	JJH A71
14	JJH A65	19	JJH A73
15	JJH A66	20	JJH A75

TABLE NO: 1

CR-POOR CLINOPYROXENE MEGACRYSTS

	21	22	23	24	25	26	27	28	29	30
SiO_2	55.49	54.82	56.16	55.22	55.19	54.02	54.43	54.15	55.43	55.31
TiO_2	.26	.40	.40	.32	.36	.53	.33	.37	.35	.41
Al_2O_3	3.54	3.00	3.12	3.17	2.74	2.56	2.63	2.45	3.34	2.86
Cr_2O_3	.55	.28	.26	.28	.40	.20	.37	.16	.35	.30
FeO	5.03	5.62	5.67	5.75	5.95	6.32	5.69	6.39	5.48	5.47
MnO	.12	.09	.15	.12	.28	ND	.14	.12	.11	.15
MgO	20.97	18.46	18.37	19.90	20.26	18.17	21.00	19.51	20.13	18.49
CaO	11.66	15.01	15.00	13.86	13.49	15.40	12.77	14.32	13.01	15.49
Na_2O	2.36	2.31	2.03	2.06	1.52	1.92	1.74	1.62	2.28	2.11
K_2O	ND	ND	ND	ND	ND	ND	ND	ND	ND	ND
TOTAL	99.99	100.00	101.17	100.69	100.20	99.14	99.11	99.10	100.49	100.60

** ATOMIC PROPORTIONS BASED ON SELECTED NO. OF OXYGENS **

OXYGEN	6	6	6	6	6	6	6	6	6	6
SI	1.974	1.976	1.993	1.969	1.976	1.972	1.967	1.971	1.973	1.981
TI	.007	.011	.011	.009	.010	.015	.009	.010	.009	.011
AL	.148	.127	.131	.133	.116	.110	.112	.105	.140	.121
CR	.015	.008	.007	.008	.011	.006	.011	.005	.010	.008
FE2+	.150	.169	.168	.171	.178	.193	.172	.195	.163	.164
MN	.004	.003	.005	.004	.008	.-	.004	.004	.003	.005
MG	1.112	.991	.972	1.057	1.081	.989	1.131	1.058	1.068	.987
CA	.445	.580	.570	.530	.518	.602	.495	.559	.496	.594
NA	.163	.161	.140	.142	.106	.136	.122	.114	.157	.147
K	-	-	-	-	-	-	-	-	-	-
SUM	4.018	4.027	3.997	4.023	4.004	4.023	4.024	4.021	4.021	4.017
	CA 26.05	CA 33.30	CA 33.35	CA 30.11	CA 29.13	CA 33.77	CA 27.51	CA 30.83	CA 28.73	CA 34.06
	MG 65.17	MG 56.97	MG 56.81	MG 60.14	MG 60.84	MG 55.42	MG 62.92	MG 58.43	MG 61.83	MG 56.55
	FE 8.77	FE 9.73	FE 9.84	FE 9.75	FE 10.03	FE 10.82	FE 9.57	FE 10.74	FE 9.45	FE 9.39
	M: 88.14	M: 85.41	M: 85.24	M: 86.05	M: 85.85	M: 83.67	M: 86.80	M: 84.47	M: 86.75	M: 85.76
	C: 28.56	C: 36.89	C: 36.99	C: 33.37	C: 32.37	C: 37.86	C: 30.42	C: 34.54	C: 31.73	C: 37.59

**** SAMPLE DIRECTORY ****

SAMPLE NO.	DESCRIPTION	SAMPLE NO.	DESCRIPTION
21	JJH A79	26	JJH A95
22	JJH A82	27	JJG 1858
23	JJH A83	28	JJG 1859
24	JJH A85	29	JJG 1868
25	JJH A87	30	JJH B38 INCLUSION IN GARNET

TABLE NO: 1

CR-POOR CLINOPYROXENE MEGACRYSTS

	31	32	33	34	35
SiO_2	55.83	55.31	55.26	54.71	55.04
TiO_2	.39	.45	.26	.34	.47
Al_2O_3	2.97	3.17	2.65	3.54	2.86
Cr_2O_3	.39	.22	.28	.32	.23
FeO	5.32	5.71	5.73	5.69	6.03
MnO	.10	.16	.13	.14	.09
MgO	18.75	17.93	20.36	18.31	17.90
CaO	14.98	15.26	13.39	14.46	15.14
Na_2O	2.13	2.20	1.44	2.33	1.77
K_2O	ND	ND	ND	ND	.04
TOTAL	100.87	100.42	99.51	99.85	99.57

** ATOMIC PROPORTIONS BASED ON SELECTED NO. OF OXYGENS **

OXYGEN	6	6	6	6	6
SI	1.987	1.984	1.986	1.972	1.991
TI	.010	.012	.007	.009	.013
AL	.125	.134	.112	.150	.122
CR	.011	.006	.008	.009	.007
FE2+	.158	.171	.172	.171	.182
MN	.003	.005	.004	.004	.003
MG	.995	.958	1.091	.983	.965
CA	.571	.586	.516	.558	.587
NA	.147	.153	.100	.163	.124
K	-	-	-	-	.002
SUM	4.008	4.011	3.997	4.021	3.995
	CA 33.13	CA 34.17	CA 28.99	CA 32.59	CA 33.84
	MG 57.68	MG 55.85	MG 61.32	MG 57.40	MG 55.64
	FE 9.18	FE 9.98	FE 9.68	FE 10.01	FE 10.52
	M: 86.26	M: 84.84	M: 86.36	M: 85.15	M: 84.10
	C: 36.48	C: 37.96	C: 32.10	C: 36.22	C: 37.82

**** SAMPLE DIRECTORY ****

SAMPLE NO.	DESCRIPTION	SAMPLE NO.	DESCRIPTION
31	JJH B53 INCLUSION IN GARNET		
32	JJH B78 INCLUSION IN GARNET		
33	JJH B83 INCLUSION IN GARNET		
34	JJH B87 INCLUSION IN GARNET		
35	JJH B89 INCLUSION IN GARNET		

TABLE NO: 2

CR-POOR GARNET MEGACRYSTS

	1	2	3	4	5	6	7	8	9	10
SiO_2	41.34	41.67	41.50	41.70	41.74	41.86	42.43	41.16	42.78	42.26
TiO_2	1.01	.86	.96	.81	.56	.72	.75	.95	.59	.87
Al_2O_3	21.71	21.78	21.21	21.75	22.45	22.02	22.81	22.00	22.78	22.52
Cr_2O_3	.62	1.27	.91	.92	.87	1.04	.66	.86	.91	.65
FeO	10.50	9.09	9.50	9.06	8.25	8.43	9.84	9.62	8.41	10.15
MnO	.34	.22	.24	.23	.23	.24	.28	.27	.26	.24
MgO	19.14	20.09	20.82	20.56	20.91	20.92	20.28	19.95	21.12	19.98
CaO	4.24	4.46	4.40	4.25	3.99	4.15	4.12	4.28	3.96	4.14
Na_2O	.12	.07	.10	.10	.08	.10	.12	.11	.10	.11
K_2O	-	-	-	-	-	-	-	-	-	-
TOTAL	99.02	99.51	99.64	99.38	99.08	99.48	101.29	99.20	100.91	100.92

** ATOMIC PROPORTIONS BASED ON SELECTED NO. OF OXYGENS **

OXYGEN	12	12	12	12	12	12	12	12	12	12
SI	2.996	2.990	2.982	2.992	2.988	2.991	2.989	2.969	3.004	2.993
TI	.055	.046	.052	.044	.030	.039	.040	.052	.031	.046
AL	1.855	1.842	1.796	1.840	1.894	1.855	1.894	1.870	1.886	1.880
CR	.036	.072	.052	.052	.049	.059	.037	.049	.051	.036
FE2+	.636	.546	.571	.544	.494	.504	.580	.580	.494	.601
MN	.021	.013	.015	.014	.014	.015	.017	.016	.015	.014
MG	2.067	2.149	2.229	2.199	2.230	2.228	2.129	2.145	2.210	2.109
CA	.329	.343	.339	.327	.306	.318	.311	.331	.298	.314
NA	.017	.010	.014	.014	.011	.014	.016	.015	.014	.015
K	-	-	-	-	-	-	-	-	-	-
SUM	8.012	8.011	8.049	8.025	8.016	8.021	8.014	8.028	8.003	8.010
	CA 10.86	CA 11.29	CA 10.79	CA 10.65	CA 10.10	CA 10.42	CA 10.30	CA 10.83	CA 9.92	CA 10.39
	MG 68.16	MG 70.75	MG 71.02	MG 71.64	MG 73.61	MG 73.06	MG 70.50	MG 70.18	MG 73.62	MG 69.73
	FE 20.98	FE 17.96	FE 18.19	FE 17.72	FE 16.30	FE 16.52	FE 19.20	FE 18.99	FE 16.45	FE 19.88
	M: 76.46	M: 79.75	M: 79.61	M: 80.17	M: 81.87	M: 81.56	M: 78.60	M: 78.70	M: 81.74	M: 77.82

**** SAMPLE DIRECTORY ****

SAMPLE NO.	DESCRIPTION	SAMPLE NO.	DESCRIPTION
1	JJH B1	6	JJH B7
2	JJH B2	7	JJH B8
3	JJH B3	8	JJH B9
4	JJH B4	9	JJH B11
5	JJH B6	10	JJH B12

TABLE NO: 2

CR-POOR GARNET MEGACRYSTS

	11	12	13	14	15	16	17	18	19	20
SiO_2	41.58	42.29	41.59	41.40	41.13	42.06	41.93	41.07	40.80	42.29
TiO_2	.90	.81	.98	1.00	1.01	.93	.86	1.00	.99	1.00
Al_2O_3	21.97	21.88	21.38	21.37	21.72	21.29	22.07	22.13	21.93	21.71
Cr_2O_3	1.16	.88	1.05	.92	.50	1.01	.78	.63	.49	.82
FeO	9.32	9.43	8.98	9.38	10.87	9.19	9.20	10.64	10.98	9.74
MnO	.25	.29	.26	.24	.26	.29	.21	.29	.31	.25
MgO	20.07	20.00	20.29	19.72	19.30	20.13	19.93	19.37	19.20	19.55
CaO	4.24	4.23	4.41	4.46	4.42	4.48	4.12	4.24	4.26	4.24
Na_2O	.10	.08	.11	.08	.12	.09	.10	.10	.14	.13
K_2O	-	-	-	-	-	-	-	-	-	-
TOTAL	99.59	99.89	99.05	98.57	99.33	99.47	99.20	99.47	99.10	99.73

** ATOMIC PROPORTIONS BASED ON SELECTED NO. OF OXYGENS **

OXYGEN	12	12	12	12	12	12	12	12	12	12
SI	2.983	3.019	2.997	3.002	2.979	3.019	3.010	2.966	2.964	3.028
TI	.049	.043	.053	.055	.055	.050	.046	.054	.054	.054
AL	1.858	1.841	1.816	1.827	1.854	1.801	1.867	1.884	1.878	1.832
CR	.066	.050	.060	.053	.029	.057	.044	.036	.028	.046
FE2+	.559	.563	.541	.569	.658	.552	.552	.643	.667	.583
MN	.015	.018	.016	.015	.016	.018	.013	.018	.019	.015
MG	2.146	2.128	2.179	2.131	2.083	2.153	2.132	2.085	2.078	2.086
CA	.326	.324	.341	.347	.343	.345	.317	.328	.332	.325
NA	.014	.011	.015	.011	.017	.013	.014	.014	.020	.018
K	-	-	-	-	-	-	-	-	-	-
SUM	8.014	7.997	8.019	8.009	8.033	8.008	7.995	8.027	8.039	7.988
	CA 10.75	CA 10.73	CA 11.13	CA 11.37	CA 11.12	CA 11.30	CA 10.56	CA 10.74	CA 10.78	CA 10.86
	MG 70.80	MG 70.59	MG 71.19	MG 69.95	MG 67.54	MG 70.61	MG 71.04	MG 68.23	MG 67.55	MG 69.66
	FE 18.45	FE 18.68	FE 17.68	FE 18.67	FE 21.34	FE 18.09	FE 18.40	FE 21.03	FE 21.68	FE 19.48
	M: 79.33	M: 79.08	M: 80.10	M: 78.93	M: 75.98	M: 79.61	M: 79.43	M: 76.44	M: 75.70	M: 78.15

**** SAMPLE DIRECTORY ****

SAMPLE NO.	DESCRIPTION	SAMPLE NO.	DESCRIPTION
11	JJH B13	16	JJH B18
12	JJH B14	17	JJH B19
13	JJH B15	18	JJH B20
14	JJH B16	19	JJH B21
15	JJH B17	20	JJH B22

TABLE NO: 2

CR-POOR GARNET MEGACRYSTS

	21	22	23	24	25	26	27	28	29	30
SiO_2	41.27	41.82	41.98	41.47	41.25	41.66	42.03	41.73	41.02	42.11
TiO_2	.96	.74	.77	.88	.96	.85	.94	.72	1.22	.58
Al_2O_3	21.40	22.06	22.24	21.62	21.66	21.90	21.77	21.66	20.91	21.94
Cr_2O_3	.68	.58	.65	.97	.80	.83	.71	1.07	.73	1.00
FeO	10.23	10.22	10.02	9.84	9.86	9.64	9.90	8.22	11.13	8.08
MnO	.20	.28	.22	.27	.24	.25	.24	.32	.31	.24
MgO	19.94	19.72	19.76	19.64	20.12	20.25	19.97	21.52	19.16	21.37
CaO	4.41	4.25	4.09	4.27	4.36	4.17	4.37	4.00	4.54	4.11
Na_2O	.10	.12	.13	.11	.11	.10	.10	.10	.12	.11
K_2O	-	-	-	-	-	-	-	-	-	-
TOTAL	99.19	99.79	99.86	99.07	99.36	99.65	100.03	99.34	99.14	99.54

** ATOMIC PROPORTIONS BASED ON SELECTED NO. OF OXYGENS **

OXYGEN	12	12	12	12	12	12	12	12	12	12
SI	2.985	3.000	3.003	2.997	2.975	2.988	3.005	2.986	2.987	3.001
TI	.052	.040	.041	.048	.052	.046	.051	.039	.067	.031
AL	1.825	1.865	1.875	1.842	1.841	1.851	1.835	1.827	1.794	1.843
CR	.039	.033	.037	.055	.046	.047	.040	.061	.042	.056
FE2+	.619	.613	.600	.595	.595	.578	.592	.492	.678	.482
MN	.012	.017	.013	.017	.015	.015	.015	.019	.019	.014
MG	2.150	2.108	2.107	2.115	2.162	2.164	2.128	2.295	2.079	2.270
CA	.342	.327	.314	.331	.337	.320	.335	.307	.354	.314
NA	.014	.017	.018	.015	.015	.014	.014	.014	.017	.015
K	-	-	-	-	-	-	-	-	-	-
SUM	8.038	8.020	8.008	8.014	8.038	8.024	8.014	8.039	8.037	8.026
	CA 10.99	CA 10.72	CA 10.38	CA 10.87	CA 10.89	CA 10.46	CA 10.96	CA 9.91	CA 11.39	CA 10.24
	MG 69.11	MG 69.17	MG 69.77	MG 69.57	MG 69.89	MG 70.66	MG 69.66	MG 74.18	MG 66.83	MG 74.05
	FE 19.90	FE 20.12	FE 19.85	FE 19.56	FE 19.22	FE 18.88	FE 19.38	FE 15.90	FE 21.79	FE 15.71
	M: 77.65	M: 77.47	M: 77.85	M: 78.05	M: 78.43	M: 78.92	M: 78.24	M: 82.35	M: 75.42	M: 82.50

**** SAMPLE DIRECTORY ****

SAMPLE NO.	DESCRIPTION	SAMPLE NO.	DESCRIPTION
21	JJH B24	26	JJH B30
22	JJH B25	27	JJH B32
23	JJH B26	28	JJH B33
24	JJH B27	29	JJH B34
25	JJH B29	30	JJH B35

TABLE NO: 2

CR-POOR GARNET MEGACRYSTS

	31	32	33	34	35	36	37	38	39	40
SiO_2	41.51	41.75	41.00	41.55	41.64	42.05	41.55	41.77	42.10	41.12
TiO_2	.83	.79	.95	.92	.67	.86	.56	.89	.97	1.05
Al_2O_3	21.49	21.95	21.92	21.46	22.17	21.77	22.26	21.69	21.31	21.85
Cr_2O_3	.98	.95	.64	.80	.94	.94	1.08	.95	.91	.58
FeO	9.10	8.70	10.17	9.85	8.62	9.40	8.19	9.27	10.27	11.20
MnO	.21	.18	.23	.29	.23	.25	.20	.23	.27	.30
MgO	20.28	20.69	20.08	19.83	20.64	20.31	21.14	20.53	19.63	19.41
CaO	4.29	4.11	4.36	4.27	4.14	4.34	4.06	4.33	4.09	4.35
Na_2O	.10	.10	.11	.11	.11	.10	.11	.09	.13	.14
K_2O	-	-	-	-	-	-	-	-	-	-
TOTAL	98.79	99.22	99.46	99.08	99.16	100.02	99.15	99.75	99.68	100.00

** ATOMIC PROPORTIONS BASED ON SELECTED NO. OF OXYGENS **

OXYGEN	12	12	12	12	12	12	12	12	12	12
SI	2.998	2.993	2.958	3.002	2.987	3.002	2.976	2.990	3.025	2.964
TI	.045	.043	.052	.050	.036	.046	.030	.048	.052	.057
AL	1.830	1.855	1.864	1.828	1.874	1.832	1.879	1.830	1.805	1.856
CR	.056	.054	.037	.046	.053	.053	.061	.054	.052	.033
FE2+	.550	.522	.614	.595	.517	.561	.491	.555	.617	.675
MN	.013	.011	.014	.018	.014	.015	.012	.014	.016	.018
MG	2.183	2.211	2.159	2.135	2.206	2.161	2.256	2.190	2.102	2.085
CA	.332	.316	.337	.331	.318	.332	.312	.332	.315	.336
NA	.014	.014	.015	.015	.015	.014	.015	.012	.018	.020
K	-	-	-	-	-	-	-	-	-	-
SUM	8.021	8.017	8.048	8.019	8.021	8.016	8.032	8.026	8.003	8.044
	CA 10.83	CA 10.36	CA 10.84	CA 10.80	CA 10.46	CA 10.87	CA 10.19	CA 10.79	CA 10.38	CA 10.85
	MG 71.23	MG 72.53	MG 69.43	MG 69.76	MG 72.54	MG 70.75	MG 73.77	MG 71.17	MG 69.28	MG 67.34
	FE 17.94	FE 17.11	FE 19.73	FE 19.44	FE 17.00	FE 18.38	FE 16.04	FE 18.03	FE 20.34	FE 21.81
	M: 79.88	M: 80.91	M: 77.87	M: 78.20	M: 81.01	M: 79.38	M: 82.14	M: 79.78	M: 77.30	M: 75.54

**** SAMPLE DIRECTORY ****

SAMPLE NO.	DESCRIPTION	SAMPLE NO.	DESCRIPTION
31	JJH B36	36	JJH B41
32	JJH B37	37	JJH B42
33	JJH B38	38	JJH B44
34	JJH B39	39	JJH B45
35	JJH B40	40	JJH B46

TABLE NO: 2

CR-POOR GARNET MEGACRYSTS

	41	42	43	44	45	46	47	48	49	50
SiO_2	41.85	41.07	41.75	40.74	41.44	41.58	41.91	41.41	41.10	42.16
TiO_2	.93	.99	.85	.94	1.04	.86	.66	.90	.82	.90
Al_2O_3	21.75	21.77	22.28	22.32	21.80	21.84	21.69	22.39	21.80	21.74
Cr_2O_3	.70	.60	.71	.62	.72	1.04	.80	.38	.92	.76
FeO	9.86	10.49	9.98	9.98	10.13	8.42	9.83	11.40	9.55	10.48
MnO	.36	.27	.22	.26	.22	.24	.28	.31	.22	.26
MgO	19.95	19.65	20.57	20.46	20.50	21.14	19.96	19.33	20.56	19.89
CaO	4.23	4.29	4.32	4.20	4.53	4.20	4.20	4.21	3.99	4.13
Na_2O	.10	.13	.13	.12	.10	.19	.13	.12	.11	.12
K_2O	-	-	-	-	-	-	-	-	-	-
TOTAL	99.73	99.26	100.81	99.64	100.48	99.51	99.46	100.45	99.07	100.44

** ATOMIC PROPORTIONS BASED ON SELECTED NO. OF OXYGENS **

OXYGEN	12	12	12	12	12	12	12	12	12	12
SI	3.002	2.972	2.965	2.932	2.960	2.975	3.013	2.968	2.966	3.008
TI	.050	.054	.045	.051	.056	.046	.036	.049	.045	.048
AL	1.839	1.857	1.865	1.893	1.835	1.842	1.838	1.891	1.855	1.828
CR	.040	.034	.040	.035	.041	.059	.045	.022	.052	.043
FE2+	.591	.635	.593	.601	.605	.504	.591	.683	.576	.625
MN	.022	.017	.013	.016	.013	.015	.017	.019	.013	.016
MG	2.133	2.119	2.177	2.194	2.182	2.254	2.138	2.065	2.212	2.115
CA	.325	.333	.329	.324	.347	.322	.323	.323	.309	.316
NA	.014	.018	.018	.017	.014	.026	.018	.017	.015	.017
K	-	-	-	-	-	-	-	-	-	-
SUM	8.016	8.038	8.046	8.062	8.053	8.042	8.019	8.036	8.043	8.016
	CA 10.66	CA 10.78	CA 10.61	CA 10.38	CA 11.06	CA 10.45	CA 10.60	CA 10.53	CA 9.96	CA 10.33
	MG 69.94	MG 68.66	MG 70.26	MG 70.36	MG 69.63	MG 73.19	MG 70.04	MG 67.22	MG 71.42	MG 69.21
	FE 19.40	FE 20.57	FE 19.13	FE 19.26	FE 19.31	FE 16.36	FE 19.36	FE 22.25	FE 18.62	FE 20.46
	M: 78.29	M: 76.95	M: 78.60	M: 78.51	M: 78.29	M: 81.73	M: 78.35	M: 75.13	M: 79.32	M: 77.18

**** SAMPLE DIRECTORY ****

SAMPLE NO.	DESCRIPTION	SAMPLE NO.	DESCRIPTION
41	JJH B47	46	JJH B52
42	JJH B48	47	JJH B55
43	JJH B49	48	JJH B57
44	JJH B50	49	JJH B58
45	JJH B51	50	JJH B59

TABLE NO: 2

CR-POOR GARNET MEGACRYSTS

	51	52	53	54	55	56	57	58	59	60
SiO_2	42.05	42.12	41.92	41.72	41.44	41.54	41.67	41.60	41.22	41.33
TiO_2	.77	.89	1.03	1.05	.97	1.00	.94	.87	1.10	1.09
Al_2O_3	21.69	22.06	21.06	21.74	21.10	20.88	21.87	21.41	21.52	20.76
Cr_2O_3	1.25	.64	.81	.87	.84	.82	.44	.61	.68	.72
FeO	9.65	10.10	10.35	10.30	10.33	9.79	11.46	9.96	10.78	10.48
MnO	.25	.26	.24	.27	.27	.28	.31	.29	.28	.25
MgO	19.97	20.20	20.32	20.10	19.90	20.21	19.21	19.99	19.81	19.91
CaO	4.15	4.10	4.43	4.49	4.39	4.37	4.16	4.20	4.46	4.42
Na_2O	.13	.12	.11	.11	.10	.10	.12	.10	.11	.09
K_2O	-	-	-	-	-	-	-	-	-	-
TOTAL	99.91	100.49	100.27	100.65	99.34	98.99	100.18	99.03	99.96	99.05

** ATOMIC PROPORTIONS BASED ON SELECTED NO. OF OXYGENS **

OXYGEN	12	12	12	12	12	12	12	12	12	12
SI	3.009	2.997	3.002	2.976	2.996	3.007	2.994	3.006	2.969	3.000
TI	.041	.048	.055	.056	.053	.054	.051	.047	.060	.059
AL	1.829	1.850	1.778	1.828	1.798	1.781	1.852	1.824	1.827	1.776
CR	.071	.036	.046	.049	.048	.047	.025	.035	.039	.041
FE2+	.577	.601	.620	.615	.625	.593	.689	.602	.649	.636
MN	.015	.016	.015	.016	.017	.017	.019	.018	.017	.015
MG	2.130	2.142	2.169	2.137	2.144	2.180	2.057	2.153	2.126	2.154
CA	.318	.313	.340	.343	.340	.339	.320	.325	.344	.344
NA	.018	.017	.015	.015	.014	.014	.017	.014	.015	.013
K	-	-	-	-	-	-	-	-	-	-
SUM	8.009	8.020	8.039	8.036	8.035	8.032	8.024	8.024	8.046	8.038
	CA 10.52	CA 10.23	CA 10.87	CA 11.09	CA 10.94	CA 10.89	CA 10.45	CA 10.56	CA 11.03	CA 10.97
	MG 70.39	MG 70.10	MG 69.32	MG 69.05	MG 68.97	MG 70.06	MG 67.09	MG 69.90	MG 68.16	MG 68.73
	FE 19.09	FE 19.67	FE 19.81	FE 19.86	FE 20.09	FE 19.05	FE 22.46	FE 19.54	FE 20.81	FE 20.30
	M: 78.67	M: 78.09	M: 77.77	M: 77.67	M: 77.44	M: 78.63	M: 74.92	M: 78.15	M: 76.61	M: 77.20

**** SAMPLE DIRECTORY ****

SAMPLE NO.	DESCRIPTION	SAMPLE NO.	DESCRIPTION
51	JJH B60	56	JJH B69
52	JJH B62	57	JJH B70
53	JJH B63	58	JJH B71
54	JJH B65	59	JJH B72
55	JJH B66	60	JJH B73

TABLE NO: 2

CR-POOR GARNET MEGACRYSTS

	61	62	63	64	65	66	67	68	69	70
SiO_2	42.16	42.24	41.40	41.70	41.76	42.49	42.64	41.26	41.67	41.89
TiO_2	.86	.88	.84	.95	1.00	.57	.90	.98	1.11	.86
Al_2O_3	22.03	21.59	21.11	22.07	21.26	21.92	21.18	21.34	21.02	21.92
Cr_2O_3	.71	.69	.92	.64	.72	1.06	1.02	.83	1.00	.62
FeO	10.30	9.80	9.46	10.97	10.49	8.41	9.30	9.82	9.33	9.92
MnO	.32	.21	.26	.35	.27	.27	.21	.28	.27	.30
MgO	19.80	20.39	20.61	19.38	19.63	20.92	20.75	20.07	20.39	19.85
CaO	4.17	4.38	4.31	4.15	4.34	3.99	4.35	4.32	4.41	4.10
Na_2O	.10	.11	.11	.12	.11	.13	.11	.09	.14	.09
K_2O	-	-	-	-	-	-	-	-	-	-
TOTAL	100.45	100.29	99.02	100.33	99.58	99.76	100.46	98.99	99.34	99.55

** ATOMIC PROPORTIONS BASED ON SELECTED NO. OF OXYGENS **

OXYGEN	12	12	12	12	12	12	12	12	12	12
SI	3.005	3.011	2.992	2.987	3.010	3.023	3.029	2.987	3.001	3.007
TI	.046	.047	.046	.051	.054	.030	.048	.053	.060	.046
AL	1.851	1.814	1.798	1.863	1.806	1.838	1.773	1.821	1.784	1.855
CR	.040	.039	.053	.036	.041	.060	.057	.048	.057	.035
FE2+	.614	.584	.572	.657	.632	.500	.552	.594	.562	.596
MN	.019	.013	.016	.021	.016	.016	.013	.017	.016	.018
MG	2.103	2.166	2.220	2.069	2.109	2.218	2.197	2.165	2.188	2.123
CA	.318	.335	.334	.319	.335	.304	.331	.335	.340	.315
NA	.014	.015	.015	.017	.015	.018	.015	.013	.020	.013
K	-	-	-	-	-	-	-	-	-	-
SUM	8.011	8.023	8.045	8.020	8.020	8.007	8.015	8.032	8.028	8.008
	CA 10.49	CA 10.84	CA 10.68	CA 10.46	CA 10.90	CA 10.06	CA 10.75	CA 10.83	CA 11.01	CA 10.39
	MG 69.28	MG 70.22	MG 71.03	MG 67.95	MG 68.55	MG 73.38	MG 71.31	MG 69.96	MG 70.81	MG 69.98
	FE 20.23	FE 18.94	FE 18.29	FE 21.59	FE 20.56	FE 16.55	FE 17.94	FE 19.21	FE 18.18	FE 19.63
	M: 77.40	M: 78.76	M: 79.52	M: 75.89	M: 76.93	M: 81.59	M: 79.90	M: 78.46	M: 79.57	M: 78.10

**** SAMPLE DIRECTORY ****

SAMPLE NO.	DESCRIPTION	SAMPLE NO.	DESCRIPTION
61	JJH B74	66	JJH B82
62	JJH B76	67	JJH B83
63	JJH B77	68	JJH B84
64	JJH B78	69	JJH B85
65	JJH B80	70	JJH B87

TABLE NO: 2

CR-POOR GARNET MEGACRYSTS

	71	72	73	74	75	76	77	78	79
SiO_2	41.08	40.98	41.37	41.21	41.59	41.55	42.15	41.46	42.22
TiO_2	1.10	.99	.86	1.08	.95	.75	.53	.88	.84
Al_2O_3	21.20	21.16	21.60	20.68	21.73	22.14	21.89	21.80	22.03
Cr_2O_3	.74	.85	.78	.77	.79	.81	1.35	.61	.92
FeO	11.08	10.21	9.52	10.76	10.28	10.22	8.06	10.96	9.80
MnO	.24	.28	.30	.30	.23	.25	.25	.27	.25
MgO	19.48	20.11	20.27	19.95	19.80	19.83	21.55	19.14	19.87
CaO	4.26	4.42	4.02	4.38	4.20	4.02	3.65	4.08	4.16
Na_2O	.13	.11	.10	.09	.09	.11	.09	.10	.11
K_2O	-	-	-	-	-	-	-	-	-
TOTAL	99.31	99.11	98.82	99.22	99.66	99.68	99.52	99.30	100.20

** ATOMIC PROPORTIONS BASED ON SELECTED NO. OF OXYGENS **

OXYGEN	12	12	12	12	12	12	12	12	12
SI	2.981	2.972	2.991	2.992	2.991	2.985	3.002	2.999	3.009
TI	.060	.054	.047	.059	.051	.041	.028	.048	.045
AL	1.813	1.809	1.841	1.770	1.842	1.875	1.838	1.859	1.851
CR	.042	.049	.045	.044	.045	.046	.076	.035	.052
FE2+	.672	.619	.576	.653	.618	.614	.480	.663	.584
MN	.015	.017	.018	.018	.014	.015	.015	.017	.015
MG	2.107	2.174	2.184	2.159	2.122	2.123	2.288	2.063	2.112
CA	.331	.343	.311	.341	.324	.309	.279	.316	.318
NA	.018	.015	.014	.013	.013	.015	.012	.014	.015
K	-	-	-	-	-	-	-	-	-
SUM	8.040	8.053	8.027	8.049	8.020	8.022	8.019	8.013	8.002
	CA 10.65	CA 10.95	CA 10.14	CA 10.81	CA 10.56	CA 10.16	CA 9.14	CA 10.39	CA 10.54
	MG 67.73	MG 69.30	MG 71.12	MG 68.47	MG 69.26	MG 69.69	MG 75.09	MG 67.82	MG 70.07
	FE 21.62	FE 19.75	FE 18.74	FE 20.72	FE 20.18	FE 20.15	FE 15.76	FE 21.79	FE 19.39
	M: 75.80	M: 77.83	M: 79.14	M: 76.77	M: 77.44	M: 77.57	M: 82.65	M: 75.68	M: 78.33

**** SAMPLE DIRECTORY ****

SAMPLE NO.	DESCRIPTION	SAMPLE NO.	DESCRIPTION
71	JJH B89	76	JJH A69 INCLUSION IN CPX
72	JJH B90	77	JJH A79 INCLUSION IN CPX
73	JJH B91	78	JJH A83 INCLUSION IN CPX
74	JJH B92	79	JJH B53
75	JJH A56 INCLUSION IN CPX		

TABLE NO: 3

CR-POOR OLIVINE MEGACRYSTS/DUNITES

	1	2	3	4	5	6	7	8	9	10
SiO_2	39.93	39.43	39.85	39.67	40.14	39.65	39.71	39.77	40.04	39.70
TiO_2	ND	ND	ND	ND	ND	ND	ND	ND	ND	ND
Al_2O_3	.06	ND	ND	ND	.05	ND	.05	ND	ND	ND
Cr_2O_3	ND	ND	ND	ND	ND	ND	ND	ND	ND	ND
FeO	13.20	12.53	13.68	14.74	12.95	14.80	13.02	13.85	13.82	13.79
MnO	.08	.11	.11	.14	.12	.11	.16	.14	.12	.13
MgO	46.75	46.61	46.08	44.63	46.78	44.79	46.08	45.61	46.37	45.93
CaO	.09	.09	.08	.04	.08	.06	.07	.06	.09	.06
Na_2O	-	-	-	-	-	-	-	-	-	-
K_2O	-	-	-	-	-	-	-	-	-	-
NiO	.32	.27	.22	.19	.34	.19	.30	.19	.33	.23
TOTAL	100.45	99.07	100.05	99.44	100.48	99.63	99.41	99.65	100.80	99.87

** ATOMIC PROPORTIONS BASED ON SELECTED NO. OF OXYGENS **

OXYGEN	4	4	4	4	4	4	4	4	4	4
SI	.991	.990	.995	1.001	.995	.999	.996	.998	.993	.994
TI	-	-	-	-	-	-	-	-	-	-
AL	.002	-	-	-	.001	-	.001	-	-	-
CR	-	-	-	-	-	-	-	-	-	-
FE2+	.274	.263	.286	.311	.268	.312	.273	.291	.287	.289
MN	.002	.002	.002	.003	.003	.002	.003	.003	.003	.003
MG	1.730	1.745	1.715	1.678	1.728	1.682	1.722	1.705	1.714	1.714
CA	.002	.002	.002	.001	.002	.002	.002	.002	.002	.002
NA	-	-	-	-	-	-	-	-	-	-
K	-	-	-	-	-	-	-	-	-	-
NI	.006	.005	.004	.004	.007	.004	.006	.004	.007	.005
SUM	3.008	3.009	3.005	2.999	3.004	3.001	3.003	3.002	3.006	3.006
	FO 86.32	FO 86.89	FO 85.72	FO 84.36	FO 86.55	FO 84.36	FO 86.31	FO 85.44	FO 85.67	FO 85.58
	FA 13.68	FA 13.11	FA 14.28	FA 15.64	FA 13.45	FA 15.64	FA 13.69	FA 14.56	FA 14.33	FA 14.42

**** SAMPLE DIRECTORY ****

SAMPLE NO.	DESCRIPTION	SAMPLE NO.	DESCRIPTION
1	JJH D1	6	JJH D18
2	JJH D2	7	JJH D19
3	JJH D3	8	JJH D21
4	JJH D5	9	JJH D23
5	JJH D9	10	JJH 5

TABLE NO: 3

CR-POOR OLIVINE MEGACRYSTS/DUNITES

	11	12	13	14
SiO_2	40.08	39.82	39.78	40.25
TiO_2	ND	ND	ND	ND
Al_2O_3	NO	.05	.06	.07
Cr_2O_3	.05	ND	NO	ND
FeO	11.75	13.27	13.78	11.77
MnO	.13	.12	.13	.10
MgO	47.27	45.68	45.36	46.47
CaO	.08	.09	.07	.08
Na_2O	-	-	-	-
K_2O	-	-	-	-
NiO	.31	.30	.20	.19
TOTAL	99.69	99.35	99.40	98.95

** ATOMIC PROPORTIONS BASED ON SELECTED NO. OF OXYGENS **

OXYGEN	4	4	4	4
SI	.996	.999	1.000	1.006
TI	-	-	-	-
AL	-	.001	.002	.002
CR	.001	-	-	-
FE2+	.244	.279	.290	.246
MN	.003	.003	.003	.002
MG	1.751	1.709	1.699	1.731
CA	.002	.002	.002	.002
NA	-	-	-	-
K	-	-	-	-
NI	.006	.006	.004	.004
SUM	3.003	3.000	2.999	2.993
	FO 87.76	FO 85.98	FO 85.44	FO 87.56
	FA 12.24	FA 14.02	FA 14.56	FA 12.44

**** SAMPLE DIRECTORY ****

SAMPLE NO.	DESCRIPTION	SAMPLE NO.	DESCRIPTION
11	JJH B35 INCLUSION IN GARNET		
12	JJH B54 INCLUSION IN GARNET		
13	JJH B86 INCLUSION IN GARNET		
14	JJH A66 INCLUSION IN CPX		

TABLE NO: 4

CR-POOR ORTHOPYROXENE MEGACRYSTS

	1	2	3	4	5	6	7	8	9	10
SiO_2	57.79	56.44	57.27	55.72	57.07	57.11	56.98	56.15	57.05	57.29
TiO_2	.12	.25	.19	.24	.22	.20	.24	.15	.22	.20
Al_2O_3	1.18	.97	1.17	.93	1.10	1.02	1.03	.79	1.25	1.16
Cr_2O_3	.07	ND	.12	.05	.10	.07	ND	ND	.17	.42
FeO	7.65	9.30	7.87	9.10	7.65	8.44	8.71	11.04	7.61	6.06
MnO	.10	.08	.13	.15	.12	.14	.17	.18	.11	.13
MgO	32.58	31.73	32.34	32.96	32.87	32.24	32.28	30.88	32.43	32.78
CaO	1.36	1.02	1.30	.93	1.27	1.03	1.06	.78	1.26	1.47
Na_2O	.38	.32	.33	.27	.33	.27	.27	.19	.27	.29
K_2O	ND	ND	ND	ND	ND	ND	ND	ND	ND	ND
TOTAL	101.24	100.13	100.73	100.36	100.74	100.53	100.76	100.18	100.38	99.81

** ATOMIC PROPORTIONS BASED ON SELECTED NO. OF OXYGENS **

OXYGEN	6	6	6	6	6	6	6	6	6	6
SI	1.984	1.974	1.979	1.948	1.971	1.981	1.975	1.977	1.976	1.983
TI	.003	.007	.005	.006	.006	.005	.006	.004	.006	.005
AL	.048	.040	.048	.038	.045	.042	.042	.033	.051	.047
CR	.002	-	.003	.001	.003	.002	-	-	.005	.011
FE2+	.220	.272	.227	.266	.221	.245	.253	.325	.220	.175
MN	.003	.002	.004	.004	.004	.004	.005	.005	.003	.004
MG	1.667	1.654	1.665	1.717	1.692	1.666	1.668	1.621	1.674	1.692
CA	.050	.038	.048	.035	.047	.038	.039	.029	.047	.054
NA	.025	.022	.022	.018	.022	.018	.018	.013	.018	.019
K	-	-	-	-	-	-	-	-	-	-
SUM	4.001	4.010	4.002	4.035	4.011	4.002	4.007	4.009	4.000	3.992
	CA 2.58	CA 1.95	CA 2.48	CA 1.73	CA 2.40	CA 1.96	CA 2.01	CA 1.49	CA 2.41	CA 2.81
	MG 86.07	MG 84.20	MG 85.80	MG 85.09	MG 86.33	MG 85.48	MG 85.10	MG 82.05	MG 86.24	MG 88.03
	FE 11.34	FE 13.85	FE 11.72	FE 13.18	FE 11.27	FE 12.56	FE 12.89	FE 16.46	FE 11.36	FE 9.13
	M: 88.36	M: 85.88	M: 87.98	M: 86.59	M: 88.45	M: 87.19	M: 86.85	M: 83.29	M: 88.36	M: 90.60
	C: 2.91	C: 2.26	C: 2.81	C: 1.99	C: 2.70	C: 2.25	C: 2.31	C: 1.78	C: 2.72	C: 3.12

**** SAMPLE DIRECTORY ****

SAMPLE NO.	DESCRIPTION	SAMPLE NO.	DESCRIPTION
1	JJH C1	6	JJH C18
2	JJH C5	7	JJH C19
3	JJH C13	8	JJH C20
4	JJH C14	9	JJH A75 INCLUSION IN CPX
5	JJH C16	10	JJH B24 INCLUSION IN GARNET

TABLE NO: 5

MG-RICH OLIVINE MEGACRYSTS/DUNITES

	1	2	3	4	5	6	7	8	9	10
SiO_2	41.07	41.16	40.92	40.81	41.21	41.54	41.19	41.37	41.09	40.40
TiO_2	ND	ND	ND	ND	ND	ND	ND	ND	ND	ND
Al_2O_3	ND	ND	ND	ND	ND	ND	ND	ND	ND	ND
Cr_2O_3	.05	ND	ND	ND	ND	ND	ND	ND	ND	.05
FeO	5.57	7.37	6.61	6.48	7.10	5.92	6.01	6.01	6.12	6.95
MnO	.08	.07	.08	.11	.09	ND	.04	.07	.10	.09
MgO	52.05	50.63	51.56	51.40	51.08	52.22	51.82	52.42	51.51	52.11
CaO	ND	ND	ND	ND	ND	ND	ND	ND	ND	ND
Na_2O	-	-	-	-	-	-	-	-	-	-
K_2O	-	-	-	-	-	-	-	-	-	-
NiO	.24	.34	.31	.34	.30	.26	.31	.28	.30	.27
TOTAL	99.09	99.61	99.52	99.18	99.82	100.01	99.41	100.19	99.16	99.90

** ATOMIC PROPORTIONS BASED ON SELECTED NO. OF OXYGENS **

OXYGEN	4	4	4	4	4	4	4	4	4	4
SI	.997	1.002	.995	.995	1.000	1.000	.999	.995	.999	.981
TI	-	-	-	-	-	-	-	-	-	-
AL	-	-	-	-	-	-	-	-	-	-
CR	.001	-	-	-	-	-	-	-	-	.001
FE2+	.113	.150	.134	.132	.144	.119	.122	.121	.124	.141
MN	.002	.001	.002	.002	.002	-	.001	.001	.002	.002
MG	1.884	1.837	1.868	1.868	1.847	1.874	1.873	1.880	1.867	1.886
CA	-	-	-	-	-	-	-	-	-	-
NA	-	-	-	-	-	-	-	-	-	-
K	-	-	-	-	-	-	-	-	-	-
NI	.005	.007	.006	.007	.006	.005	.006	.005	.006	.005
SUM	3.002	2.998	3.005	3.005	3.000	2.999	3.001	3.004	3.000	3.018
	FO 94.33	FO 92.45	FO 93.29	FO 93.39	FO 92.76	FO 94.02	FO 93.89	FO 93.96	FO 93.75	FO 93.04
	FA 5.67	FA 7.55	FA 6.71	FA 6.61	FA 7.24	FA 5.98	FA 6.11	FA 6.04	FA 6.25	FA 6.96

**** SAMPLE DIRECTORY ****

SAMPLE NO.	DESCRIPTION	SAMPLE NO.	DESCRIPTION
1	JJH D4	6	JJH D11
2	JJH D6	7	JJH D12
3	JJH D7	8	JJH 013
4	JJH D8	9	JJH D14
5	JJH D10	10	JJH D16

TABLE NO: 5

MG-RICH OLIVINE MEGACRYSTS/DUNITES

	11	12
SiO_2	41.47	40.81
TiO_2	ND	ND
Al_2O_3	ND	ND
Cr_2O_3	ND	ND
FeO	5.84	6.86
MnO	.10	.08
MgO	52.01	52.01
CaO	ND	ND
Na_2O	-	-
K_2O	-	-
NiO	.32	.24
TOTAL	99.78	100.04

** ATOMIC PROPORTIONS BASED ON SELECTED NO. OF OXYGENS **

OXYGEN	4	4
SI	1.001	.988
TI	-	-
AL	-	-
CR	-	-
FE2+	.118	.139
MN	.002	.002
MG	1.871	1.877
CA	-	-
NA	-	-
K	-	-
NI	.006	.005
SUM	2.999	3.011
	FO 94.07	FO 93.11
	FA 5.93	FA 6.89

**** SAMPLE DIRECTORY ****

SAMPLE NO.	DESCRIPTION	SAMPLE NO.	DESCRIPTION
11	JJH D17		
12	JJH D20		

TABLE NO: 6

GRANNY SMITH DIOPSIDES

	1	2	3	4	5	6	7	8	9	10
SiO_2	54.75	53.80	54.40	54.74	54.65	54.80	54.29	54.64	54.60	54.47
TiO_2	.18	.17	.29	.15	.14	.18	.20	.23	.29	.17
Al_2O_3	.48	.37	1.22	.34	.21	.39	.46	1.29	1.68	.39
Cr_2O_3	1.33	1.23	1.56	1.30	1.40	1.22	1.16	2.44	2.97	1.24
FeO	2.15	1.94	2.76	2.00	2.04	1.88	2.17	2.50	2.38	2.16
MnO	.08	.07	.06	.05	.10	.07	.11	.10	.06	.05
MgO	17.74	17.66	17.18	17.86	17.39	17.76	17.62	17.46	16.41	18.06
CaO	21.80	21.66	20.41	22.24	22.63	22.04	21.97	19.34	19.11	22.64
Na_2O	1.19	2.46	1.75	1.09	1.02	1.09	1.14	1.91	2.53	1.09
K_2O	ND	ND	ND	ND	ND	ND	ND	.05	ND	ND
TOTAL	99.71	99.37	99.64	99.78	99.59	99.44	99.13	99.96	100.04	100.28

** ATOMIC PROPORTIONS BASED ON SELECTED NO. OF OXYGENS **

OXYGEN	6	6	6	6	6	6	6	6	6	6
SI	1.991	1.973	1.981	1.990	1.993	1.995	1.988	1.980	1.979	1.975
TI	.005	.005	.008	.004	.004	.005	.006	.006	.008	.005
AL	.021	.016	.052	.015	.009	.017	.020	.055	.072	.017
CR	.038	.036	.045	.037	.040	.035	.034	.070	.085	.036
FE2+	.065	.060	.084	.061	.062	.057	.066	.076	.072	.066
MN	.002	.002	.002	.002	.003	.002	.003	.003	.002	.002
MG	.961	.965	.932	.967	.945	.964	.961	.943	.886	.976
CA	.849	.851	.796	.866	.884	.860	.862	.751	.742	.880
NA	.084	.175	.124	.077	.072	.077	.081	.134	.178	.077
K	-	-	-	-	-	-	-	.002	-	-
SUM	4.017	4.084	4.025	4.019	4.014	4.013	4.021	4.020	4.024	4.032
	CA 45.27	CA 45.37	CA 43.93	CA 45.72	CA 46.75	CA 45.72	CA 45.61	CA 42.43	CA 43.64	CA 45.79
	MG 51.24	MG 51.45	MG 51.43	MG 51.07	MG 49.96	MG 51.24	MG 50.88	MG 53.28	MG 52.12	MG 50.80
	FE 3.49	FE 3.17	FE 4.64	FE 3.21	FE 3.29	FE 3.04	FE 3.52	FE 4.28	FE 4.24	FE 3.41
	M: 93.63	M: 94.19	M: 91.73	M: 94.09	M: 93.82	M: 94.39	M: 93.54	M: 92.56	M: 92.47	M: 93.71
	C: 46.91	C: 46.86	C: 46.07	C: 47.24	C: 48.34	C: 47.15	C: 47.27	C: 44.33	C: 45.57	C: 47.40

**** SAMPLE DIRECTORY ****

SAMPLE NO.	DESCRIPTION	SAMPLE NO.	DESCRIPTION
1	JJH A9	6	JJH A15
2	JJH A10	7	JJH A16
3	JJH A11	8	JJH A17
4	JJH A13	9	JJH A18
5	JJH A14	10	JJH A19

TABLE NO: 6

GRANNY SMITH DIOPSIDES

	11	12	13	14	15	16	17	18	19	20
SiO_2	54.65	54.79	54.15	54.75	54.21	54.21	54.13	54.37	54.52	55.02
TiO_2	.20	.15	.23	.32	.12	.26	.20	.26	.31	.24
Al_2O_3	.37	.24	.84	1.16	1.40	1.02	.92	.94	1.34	1.02
Cr_2O_3	1.11	1.69	2.20	1.38	3.37	2.68	1.47	2.73	2.18	2.89
FeO	2.05	2.20	1.98	3.05	2.06	2.02	2.67	1.83	2.45	1.90
MnO	.06	.06	ND	.09	.05	.08	.04	.08	.08	.09
MgO	18.11	17.32	17.35	17.50	16.78	16.95	17.44	17.22	16.72	16.94
CaO	22.11	22.32	20.93	20.78	19.10	20.55	21.03	20.87	19.96	20.86
Na_2O	1.10	1.28	1.56	1.37	2.23	1.70	1.49	1.67	1.93	1.85
K_2O	ND	ND	ND	ND	.10	ND	ND	ND	ND	ND
TOTAL	99.77	100.06	99.28	100.41	99.42	99.48	99.40	99.98	99.50	100.82

** ATOMIC PROPORTIONS BASED ON SELECTED NO. OF OXYGENS **

OXYGEN	6	6	6	6	6	6	6	6	6	6
SI	1.986	1.991	1.978	1.979	1.977	1.977	1.978	1.974	1.985	1.980
TI	.005	.004	.006	.009	.003	.007	.005	.007	.008	.006
AL	.016	.010	.036	.049	.060	.044	.040	.040	.058	.043
CR	.032	.049	.064	.039	.097	.077	.042	.078	.063	.082
FE2+	.062	.067	.060	.092	.063	.062	.082	.056	.075	.057
MN	.002	.002	-	.003	.002	.002	.001	.002	.002	.003
MG	.981	.938	.945	.943	.912	.921	.950	.932	.907	.909
CA	.861	.869	.819	.805	.746	.803	.824	.812	.779	.805
NA	.078	.090	.111	.096	.158	.120	.106	.118	.136	.129
K	-	-	-	-	.005	-	-	-	-	-
SUM	4.023	4.021	4.021	4.016	4.022	4.015	4.028	4.019	4.014	4.015
	CA 45.22	CA 46.38	CA 44.91	CA 43.75	CA 43.36	CA 44.97	CA 44.39	CA 45.13	CA 44.23	CA 45.44
	MG 51.51	MG 50.05	MG 51.78	MG 51.24	MG 52.99	MG 51.58	MG 51.21	MG 51.79	MG 51.53	MG 51.33
	FE 3.27	FE 3.57	FE 3.32	FE 5.01	FE 3.65	FE 3.45	FE 4.40	FE 3.09	FE 4.24	FE 3.23
	M: 94.03	M: 93.35	M: 93.98	M: 91.09	M: 93.55	M: 93.73	M: 92.09	M: 94.37	M: 92.40	M: 94.08
	C: 46.75	C: 48.09	C: 46.45	C: 46.05	C: 45.01	C: 46.57	C: 46.44	C: 46.56	C: 46.19	C: 46.96

**** SAMPLE DIRECTORY ****

SAMPLE NO.	DESCRIPTION	SAMPLE NO.	DESCRIPTION
11	JJH A20	16	JJH A28
12	JJH A21	17	JJH A30
13	JJH A22	18	JJH A31
14	JJH A25	19	JJH A34
15	JJH A26	20	JJH A36

TABLE NO: 6

GRANNY SMITH DIOPSIDES

	21	22	23	24	25	26	27	28	29	30
SiO_2	54.77	54.26	55.24	55.04	54.65	54.20	54.86	54.61	55.09	54.76
TiO_2	.21	.33	.25	.26	.25	.18	.32	.31	.22	.29
Al_2O_3	.67	1.42	.79	1.05	.89	.41	1.61	1.23	.82	.99
Cr_2O_3	1.13	2.11	2.61	2.96	2.92	1.39	1.86	1.10	.98	2.17
FeO	2.34	2.52	1.79	1.96	1.88	2.00	2.90	2.63	2.82	2.10
MnO	.10	.10	ND	.06	.09	ND	ND	.09	.07	.05
MgO	16.77	16.82	16.65	16.90	16.56	17.26	16.09	17.02	17.09	17.33
CaO	22.12	19.88	21.58	20.77	20.66	22.79	19.88	20.93	21.92	20.85
Na_2O	1.12	1.96	1.61	1.86	1.74	1.09	1.91	1.54	1.25	1.66
K_2O	ND	ND	ND	ND	ND	ND	ND	ND	ND	ND
TOTAL	99.24	99.41	99.94	100.55	100.87	99.65	99.34	99.45	99.47	100.27

** ATOMIC PROPORTIONS BASED ON SELECTED NO. OF OXYGENS **

OXYGEN	6	6	6	6	6	6	6	6	6	6
SI	2.001	1.979	1.992	1.980	1.989	1.984	1.997	1.989	1.995	1.981
TI	.006	.009	.007	.007	.007	.005	.009	.008	.006	.008
AL	.029	.061	.034	.045	.038	.018	.069	.053	.035	.042
CR	.033	.061	.074	.084	.084	.040	.054	.032	.028	.062
FE2+	.072	.077	.054	.059	.057	.061	.088	.080	.085	.064
MN	.003	.003	-	.002	.003	-	-	.003	.002	.002
MG	.913	.914	.895	.906	.898	.941	.873	.924	.922	.934
CA	.866	.777	.834	.801	.806	.894	.775	.817	.850	.808
NA	.079	.139	.113	.130	.123	.77	.135	.109	.088	.116
K	-	-	-	-	-	-	-	-	-	-
SUM	4.002	4.020	4.004	4.014	4.005	4.021	4.001	4.015	4.012	4.018
	CA 46.79	CA 43.94	CA 46.78	CA 45.34	CA 45.75	CA 47.13	CA 44.65	CA 44.86	CA 45.77	CA 44.75
	MG 49.34	MG 51.71	MG 50.20	MG 51.32	MG 51.00	MG 49.64	MG 50.26	MG 50.74	MG 49.63	MG 51.73
	FE 3.86	FE 4.35	FE 3.03	FE 3.34	FE 3.25	FE 3.23	FE 5.08	FE 4.40	FE 4.60	FE 3.52
	M: 92.74	M: 92.24	M: 94.31	M: 93.89	M: 94.01	M: 93.89	M: 90.81	M: 92.02	M: 91.52	M: 93.63
	C: 48.67	C: 45.94	C: 48.24	C: 46.91	C: 47.28	C: 48.70	C: 47.04	C: 46.93	C: 47.98	C: 46.38

**** SAMPLE DIRECTORY ****

SAMPLE NO.	DESCRIPTION	SAMPLE NO.	DESCRIPTION
21	JJH A37	26	JJH A90
22	JJH A41	27	JJH A91
23	JJH A51	28	JJH A92
24	JJH A53	29	JJH A93
25	JJH A76	30	JJG 1841

TABLE NO: 6

GRANNY SMITH DIOPSIDES

	31	32	33	34	35	36	37	38	39	40
SiO_2	54.40	54.12	54.53	54.72	54.62	54.69	54.86	54.68	54.98	55.40
TiO_2	.25	.28	.20	.22	.21	.21	.29	.21	.22	.32
Al_2O_3	.78	.89	1.63	.65	.41	.73	1.36	.44	.73	1.37
Cr_2O_3	2.09	1.43	1.01	.82	1.38	1.63	1.45	1.30	2.19	2.33
FeO	2.01	2.78	2.82	2.99	2.07	2.23	3.02	2.13	2.09	2.40
MnO	.05	.11	.07	.07	.04	.11	.08	.09	.04	.05
MgO	17.20	17.38	16.87	17.32	17.42	17.42	17.08	17.81	17.28	16.42
CaO	21.16	20.35	20.65	21.38	21.96	20.98	20.18	22.49	21.42	20.36
Na_2O	1.45	1.42	1.88	1.21	1.19	1.47	1.79	1.14	1.50	1.90
K_2O	.05	.13	ND	ND	ND	ND	ND	ND	ND	ND
TOTAL	99.44	98.89	99.67	99.39	99.31	99.48	100.12	100.30	100.46	100.56

** ATOMIC PROPORTIONS BASED ON SELECTED NO. OF OXYGENS **

OXYGEN	6	6	6	6	6	6	6	6	6	6
SI	1.984	1.986	1.983	1.998	1.994	1.992	1.987	1.981	1.986	1.995
TI	.007	.008	.005	.006	.006	.006	.008	.006	.006	.009
AL	.034	.038	.070	.028	.018	.031	.058	.019	.031	.058
CR	.060	.041	.029	.024	.040	.047	.042	.037	.063	.066
FE2+	.061	.085	.086	.091	.063	.068	.091	.065	.063	.072
MN	.002	.003	.002	.002	.001	.003	.002	.003	.001	.002
MG	.935	.950	.914	.942	.948	.945	.922	.962	.930	.881
CA	.827	.800	.805	.836	.859	.819	.783	.873	.829	.785
NA	.103	.101	.133	.086	.084	.104	.126	.080	.105	.133
K	.002	.006	-	-	-	-	-	-	-	-
SUM	4.015	4.020	4.028	4.014	4.014	4.016	4.019	4.025	4.014	4.001
	CA 45.36	CA 43.58	CA 44.59	CA 44.72	CA 45.94	CA 44.69	CA 43.59	CA 45.97	CA 45.49	CA 45.17
	MG 51.28	MG 51.77	MG 50.66	MG 50.39	MG 50.68	MG 51.61	MG 51.32	MG 50.63	MG 51.04	MG 50.67
	FE 3.36	FE 4.65	FE 4.75	FE 4.88	FE 3.38	FE 3.71	FE 5.09	FE 3.40	FE 3.46	FE 4.16
	M: 93.85	M: 91.76	M: 91.42	M: 91.17	M: 93.75	M: 93.30	M: 90.97	M: 93.71	M: 93.64	M: 92.42
	C: 46.94	C: 45.71	C: 46.81	C: 47.02	C: 47.54	C: 46.41	C: 45.93	C: 47.59	C: 47.12	C: 47.13

**** SAMPLE DIRECTORY ****

SAMPLE NO.	DESCRIPTION	SAMPLE NO.	DESCRIPTION
31	JJG 1842	36	JJG 1849
32	JJG 1843	37	JJG 1856
33	JJG 1844	38	JJG 1862
34	JJG 1846	39	JJG 1865
35	JJG 1847	40	JJG 1866

TABLE NO: 6

GRANNY SMITH DIOPSIDES

	41
SiO_2	54.75
TiO_2	.28
Al_2O_3	.83
Cr_2O_3	2.24
FeO	1.91
MnO	.09
MgO	17.62
CaO	21.07
Na_2O	1.53
K_2O	ND
TOTAL	100.33

** ATOMIC PROPORTIONS BASED ON SELECTED NO. OF OXYGENS **

OXYGEN	6
SI	1.978
TI	.008
AL	.035
CR	.064
FE2+	.058
MN	.003
MG	.949
CA	.816
NA	.107
K	-
SUM	4.018

CA 44.77
MG 52.07
FE 3.17

M: 93.64
C: 47.12

**** SAMPLE DIRECTORY ****

SAMPLE NO.	DESCRIPTION	SAMPLE NO.	DESCRIPTION
41	JJG 1869		

APPENDIX 5

THERMOBAROMETRY

SAMPLE NO.	FB86 (°C)	MC74 (kbar)	OW79 (°C)	NG85 (kbar)	BM85 (°C)	NG85 (kbar)
JJH 1	1152	55.1	1086	46.0	1143	48.6
JJH 2	1264	59.5	1206	49.3	1244	51.2
JJH 3	1296	59.8	1220	48.6	1263	50.6
JJH 4	1296	60.5	1058	41.6	1262	51.5
JJH 6			1135	59.0		
JJH 7	1375	63.3	1223	47.0	1335	52.4
JJH 8	1282	61.2	1229	51.4	1257	52.7
JJH 9			1196	57.8		
JJH 10	1290	59.6	1289	52.9	1251	50.9
JJH 11	1336	62.9	1241	50.3	1312	53.8
JJH 12	1366	63.9	1297	51.3	1321	52.5
JJH 13	1310	60.9	1269	51.7	1261	51.4
JJH 14	1174	56.6	1261	56.5	1163	51.5
JJH 15	1329	62.3	1334	54.8	1303	53.3
JJH 17	1179	56.7	1281	56.9	1168	50.8
JJH 18	1302	61.6	1234	51.3	1269	53.0
JJH 19			1166	44.9		
JJH 20	1268	60.2	1222	51.0	1243	52.0
JJH 26	1234	57.1	1185	48.1	1219	50.0
JJH 28	1174	55.2	1066	44.1	1188	50.6
JJH 29			1106	45.2		
JJH 30	1327	61.3				
JJH 31	1405	64.7	1172	42.1	1361	50.2
JJH 32	1264	59.2	1222	50.1	1264	52.2
JJH 33	1126	53.2	1198	52.6	1169	51.1
JJH 34	1299	59.7	1226	48.9	1268	51.0
JJH 35	1109	52.9	1186	52.9	1132	50.3
JJH 36	1297	61.8	1257	52.5	1302	54.3
JJH 37	1297	58.6	1200	47.1	1278	51.0
JJH 38	1275	58.4	1209	47.4	1258	49.8
JJG 1710	1255	59.0	1273	53.1	1271	53.0
JJG 1713	1361	61.5	1336	52.1	1344	52.4
JJG 1729	1231	57.9	745	28.0	1196	53.9
JJG 1753	1313	58.7	1244	48.7	1294	51.2
JJG 1798	1298	61.4	1206	47.3	1284	50.3
J 117	1359	61.7	1263	49.0	1332	52.6

FB86 = Finnerty and Boyd (1986)
MC74 = MacGregor (1974)
OW79 = O'Neill and Wood (1979)
BM85 = Bertrand and Mercier (1985)
NG85 = Nickel and Green (1985)

APPENDIX 6

ANALYTICAL TECHNIQUES-ISOTOPE ANALYSIS

Isotope analyses were performed at the Max Planck Institute (MPI) in Mainz, West Germany and at the Bernard Price Institute for Geophysics (BPI) at the University of the Witwatersrand, Johannesburg, South Africa.

Rock-crushing and mineral separation:

Peridotite and megacryst xenoliths were initially crushed with either a small steel or agate mortar and pestle. Crushed samples were then separated into size fractions using disposable nylon mesh. The 200-400 micron (MPI) and 280-500 micron (BPI) size fractions were chosen for analysis because Smith (1984) had noted that this size fraction was most accurately cleaned and sorted under a binocular microscope. The 200-400 micron peridotite sample was then passed through a Frantz magnetic separator for preconcentration of garnet and clinopyroxene. All samples were washed in acetone and distilled water with ultrasonic agitation before handpicking under a binocular microscope.

Handpicking:

The handpicking was done first under fibre optic illumination and then followed by a second more rigorous examination in ethanol with a horizontal light source (MPI) or a dark field annular illuminator (BPI).

Approximately 10 mg of clinopyroxene and 20 mg of garnet were used in analyses at the MPI, and approximately 20 mg of clinopyroxene was used in analyses at the BPI.

Leaching:

All samples were leached overnight in 6N HCl, this was followed by ultrasonic agitation and rinsing in distilled H_2O. The clinopyroxene separates were leached for approximately 10 minutes in 5% HF and washed several times in distilled H_2O with ultrasonic agitation. The garnet separates were leached for approximately 30 minutes in 5% HF and washed several times in 3* H_2O with ultrasonic agitation.

Dissolution:

All samples were dissolved in teflon bombs in a 3:1 HF to $HClO_4$ solution. At the MPI samples were initially microwaved at high power for three 10 minute intervals and then left in an oven at appproximately 100°C for 5 days. At the BPI samples were initially heated on a hotplate for approximately 30 minutes and then left in an oven at approximately 100°C for 5 days.

The excess HF and $HClO_4$ was then evaporated on a hotplate and 6N HCl was added to determine whether the sample had dissolved.

Splitting and spiking:

The 6N HCl was evaporated and 500 ul of 2.59N HCl added to the sample. This was split in the ratio 4:1 for isotopic concentration and isotope dilution procedures respectively.

The samples were spiked with a mixed spike at MPI and separately with ^{149}Sm, ^{146}Nd and ^{84}Sr spikes at the BPI.

Ion-exchange chemistry:

The routine methods employed by E.Jagoutz at the MPI were followed (Jagoutz and Wanke, 1986), and similar methods were then employed at the BPI.

Filaments:

All samples were loaded in HNO_3 onto outgassed filaments.

MPI: Sm and Nd - single Re

Sr - single W (with TaF)

BPI: Sm and Nd - single Re (graphite/platinum solution)

Sr - single Ta

Mass-spectrometric procedures:

Isotopic measurements at the MPI were made on an instrument constucted by E. Jagoutz. Nd was measured as an oxide, and normalized to $^{146}Nd/^{142}Nd = .632285$ (equivalent to $^{146}Nd/^{144}Nd = .7219$). It is reported relative to $^{143}Nd/^{144}Nd = .511890 \pm 5$ for the La Jolla standard and $^{143}Nd/^{144}Nd = .51264$ for BCR-1. Ba and BaF were absent or negligible during these runs. Sr was measured as a metal, and normalized to $^{86}Sr/^{88}Sr = .1194$. It is reported relative to $^{87}Sr/^{86}Sr = .70802 \pm 2$ for the E&A standard.

Sr and Nd isotopic measurements at the BPI were determined on a VG354, and Sm and Nd concentrations were determined on a VG Micromass 30 mass spectrometer. Nd is reported relative to $^{143}Nd/^{144}Nd = .511850 \pm 30$ for the La Jolla

standard. Sr is reported relative to $^{87}Sr/^{86}Sr = .708002 \pm 35$ for the E&A standard.

Estimated precision of concentrations is approximately .05% for Sr, and .01% for Sm and Nd.

Total procedural blank measurements were 60 pg for Sr and 18 pg for Nd. No blank corrections were made to the data.

Values for Bulk Earth used in calculations were:

$$^{87}Sr/^{86}Sr_p = .7045$$

$$^{87}Rb/^{86}Sr = .0827$$

$$^{143}Nd/^{144}Nd_p = .51264$$

$$^{147}Sm/^{144}Nd\ .1967$$

APPENDIX 7

ISOTOPE ANALYSES

TABLE 1 - HIGH-TEMPERATURE PERIDOTITES

TABLE 2 - CR-POOR MEGACRYSTS

TABLE 3 - GRANNY SMITH CLINOPYROXENES

- = no data available

All concentrations are given in ppm. Isotopic ratios with subscript p are present day (measured) ratios with in-run 2 std errors on the mean.

TABLE 1

HIGH-TEMPERATURE PERIDOTITES

Sample	weight (mg)	Sr (ppm)	$^{87}Sr/^{86}Sr$
JJH 10			
cpx	4	102	.70320 ± 6
cpx	16	98.2	.70316 ± 2
gnt	9	.52	-
JJH 12			
cpx	9	100	.70290 ± 4
gnt	14	.89	.7032 ± 1
JJH 26			
cpx	3	96.6	.70243 ± 6
gnt	13	.74	-
gnt	24	-	-
JJH 35			
cpx	3	76.5	.7034 ± 1
cpx	5	82.2	-
gnt	10	.35	-
JJG 1713			
cpx	3	87.1	.70310 ± 6
gnt	13	.59	-
JJG 1729			
cpx	21	113	.70252 ± 3
gnt	17	.40	-
JJG 1753			
cpx	20	102	.70288 ± 3
gnt	20	-	.70395 ± 4

cpx = clinopyroxene
gnt = garnet

All analyses determined at the Max Planck Institute, Mainz

TABLE 1 cont.

HIGH-TEMPERATURE PERIDOTITES

Sample	Sm (ppm)	Nd (ppm)	$^{143}Nd/^{144}Nd_p$	$^{147}Sm/^{144}Nd$
JJH 10				
cpx	1.55	5.99	.51275 ± 2	.156
cpx	1.50	5.68	-	.160
gnt	.75	.97	.51306 ± 6	.468
JJH 12				
cpx	1.69	5.97	.51285 ± 3	.171
gnt	1.22	1.36	.5129 ± 1	.542
JJH 26				
cpx	1.37	4.74	.51323 ± 2	.175
gnt	.61	.73	.5134 ± 1	.505
gnt	.62	.59	.51345 ± 2	.639
JJH 35				
cpx	.26	2.48	.51287 ± 2	.063
cpx	.30	2.62	.51266 ± 3	.070
gnt	.41	1.21	.51287 ± 3	.205
JJG 1713				
cpx	1.44	5.20	.51284 ± 3	.167
gnt	-	1.04	.51295 ± 2	
JJG 1729				
cpx	1.58	6.11	.51292 ± 2	.156
gnt	.78	.87	.51310 ± 3	.542
JJG 1753				
cpx	1.67	6.13	.51287 ± 2	.164
gnt	.73	.85	.51310 ± 2	.520

cpx = clinopyroxene
gnt = garnet

All analyses determined at the Max Planck Institute, Mainz

TABLE 2

CR-POOR MEGACRYSTS

Sample	weight (mg)	Sr (ppm)	$^{87}Sr/^{86}Sr$
Clinopyroxene:			
JJH A59			
	12*	76.9	.70304 ± 3
	15*	89.7	.70308 ± 4
JJH A83			
	4+	99.9	.70318 ± 4
	2+	88	-
JJH A95			
	5+	111	.7029 ± 1
	11+	105	.70314 ± 8
	10*	106	.70303 ± 2
JJG 1859			
	10*	100	.70309 ± 4
	23*	-	.70325 ± 2
Garnet:			
JJH B38			
	12+	1.28	.70383 ± 9
JJH B53			
	20+	.96	.70535 ± 6
JJH B87			
	14+	1.54	-

+ Analyses determined at the Max Planck Institute, Mainz

* Analyses determined at the Bernard Price Institute

TABLE 2 cont.

CR-POOR MEGACRYSTS

Sample	Sm (ppm)	Nd (ppm)	$^{143}Nd/^{144}Nd_p$	$^{147}Sm/^{144}Nd$
Clinopyroxene:				
JJH A59				
	2.22	-	-	-
	1.37	4.50	.51286 ± 2	.184
JJH A83				
	1.79	-	.51287 ± 2	-
	1.50	5.38		.169
JJH A95				
	2.07	7.36	.51297 ± 4	.170
	1.95	6.92	.51281 ± 2	.170
	2.05	8.14	.51284 ± 3	.152
JJG 1859				
	1.86	-	.51281 ± 2	-
	1.66	5.12	.51275 ± 2	.196
Garnet:				
JJH B38				
	.94	1.02	.51310 ± 2	.558
JJH B53				
	-	.93	.51350 ± 3	-
JJH B87				
	.75	-	.51305 ± 2	-

TABLE 3

GRANNY SMITH CLINOPYROXENES

Sample	weight (mg)	Sr (ppm)	$^{87}Sr/^{86}Sr$
JJH A10			
	10*	182	.70367 ± 2
	21*	177	.70361 ± 6
JJH A90			
	3+	201	.7045 ± 1
JJG 1869			
	7*	132	.70386 ± 2
	16*	122	.70390 ± 2

+ Analyses determined at the Max Planck Institute, Mainz

* Analyses determined at the Bernard Price Institute

TABLE 3 cont.

GRANNY SMITH CLINOPYROXENE

Sample	Sm (ppm)	Nd (ppm)	$^{143}Nd/^{144}Nd_p$	$^{147}Sm/^{144}Nd$
JJH A10				
	-	10.5	-	-
	2.17	9.15	.51284 ± 2	.143
JJH A90				
	3.62	13.7	.51275 ± 2	.160
JJG 1869				
	2.04	7.28	-	.169
	1.79	5.71	.51277 ± 2	.189